FINAL REPORT

Development Of Assessment Tools For Evaluation Of The Benefits Of DNAPL Source Zone Treatment

SERDP Project ER-1293

SEPTEMBER 2008

Linda M. Abriola
Tufts University

Pierre Goovaerts
Biomedware

Kurt D. Pennell
Frank E. Löffler
Georgia Institute of Technology

Strategic Environmental Research and Development Program

Report Documentation Page

Form Approved
OMB No. 0704-0188

1. REPORT DATE	2. REPORT TYPE	3. DATES COVERED
SEP 2008	**N/A**	**-**

4. TITLE AND SUBTITLE	5a. CONTRACT NUMBER
Development Of Assessment Tools For Evaluation Of The Benefits Of DNAPL Source Zone Treatment	5b. GRANT NUMBER
	5c. PROGRAM ELEMENT NUMBER
6. AUTHOR(S)	5d. PROJECT NUMBER
	5e. TASK NUMBER
	5f. WORK UNIT NUMBER
7. PERFORMING ORGANIZATION NAME(S) AND ADDRESS(ES) **Tufts University**	8. PERFORMING ORGANIZATION REPORT NUMBER
9. SPONSORING/MONITORING AGENCY NAME(S) AND ADDRESS(ES)	10. SPONSOR/MONITOR'S ACRONYM(S)
	11. SPONSOR/MONITOR'S REPORT NUMBER(S)

12. DISTRIBUTION/AVAILABILITY STATEMENT
Approved for public release, distribution unlimited

13. SUPPLEMENTARY NOTES
The original document contains color images.

14. ABSTRACT

15. SUBJECT TERMS

16. SECURITY CLASSIFICATION OF:			17. LIMITATION OF ABSTRACT	18. NUMBER OF PAGES	19a. NAME OF RESPONSIBLE PERSON
a. REPORT	b. ABSTRACT	c. THIS PAGE			
unclassified	**unclassified**	**unclassified**	**UU**	**173**	

Table of Contents

List of Figures

List of Tables

List of Acronyms

Acronym	Definition
1D	One dimension
2D	Two dimensions
3D	Three dimensions
BDI	Bio-Dechlor INOCULUM
BTC	Breakthrough Curve
ccdf	Conditional cumulative distribution function
cis-DCE	*cis*-dichloroethene
DMD	Density modified displacement
DMD-EM	Density modified displacement – emulsion delivery
DNA	Deoxyribonucleic Acid
DNAPL	Dense non-aqueous phase liquid
DOD	Department of defense
ER	Environmental restoration
FID	Flame ionization detector
GAC	Granular activated carbon
GC	Gas chromatograph
GTP	Ganglia to pool
HD	Hexadecane
HP	Hewlett Packard
IFT	Interfacial tension
ITRC	Interstate Technology & Regulatory Council
LNAPL	Light non-aqueous phase liquid
LT	Light transmission
MAEP	Mean absolute error of prediction
MCDM	Multiple criteria decision making
MISER	Michigan subsurface environmental remediation simulator
MT3D	Modular three-dimensional transport simulator
NAPL	Non-aqueous phase liquid
PCE	Tetrachloroethene or perchloroethene
PFM	Passive flux meter
PI	Probability interval
PV	Pore volume
qPCR	Quantitative, real-time polymerase chain reaction
rRNA	Ribosomal ribonucleic acid
SEAR	Surfactant enhanced aquifer remediation
SEAR-CAT	SEAR – Cost analysis tool
SGS	Sequential Gaussian simulation
SIS	Sequential indicator simulation
SOL	Solubilization
SOL+MOB	Solubilization plus mobilization

SON	Statement of need
TCE	Trichloroethene
TES	N-tris[hydroxymethyl]methyl-2-aminoethane-sulfonic acid
trans-DCE	*trans*-dichloroethene
UTCHEM	University of Texas chemical simulator
VC	Vinyl chloride

Acknowledgements

Over the course of this research project, many faculty, staff and students have contributed time, energy and thoughtful research, which when combined, provides the sponsoring agency with new insight that is expected to aid in the management of numerous federal and state sites contaminated with chlorinated solvent dense nonaqueous phase liquids. This work could not have been completed without the help of the following individuals: Dr Linda Abriola (Tufts U), Dr Pierre Goovaerts (Biomedware), Dr Frank Löffler (Georgia Tech), Dr Kurt Pennell (Georgia Tech), Dr C. Andrew Ramsburg (Tufts U), Dr Lawrence Lemke (Wayne State U.), Dr Tom Phelan (Geosyntec), Dr John Christ (US Air Force Academy), Dr Eric Suchomel (Geosyntec Consultants), Dr Ben Amos (Georgia Tech), Dr Ke (Betty) Li (TetraTech), Dr Yusong Li (Tufts U), Dr John Lang (University of Michigan), and Dr Natalie Cápiro (Georgia Tech). Additionally, the administrative, laboratory and support staff at the Tufts University, the Georgia Institute of Technology, and the University of Michigan are gratefully acknowledged.

Our sincere thanks is extended to the members of the SERDP DNAPL Review Panel for their knowledge, insights and energy that helped keep us outcome focused and made this work stronger. We are also grateful to our Project Officers, for their invaluable assistance in financial management and most especially, helping us navigates the transfer of this contract to Tufts University. The SERDP staff has supported us in countless ways, always responding in a professional and cheerful manner. Our very special thanks are extended to Andrea Leeson and Jeff Marqusee, without whose vision and support this work would never have taken place.

Executive Summary

Since its commencement in September 2002, SERDP Project ER-1293 has supported 4 doctoral students at three universities and resulted in over 40 conference proceedings/technical abstracts and over 20 peer-reviewed publications. These presentations and publications, as referenced in this final report, describe various aspects of the research investigations and tools that have been developed to enhance design and assessment of DNAPL source zone treatment. In general, research in ER-1293 has led to the development and validation of four important concepts: (i) partial source zone mass removal may result in substantial local concentration and mass flux reductions; (ii) potential remediation efficiency is closely linked to source zone architecture (ganglia to pool ratios); (iii) biostimulation and bioaugmentation approaches are feasible for treatment of DNAPL source zones; and (iv) the uncertainty in mass discharge ([M/T]) estimates can be quantified through application of geostatistical methods to field measurements. Major contributions of this research include (i) establishment that rates of metabolic reductive dechlorination can exceed rates of DNAPL dissolution, resulting in aqueous contaminant concentrations in the presence of DNAPL that are substantially lower than saturation levels and are not toxic to the dechlorinating organisms; (ii) enhancements in dissolution will be transient and a function of physico-chemical and biological conditions adjacent to the DNAPL; (iii) demonstration that mass flux reduction behavior can be directly linked to DNAPL source zone architecture; (iv) development of a series of geostatistical approaches capable of quantifying mass discharge uncertainty and guiding real-time sampling design for uncertainty reduction through hot spot delineation ; and (v) creation of a source zone remediation cost estimation tool. These accomplishments provide DOD site managers, federal and state regulators, and other stakeholders with new insight on the mechanisms controlling the strategies employed to remediate and manage chlorinated solve-DNAPL sites.

An ensemble of two- (2D) and three-dimensional (3D) multiphase, compositional simulations were combined with 2D aquifer cell experiment results to quantify the linkage between source zone mass removal and down-gradient flux (or concentration) reduction. Numerical simulations were performed in nonuniform permeability fields conditioned to samples collected at the Bachman Road (MI) field site *(Abriola et al. 2005; Ramsburg et al. 2005).* Several geostatistical simulation methodologies were employed to examine the influence of modeling methodology on simulation results and to generate a set of numerical realizations that encompass the variety of source zone architectures that may be expected in the field *(Lemke et al. 2004).* Source zone architectures were quantified using traditional statistics and spatial metrics (e.g., max DNAPL saturation, central moments) along with innovative metrics developed as part of this project. The ganglia to pool (GTP) ratio was developed to link the source zone architecture to the down-gradient flux signal. Observations of the numerical simulations demonstrated that contaminant flux signals eluting from source zone architectures dominated by DNAPL pools (high saturation, low specific interfacial area DNAPL zones) would evolve differently than those dominated by DNAPL ganglia (low saturation, high specific interfacial area DNAPL zones). Moderate mass removal from source zones characterized as low GTP could result in significant contaminant flux reductions, while the same level of mass removal in a high GTP source zone would lead to minimal reduction in contaminant flux *(Lemke et al. 2004; Phelan et al. 2004; Lemke and Abriola 2006).* Unlike traditional statistical or spatial metrics, the GTP acknowledges this

difference, facilitating the prediction of future source zone response to remedial action *(Christ et al. 2006)*. The relevance of the GTP metric was demonstrated in 2D aquifer cell experiments that employed a novel light transmission methodology to quantify not only the source zone DNAPL saturations, but the saturation architecture as mass was removed *(Suchomel and Pennell 2006)*. As predicted by the numerical simulations and quantified by the GTP metric, light transmission results showed high saturation ganglia zones dissolved rapidly followed by the slow elution of contaminant from persistent DNAPL pools. These encouraging results suggest that aggressive mass removal may result in significant down-gradient flux reduction, potentially leading to the design of remediation strategies that couple the expected flux reduction due to aggressive mass removal with the natural attenuation capacity of the aquifer to manage the contaminant source and plume over the long term. Dfaddfad a

Although the majority of the numerical and experimental source zone architecture studies were performed in 2D, an investigation using a 3D compositional multiphase simulator demonstrated that 3D and 2D source zone architecture metrics (statistical, spatial, and GTP) were not statistically different in low- to-moderately nonuniform permeability fields *(Christ et al. 2005)*.

Anticipated reductions in contaminant flux due to aggressive source zone mass removal suggested the potential to couple source zone mass removal technologies with source zone polishing technologies, such as biostimulation or bioaugmentation *(Christ et al. 2005)*. Bioactivity in the source zone can reduce bulk aqueous phase contaminant concentrations, increasing the concentration gradient and DNAPL dissolution. Batch, column, and 2D aquifer cell experiments were combined with one- (1D) and two-dimensional numerical modeling to examine the significance of metabolic reductive dechlorination on DNAPL dissolution in chlorinated solvent source zones. Batch experiments using four pure cultures: *Desulfuromonas michiganensis* strain BB1, *Sulfurospirillum multivorans*, *Geobacter lovleyi* strain SZ, and *Desulfitobacterium* sp. strain Viet1, demonstrated the tolerance of dechlorinating cultures to aqueous phase tetrachloroethene (PCE). Contrary to several studies in the literature, this work identified an aqueous phase PCE threshold concentration above which metabolic reductive dechlorination ceased: 90 mg PCE per liter. In all pure cultures studied, dechlorination became negligible when PCE concentrations exceeded the 90 mg/L threshold. Dechlorination in the presence of PCE-DNAPL did occur, however, in those cultures with dechlorination rates exceeding the dissolution rate (e.g., *S. multivorans*). In these cases, active dechlorinating cultures maintained an aqueous phase PCE concentration below the threshold, resulting in complete dissolution and dechlorination of the PCE-DNAPL *(Amos et al. 2007a)*. These observations were supported in three 1D column experiments designed to have a 10cm long source zone followed by a 50cm plume region. In two of the three column experiments a mixed NAPL (PCE/hexadecane) was employed to ensure aqueous phase PCE concentrations remained below the threshold concentration identified in the batch experiments. In the third column a pure PCE-DNAPL was employed, resulting in aqueous phase PCE concentrations exceeding the threshold concentration. In the later column with solubility PCE concentrations (~150 – 200 mg/L) no enhancement, bacterial growth, or dechlorination was observed, while in the former columns significant dissolution enhancement (4X) and dechlorination was observed *(Amos et al. 2008a, 2008b)*, supporting the batch experiment conclusions. A novel 2D multiphase compositional simulator that coupled dissolution enhancement to aqueous phase metabolic reductive dechlorination was developed and applied to examine the conditions controlling the

degree of dissolution enhancement in 1D and 2D experimental settings. Simulation results demonstrated the degree of dissolution enhancement would evolve as the DNAPL dissolved and the saturation distribution changed, ultimately leading to dissolution-limited conditions. Biological reaction kinetics (e.g., max utilization rate, biomass concentration, and substrate concentration), NAPL saturation, and saturation distribution were all factors found to influence the degree of dissolution enhancement *(Christ and Abriola 2007)*.

Ramsburg et al. *(2004)* suggested residual flushing solution (i.e., surfactant) could provide adequate substrate to drive source zone metabolic reductive dechlorination. This fortuitous observation in the field, however, required documentation in the laboratory. Toward this end, a series of batch experiments were performed to evaluate the effect of Tween 80 on metabolic reductive dechlorination. Batch experiments considered a variety of pure and mixed cultures at multiple Tween 80 concentrations. All results except those of the *Dehalococcoides* cultures, indicated that the affects of Tween 80 on dechlorination were negligible, suggesting the potential for residual flushing solution to stimulate source zone and down-gradient metabolic reductive dechlorination. The effect of Twen 80 on *Dehalococcoides* spp., however, was reversible and would likely be negligible in the field due to surfactant transport, dilution, and degradation *(Amos et al. 2007b)*.

2D aquifer cell experiments designed to examine metabolic reductive dechlorination in realistic nonuniform PCE-DNAPL source zones were shown to result in localized source zone regions with environmental conditions favorable for metabolic reductive dechlorination. These experiments, performed following a similar methodology to that used in the abiotic experiments outlined above, released a pure PCE-DNAPL into an aquifer cell comprised of low permeability lenses set in high permeability media, generating a source zone architecture with a relatively low GTP. Surfactant floods were then applied to remove the majority of the DNAPL mass before augmenting with dechlorinating microbial cultures, much like a combined remediation strategy that might be applied for long-term management of a chlorinated solvent-DNAPL source zone. Even though microbial reductive dechlorination did not occur in regions with high aqueous phase PCE concentrations (i.e., minimal dissolution enhancement due to dechlorination), aqueous phase PCE concentrations in the effluent were reduced, suggesting a combined strategy may be an effective methodology for long-term management of a persistent DNAPL source zone.

The recognized inability to reduce contaminant concentrations below a regulatory threshold (e.g., the Maximum Contaminant Level) at most sites and the unclear relationship between partial source mass removal and plume response have led a number of researchers seeking alternative metrics to evaluate the benefits of partial source depletion. Indeed, differing from a point concentration-based metric (e.g., concentration at the extraction well), contaminant mass discharge through an entire down-gradient boundary has been widely acknowledged as an alternative metric because it represents the amount of contaminant mass emanating from the source to the plume, thus closely relates to both the source and the plume . Use of contaminant mass discharge as a metric, however, requires improved understanding of the uncertainty associated with the reported single-value estimate. Contaminant mass discharge can be computed by integrating water flux and contaminant concentration, or mass flux ($[M/T \cdot L^2]$) over a down-gradient control plane. Fiscal and practical constraints, however, always prevent

exclusive sampling of the control plane. Regionalization of local measurements of concentration and water flux, or mass flux thus introduces uncertainty into mass discharge estimate.. To better understand this uncertainty and to provide a tool to aid remedial site managers with quantified mass discharge uncertainty, two geostatistical-based stochastic simulation approaches were developed. These approaches can take transect measurements or mass flux measurements obtained in the field and provide an empirical probability distribution of mass discharge, which fully characterizes the uncertainty space of mass discharge without arbitrary assumptions of the distribution function shape or type. In addition to uncertainty quantification, these approaches can also provide equal-probable maps (realizations) of local mass flux on the control plane (*Li et al., 2007*). Application of the approaches to 3D field-scale numerically simulated plume data suggest that even for a mildly heterogeneous aquifer, the heterogeneity of the contaminant concentration field may still lead to great uncertainty in the mass discharge estimate. Under a typical regular sampling design, the control plane may need to be sampled to an extremely high degree (6~7% of the transect area) for an accurate model of uncertainty for mass discharge. However, this level of sampling effort is typically impractical in the field. As a result, a multi-stage sampling algorithm has been developed to optimize sampling locations and collect sample data efficiently. This algorithm was designed to preferentially sample the most uncertain locations in the vicinity of hot spot areas which contributes the most to the uncertainty of mass discharge (*Li and Abriola, 2006).* Application of the sampling algorithm to numerically simulated plume data shows that its use can reduce the sampling cost by as much as 50% over regular sampling schemes, suggesting a potentially significant cost saving.

A second tool designed with the practitioner in mind was developed to guide cost estimating and remediation technology selection. The surfactant enhanced aquifer remediation Cost Analysis Tool (SEAR-CAT) was developed using practitioner (HSI-Geotrans) input to provide a comprehensive ability to cost-estimate SEAR applications, including below- and above-ground treatment components (e.g. air-strippers, GAC units) for complex, multi-component NAPL compositions and architectures. Mass recovery-mass flux type curves, developed using the results of abiotic numerical simulations and 2D aquifer cell experiments, were incorporated to enable the evaluation of various initial source zone architectures. The user is able to estimate either the volume of surfactant flushing required to attain a specific flux reduction or the flux reduction accompanying a given volume of surfactant flushing for a set of representative source zone architectures. Overall treatment cost as a function of either mass flux reduction and/or source zone mass removal can then be estimated for a site-specific source zone architecture.

The observations made combined with the tools developed as parts of this project provide profound improvements in the general understanding of the mechanisms controlling DNAPL source zone behavior. In fact, these results (e.g., the GTP metric) have already found their way into language describing new research needs (e.g., FY08 statement of need [SON]) and are fully expected to provide improved DNAPL site management strategies. A summary of lessons learned include:

- Significant reductions in contaminant flux (2 orders of magnitude) may be realized at moderate levels of DNAPL mass removal
- Flux reduction and mass recovery will depend on DNAPL architecture, quantified according to the ganglia to pool ratio

- DNAPL source zone ganglia to pool ratios cannot be predicted *a priori* using release volume or subsurface variation in hydraulic or capillary parameter information
- Significant DNAPL mass may persist and concentration levels can be locally high following aggressive mass removal
- Metabolic reductive dechlorination is achievable within a source zone if aqueous phase PCE concentrations remain below a deactivation threshold: ~90mg/L
- Dissolution enhancements due to metabolic reductive dechlorination are possible, but will be limited in effect and transient in extent
- Residual flushing solutions may stimulate metabolic reductive dechlorination
- Aggressive mass removal, coupled with source zone biopolishing, offers much promise for plume management
- Remediation efficacy will depend heavily on nonuniformities in the permeability field and saturation distribution
- Most field applications to date may not have been based upon a sample size sufficient to accurately quantify the uncertainty of mass discharge, and the estimated mass discharge may have large errors.
- Geostatistical approaches can be used successfully to estimate downstream contaminant mass discharge and quantify the associated uncertainty using multi-level transect measurements or mass flux measurements
- Optimization of sampling locations using the multi-stage adaptive sampling algorithm can reduce sampling volumes for mass discharge uncertainty quantification, and reduce the uncertainty
- The SEAR-CAT may be used to guide remediation site managers in the implementation of SEAR technologies

Through the course of this project continuing challenges have been identified. Challenges worth additional inspection include, but are not limited to:

- Quantification of source zone architecture for improved remedial performance design and assessment.
- Source zone dechlorination, if incomplete, may lead to increased risk. Additional factors due for exploration include solvent toxicity, electron donor limitations, gas production, and pH changes.
- Novel delivery and maintenance of electron donor levels in DNAPL source zones under heterogeneous conditions may lead to improved dissolution enhancement.
- Development of simplified (e.g., upscaled) prediction tools for treatment design and assessment.
- Design of reliable monitoring protocols and tools for uncertainty assessment for all mass discharge estimation technologies.

Objectives

This project was one of three DNAPL-related funded projects in 2002 in response to the SERDP FY2001 statement of need (SON). This SON identified the following research needs: (i) exploration of the effects of source zone treatment and benefits of partial mass removal from sources, (ii) source delineation, characterization and flux analysis, (iii) investigation of source zone bioremediation and bioaugmentation, and (iv)a better understanding of existing technologies.

The accomplished research represents a multidisciplinary integration of laboratory, field, and modeling studies designed to provide a more comprehensive understanding of the impacts of DNAPL source zone treatment on contaminant concentrations and mass fluxes in heterogeneous field settings and to develop tools and protocols for field monitoring and cost/benefit remediation analyses for such DNAPL sites. The primary objective of the research was to develop and evaluate a suite of tools that can be utilized by site managers to: (1) predict and monitor plume development following DNAPL source zone treatment and (2) perform cost/benefit analysis during the selection of a source zone remediation technology. Emphasis was placed on remediation of chlorinated solvent sources residing within the saturated groundwater zone. The research focused on examination of relatively favorable remediation scenarios for source removal technologies (i.e. unconsolidated media and environments favorable for microbial attenuation) and addressed near source mass fluxes and plume development under natural gradient conditions.

Specific objectives included: (i) evaluation of DNAPL recovery and subsequent dissolved-phase contaminant fluxes from heterogeneous source zones for a variety of treatment technologies and treatment levels at the laboratory-scale; (ii) evaluation of the impact of treatment technologies on the potential for natural attenuation within the source zone; (iii) refinement and validation of a numerical simulator for the prediction of the effects of source zone treatment on spatial and temporal changes in dissolved-phase contaminant concentrations; (iv) development and evaluation of alternative protocols/tools for the estimation of mass discharge/fluxes and the associated uncertainty, and the assessment of the potential for natural attenuation within post-treatment source zones; and (v) development of cost-benefit analysis tools to evaluate and compare source zone treatment technologies.

I. Background

When released to the subsurface, DNAPLs tend to migrate downward through both the unsaturated and saturated zones until a capillary barrier (a finer grained or low permeability material) is encountered. The combined high density and low viscosity of many of these solvents also creates a tendency for the formation of gravity fingers (narrow and tortuous migration pathways) within the saturated zone *(Chouke et al. 1959; Homsy 1987).* The migration pathways and entrapment of DNAPLs in natural formations are largely governed by the spatial distribution of subsurface properties, such as permeability, porosity, and mineralogy *(Kueper et al. 1993; Dekker and Abriola 2000).* Even relatively low levels of heterogeneity have been shown to result in enhanced spreading and highly complex migration pathways and entrapment configurations *(Kueper and Frind 1991; Essaid and Hess 1993).* Once infiltration and migration have ceased, the DNAPL distribution in the subsurface is typically characterized by highly irregular patterns of residual droplets or ganglia entrapped within the porous medium by capillary forces and regions of high DNAPL saturation or "pools" above fine layers.

At the start of this research, the most common technology implemented for aquifer remediation was "pump-and treat", which was selected for groundwater treatment at 98% of over 600 National Priority List (NPL) sites *(USEPA 1997).* Although plume containment can often be achieved using this technology, its application to source zone treatment relies on the dissolution and desorption of contaminants into the aqueous phase. These processes occur over very long time scales and, thus, the use of conventional pump and treat technologies to restore a DNAPL contaminated aquifer to a specific health or risk based standard (e.g., an aqueous- or solid-phase concentration) is usually not achievable within an acceptable time frame. In addition, the costs associated with maintaining a pump and treat system, in particular water treatment components, and monitoring contaminant levels in groundwater over long periods of time can be exorbitant.

Table 1. Comparison of DNAPL source zone treatment outcomes.

	Source Zone Treatment Technology					
Expected Outcome	Pump and Treat	Chemical Oxidation	Co-Solvent Flushing	Surfactant Flushing	Steam Flushing	Air-Sparging
Mass Removal	Low	Medium	High	High	High	Low/Medium
Treatment Time	Long	Short	Short	Short	Short	Medium
Mass Flux Reduction	Low	Medium (?)	Medium/High (?)	High (?)	High (?)	Low/Medium
Overall Cost	High	Medium/High	Medium/High	Medium/High	Medium/High	Low
Major Cost Components	Effluent Trt. O & M	Chemicals, Injection Sys.	Chemicals, Effluent Trt.	Chemicals, Effluent Trt., Recycle Sys.	Energy, Injection Sys., Effluent Trt.	Injection and Extraction Sys.
Limitations and Drawbacks	Ineffective, Containment only, Long trt. time	Toxicity to microflora, Uncontrolled reaction, Hazardous	Toxicity to microflora, Fluid density contrast, Flammability	Risk of displacement, Recycle system	Toxicity to microflora, Uncontrolled DNAPL migration	Preferential flow paths, Contaminant volatility

Over the past decade, considerable research focused on the development and demonstration of alternative technologies for DNAPL mass recovery in the saturated zone, including surfactant enhanced aquifer remediation (SEAR), solvent flushing, air sparging, steam flushing, and in situ chemical oxidation *(NRC 1997; Pennell and Abriola 1997)* (see Table 1).

Although each of the above technologies may present distinct advantages and disadvantages in a particular contamination scenario, the successful application of any of these requires both the delivery of fluids to the contaminated source zone and contact with the DNAPL. Most techniques also require the subsequent recovery of contaminant mass (whether solubilized, volatilized, or mobilized as a separate phase). At the laboratory bench scale, these technologies have been shown to greatly reduce overall remediation time and enhance contaminant mass recovery/destruction in comparison to conventional pump-and-treat approaches. In field applications, however, fluid delivery and recovery is governed in large measure by subsurface heterogeneity. Thus, pilot-scale chemical flushing and air sparging trials involving DNAPL source zones have yielded mixed results, and in a number of cases failed to reach desired clean up goals (e.g. *Fountain et al. 1996; AATDF 1997; Smith et al. 1997)* . Although under more controlled and homogeneous field conditions some chemical flushing field trials were far more successful *(AATDF 1997; Jawitz et al. 1998), in-situ* flushing strategies cannot be expected to recover more than 80 to 90% of the contaminant mass even under ideal, pilot-scale field conditions. For more extensive or complex source zone scenarios, realistic recovery rates may be on the order of 50-70%. The contaminant remaining after treatment is likely to exist within thin pools of free product residing above low permeability lenses or confining layers, entrapped within low permeability media, and/or sorbed by the solid phase. Active ingredients in the flushing solution, such as surfactant, that are not completely extracted from the swept volume may also be present in low permeability zones and sorbed by the solid-phase. Thus, a post-treatment source zone is likely to contain substantial amounts of DNAPL contaminant and flushing solution constituents, even though overall mass recoveries may be quite high.

The definition and quantification of 'success' with respect to source zone remediation is a controversial subject and was the focus of a National Ground Water Association Theis Conference (November 12-15, 1999). The efficient recovery or removal of 80 to 90% of the contaminant mass from a source zone is a vast improvement over conventional technologies. From a regulatory perspective, however, the post-treatment contaminant mass (10%-20%) may still pose a significant risk to human health and the environment. Two approaches to the quantification of source zone remediation 'success' may be identified. The first involves quantification of the potential reduction in remediation and containment costs associated with the application of a particular source treatment scheme. This measure is linked to mass removal efficiency. The second approach involves the evaluation of the reduction in contaminant mass flux from the source zone subsequent to treatment. Such reductions in mass flux could be associated with DNAPL mass removal or enhancements of DNAPL bioavailability within the source zone. An analytical modeling investigation, based upon simplified source zone conditions (such as uniform groundwater flow, a constant interphase mass transfer coefficient, and simplified entrapment configurations) concluded that effective mass transfer rates of contaminants from source zones will be 'largely independent of DNAPL saturations within DNAPL subzones' and that 'remediations (sic) that reduce DNAPL saturations will have little effect on near-term groundwater quality'*(Sale and McWhorter 2001)*. Such conclusions, however, may not be valid in more heterogeneous flow environments and would appear to be contradicted by recent sand box experiment observations of source zone mass fluxes (e.g. *Taylor et al. 2001*) and numerical simulations of contaminant concentrations under flushing conditions (e.g. *Dekker and Abriola 2000*) in slightly heterogeneous media.

Despite its obvious importance to the evaluation of alternative site remediation/management options, relatively little research had been conducted to assess the post-

treatment distribution, mass transfer, and biotransformation of DNAPLs following *in-situ* flushing treatments. Although microbial transformation of DNAPLs in source zones had generally been assumed to be inhibited, more recent findings suggested that some PCE-dechlorinating bacteria were able to tolerate high concentrations of chlorinated solvents and can reductively dechlorinate PCE in the presence of DNAPLs (*Sung et al., 2003; Yang and McCarty*, 2000). These observations are of tremendous relevance for the remediation of chlorinated solvent source zones, suggesting microbial stimulation as a post-flushing treatment. It is likely, however, that the selected remediation technology will strongly influence the potential for natural attenuation in the source zone area and in the plume. For example, one study suggested that ethanol flushing significantly decreased the viable bacteria in the PCE/TCE source zone *(Helton et al. 2000).* Chemical oxidation and steam flooding are also likely to adversely affect viable biomass. In contrast, other studies suggested that certain classes of surfactants (e.g. Tween series) may not only induce anaerobiosis but also provide reducing equivalents to the reductively dechlorinating populations *(Yeh and Pavlostathis 2004).*

Field scale prediction or assessment of contaminant mass flux reductions from a treated source zone is further complicated by subsurface heterogeneity. Numerical modeling studies have indicated that the prediction of DNAPL flow pathways is very sensitive to small-scale heterogeneity in permeability and capillary characteristics *(Bradford et al. 1998; Dekker and Abriola 2000).* The prediction of DNAPL distribution, long term DNAPL persistence, and the evolution of contaminated plumes emanating from DNAPL source zones in natural aquifer environments is, thus, predicated upon a realistic representation of heterogeneity at a range of scales (from centimeters to tens or hundreds of meters). The presence of heterogeneity also complicates the estimation of mass fluxes from field measurements. In investigations relating to contaminant plume attenuation, two general methods have been applied to estimate dissolved mass flux *(Einarson and Mackay*, 2001*).* In the first, hydraulic conductivity and solute concentrations are sampled from multiple points across one or more transects (e.g., *Borden et al. 1997; Semprini et al. 1995; Wilson, et al.,* 2000). Uncertainty corresponding to mass flux estimates generated in this way is difficult to quantify, and few attempts have been documented in the literature (*Wilson et al. 2000).* For heterogeneous aquifer systems, the influence of sample density and interpolation method on the uncertainty in contaminant mass flux estimates is poorly understood. The second method for estimating mass flux is based on the inversion of time series concentration measurements made during short-term pumping tests *(Holder et al. 1998; Schwarz et al. 1998)*. This emerging approach involves simultaneous or sequential pumping of extraction wells located along a plane perpendicular to groundwater flow. Although this approach offers the advantage of integrating contaminant mass measurements over the capture zone volume, the potential for altered mass flux due to perturbation of the flow field during the pumping test has not yet been fully explored nor has the uncertainty associated with the inversion solutions for contaminant mass distribution and average mass flux estimates.

Relatively few mathematical models have been developed for the simulation of field-scale multiphase flushing (i.e. surfactant, co-solvent, or air sparging) remediation technologies. Most advanced simulators are based upon an adaptation of enhanced oil recovery models *(Brown et al. 1994; Delshad et al. 1996)*, and are predicated on assumptions of local thermodynamic equilibrium between phases**.** Some data from laboratory experiments of surfactant-enhanced solubilization and soil vapor extraction, however, indicate that local interphase mass transfer rates can severely limit DNAPL recovery *(*e.g. *Abriola et al. 1993).* Mass transfer rate limitations are commonly observed at the field scale (e.g., *Fountain et al. 1996)* in applications

of remedial technologies. While these field observations may also be the consequence of irregular DNAPL distributions and flow bypassing, the controlling scale of heterogeneity will likely require a numerical model that accounts for such rate limitations on the grid scale, incorporating both temporal and spatial variability of mass transfer rates. Without incorporating such rate limitations, models tend to over predict remedial mass recoveries and under predict mass fluxes from DNAPL residual zones. Few modeling investigations have considered the influence of subsurface heterogeneity and rate-limited mass transfer on source zone mass fluxes (e.g. *Dekker and Abriola*, 2000b) or long-term (post treatment) elution.

II. Materials and Methods

II.1 BATCH BIOTIC EXPERIMENTS

II.1.1 Evaluation of aqueous-phase PCE tolerance and microbially enhanced PCE dissolution

For the microbial reductive dechlorination process to be widely accepted as a source zone treatment strategy applicable to a wide range of sites and environmental conditions, mechanisms controlling microbial activity in the presence of DNAPL must be elucidated. The objectives of the research outlined in this section were to evaluate the dechlorination performance of four pure dechlorinating microbial cultures at elevated PCE concentrations and to investigate the ability of the cultures to dechlorinate in the presence of PCE DNAPL. Additional information on the motivation for this research and the experimental methodology is available in Amos et al. *(2007a)*.

II.1.1.1 Chemicals

PCE (≥99.9%) and TCE (≥99.5%) were purchased from Sigma-Aldrich Co. (St. Louis, MO). *cis*-DCE (99.9%) and *trans*-1,2-dichloroethene (*trans*-DCE, 99.9%) were obtained from Supelco Co. (Bellefonte, PA). Methanol (≥99.9%) was obtained from Fisher Scientific (Hampton, NH). All of the other chemicals used were reagent grade or better unless otherwise specified.

II.1.1.2 Cultures and medium preparation

The following pure cultures were used in this study: *Desulfuromonas michiganensis* strain BB1 (DSM 15941, *(Sung et al. 2003)*), *S. multivorans* (DSM 12446, *(Neumann et al. 1994; Luijten et al. 2003)*), *Geobacter lovleyi* sp. strain SZ (DSM 17278, *(Sung et al. 2006)*), and *Desulfitobacterium* sp. strain Viet1 *(Löffler et al. 1997; Löffler et al. 1999)*. Reduced anaerobic mineral salts medium was prepared as described *(Löffler et al. 1996)* with the following modifications: KH_2PO_4, 0.2 mM; resazurin, 1 μM; Na_2S x $9H_2O$, 0.05 mM (unless otherwise noted); dithiothreitol, 0.5 mM; anhydrous L-cysteine hydrochloride, 0.22 mM; and TES (N-tris[hydroxymethyl]methyl-2-aminoethane-sulfonic acid), 10 mM. Vitamins (200-fold concentrated) and KH_2PO_4 (200 mM) were added from sterile, anoxic stock solutions after autoclaving. The final vitamin concentrations were as described *(Löffler et al. 1996)*, except vitamin B_{12} was at twice the concentration. Serum bottles (160 mL nominal capacity, Wheaton Co., Millville, NJ) were prepared with a N_2/CO_2 (80%/20% [vol/vol]) headspace and sealed with Teflon-lined, gray butyl rubber septa (#1014-4937, West Pharmaceuticals, Lionville, PA) and aluminum crimp caps (Wheaton Co., Millville, NJ). PCE was added as described below, sterile hydrogen gas was added via syringe (where indicated), and acetate or pyruvate were added to individual bottles from sterile, anoxic stock solutions using a syringe. The final aqueous volume following all amendments was 101 ± 1 mL.

II.1.1.3 Determination of dissolved-phase PCE tolerance

In this study, PCE tolerance is defined as the ability to dechlorinate dissolved-phase PCE completely to the strain-specific dechlorination end product (i.e., TCE, *cis*-DCE). In the

dissolved-phase PCE tolerance experiments, culture vessels received PCE dissolved in a water miscible carrier phase (i.e., methanol) to facilitate the immediate availability of dissolved-phase PCE to the microorganisms. Preparation of anoxic methanol and the anoxic PCE/methanol stock solution (350 μL PCE/15 mL methanol) is described in the *Supporting Information* of reference *(Amos et al. 2007a)*. Bottles containing medium were amended with the anoxic PCE/methanol stock solution (0.2 mL) and allowed to equilibrate for 2 days, resulting in measured initial aqueous phase PCE concentrations of 240-310 μM after equilibration (i.e., partitioning between the headspace and aqueous phases). Electron donors and/or carbon sources were added as described above, were in excess throughout the experiment, and varied for each culture: acetate (5 mM) for strain BB1, acetate (5 mM) and hydrogen (10 mL) for *S. multivorans* and strain SZ, and pyruvate (5 mM) and hydrogen (10 mL) for strain Viet1. Each culture was initiated with a 5% (vol/vol) inoculum from a dechlorinating culture grown with PCE (0.33 mM) as the electron acceptor. After significant dechlorination (>80%) of the initial amount of PCE, a series of bottles received different volumes from the PCE/methanol stock solution (aqueous phase PCE concentrations after equilibration are given in parentheses): 0.2 mL (295 ± 10 μM), 0.4 mL (560 ± 45 μM), 0.6 mL (830 ± 15 μM), 0.8 mL (1,050 ± 5 μM), or 1.0 mL (1,200 ± 100 μM). The aqueous methanol concentration was adjusted to 1.2% (vol/vol)) in all bottles. Exploratory experiments demonstrated that the final methanol concentration did not affect culture performance (i.e., toxicity), pH, or analyte partitioning. Cultures were immediately shaken by hand and sampled after amendment with the PCE/methanol solution and/or pure methanol. Cultures were incubated upright at 22°C on a platform shaker at 175 rpm.

II.1.1.4 Dechlorination studies in the presence of PCE DNAPL

Dechlorination studies in the presence of PCE DNAPL were performed with strain BB1, strain SZ, and *S. multivorans.* Electron donors and/or carbon sources were added as described above and varied for each culture: acetate (5 mM) for strains BB1 and SZ and pyruvate (5 mM) and hydrogen (5 mL) for *S. multivorans*. In these experiments, the concentration of $NaHCO_3$ was increased to 60 mM to increase the buffering capacity and the concentrations of Na_2S and L-cysteine were increased to 0.1 mM and 0.27 mM, respectively. Serum bottles containing medium were amended with 0.2 mL of the anoxic PCE/methanol stock solution and allowed to equilibrate for 2 days to yield initial aqueous phase PCE concentrations of approximately 300 μM. The bottles received a 5% (vol/vol) inoculum of a dechlorinating culture grown with PCE (0.33 mM) as the electron acceptor. Triplicate cultures of strain BB1, strain SZ, and *S. multivorans* were incubated at 22°C and shaken upright at 150 rpm on a platform shaker. Following complete dechlorination of the initial PCE amendment, the cultures were amended with an additional 0.2 mL of the anoxic PCE/methanol stock solution. After complete dechlorination of dissolved-phase PCE, a 500 μL gastight syringe (#1750, Hamilton Co., Reno, NV) was used to amend the bottles with 50 μL neat PCE to form a single PCE droplet (DNAPL). Control cultures operated under identical conditions were inactivated by the addition of sterile O_2 gas (10 mL) after growth of *S. multivorans* on dissolved-phase PCE but before amendment of PCE DNAPL. The control cultures were used to determine the PCE dissolution rate. Additions of hydrogen gas (10 mL at Day 2, 5 mL for all other amendments) to the cultures of *S. multivorans* were performed on Days 2, 4, 5, 6.5, 7, 10, 12, and 15 after DNAPL addition. The experiment with *S. multivorans* was repeated in duplicate vessels shaken at increased agitation (175 rpm), which was assumed to increase the rate of PCE dissolution from the DNAPL phase.

The *cis*-DCE production following DNAPL addition was determined by subtracting the *cis*-DCE aqueous phase concentration present before DNAPL addition from the *cis*-DCE concentrations measured following DNAPL addition.

II.1.1.5 Analytical methods

Chlorinated ethenes were quantified via gas chromatography. Aqueous phase samples (1 mL) were analyzed on a Hewlett-Packard (HP) 7694 headspace autosampler and a HP 6890 gas chromatograph (GC) equipped with a HP-624 column (60 m by 0.32 mm; film thickness, 1.8 μm nominal) and a flame ionization detector (FID). Standards for chlorinated ethenes were prepared as described *(Gossett 1987; Löffler et al. 1997)*. Additional information on sample and standard preparation as well as GC and autosampler operational parameters is provided in the *Supporting Information* of Amos et al. *(2007a)*.

II.1.2 Effects of Tween 80 on microbial reductive dechlorination

Recent field studies have indicated synergistic effects of coupling microbial reductive dechlorination with physicochemical remediation (e.g., surfactant flushing) of DNAPL source zones. In a staged treatment scenario, the physicochemical remedy removes significant contaminant mass, and, in case of surfactant or co-solvent flushing, delivers electron donors that may stimulate microbial reductive dechlorination activity *(Mravik et al. 2003; Ramsburg et al. 2004; Ramakrishnan et al. 2005)*. Hence, in this sequential approach, reductive dechlorination acts as a "polishing" step that detoxifies residual contaminants, thereby reducing contaminant mass flux and controlling long-term plume development. Understanding the effects of surfactants on dechlorinating bacteria is vital for successfully applying sequential remedies to a broad range of contaminated sites. Therefore, the objective of the research outlined in this section was to determine the influence of Tween 80 on key chlorinated ethene-dechlorinating bacteria at surfactant concentrations similar to those observed following SEAR at the Bachman Road site *(Ramsburg et al. 2004)*. Additional information on the motivation for this research and the experimental methodology is available in Amos et al. *(2007b)*.

II.1.2.1 Chemicals

Tween 80 (polyoxyethylene [20] sorbitan monooleate) was obtained from Uniqema (New Castle, DE) and used without further purification. Tween 80 has an average molecular weight of 1,310 g/mole *(Pennell et al. 1997)*. PCE (≥99.9%) and TCE (≥99.5%) were purchased from Sigma-Aldrich Co. (St. Louis, MO). *cis*-DCE (99.9%) and *trans*-1,2-dichloroethene (*trans*–DCE, 99.9%) were obtained from Supelco Co. (Bellefonte, PA). Gaseous VC (≥99.5%) was obtained from Fluka Chemical Corp. (Ronkonkoma, NY), and ethene (99.5%) was purchased from Scott Specialty Gases (Durham, NC). All of the other chemicals used were reagent grade or better unless otherwise specified.

II.1.2.2 Cultures and medium preparation

The following pure cultures were used in this study: *Sulfurospirillum multivorans* (DSM 12446, *(Scholz-Muramatsu et al. 1995)*), *Geobacter lovleyi* sp. strain SZ (DSM 17278, *(Sung et al.*

2006)), "*Clostridium bifermentans*" strain DPH-1 *(Chang et al. 2000)*, *Desulfitobacterium* sp. strain Viet1 *(Löffler et al. 1997; Löffler et al. 1999)*, *Dehalococcoides* sp. strain BAV1 *(He et al. 2003)*, and *Dehalococcoides* sp. strain FL2 *(He et al. 2005)*. In addition to the six pure cultures, two PCE-to-ethene dechlorinating mixed cultures were tested: the OW consortium *(Daprato et al. 2007)* and Bio-Dechlor INOCULUM (BDI), a microbial consortium that has been successfully used for bioaugmentation at chlorinated ethene-contaminated sites *(Ritalahti et al. 2005)*.

The detailed preparation of reduced anaerobic mineral salts medium is described in the *Supporting Information* of Amos et al. *(2007b)*. Experiments with pure cultures and the BDI consortium used 160-mL (nominal volume) serum bottles containing 100 mL ± 1 mL of medium (unless otherwise noted) and a N_2/CO_2 or H_2/CO_2 (80%/20% [vol/vol]) headspace. For experiments with the OW consortium, 70-mL (nominal volume) serum bottles containing ~50 mL of medium and a H_2/CO_2 (80%/20% [vol/vol]) headspace were used. Tween 80 was added from filter-sterilized anoxic stock solutions (23 or 50 g/L), which were prepared with anoxic, deionized water or reduced mineral salts medium in a glove box (Coy Laboratory Products, Ann Arbor, MI) filled with 95% N_2 and 5% H_2 [vol/vol]. Chlorinated ethenes were added at non-inhibitory concentrations as described *(Amos et al. 2007a)*. Electron donors and/or carbon sources were chosen based on strain-specific requirements and added in excess (i.e., did not limit dechlorination activity).

II.1.2.3 Tween 80 exposure

The pure cultures and BDI were incubated in the presence Tween 80 at concentrations ranging from 50 to 5,000 mg/L (Table 2), which are similar to concentrations (50 – 2,750 mg/L) observed in the Bachman aquifer following surfactant flushing *(Ramsburg et al. 2004)*. Control cultures did not receive Tween 80 but instead were amended with equal volumes of sterile medium. Each vial was allowed to equilibrate for ≥2 days after the addition of a chlorinated ethene before inoculation with 2-5% (vol/vol) from actively dechlorinating stock cultures. Experiments were conducted in triplicate or replicate, independent assays incubated at 22ºC or 30ºC (see Supporting Information, Table S1 of Amos et al. *(2007b)*).

II.1.2.4 Biomass effects on Tween 80 inhibition

To explore the effect of biomass concentration on Tween 80 inhibition, the dechlorination performances of undiluted and 100-fold diluted OW cultures were compared. Aliquots (50 mL) from the 20-L stock culture of the OW consortium, which was grown in semi-batch mode with PCE as the electron acceptor and methanol as the electron donor *(Daprato et al. 2007)*, were dispensed into triplicate, sterile, N_2-flushed serum bottles. The bottles were sparged with H_2/CO_2 (80%/20% [vol/vol]) to remove residual chlorinated ethene. Aliquots (0.5 mL) were then diluted 100-fold into triplicate bottles containing reduced medium. Each bottle received PCE (1.25 μL) and Tween 80 (final concentration of 1,000 mg/L) to bring the total volume per vessel to 50 mL. Triplicate control cultures did not receive Tween 80, but instead received equal volumes of medium. All OW cultures were incubated at 22ºC. Particulate organic carbon (POC) measurements estimated steady-state biomass concentrations from stock cultures of both the OW and BDI consortia as described *(Okutman Tas et al. 2006)*. To collect POC, samples were

filtered through a glass microfiber filter (Whatman Inc., Florham Park, NJ) with 0.7 μm (nominal diameter) pores.

II.1.2.5 Effect of Tween 80 on Dehalococcoides cell numbers

To evaluate the effect of Tween 80 on *Dehalococcoides* cell numbers, BDI cultures were monitored under three different incubation conditions, each maintained at 22ºC. The BDI consortium was chosen for this experiment since it is a robust culture that is easily maintained in the laboratory, contains multiple *Dehalococcoides* strains *(Ritalahti et al. 2006),* and has been successfully used in bioaugmentation field applications *(Ritalahti et al. 2005).* Triplicate vessels were amended with 250 mg/L Tween 80. An additional set of triplicates did not receive VC or Tween 80 and served as electron acceptor-starved controls. Duplicate bottles without Tween 80 served as positive control cultures. Each culture vessel received 3 mL of sterile VC gas (unless otherwise indicated) as electron acceptor. Following a 2-day equilibration period, the vessels were inoculated with 15% (vol/vol) from an actively dechlorinating BDI consortium grown with PCE as the electron acceptor. Before inoculation, 200 mL of BDI was placed into sterile, N_2-flushed serum bottles, and a filter-sterilized stream of N_2/CO_2 (80%/20% [vol/vol]) was bubbled through the cell suspension for 15 minutes to remove residual chlorinated ethenes. Before distribution of the inoculum to individual experimental bottles, a sample of the inoculum was collected for quantitative, real-time PCR (qPCR) analysis. The experiment was repeated with a longer incubation time for the Tween 80-exposed treatment and the positive control bottles. Samples were taken periodically for DNA extraction and qPCR analysis (see the *Supporting Information* of Amos et al. *(2007b)* for procedural details). The terms "16S rRNA gene copies" and "cell numbers" are per mL of culture fluid and are used interchangeably because the known *Dehalococcoides* organisms contain one 16S rRNA gene copy per genome *(Kube et al. 2005; Seshadri et al. 2005).*

II.1.2.6 Reversibility experiments

To determine the reversibility of Tween 80 inhibition of *Dehalococcoides* organisms, aqueous samples (1 mL) were collected from triplicate bottles of the BDI consortium exposed to 250 mg/L Tween 80 for 21 days. Samples were also collected after 21 days of incubation from BDI cultures without surfactant (duplicate positive control cultures) or in the absence of chlorinated ethenes (triplicate electron acceptor-starved control cultures). Samples collected from duplicate BDI cultures exposed to filter-sterilized air for 21 days served as negative controls. The biomass was collected by centrifugation for 30 minutes at 4,300 × g using a microcentrifuge placed inside a glove box. The supernatant was decanted, and the biomass from 15 1-mL samples of culture suspension was collected in the same tube. The resulting pellets were suspended (i.e., washed) in 1.5 mL of reduced mineral salts medium, and the centrifugation step was repeated. Each pellet was then suspended in 1 mL of medium and served as inoculum for Tween 80-free medium that had been equilibrated with 3 mL of VC. The cultures were then incubated at 22ºC. The pH of all vials was determined on Day 48 and adjusted with 6N NaOH to pH 7.2 ± 0.1, if necessary.

Table 2. Summary of dechlorination performance of pure and mixed cultures in the presence of Tween 80 *(Amos et al. 2007b).*

	Culture	Provided Electron Acceptor	Tween 80 Concentrations (mg/L)	Dechlorination End Product	
				Control[a]	With Tween 80
Pure Cultures	*Desulfuromonas michiganensis* strain BB1	PCE	1000, 5000	*cis*-DCE	*cis*-DCE
	Sulfurospirillum multivorans	PCE	500, 1000, 5000	*cis*-DCE	*cis*-DCE
	Geobacter lovleyi strain SZ	PCE	500, 1000, 5000	*cis*-DCE	*cis*-DCE
	"*Clostridium bifermentans*" strain DPH-1	PCE	500	*cis*-DCE	*cis*-DCE
	Desulfitobacterium sp. strain Viet 1	PCE	500, 1000, 5000	TCE	TCE
	Dehalococcoides sp. strain BAV1	*cis*-DCE	50, 250	ethene	—[b]
	Dehalococcoides sp. strain FL2	TCE	250	VC	—[b]
Mixed Cultures	Bio-Dechlor INOCULUM (BDI)	PCE	500, 1000, 5000	ethene	*cis*-DCE
	OW Consortium	PCE	1000	ethene	*cis*-DCE/ethene[c]

[a] Cultures incubated without Tween 80
[b] No dechlorination observed
[c] The biomass concentration affected product formation (see text for details)

II.1.2.7 Analytical methods

Aqueous phase (1 mL) or headspace (0.1 ml) samples were collected periodically for chlorinated ethene and ethene quantification by gas chromatography. Aqueous phase samples were analyzed with a Hewlett-Packard (HP) 7694 headspace autosampler connected to a HP 6890 gas chromatograph (GC) equipped with a HP-624 column (60 m by 0.32 mm; film thickness, 1.8 μm nominal) and a flame ionization detector (FID) as described *(Amos et al. 2007a)*. Headspace samples were manually injected into the HP 6890 GC and analyzed as described *(Sung et al. 2003)*. Standard calibration curves for chlorinated ethenes and ethene analysis were prepared as described *(Gossett 1987; Löffler et al. 1997)*. Additional information on sample analysis, including corrections to account for surfactant influences on contaminant partitioning and quantification, is provided in the *Supporting Information* of Amos et al. *(2007b)*.

II.2 BIOTIC 1D COLUMN EXPERIMENTS

Several batch, one-dimensional (1D) column, and two-dimensional (2D) sand box experiments have been conducted to evaluate microbial reductive dechlorination performance and bioenhanced dissolution in PCE-DNAPL source zones *(Carr et al. 2000; Yang and McCarty 2000; Cope and Hughes 2001; Yang and McCarty 2002; Adamson et al. 2004; Sleep et al. 2006)*. These studies suggest dechlorination activity in the vicinity of PCE-DNAPL. While these initial results are promising, the activity of relevant microbial species within DNAPL source zones and the effect(s) of microbial distribution on dissolution enhancement remain poorly understood. To better understand the process of bioenhanced PCE dissolution, continuous-flow column experiments were performed under precisely controlled conditions. The column design allowed for assessment of the spatial distribution and activity of key dechlorinating isolates within PCE-NAPL source zones and the associated plume areas. Additional information on the motivation for this research and the experimental methodology is available in Amos et al. *(2008a, 2008b)* .

Column experiments explored bioenhanced dissolution with a PCE-to-*cis*-DCE dechlorinating, strictly anaerobic pure culture, *Sulfurospirillum multivorans* (DSM 12446, *(Neumann et al. 1994; Luijten et al. 2003)*). *S. multivorans* was selected for evaluation in the 1-D column experiments due to its ease of handling, robust growth characteristics, and the fact that it was observed to dechlorinate in the presence of PCE-DNAPL *(Amos et al. 2007a)*. An additional column experiment was undertaken with BDI-SZ, a PCE-to-ethene dechlorinating consortium that contained multiple *Dehalococcoides* spp. as well as two PCE-to-*cis*-DCE dechlorinating populations (*Geobacter lovleyi* strain SZ and a *Dehalobacter* species). The dechlorinating consortium was utilized for the following reasons: efficient and complete dechlorination of PCE to ethene depends on the presence of multiple dechlorinating organisms, dechlorinating consortia are often used as bioaugmentation inocula *(Major et al. 2002; Ritalahti et al. 2005)*, and complex microbial communities dominate subsurface environments at contaminanted sites.

II.2.1 Materials

HPLC-grade tetrachloroethene (PCE) was purchased from Fisher Scientific (Fair Lawn, New Jersey). PCE has an equilibrium aqueous phase solubility of ca. 1,200 μM (200 mg/L) *(Perry et*

al. 1997) and a liquid density of 1.625 g/mL *(Huling and Weaver 1991)*. Hexadecane (HD; 99% purity) was obtained from Sigma-Aldrich Co. (St. Louis, Missouri). HD has an equilibrium aqueous phase solubility of ca. 0.016 μM (0.0036 mg/L) and a liquid density of 0.77 g/mL *(Schwarzenbach et al. 2003)*. Oil-Red-O ($C_{26}H_{24}N_4O$), a hydrophobic dye, was obtained from Fisher Scientific and used to aid in visualization of entrapped NAPL within the column. For analytical standard curves, PCE (≥99.9%) and TCE (≥99.5%) were purchased from Sigma-Aldrich Co., *cis*-DCE (99.9%) and *trans*-1,2-dichloroethene (*trans*–DCE, 99.9%) were obtained from Supelco Co. (Bellefonte, Pennsylvania). Gaseous VC (≥99.5%) was obtained from Fluka Chemical Corp. (Ronkonkoma, New York), and ethene (99.5%) was purchased from Scott Specialty Gases (Durham, North Carolina). All of the other chemicals used were reagent grade or of higher purity. Federal Fine Ottawa sand (30-140 mesh; U.S. Silica Company, Berkeley Spring, West Virginia) was selected for the column experiments due to its low organic carbon content (below the detection limit of 0.1 g organic carbon per kg solid) and light color, which facilitated the observation of dyed NAPL within the column. The mean grain size and intrinsic permeability of Federal Fine Ottawa sand are 0.32 mm and 4.2 x 10^{-11} m^2, respectively *(Suchomel et al. 2007)*.

II.2.2 NAPL preparation

Two different PCE-NAPLs were used in the column experiments: pure PCE-DNAPL and a mixed NAPL, both of which were dyed with Oil-Red-O at a concentration of 0.4 mM. The mixed NAPL, comprised of PCE and HD, was utilized to (i) simulate a PCE-containing NAPL consisting of a recalcitrant organic fraction with low aqueous solubility and (ii) reduce equilibrium dissolved-phase PCE concentrations below the level inhibitory to many dechlorinating organisms (< 540 μM [90 mg/L]) *(Amos et al. 2007a)*. The PCE/HD mixed NAPL was prepared in an anoxic glove box (Coy Laboratory Products, Ann Arbor, Michigan) by diluting anoxic, N_2-flushed PCE into anoxic, N_2-flushed HD to a final ratio of 0.25/0.75 (mol/mol) (e.g., 10.4 mL PCE and 89.6 mL HD). The aqueous phase solubility of PCE in equilibrium with the mixed NAPL was ca. 300 μM (50 mg/L) based on equilibrium aqueous phase solubility of pure PCE (ca. 1,200 μM) times the mole fraction of PCE in the mixed NAPL (0.25); the aqueous phase solubility of PCE in equilibrium with the mixed NAPL was verified experimentally (data not shown). The density of the mixed NAPL was determined to be 0.86 g/mL using a 2-mL pycnometer (Ace Glass Incorporated, Vineland, New Jersey).

II.2.3 Medium preparation and column inoculum

Reduced, anaerobic mineral salts medium with low chloride content was prepared as described *(Sung et al. 2003)*, except for changes as described below. For experiments with *S. multivorans*, changes to the concentrations of the following components were made: Na_2S x 9 H_2O, 1 mM; anhydrous L-cysteine hydrochloride, 0.2 mM; $NaHCO_3$, 60 mM; and resazurin, 2 μM. For experiments with BDI-SZ, the same changes were performed except the concentration of $Na_2S \cdot 9H_2O$ was reduced to 0.2 mM and the concentration of anhydrous L-cysteine hydrochloride was increased to 1 mM. *N*-tris[hydroxymethyl]methyl-2-aminoethane-sulfonic acid (TES) was also included at a final concentration of 10 mM in the media for *S. multivorans* and BDI-SZ. The reduced medium (1 L) was prepared in 2-liter Schott Duran glass bottles (Fisher Scientific), each of which was capped with a sidearm plug (19 mm i.d.; Wheaton Co., Millville, New Jersey) and

a modified 25-mL anaerobic culture (Balch) tube (Bellco Glass Inc., Vineland, New Jersey) sealed with a black butyl-rubber stopper (Geo-Microbial Technologies, Inc., Ochelata, Oklahoma) and an aluminum crimp cap (Wheaton). Each 2-L bottle contained a N_2/CO_2 (80%/20% [vol/vol]) headspace. Sterile, anoxic sodium/potassium phosphate (Na_2HPO_4/KH_2PO_4; 200 mM) solution was added to the medium to a final concentration of 2 mM after autoclaving. Vitamins were added as described, except vitamin B_{12} was at twice the concentration *(Löffler et al. 1996)*. Where indicated, 20 mM pyruvate or 20 mM lactate was added as electron donor and carbon source from an anoxic, filter-sterilized stock solution for experiments with *S. multivorans* or BDI-SZ, respectively.

Cultures of *S. multivorans* (1 L) were grown with 20 mM pyruvate as the sole carbon and energy source and served as inocula for the column experiments when the pyruvate had been completely consumed. Before the columns were packed, samples of the inocula were collected for DNA extraction and quantitative real-time PCR (qPCR) analysis.

The PCE-to-ethene dechlorinating culture used as inoculum for the column experiment was developed by mixing cultures of the PCE-to-*cis*-DCE dechlorinating isolate, *Geobacter lovleyi* strain SZ (DSM 17278, *(Sung et al. 2006)*), with a PCE-to-ethene dechlorinating consortium, Bio-Dechlor INOCULUM (BDI). BDI has been successfully used in bioaugmentation field applications *(Ritalahti et al. 2005)* and contains *Dehalococcoides* organisms *(Ritalahti et al. 2006)* and a PCE-to-*cis*-DCE dechlorinating *Dehalobacter* species *(Amos et al. 2007b)*. *G. lovleyi* strain SZ was added to BDI since strain SZ-like organisms are widely distributed in the environment and present at many contaminanted sites *(Duhamel et al. 2004; Duhamel and Edwards 2006; Amos et al. 2007c; Duhamel and Edwards 2007)*. In addition, a strain SZ-like population is present in the bioaugmentation inoculum KB-1, which has been used successfully at a number of sites *(Geosyntec 2005.; Major et al. 2002)* and is commercially available (SiREM; http://www.siremlab.com). Recent studies have demonstrated growth of SZ-like organisms in the KB-1 consortium during PCE and TCE dechlorination to *cis*-DCE *(Duhamel and Edwards 2007)*. The development of the PCE-to-ethene dechlorinating consortium, subsequently referred to as BDI-SZ, allowed for simultaneous assessment of multiple, environmentally-relevant dechlorinating populations during bioenhanced dissolution. The BDI-SZ consortium received periodic additions of PCE (0.33 mM) as electron acceptor and lactate (20 mM) as electron donor. The dechlorination performance of BDI-SZ was stable over a period of several months before initiation of the column experiment. Before the column was packed, samples of the BDI-SZ consortium were collected for DNA extraction and qPCR analysis.

II.2.4 Column design and construction

A borosilicate glass column (60 cm length x 4.8 cm inside diameter [i.d.]; Kontes Glass Company, Vineland, New Jersey) equipped with Teflon end-plates was retrofitted with eleven sampling side ports, located on alternating sides of the column at 5 cm intervals (Figure 1). The port nearest to the column influent (5 cm down-gradient) was designated as Port 1, and the ports were numbered sequentially with increasing distance from the influent (Figure 1). Each side port consisted of the upper portion of a 2-mL glass screw-cap HPLC vial (Fisher Scientific) fused to the column via a glass capillary tube (2 mm i.d.). The column contained three regions: a ~10 cm long source zone containing uniformly distributed residual PCE-NAPL, a ~10 cm long transition

zone directly down-gradient of the source zone containing some nonuniformly-distributed NAPL ganglia, and a 40 cm long plume region down-gradient of the transition zone. Ports 1 and 2 were located within the source zone, Ports 3 and 4 were in a transition zone, and Ports 5-11 were in the plume region that did not contain any NAPL.

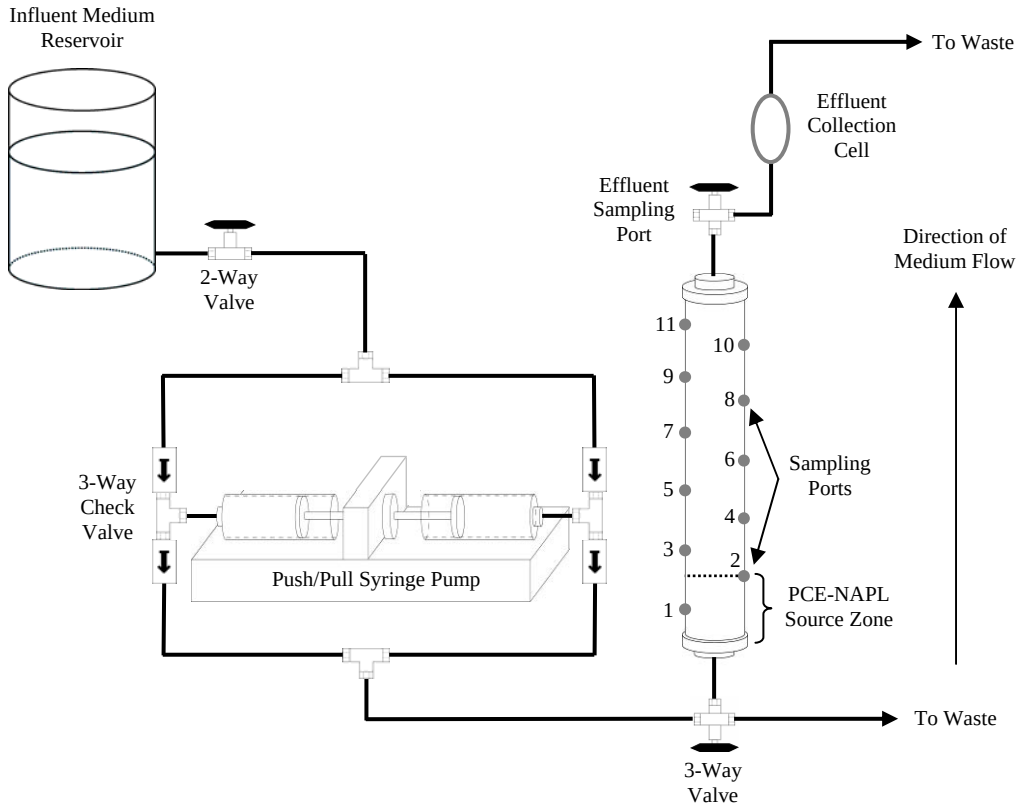

Figure 1: Schematic diagram of the 1-D column system *(Amos et al. 2008a)*.

An influent system was designed to operate continuously at flow rates of less than 1 mL/min under anaerobic conditions. The 2-L bottle containing the influent medium was connected to the column via stainless steel tubing (0.175 i.d.; 0.318 cm outside diameter [o.d.]). The influent medium reservoir was routinely replaced with another reservoir containing freshly-prepared medium to maintain uninterrupted flow. Since medium was continuously withdrawn, the reservoir was pressurized daily to 15 psig with sterile N_2 to prevent intrusion of air into the anoxic influent system. Medium was pumped from the influent reservoir to the column via two 25 mL gas-tight glass syringes (Hamilton Co., Reno, Nevada) using a syringe pump (model PHD 2000 push/pull, Harvard Apparatus, Holliston, Massachusetts). The pump was capable of simultaneous infusion and withdrawal, allowing for continuous operation (i.e., one syringe was infusing medium into the column, while the other was withdrawing medium from the influent reservoir). An in-line effluent collection cell of ca. 25 mL volume was custom-built from a single piece of glass tubing (0.15 i.d.; 0.23 o.d.) and connected to the exit of the column via a four-way valve (Hamilton) and Teflon tubing (0.318 cm o.d.; 0.159 cm i.d.).

II.2.5 Column packing

Three separate columns were constructed: one containing *S. multivorans* and a pure PCE-DNAPL source zone, one containing *S. multivorans* and a mixed-NAPL source zone, and one containing BDI-SZ and a mixed-NAPL source zone. The columns were packed with autoclaved, N_2-sparged Federal Fine Ottawa sand under water-saturated conditions in approximately 2 cm increments with cultures of *S. multivorans* or BDI-SZ as the resident aqueous phase. Packing was conducted inside a glove bag system continuously flushed with nitrogen to maintain anoxic conditions. Use of the microbial culture as the residence aqueous phase, as opposed to culture injection into the column, ensured a uniform initial distribution of bacteria within the column. The pore volumes (PV) were calculated to range from 397-407 mL for the three columns based on the mass of sand added and the total column volume.

II.2.6 Column operation for the S. multivorans column experiments

Following column packing with cultures of *S. multivorans*, reduced medium without pyruvate was continuously flushed through the column at 0.25 mL/min yielding a hydraulic retention (residence) time of ca. 1.1 days. The pure PCE-DNAPL and mixed-NAPL *S. multivorans* columns were flushed for 3.3 and 4.3 PV, respectively, and the elution (i.e., washout) of *S. multivorans* cells was monitored by daily collection of effluent samples (10-20 mL) for DNA extraction and qPCR analysis. Cumulative cell recovery was determined by multiplying the cell titer by the corresponding effluent volume. Percent cell recovery was calculated from the difference between the cumulative cell recovery and the total number of cells added to the column, which was estimated by multiplying the inoculum cell titer by the total PV of the column. Since the influent medium did not contain growth substrate during this phase of the experiment, the calculated percent recovery was based on an assumption of no growth or decay of *S. multivorans*.

At the conclusion of the microbial elution phase, a syringe pump (model 22, Harvard Apparatus) was used to inject the anoxic, mixed or pure PCE-NAPL into the column at a constant flow rate of 1 mL/min until NAPL was visually observed in the first 10 cm (nominal) of the column. NAPL injection was then terminated, and the column was operated in a down-flow mode (1 mL/min) for approximately 1 hour to remove mobile NAPL and establish entrapped NAPL ganglia. At the conclusion of down-flow operation, the source zones for the mixed NAPL and pure PCE-DNAPL *S. multivorans* columns contained approximately 14 mL and 9 mL of NAPL, respectively, corresponding to organic phase saturations of approximately 0.21 and 0.13, respectively, over the first 10 cm (Ports 1 and 2) of the column. Although the NAPL distribution within the source zone was relatively uniform in both column experiments, some nonuniformly-distributed NAPL ganglia were present along the right-hand side of the column (even-numbered ports) in the transition zone (10-20 cm, Ports 3 and 4) between the source zone (0-10 cm, Ports 1 and 2) and the down-gradient, NAPL-free region (20-60 cm, Ports 5-11).

After NAPL imbibition, the influent medium contained 20 mM pyruvate, and the columns were continuously operated at a flow rate of 0.25 mL/min. Effluent samples (~20 mL) were collected every 1-2 days for chlorinated ethene, pH, and microbial analyses. For the mixed NAPL column

experiment, the side ports were sampled (1 mL) for chlorinated ethenes after 5, 11, and 17.5 PV of flushing, and additional 1-mL side port samples were taken from each port for microbial analysis following the 17.5 PV sampling event. In order to minimize disruption of flow within the column during side port sampling, aqueous samples were taken at a constant rate (0.1 mL/min) using a 2.5 mL gas-tight syringe (Hamilton) connected to a syringe pump (model 22, Harvard Apparatus) operating in withdrawal mode. Cumulative chlorinated ethene recoveries, on a molar as well as a percent basis, and mass transfer enhancement factors were calculated as described in the *Supplementary Material* of Amos et al. *(2008a)*. For the mixed NAPL column experiment, the expected mass recovery under abiotic conditions was estimated by assuming an initial aqueous phase PCE solubility of ~300 μM, accounting for changing NAPL composition with PCE mass depletion, and assuming equilibrium mass transfer at the operational column flow rate of 0.25 mL/min (see the *Supplementary Material* of Amos et al. *(2008a)* for details). A cumulative mass transfer enhancement factor was calculated by dividing the experimental mass recovery by the expected mass recovery (see the *Supplementary Material* of Amos et al. *(2008a)* for details).

At the conclusion of the mixed-NAPL *S. multivorans* column experiment, the column was sectioned into six 10-cm long cores inside a N_2-flushed glove bag system. Cores were recovered from the column by sequentially driving sterilized aluminum cylinders (3.81 cm o.d., 3.63 cm i.d.) into the uppermost 10 cm of column material. The top of the cylinders were sealed, and the cores, which remained encased in the aluminum cylinders, were removed from the column and frozen overnight (-20°C) to prevent additional microbial activity and redistribution of the liquid phases. Each core was then thawed, removed from the aluminum cylinder under sterile conditions, and divided into 2-cm sections. These subsections were homogenized and stored at -20°C until genomic DNA extraction was performed.

II.2.7 Column operation for the BDI-SZ column experiment

Following column packing with the BDI-SZ culture, reduced medium without lactate was continuously flushed through the column at 0.25 mL/min for 3.3 PV. The elution (i.e., washout) of dechlorinating bacteria (e.g., *Dehalococcoides*) was monitored by daily collection of effluent samples (10-20 mL) for DNA extraction and qPCR analysis. Cumulative and percent cell recoveries were calculated as described above for the *S. multivorans* column experiments.

Following the microbial elution phase, the column was imbibed with the anoxic mixed-NAPL as described for the *S. multivorans* column experiments. The 10 cm (nominal) source zone contained approximately 16 mL of residual (entrapped) NAPL ganglia, corresponding to an organic phase saturation of approximately 0.24 over the first 10 cm of the column. Although the NAPL distribution within the source zone was relatively uniform, some fingering of the NAPL was apparent. Ports 1 and 2 were within the source zone, and Ports 4-11 were in the plume region. Due to some fingering of the imbibed NAPL, Port 3 was in a transition zone between the source zone and the plume region.

After NAPL imbibition, the column was continuously operated and dechlorination activity monitored for approximately 3 months. During this time, the influent contained 20 mM lactate. The influent system was initially operated at 0.25 mL/min (hydraulic retention [residence] time

of approximately 1.1 days). At 21.6 PV of flushing, the flow was reduced to 0.1 mL/min (residence time of approximately 2.8 days) for the remainder of the experiment. An unintentional flow interruption occurred for approximately 22 hours at 16.8 PV. Effluent samples (ca. 20 mL) were collected every 1-3 days and divided into separate sub-samples for chlorinated ethene, pH, and microbial analyses. The side ports along the length of the column were also sampled periodically for chlorinated ethenes and/or microbial analysis. Sampling was performed as described for the *S. multivorans* column experiments.

After depletion of PCE from the mixed-NAPL and a decline in chlorinated ethene effluent concentrations to < 5 μM, a ca. 1.1 pore volume pulse (451 mL) of VC-amended medium was injected into the column between 32.8 and 33.9 PV of column operation to assess whether conditions within the column were favorable for ethene production. During injection of the pulse, aqueous phase VC concentrations within the influent were periodically monitored and decreased from 97.5 μM to 62.5 μM during the pulse. The decrease in aqueous phase VC concentrations in the influent is likely a result of the changing ratio between the headspace and aqueous phase volumes within the influent reservoir. The ratio between the headspace and aqueous phase volumes changed since medium was continuously withdrawn from the reservoir. VC is a volatile compound that partitions between the aqueous phase and headspace; therefore, a larger headspace volume would result in reduced aqueous phase VC concentrations. Alternatively, VC sorption to the influent medium reservoir septum may have occurred and resulted in the reduced aqueous phase VC concentrations. Based on measured aqueous phase VC concentrations in the influent, approximately 34.6 μmol of VC was injected into the column during this pulse. VC elution and/or ethene production were monitored in effluent samples for the duration of the experiment to estimate recovery of the pulse as VC and/or ethene. At the conclusion of the column experiment, the column was destructively sampled as described for the *S. multivorans* column experiments. Calculation of cumulative mass recovery and mass transfer enhancement factors was performed as described above for the *S. multivorans* column experiment.

II.2.8 Abiotic column experiments

Two independent abiotic experiments were performed to characterize the hydrodynamic properties of the packed columns. A pulse of non-reactive tracer solution (0.01 M potassium iodide) was introduced into the column at a flow rate of either 2.0 or 0.25 mL/min, and effluent samples were collected continuously. Effluent breakthrough curves (BTCs) obtained from both non-reactive tracer experiments were symmetrical and did not exhibit tailing, indicating the absence of preferential flow paths or immobile water. The measured BTC data were fit to a 1-D form of the advective-dispersion reactive (ADR) transport equation (CXTFIT version 2.0 *(Toride et al. 1995)*). The resulting Peclet number, $Pe = vL/D_H$,where v is the pore-water velocity, L is the column length, and D_H is the hydrodynamic dispersion coefficient, ranged from 590 to 850 depending on the flow rate, and corresponded to dispersivity ($\alpha_D = D_H/v$) values of 0.07 cm and 0.1 cm. The overall pore volumes of the packed columns determined from the simulated BTCs were 390 and 400 mL, consistent with the experimentally measured pore volumes. In a third abiotic experiment, a uniform residual saturation of mixed NAPL was established in the column

to evaluate PCE dissolution from the mixed NAPL. At a flow rate of 0.25 mL/min, dissolved-phase PCE concentrations at early times were similar to those expected from equilibrium calculations (i.e., 300 μM, 50 mg/L) along the entire length of the column, indicating the absence of abiotic mass transfer limitations.

II.2.9 DNA extraction

Biomass was collected from 10-20 mL effluent samples by centrifugation at 4°C for 30 minutes at 3,220 x *g*. All but ca. 1 mL of the supernatant was decanted, and the cell pellet was suspended in the remaining liquid. Centrifugation was repeated at 16,000 x *g* for 10 minutes. For the side port samples, 1 mL liquid samples were centrifuged at 16,000 x *g* at room temperature for 10 minutes. After removing the supernatant, the pellets were stored at -20°C until genomic DNA was extracted using the QIAamp DNA Mini Kit (Qiagen, Valencia, California) following the modifications described by Ritalahti et al. *(2006)*. DNA was obtained in final volumes of 200 μL buffer AE (provided with the QIAamp DNA Mini Kit) and stored at -20°C until qPCR analysis. DNA was also extracted from representative solid-phase samples (ca. 1 g of wet sand) using the UltraClean Soil DNA Isolation Kit (MoBio Laboratories, Inc., Solana Beach, California). The selected solid-phase samples corresponded to the location of the aqueous phase side ports. DNA was obtained in a final volume of 50 μL of solution S5 (provided with the UltraClean Soil DNA Isolation Kit) and stored at -20°C until qPCR analysis.

II.2.10 Quantitative real-time PCR (qPCR) analysis

qPCR analysis to quantify the number of *S. multivorans* cells used SYBR Green-based detection chemistry and primers (SpSm1f, 5'-TCGTTGCAGGTATCGCTATG-3'; SpSm1r, 5'-TTCAACAGCAAAGGCAACTG-3') to target the *pceA* reductive dehalogenase gene of *S. multivorans (Regeard et al. 2004)*. The specificity of the primer pair was experimentally confirmed with DNA from select reductively dechlorinating bacteria (*Dehalococcoides* sp. strain BAV1, *Dehalobacter restrictus*, *Desulfuromonas michiganensis* strain BB1, *Desulfitobacterium* sp. strain Viet1, *Geobacter lovleyi* strain SZ, and *Anaeromyxobacter dehalogenans* strain 2CP-C). The qPCR reaction mixture contained 15 μL of QuantiTect SYBR Green PCR master mix (Qiagen, Valencia, California), 300 nM of each primer, and 3 μL of template DNA in a total reaction volume of 30 μL. The PCR temperature program was as follows: 2 min at 50ºC, 15 min at 95ºC, followed by 40 cycles of 15 sec at 94°C, 30 sec at 52°C, and 30 sec at 72°C. qPCR was carried out in an Applied Biosystems (ABI) Prism 7000 Sequence Detection System. Standard curves were generated following the procedure of Ritalahti et al. *(2006)* using a 10-fold dilution series of quantified genomic DNA of *S. multivorans*. The initial DNA concentration was determined spectrophotometrically at 260 nm. The number of gene copies in each standard was estimated from the DNA concentrations as described *(Ritalahti et al. 2006)*, assuming one copy of the *pceA* gene per genome (G. Diekert, personal communication) and an estimated 1.64 Mb genome size for *S. multivorans (Parkhill et al. 2000)*. The terms "*pceA* gene copies" and "cell numbers" are used interchangeably and are expressed per mL of fluid or per gram of column material. The linear range for quantification was 10^2 - 10^8 *pceA* gene copies per μL of template DNA (R^2 = 0.993; amplification efficiency = 1.89 *(Pfaffl 2001)*), resulting in a quantification limit of ~100 *pceA* gene copies per μL of template DNA. To identify false positives, template DNA was replaced with sterile water.

For quantification of *Dehalococcoides* spp., *Dehalobacter* spp., and *Geobacter lovleyi* strain SZ, qPCR analysis was performed with an ABI 7500 Fast Real-Time PCR System (Applied Biosystems [ABI], Foster, California) using the standard 7500 operating mode. TaqMan-based qPCR analysis was used to quantify the number of *Dehalococcoides* 16S rRNA gene copies as described *(Ritalahti et al. 2006)*. Each well of a MicroAmp Optical 96-Well Reaction Plate (ABI) contained 1x TaqMan universal PCR master mix (ABI), 300 nM probe, 300 nM of each primer, and 3 μL of template DNA in a total reaction volume of 30 μL. The PCR temperature program was as follows: 2 min at 50°C, 10 min at 95°C followed by 40 cycles of 15 sec at 95°C and 1 min at 58°C. Standard curves were generated for the *Dehalococcoides* 16S rRNA gene as described *(Ritalahti et al. 2006)*. For *Dehalococcoides*, the terms "16S rRNA gene copies" and "cell numbers" are per mL of fluid or per gram of column material and are used interchangeably because the known *Dehalococcoides* organisms contain a single 16S rRNA gene copy per genome *(Kube et al. 2005; Seshadri et al. 2005)*.

qPCR analysis to quantify *Dehalobacter* 16S rRNA genes was performed using SYBR Green-based detection chemistry as described by Smits et al. *(Smits et al. 2004)* and Daprato et al. *(Daprato et al. 2007)*. The qPCR reaction mixture contained 15 μL of Power SYBR Green PCR master mix (ABI), 300 nM of each primer, and 3 μL of template DNA in a total reaction volume of 30 μL. The PCR temperature program was as follows: 2 min at 50°C, 15 min at 95°C followed by 40 cycles of 15 sec at 94°C, 30 sec at 58°C, and 30 sec at 72°C. Standard curves were generated following the procedure outlined in Ritalahti et al. *(Ritalahti et al. 2006)*, and used a 10-fold dilution series of quantified plasmid DNA (concentrations determined spectrophotometrically at 260 nM). Each plasmid carried a single copy of the 16S rRNA gene of *Dehalobacter restrictus* (DSM 9455). The number of 16S rRNA genes in the genome of *Dehalobacter restrictus* has not been determined; the cell number estimates reported herein assume one 16S rRNA gene copy per *Dehalobacter* cell and are reported per mL of fluid or per gram of column material.

qPCR analysis to quantify *Geobacter lovleyi* strain SZ was performed using SYBR Green-based detection chemistry and primers that targeted the 16S rRNA gene. Primer Geo73F (5'-CTTGCTCTTTCATTTAGTGG -3') was designed by Duhamel and Edwards *(Duhamel and Edwards 2006)*, while Geo196R (5'-GAATCAGGAGCATATTC-3') is the reverse complement of primer Geo196F, which was designed as part of the work described in Amos et al. *(2007c)*. The specificity of the primer pair was experimentally confirmed with DNA from close relatives (*G. thiogenes*, *G. sulfurreducens*, and *G. metallireducens*) and selected reductively dechlorinating species (*Desulfuromonas michiganensis* strain BB1, *Anaeromyxobacter dehalogenans* strain 2CP-C, *Sulfurospirillum multivorans*, *Dehalobacter restrictus*, *Dehalococcoides* sp. strain BAV1, *Desulfitobacterium* sp. strain Viet1, and culture "*Clostridium bifermentans*" strain DPH-1). The Geo73F/Geo196R primer pair amplified DNA from both *G. lovleyi* strain SZ and *G. thiogenes*, but did not amplify DNA from any of the other organisms. No amplification was observed with DNA extracted from the BDI consortium (before addition of strain SZ and development of BDI-SZ), indicating that the selected primer pair, although unable to distinguish strain SZ and *G. thiogenes*, only monitored the growth and distribution of strain SZ in samples from the column experiment. The qPCR reaction mixture contained 15 μL of Power SYBR Green PCR master mix (Applied Biosystems), 300 nM of each primer, and 3 μL of

template DNA in a total reaction volume of 30 μL. The PCR temperature program was as follows: 2 min at 50°C, 15 min at 95°C followed by 40 cycles of 30 sec at 94°C, 30 sec at 51°C, and 30 sec at 72°C. Standard curves were generated following the procedure outlined by Ritalahti et al. *(Ritalahti et al. 2006)*, and used a 10-fold dilution series of quantified plasmid (concentration determined spectrophotometrically at 260 nM) carrying a single copy of the 16S rRNA gene of *Geobacter lovleyi* strain SZ. The genome of strain SZ contains two 16S rRNA gene copies (www.jgi.doe.gov); therefore, dividing gene copy numbers by a factor of two yielded the cell numbers, which are reported per mL of fluid or per gram of column material.

II.2.11 Analytical methods

Aqueous-phase samples (1 mL) were analyzed for chlorinated ethenes as described *(Amos et al. 2007a)* with a Hewlett-Packard (HP) 7694 headspace autosampler connected to a HP 6890 gas chromatograph (GC) equipped with a HP-624 column (60 m by 0.32 mm i.d.; film thickness, 1.8 μm) and a flame ionization detector (FID). Chlorinated ethene standard curves were prepared as described *(Gossett 1987; Löffler et al. 1997)*. The pH of column effluent was measured using a VWR Model 8000 pH meter (#511710, VWR Scientific, West Chester, Pennsylvania) equipped with an Accumet gel-filled pH combination electrode (#13-620-290, Fisher Scientific). In samples from the non-reactive tracer experiments, iodide was measured using an HP 1100 series HPLC equipped with a Supelcosil 5 μm LC-18-DB column (25 cm x 4.6 mm) and a diode array detector with ultraviolet detection at 240 nm. The mobile phase consisted of 20% acetonitrile and 80% water delivered at a constant flow rate of 1 mL/min.

II.3 2D ABIOTIC AQUIFER CELL EXPERIMENTS

II.3.1. Aquifer cell design and experimental methods

A series of two-dimensional (2-D) aquifer cell experiments were conducted to quantify the effects of partial mass removal on dissolved-phase PCE or TCE concentrations and mass discharge as a function of the initial source zone saturation distribution. The body of the aquifer cell was constructed from a single piece of milled 6061 aluminum in order to minimize leakage, while the front and back panels were constructed from ½" thick, non-tempered glass. The aquifer cell had internal dimensions of 150 cm (length) × 48 cm (height) × 1.4 cm (thickness), and contained a 58-cm long "source zone" region designed to assess DNAPL mass recovery and saturation distribution, and a 92-cm long "plume region" (Figure 2). The total internal volume of the aquifer cell was approximately 10L. To allow for post-treatment plume development monitoring within the plume region of the aquifer cell the front panel was fitted with twenty low-volume (~ 0.4 mL), screw-cap sampling ports, constructed from 0.2 mm i.d. glass tubing.

Four quartz sands, Federal Fine (30-140 mesh) Ottawa sand, F-70 (40-270 mesh) Ottawa sand, 20-30 mesh Accusand and 20-50 mesh Accusand, were used as the background packing media in the aquifer cell studies. Federal Fine Ottawa sand (U.S. Silica Co.) was selected because both the grain size distribution and intrinsic permeability (4.2×10^{-11} m^2) are similar to that of aquifer material collected from the Bachman Road site in Oscoda, MI *(Ramsburg and Pennell 2001)*. The Accusands were selected for use as the background media because of their high purity (99.8% SiO_2), absence of organic carbon, and translucent to transparent properties, which

renders them well-suited to light transmission analysis *(Niemet and Selker 2001)*. The intrinsic permeabilities of 20-30 and a 1:1 mixture of 20-30 and 40-50 mesh Accusands are 2.0 x 10^{-10} m^2 and 1.6 x 10^{-11} m^2, respectively *(Schroth et al. 1996)*, while F-70 Ottawa sand (U.S. Silica Co.) has an intrinsic permeability of 8.2 x 10^{-12} m^2. The aquifer cell was packed under water-saturated conditions with a lower layer of F-70 Ottawa sand. Above this layer, the cells were packed with either the 1:1 Accusand mixture, 20-30 mesh Accusand or Federal Fine sand as the predominant or "background" aquifer material. Regions of F-70 Ottawa sand lenses were packed within the source zone region of each cell to represent permeability contrasts that would retain DNAPL during the initial release event (Figure 2).

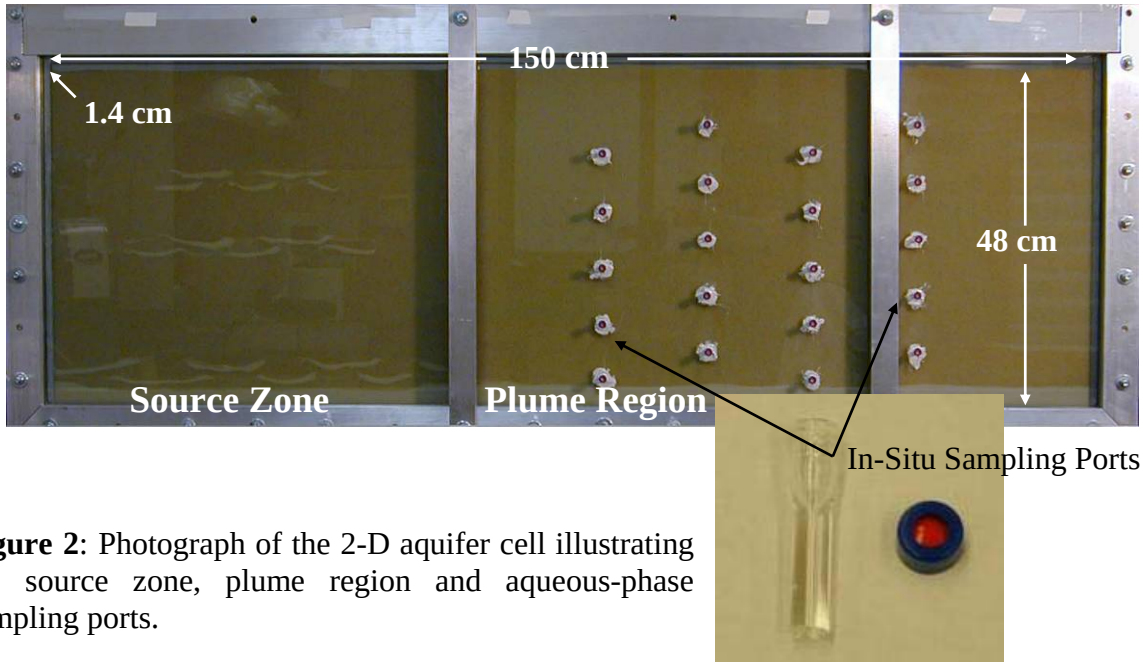

Figure 2: Photograph of the 2-D aquifer cell illustrating the source zone, plume region and aqueous-phase sampling ports.

Liquid PCE or TCE (99.9% + purity) was purchased from Sigma-Aldrich (Milwaukee, WI). PCE has a density of 1.62 g/mL at 25°C, a molecular weight of 165.8 g/mole, and an aqueous solubility of approximately 200 mg/L at 25°C *(Taylor et al. 2001)*. The aqueous solubility and liquid density of TCE at 25°C are approximately 1,100 mg/l and 1.47 g/ml, respectively (Riddick and Bunger, 1970). For visualization purposes, the DNAPLs were dyed red with an organic soluble dye, Oil-Red-O (Fisher Scientific, Fair Lawn, NJ) at a concentration of 4×10^{-4} M. Previous studies have shown that the presence of Oil-Red-O at this concentration does not significantly alter relevant physical properties of TCE- or PCE-DNAPL *(Taylor et al. 2001)*. The dyed liquid DNAPL (15 to 41 mL) was introduced into the source zone region aquifer cell at a constant flow rate of 1.0 or 0.1 mL/min. DNAPL was delivered using a Harvard Apparatus syringe pump fitted with a 15.2 cm long, 18-gauge stainless steel needle, which was located approximately 5 cm below the sand surface. Following injection, the liquid DNAPL was allowed to redistribute for a period of at least 24 h prior to water flushing of the aquifer cell.

To quantify the DNAPL distribution and saturation within the source zone, the aquifer cell was coupled to a light transmission system described by *(Suchomel and Pennell 2006)*. The light transmission (LT) system, based on the original design of *(Tidwell 1994.)*, was used to quantify

the TCE-or PCE-DNAPL saturation (S_{DNAPL}) distributions within the source zone region of the cell as shown in Figure 3. A Nikon Coolpics 900 digital camera was used to image the aquifer cell, which was illuminated with a Flathead 80 light bank (Kino Flo Inc., Burbank, CA). Local PCE or TCE saturations were estimated by comparison of the digital image to previously-generated hue-NAPL saturation calibration curves, which were developed using the experimental method of *(Darnault 1998)*. Thickness-averaged saturation distributions were calculated on a pixel basis (~0.3 mm × 0.3 mm) using MATLAB 6.5 software (MathWorks, Inc.), and summed over the entire source zone region to estimate the total volume of liquid TCE or PCE in the source zone. The DNAPL volumes obtained by LT analysis were within 5% of values calculated from the DNAPL injection flow rate and duration. The resulting DNAPL saturation distributions were expressed in terms of a ganglia-to-pool (GTP) ratio, defined as the ratio of the TCE or PCE volume present in the cell at saturations less than residual saturation of the porous media ($S_{DNAPL} \leq 11\%$ and 13% for 20-30 mesh and mixed Accusand, respectively) to the volume of DNAPL present in the cell at saturations greater than residual ($S_{DNAPL} > 11\%$ or 13%). Residual saturation values were obtained from *(Pennell 1996)* for the same size fractions of Ottawa sand, and confirmed using the intrinsic permeability-residual DNAPL saturation correlation developed by *(Powers et al. 1992)* for various sand size fractions.

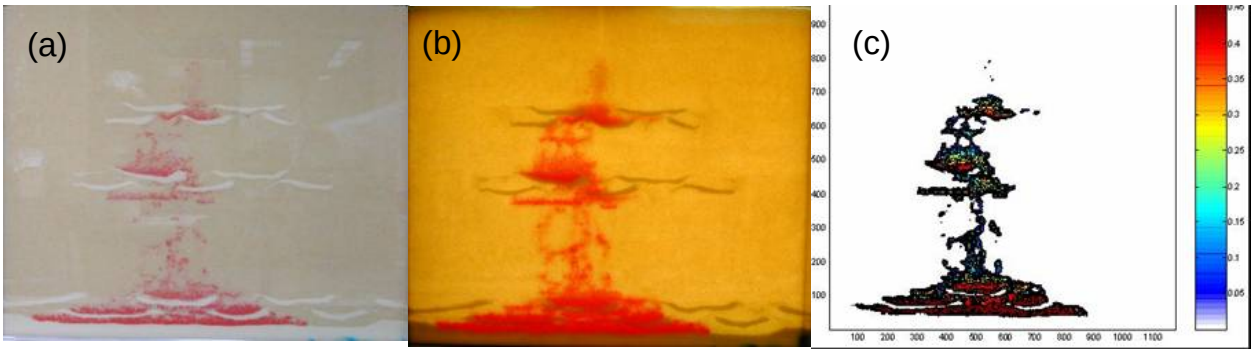

Figure 3: Images of the aquifer cell source zone following PCE-DNAPL injection (a) with natural light, (b) light transmission system, and (c) the resulting PCE-DNAPL saturation distribution.

Aqueous solutions were delivered and extracted from the aquifer cell through two fully-screened rectangular chambers that were located at each end of the cell. The well chambers were constructed from square (1.27 cm x 1.27 cm) aluminum tubing and milled with 0.203 mm slits on one side through which solutions flowed. Flow was controlled by adjusting the height of a constant head reservoir that was connected to the inlet chamber by Teflon® tubing. Following DNAPL injection and redistribution, the overall hydraulic conductivity of the cell was determined from at three steady flow rates using Darcy's law. The aqueous flow field was monitored periodically by introducing pulses of aqueous solution containing water-soluble dye, Ergioglaucine A (Fluka Chemical) at a concentration of 3×10^{-5} M. Water was flushed through the cell constant rates ranging from 1.0 to 1.5 mL/min to establish steady-state dissolved-phase DNAPL concentrations in the down-gradient plume region of the cell. A sequence of either two or three surfactant floods was then conducted at flow rates ranging from 5.5 to 8.6 mL/min to remove incremental amounts of DNAPL from the source zone via dissolution. Following each surfactant flood, several pore volumes of water were introduced into the cell at flow rates from

1.0 to 1.5 mL/min to establish a steady-state dissolved-phase plume. Aqueous samples were collected continuously from the mid-point of the effluent chamber which was connected to a Retriever II fraction collector (Isco Inc.) with Teflon tubing, and daily from sampling ports located in the plume region of the cell using a gas-tight syringe.

To mimic "aggressive" source zone treatment, the aquifer cells were flushed with two different surfactant formulations. The first surfactant, polyoxyethylene (20) sorbitan monooleate (Tween 80), was obtained from Uniqema, and was used without further purification. Tween 80, which has a molecular weight of 1310 g/mole, a liquid density of 1.08 g/cm^3, and a critical micelle concentration (CMC) of approximately 13 mg/L, is a food-grade surfactant that can be degraded under both aerobic and anaerobic conditions. The second surfactant, Aerosol MA-80I, was purchased from Cytec Industries. Aerosol MA-80I is comprised of 80% (vol.) active ingredient (sodium dihexyl sulfosuccinate), while the remaining 20% (vol.) consists of water and 2-propanol. The molecular weight and CMC of Aerosol MA-80I are 388 g/mol and approximately 550 mg/l, respectively. Additional chemicals, including sodium chloride (NaCl), calcium chloride ($CaCl_2$), and 2-propanol (IPA) were purchased from Fisher Scientific. All aqueous solutions were prepared with water that was purified using a Nanopure Analytical Deionization system (Barnstead/Thermolyne Corp.) and contained 500 mg/L $CaCl_2$ as a background electrolyte.

Dissolved-phase PCE or TCE concentrations were measured using a Hewlett Packard (HP) model 6890 gas chromatograph (GC) equipped with an HP model 7694 autosampler and a flame ionization detector (FID) and micro electron capture detector (μECD). Samples were prepared for analysis by adding approximately 0.4 ml of aqueous sample to 1.2 ml of IPA in glass auto sampler vials. A surfactant trap, consisting of a glass inlet liner packed with a 3-cm bed of 80-100 mesh Porpak Q (Alltech), was used to prevent fouling of the capillary column with surfactant. Separation was achieved isothermally (45ºC) using a 30 m (length) DB-5 column with a 0.32 mm outside diameter (Agilent Technologies). A six-point calibration curve was generated for each sequence run, and calibration check samples were run after every 10 samples. Aerosol MA concentrations were determined using an Agilent Series 1100 high-performance liquid chromatograph (HPLC) equipped with a diode array detector (DAD), based on the gradient elution method developed by *(Field 2000)*. Tween 80 analysis was adapted from the method described by *(Taylor et al. 2001)*, which involved HPLC separation followed by quantification with both a DAD and a Sedex 55 Evaporative Light Scattering Detector (ELSD). For all GC and HPLC analyses, a six-point calibration curve was generated prior to each sequence run, and a calibration check was performed after every 10 samples.

II.4 2D BIOTIC AQUIFER CELL EXPERIMENTS

A second two-dimensional aquifer cell was constructed for use in a biotic aquifer cell experiment (Figure 4). This experiment was intended to combine knowledge gained from the 1-D biotic column experiments and the 2-D abiotic aquifer cell experiments to evaluate metabolic reductive dechlorination in a heterogeneous, multidimensional setting. Additionally, this experiment was conducted to assess the feasibility of combining treatment remedies, surfactant enhanced aquifer remediation (SEAR) with bioaugmentation, for the treatment of a PCE-DNAPL source zone based on evidence from the Bachman Road site study *(Abriola et al. 2005; Ramsburg et al.*

2005). The aquifer cell design was based on the aquifer cell employed in the abiotic 2-D aquifer cell experiments, with slightly smaller overall dimensions (63.5 cm in length x 38 cm in height x 1.4 cm in thickness) and modifications to allow for continuous anaerobic operation. The front and rear faces of the aquifer cell consisted of 1.4-cm thick glass panels, which allowed for quantification of the PCE-DNAPL source zone saturation distribution using the light transmission method developed by Suchomel and Pennell *(Suchomel and Pennell 2006)*. Eighteen sampling ports were located in the front glass panel of the cell to allow for quantification of the spatial distribution of PCE and dechlorination daughter product concentrations, and the number dechlorinating microorganisms within the aquifer cell.

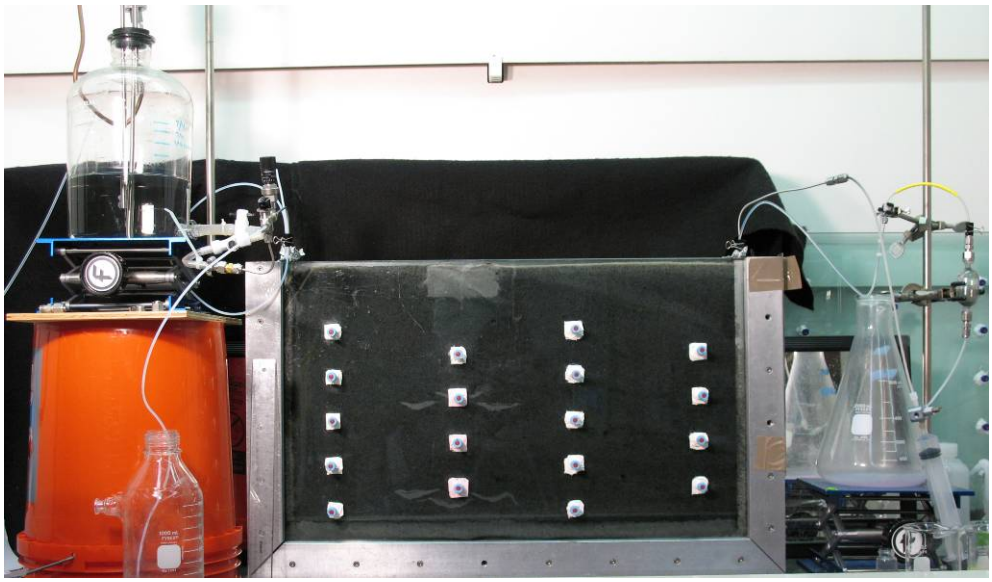

Figure 4: 2-D aquifer cell constructed for Task I, Milestone S2.1.

Construction of the medium delivery system, which was initially modeled on the system used for the 1-D biotic column experiments, was modified to prevent the development of gas bubbles inside the 2-D aquifer cell, which was observed during a preliminary biotic aquifer cell experiment. The modified flow delivery system was driven by a hydraulic gradient of less than 0.5 cm across the length of the box. Influent was stored in a 4 L mariot bottle equipped with an aspirator that was connected with flexible tubing to a screened 0.635 cm O.D. (¼") stainless steel well within the inlet end chamber of the aquifer cell. The insertion of 0.635 cm O.D. (¼") stainless steel tubing in the upper opening of the reservoir through a tight fitting rubber stopper provided for a constant head independent of the volume of water in the reservoir. The aqueous flow rate was controlled by adjusting the heights of the constant head (mariot) bottle and the effluent tubing outlet. The flow system was designed for operation at relatively low flow rates, which ranged from 0.1 mL/min to 1.0 mL/min. These flow rates correspond to pore-water (seepage) velocities ranging from 6.35 to 63.5 cm/day and corresponding aquifer cell residence times ranging from 10 to 1 days. The aquifer cell effluent collection system was equipped with a glass sampling bulb that allowed for the collection a single large sample volume (20-23 mL) for chlorinated ethenes, pH, organic acids, and biomass analysis.

Additional influent system modifications were required to maintain anaerobic conditions during reduced salts medium delivery. Prior to connecting the influent system to the aquifer cell, several influent configurations were tested in an off-line system. The final influent system included a glass column filled with powdered ferrous iron as in-line oxygen scrubbers/absorbers that was continuously flushed with argon gas. The performance of the oxygen removal system was verified using color indicators that signify the presence of trace oxygen in both the mineral salts medium and the powdered iron oxide trap.

Following system design the aquifer cell was packed under water-saturated conditions with a background porous medium comprised of a mixture of 50% 20-30 mesh and 50% 40-50 mesh Accusands. Two regions of low permeability lenses consisting of F-70 Ottawa sand (40-270 mesh) were emplaced within the background medium to simulate subsurface heterogeneity. Following packing, approximately 40 mL of anoxic PCE-DNAPL was injected into the aquifer cell at a flow rate of 0.5 mL/min and allowed to redistribute for a period of 24 hours. De-aired water was then flushed through the aquifer cell at a flow rate of 1 mL/min, and the effluent and sampling ports were periodically sampled to monitor plume development. Light transmission analysis was performed at the conclusion of the plume development phase; after approximately 7-10 pore volumes, where one pore volume is equivalent to 1450 mL, to quantify the initial PCE-DNAPL saturation distribution.

Three pore volumes of reduced mineral salts medium were flushed through the aquifer cell at a flow rate of 0.15 mL/min (7-day residence time) to develop anaerobic conditions prior to bioaugmentation. After the establishment of anaerobic conditions within the aquifer cell, lactate (10 mM) was added to the medium as an electron donor, and the lactate-amended medium was flushed through the aquifer cell at a flow rate of 0.15 mL/min. After injecting one pore volume of lactate-amended medium, the nine side- ports upstream of the source zone were manually bioaugmented with 20 mL per port with Bio-Dechlor INOCULUM (BDI) using a gas-tight syringe. Over the course of the 100 pore volume experiment, flux-averaged effluent samples were collected approximately every 1 to 3 days, and side-port samples are collected every 2 PVs (~14 to 20 days). Chlorinated ethene concentrations were measured using a head-space gas chromatography (GC) method with 1 mL from all aqueous samples taken throughout the experiment. Following bioaugmentation, an additional 1 mL from all aqueous samples was filtered and diluted for direct injection organic acid analysis on the HPLC. The pH was measured using a direct measurement probe with 5mL of effluent aqueous sample. Biomass was measured from the remaining aqueous sample taken from each sampling port (1-1.5mL) and the effluent (15 mL) for subsequent molecular analysis using quantitative polymerase chain reaction (qPCR) to quantify numbers of dechlorinating bacteria.

II.5 MATHEMATICAL MODELING

II.5.1 Modeling Metabolic Reductive Dechlorination

II.5.1.1 Batch Experiments

A conceptual model to describe metabolic reductive dechlorination was developed, incorporated into a mathematical framework and applied to simulate experimental results obtained for aqueous and aqueous-organic batch experimental studies described in II.1. The batch dechlorination model, which accounts for the activity of four microbial populations: fermentors, PCE-to-*cis*-DCE dechlorinators, *cis*-DCE-to-ethene dechlorinators, and competitors (e.g., methnogens), and eight chemical components: fermentable substrate, hydrogen, PCE, TCE, DCE, VC, ethane, competitor product (e.g., methane), was combined with an optimization algorithm to obtain best-fit dechlorination kinetic coefficients. Reductive dechlorination kinetics (Michaelis-Menten) were based on previously proposed models to account for the growth of PCE-to-*cis*-DCE dechlorinating organisms due to the dechlorination of aqueous-phase PCE to *cis*-DCE with intermediate formation of TCE. Competitive inhibition was modeled following *(Yu and Semprini 2004)* and product inhibition was neglected. Self-inhibition at high PCE concentrations was modeled after Luong *(Luong 1987)*. Unlike other self-inhibition models (e.g., Haldane) that have been used successfully to model the gradual decline in transformation rates as substrate concentration increases, experimental results presented here suggest that dechlorination ceased when PCE concentrations exceeded a maximum tolerable level for the tested cultures. The selected self-inhibition model better represents this terminal inhibition concentration and eliminates the need to quantify another kinetic parameter (i.e., inhibition constant).

Numerical simulations of dissolved phase PCE experimental results were first used to obtain best-fit initial biomass concentrations (X_0) and dechlorination kinetic parameters (k_{max}^{PCE}, k_{max}^{TCE}, K_S^{PCE}, K_S^{TCE}). While it is often difficult to fit the biomass concentration and maximum utilization rate simultaneously, assumption of a yield value from the literature combined with the simulation of a non-steady biomass enabled the estimation of X_0 and k_{max}^{PCE} /k_{max}^{TCE} simultaneously. The accuracy of the predicted best-fit initial biomass concentration for each strain was verified by comparison to data from 16S rRNA gene-targeted quantitative real-time PCR analysis on cultures grown under identical conditions. Best-fit model parameters were then used, in conjunction with a PCE mass transfer coefficient (κ^{PCE}) independently derived from an abiotic experiment, to simulate the reductive dechlorination process in the presence of dissolving PCE DNAPL.

II.5.1.2 Column Experiments

The metabolic reductive dechlorination kinetics described in II.5.1.1 was incorporated into the existing multiphase, multicomponent simulator, MISER. MISER is a well-established multiphase simulator that has been used successfully to model NAPL remediation at both the bench- (e.g., *(Rathfelder et al. 2003)*) and field-scale (e.g., *(Abriola et al. 2005)*). To ensure that the modified version of MISER solved the metabolic reductive dechlorination equations correctly, MISER simulations were compared to an existing 1-D analytical solution for sequential first-order degradation of aqueous phase contaminants *(Clement 2001)*. This

analytical model forms the foundation of the popular single-phase natural attenuation screening model BIOCHLOR *(Aziz et al. 1999)*. To facilitate the numerical-analytical comparison, interphase partitioning was neglected and the reaction terms were forced to approximate first-order. Figure 5 shows the close agreement between the analytical solution (symbols) and the modified version of MISER (solid lines), providing model verification for simplified reaction kinetics.

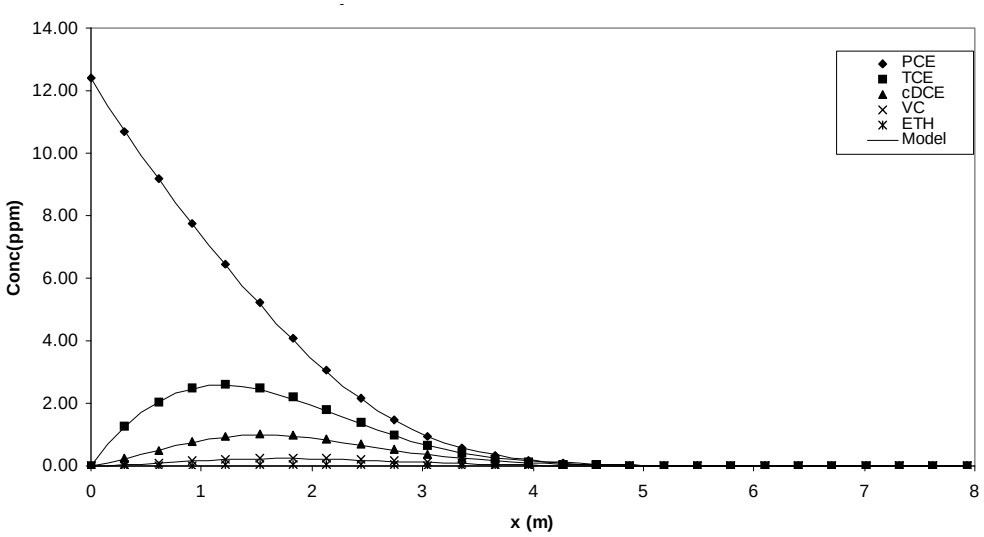

Figure 5: Comparison of numerical model developed in this work to analytical solution of *(Clement 2001)*. Symbols represent analytical solution and solid lines represent numerical model results generated using a modified version of MISER *(Christ and Abriola 2007)*.

For more complex problems that incorporate interphase partitioning and non-linear dechlorination kinetics, no analytical solutions are available and mass balance calculations are useful to evaluate model performance. Cumulative and time-step phase and component mass balances were computed following the methods outlined in *(Abriola et al. 1997)*, which generally take the form:

$$\varepsilon_{cum} = 1 - \left| \frac{\sum_{\Delta t} \left(F_{adv} + F_{mt} + F_{rxn} \right) \Delta t}{\sum_{\Delta t} \left(\Delta_{storage} \right) \Delta t} \right| \tag{1}$$

and

$$\varepsilon_{\Delta t} = 1 - \left| \frac{F_{adv} + F_{mt} + F_{rxn}}{\Delta_{storage}} \right| \tag{2}$$

for the cumulative (ε_{cum}) and time-step ($\varepsilon_{\Delta t}$) mass balance error, respectively. For each phase and component, $\Delta_{storage}$ represents the change in storage, F_{adv} represents the advective flux, F_{mt} represents changes due to interphase partitioning, and F_{rxn} represents changes due to biological reactions. Using equation 1 to evaluate model performance, cumulative (and time-step) phase and component mass balance errors were less than 0.5% for all components with concentrations greater than 1 ng/L.

As a further validation step, the modified version of MISER was used to simulate typical trends found in laboratory experiments. The modified MISER model was used to simulate the results of a laboratory experiment involving metabolic reductive dechlorination and bioenhanced dissolution in a two-phase (aqueous-organic) packed column system *(Yang and McCarty 2002)*. The intent of this comparison was not to use the model in a predictive sense, but rather to demonstrate the ability of the model to simulate metabolic reductive dechlorination in a two-phase system using parameter values consistent with those provided in the literature.

Simulated and published experimental chloroethene breakthrough curves were compared for the one-dimensional column, which was packed with aquifer material from a pristine site and contaminated by hand during packing using a syringe to an approximately uniform saturation of PCE-DNAPL (2%) *(Yang and McCarty 2002)*. Two pore volumes of an anaerobic PCE-dechlorinating mixed culture were flushed through the column at the start of the experiment to initiate metabolic reductive dechlorination. Pentanol (3.7 mM) was continuously flushed through the column to provide the necessary fermentable substrate to drive the dechlorination reactions. Retention time in the column was approximately 14 days. Although the column was operated for approximately 300 days, only the first 150 days of column operation were simulated. Biotransformation kinetic coefficients and initial biomass concentrations were taken from a recent study that used the column augmented culture to investigate the rate and extent of dechlorination for several alternative fermentable substrates *(Lee et al. 2004)*. Pentanol fermentation kinetics were assumed to be the same as those of ethanol utilizers and methanogenesis kinetics were estimated from the literature *(Fennell and Gossett 1998)*. Initial biomass was assumed to be uniformly distributed throughout the column and the PCE maximum utilization rate was adjusted (reduced by approximately one order-of-magnitude) to obtain the best fit to the effluent chloroethene concentrations.

Simulated (solid line) and experimental (closed symbols) breakthrough curves are compared in Figure 6. Simulations were consistent with experimental trends in chloroethene breakthroughs. PCE is dechlorinated to cis-DCE with no noticeable accumulation of TCE, and dechlorination beyond cis-DCE is not observed. The lack of complete dechlorination of PCE to ethene in the experimental system is likely due to the inhibition of the cis-DCE-to-ethene dechlorinating population by the high PCE concentrations, since this culture has demonstrated the ability to effect the complete conversion of PCE to ethene at lower PCE concentrations. Simulated methane discharge at the effluent boundary (~2 μmol/d) was approximately equivalent to the discharge reported by Yang and McCarty (2002) (~3μmol/d), although the model did not predict the significant spikes in discharge (~20μmol/d) that were periodically observed in the experimental results. Recall the model assumed a uniform initial PCE-DNAPL saturation in all elements, which resulted in significant inhibition of methanogens. In the experiment, however, PCE-DNAPL was only approximately uniform. Therefore, methanogens may have thrived in localized areas where PCE concentrations were low *(Chu et al. 2003)*. If more refined measurements of the PCE-DNAPL distribution had been available, this may have improved model predictions.

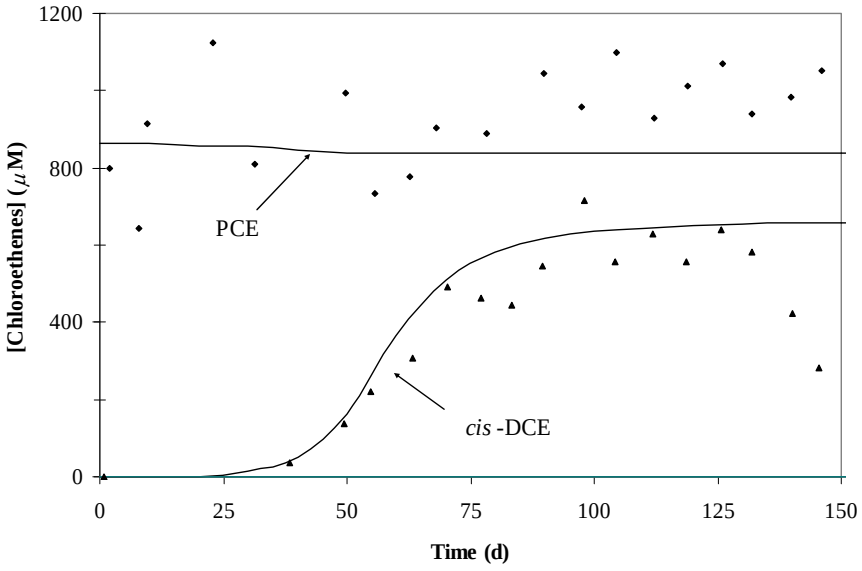

Figure 6: Comparison of simulated (solid line) and experimental (filled symbols) results for a one-dimensional column contaminated with PCE-DNAPL *(Christ and Abriola 2007).*

Comparison of simulated and experimental breakthrough curves in Figure 6 reveals relatively good agreement, except for the trend in *cis*-DCE concentration after approximately 120 days of system operation. Here simulated *cis*-DCE concentrations remain relatively constant while measured *cis*-DCE concentrations decline. Yang and McCarty *(Yang and McCarty 2002)* attribute the observed decline to the accumulation of biomass and the production of methane gas by competitors. Gas production is not considered in the model developed here. Although bio-clogging is modeled, the biophase saturation did not have a noticeable effect on the aqueous phase relative permeability in this simulation. The discrepancy between the simulation and experimental results, thus, suggests that either (i) the production of methane gas is a significant clogging mechanism in experimental systems or (ii) additional clogging mechanisms associated with biomass growth, such as production of extracellular polysaccharides, should not be neglected. The former explanation is supported by the observation of methane discharge spikes mentioned previously. These spikes occurred at about the same time as the decline in *cis*-DCE concentration. Furthermore, the addition of saturated PCE concentrations to the experimental column influent at day 150 inhibited the spikes in methane production and enabled the recovery of PCE-to-*cis*-DCE dechlorination resulting in *cis*-DCE accumulation *(Yang and McCarty 2002).*

Overall, this comparison demonstrates the ability of the model to simulate the dissolution and degradation of PCE and the accumulation of daughter products in a column contaminated with DNAPL.

II.5.2 Field-scale numerical simulations

To better understand the benefits of mass removal from DNAPL source zones suggested by the bench-scale experiments, an ensemble of field-scale two- and three-dimensional numerical simulations was performed. A set of 3-D geostatistical models conditioned to core samples

collected from the Bachman Road Site located in Oscoda, MI were used to generate three-dimensional nonuniform sandy aquifer parameter fields. Figure 7 provides the location of the field study site. Porosity was either assumed to be uniform or simulated using sequential Gaussian simulation (SGS). Permeability (hydraulic conductivity) was modeled using SGS and sequential indicator simulation (SIS) based upon geostatistical indicator classes derived from measured grain size distribution curves.

Here, two types of aquifer model ensembles are considered, which share the same porosity and permeability fields but employ different methods for representing retention characteristics. For the first type, retention characteristics were assigned employing Leverett scaling of a representative P_c-Sat curve to the geostatistical *k* fields. The Haverkamp and Parlange approach, which was based on sediment grain size distribution, was used in the second approach to estimate retention parameters. Thus, retention parameters in the second ensemble are strongly associated with the spatial distribution of independently simulated geostatistical indicator classes corresponding to sediment grain size distributions (Lemke et al., 2004a). Herein, the first ensemble is referred to as correlated realizations, while the second ensemble is referred to as independent realizations. Additional information is available in *Lemke and Abriola,(2004a)*.

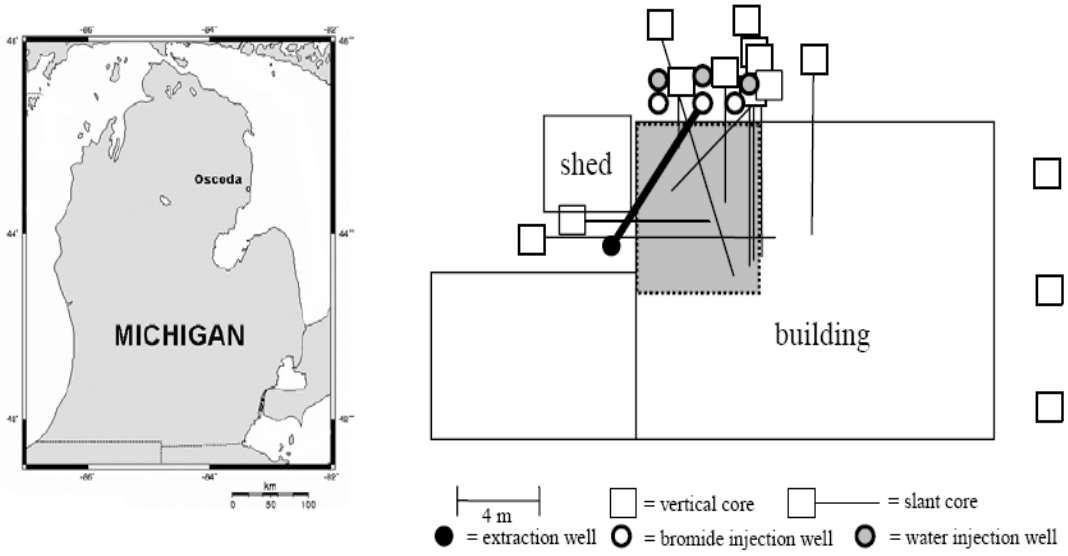

Figure 7. Location of the field study site in Oscoda, Michigan. The position of vertical and oriented soil cores is shown. The suspected PCE source zone targeted in the SEAR pilot test is shaded. The bold SE-NE line indicates the position of two-dimensional vertical profiles extracted from three-dimensional geostatistical simulations. *(Lemke and Abriola, 2004a)*

II.5.2.1 Two-dimensional simulations

Two dimensional infiltration and entrapment of a hypothetical PCE spill were modeled in profiles extracted from the three-dimensional geostatistical realizations described above. PCE infiltration was simulated using MVALOR *(Abriola et al. 1992; Rathfelder and Abriola 1998)*, a multiphase flow model. In the hypothetical spill scenario, 156 kg of PCE was released at the top

center of the model domain at a rate of 0.24 liter/day for 400 days. An additional 330 days were allowed for subsequent PCE infiltration and redistribution. Horizontal and vertical grid refinement were 30.48 cm and 7.62 cm, respectively, following the approach in *(Abriola et al. 1992; Rathfelder and Abriola 1998).*

The PCE saturation distributions generated by MVALOR were used as initial conditions for the simulation of organic recovery under Surfactant Enhanced Aquifer Remediation (SEAR) using MISER *(Abriola et al. 1997; Rathfelder et al. 2000)*, a two-dimensional compositional simulator that accounts for rate-limited NAPL dissolution and surfactant sorption. First, PCE dissolution under natural aqueous gradient (0.002) conditions for a period of 100 days was simulated. Then, 4% Tween 80 aqueous surfactant flushing was simulated at a gradient of 0.13 for two days followed by a clean water flush for another 10 days. Finally, a natural gradient flow was resumed for 100 days.

In MISER simulations, a diminishing sphere model proposed by Powers et al. *(1992)* was used for calculation of the rate limited PCE dissolution, where a single NAPL sphere class with a radius of 0.2 mm was assumed. The approach of Rathfelder et al. *(2001)* was employed to estimate the mass transfer coefficient when surfactant concentrations exceeded the critical micelle concentration. Further detail on the methodology of two-dimensional simulations can be found in *Lemke and Abriola (2004 b).*

II.5.2.2 Three-dimensional simulations

Three-dimensional (3D) DNAPL infiltration and entrapment in statistically homogeneous, nonuniform permeability fields were simulated using the University of Texas chemical simulator (UTCHEM) *(Delshad et al. 1996)*, a 3D multiphase compositional simulator. The hysteretic capillary pressure-saturation-relative permeability functions in UTCHEM were modified to simulate the Land equation and to incorporate the Brooks-Corey-Burdine (P_c-s_n-k_r) relationship. 3D simulations were compared with simulations in two-dimensional (2D) transects extracted from the 3D heterogeneity models to examine the influence of dimensionality on multiphase simulation results, as illustrated in Figure 8. In addition, a version of MT3D modified to account for DNAPL dissolution was used to investigate the effects of dimensionality on mass recovery from a DNAPL source zone. The 2D and 3D saturation distributions discussed above were used as initial conditions for MT3D simulations. Additional information on the 3D simulation methodology is available in *Christ et al. (2005a).*

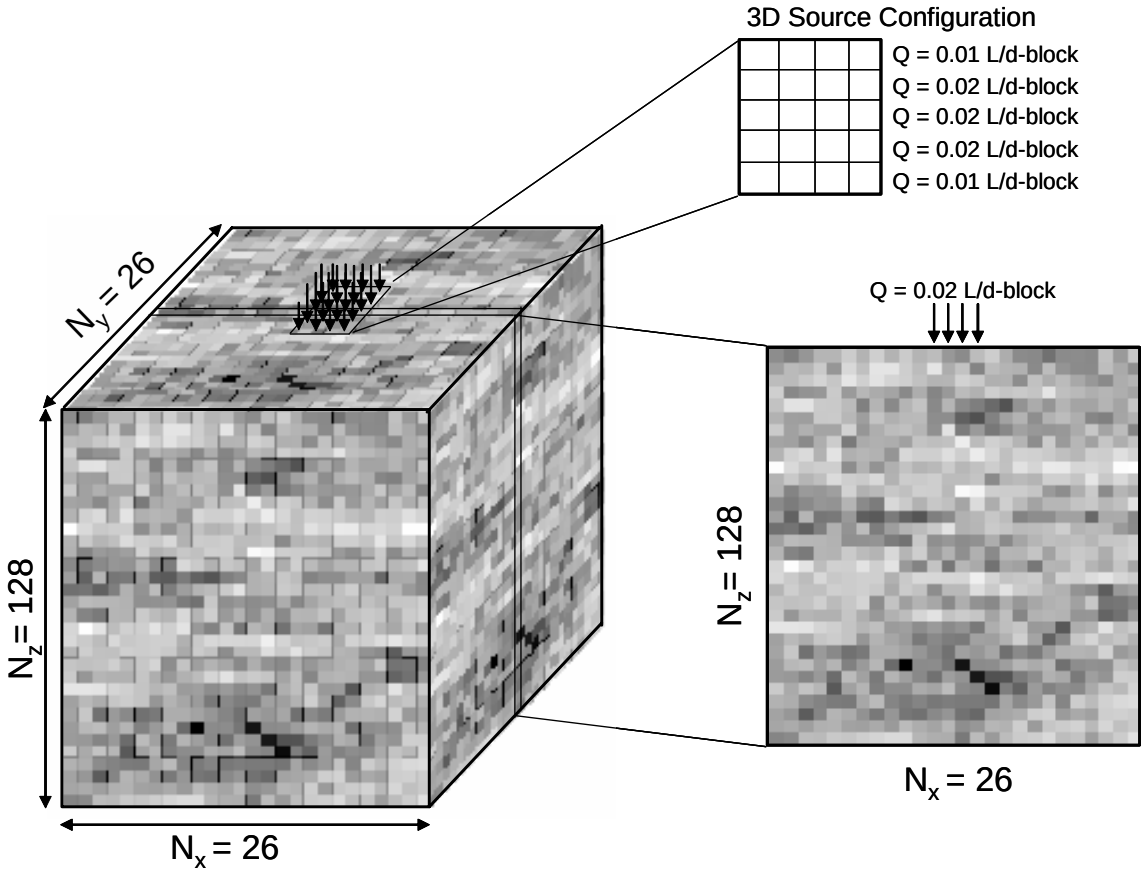

Figure 8. Model domain conceptualization for 2D and 3D simulations. The nominal width of the 2D domain is equal to the width of the 3D cross section and the release rate configuration in 3D was selected so that the sum of the rows (*x*-direction) was equal to the sum of the columns (*y*-direction). *(Christ et al. 2005a)*

II.5.2.3 Upscaling

Based upon the results of the more comprehensive numerical simulations, this work also examined the efficacy of simplified models that rely on upscaled mass transfer coefficient to approximate field scale dissolution processes. The development of these models included the integration of numerical and analytical methods to model mass discharge from DNAPL source-zone.

II.5.2.3.1 Numerical Simulations

An ensemble of 16 3-D DNAPL saturation distributions was selected from *Christ et al. (2005a),* where UTCHEM was employed to simulate hysteretic infiltration and entrapment of PCE. DNAPL saturation distributions selected included a mixture of low-saturation ganglia ($0.0001 < s_n < 0.15$) and high-saturation pooled ($0.15 \leq s_n < 0.7$) regions. Figure 9 presents an example of an initial DNAPL saturation distribution. Here, the simulation domain has been sliced through the center cross-section along the direction of flow to show the PCE-NAPL saturations in a representative *x-y* plane.

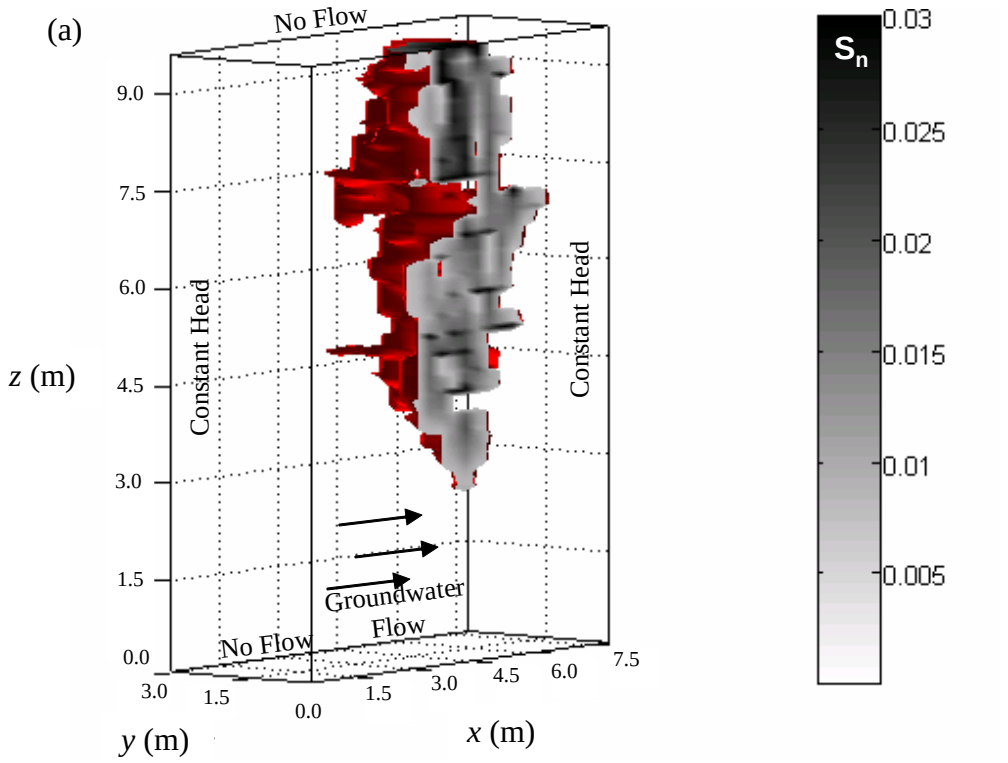

Figure 9: Example of initial DNAPL saturation distribution (GTP = 23.0) sliced through center cross-section to illustrate nonuniform DNAPL saturations in *x-y* plane. Note that the red surface represents the s_n = 0.0001 isosurface and that the range of s_n was selected to differentiate nonuniformities in low s_n values. Cells with $s_n > 0.03$ are shaded black. *(Christ et al. 2005b)*

The modular three-dimensional transport simulator (MT3D) (*Zheng and Wang, 1999*), an existing three-dimensional (3-D), multiphase compositional simulator was used to simulate DNAPL dissolution for the selected DNAPL saturation distribution fields. *Powers et al. (1994)* correlation was used to calculate mass transfer between organic liquid and aqueous phases. MODFLOW (VEERSION 1.0), modified to update aqueous phase mobility at each time step by *(Parker and Park 2004)*, was used to simulate changes in bulk aqueous-phase flow due to DNAPL dissolution. Coupled MT3D and MODFLOW was used to simulate DNAPL dissolution process until 99.99% of the DNAPL mass was removed, which resulted in simulated source longevities between 5,000 and ~30,000 days.

II.5.2.3.2 Analytical Simulations

Upscaled models have taken a variety of forms ranging from simple correlations (e.g.,*(Zhu and Sykes 2000)*) to regression-based Damkohler models, e.g., *(Parker and Park 2004)*. Typically, a steady, one-dimensional (1-D) flow field is assumed and dissolution mass transfer is approximated by a linearized Fick's law expression incorporating an upscaled mass transfer coefficient. These simplifications enable the derivation of an analytical expression describing the plume response associated with a given SZA (e.g., *(Parker and Park 2004)*):

$$\frac{\overline{C}(L)}{C^{eq}} = 1 - \exp\left(\frac{-\kappa_{eff} L}{\overline{q}}\right) \tag{3}$$

where $\overline{C}(x)$ is the flux-weighted aqueous-phase concentration of a selected component at a distance x from the source, where x is typically assumed to correspond to the down-gradient boundary ($x = L$) of the assumed 1-D domain, C^{eq} is the equilibrium aqueous solubility of the selected component, $\overline{q}$ is the equivalent average hydraulic flux assuming 1-D flow, and k_{eff} is an upscaled mass transfer coefficient represented using a correlation of domain-averaged parameters and fitting coefficients (k_o, γ, and β):

$$\kappa_{eff} = \kappa_o \left(\frac{\overline{q}}{\overline{K}}\right)^{\gamma} \left(\frac{M(t)}{M(t=0)}\right)^{\beta} \tag{4}$$

Model parameterization has generally employed regression analyses to fit the model (eqs. 3 and 4) to flux-averaged concentrations (e.g., *(Parker and Park 2004)*), precluding application of the model in a predictive sense at sites other than those for which the model was parameterized.

Most previous upscaled models predicted higher flux-weighted concentrations than those obtained for the average numerical simulations, as shown in Figure 10.

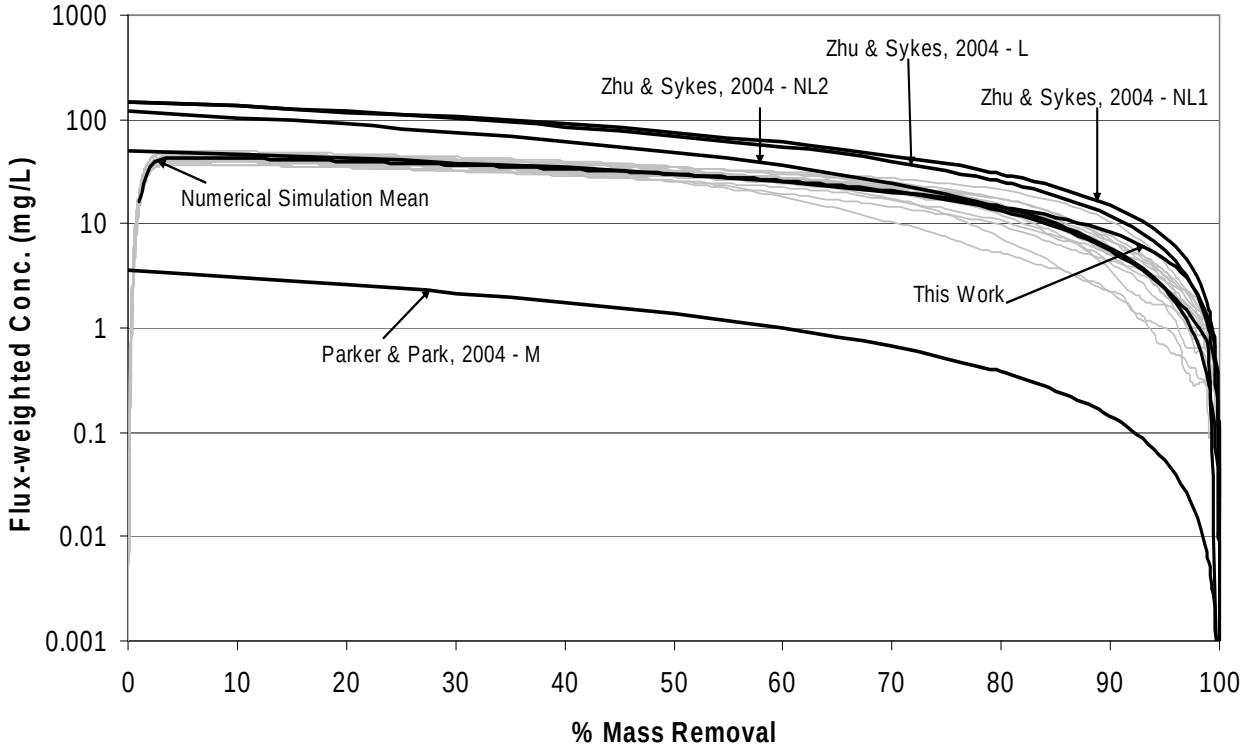

Figure 10: Flux-weighted PCE concentration as a function of mass reduction for 16 numerical simulations (light gray lines) and upscaled mass transfer models. *(Christ et al. 2005b)*

To improve the predictive capabilities of the upscaled mass transfer correlation, modifications to the previous upscaled model included (1) equating κ_o to the initial flux-weighted concentration

during site characterization and (2) relating β to the ganglia-to-pool mass ratio. The proposed new upscaled model can be expressed as:

$$\frac{\overline{C}(L)}{C^{eq}} = 1 - \left(1 - \frac{\overline{C_o}}{C^{eq}}\right)^{\left(\frac{M}{M_o}\right)^{1.5 \cdot GTP^{-0.26}}} \qquad \text{for } 1.5 < \text{GTP} < 24.0 \qquad (5)$$

The proposed upscaled model (eq 5) was further validated on the source-zone scenarios other than those used to develop the correlation. Eight realizations of source-zone scenarios were selected from *Lemke and Abriola (2006),* where GTP ratios ranged from 0.9 to 65. Two additional scenarios were based on the work by *(Zhu and Sykes 2004)* and *(Parker and Park 2004),* which have GTP mass ratios of infinity and ~0.41, respectively. Additional information on the upscaled model development is available in *Christ et al. (2005b).*

II.5.3 Modeling contaminant mass discharge uncertainty

In order to evaluate the effectiveness of source zone treatment and quantify the source strength to the downstream plume, a new metric, mass discharge, has been proposed by many researchers *(Rao et al. 2002; Stroo et al. 2003; (ITRC) 2004; Soga et al. 2004).* Defined as the contaminant mass per unit time ([M/T]) migrating across a hypothetic control plane orthogonal to the mean groundwater flow, mass discharge represents source strength from the DNAPL source zone to the downstream plume. Unlike other metrics such as source mass removal efficiency or point measurement of contaminant concentration, mass discharge provides straightforward information that links the source zone to the downstream plume, facilitating the assessment of the impact of source loading and the evaluation of source longevity. In addition to its application in the assessment of source zone depletion, mass discharge has also been widely used to estimate natural attenuation rate and evaluate the effectiveness of biodegradation for many contaminants *(Semprini et al. 1995; Borden et al. 1997; King et al. 1999; Bockelmann 2001; Kao and Wang 2001).*

Currently, technologies are available in the field to measure local system parameters for the estimation of mass discharge, such as contaminant concentration, hydraulic conductivity *(Einarson and Mackay 2001),* or mass flux ([M/T•L2]) *(Hatfield et al. 2004).* Although mass discharge estimated using these technologies is always subject to uncertainty contributed primarily by the regionalization process, this uncertainty is typically not accounted for in current practices *(Stroo et al. 2003).* In fact, in only a few studies *(Wilson et al. 2000; Annable et al. 2005)* were statistics (e.g. mean, standard deviation) of variables (e.g. hydraulic conductivity, concentration, mass flux) reported for mass discharge estimation. However, these studies are based on classical statistical approaches which may not be appropriate when the data are correlated in space. In addition, the classical way of expressing uncertainty, using mean and variance, fully characterizes the uncertainty space of a random variable only for particular distribution functions (e.g. Gaussian assumption). Developing uncertainty quantification approaches for the mass discharge estimated in the field becomes critical for proper

implementations of this metric with confidence. Information on the uncertainty associated with mass discharge estimates could also support risk-based source-plume management.

II.5.3.1 A Geostatistical Approach for Quantification of Contaminant Mass Discharge Uncertainty Using Multi-level Sampler Measurements

In this section, a geostatistical approach is presented to estimate mass discharge and to quantify its associated uncertainty using multi-level transect measurements of contaminant concentration (C) and hydraulic conductivity (K). This approach adapts the p-field simulation algorithm to propagate and upscale the uncertainty of mass discharge from the local uncertainty models of C and K.

As shown in figure 11, the proposed approach comprises four major steps: 1) model the local uncertainty (ccdfs) of C and K using indicator kriging; 2) generate unconditional, correlated p-field pairs and use them to sample the ccdfs of C and K; 3) propagate the uncertainty of local mass flux using the sampled C and K values (Monte-Carlo simulation) and generate realizations of the spatial distribution of local mass flux within the control plane; and 4) upscale the local mass flux realizations to generate the probability distribution of the mass discharge across the entire control plane.

Local uncertainty modeling of C and K is achieved by indicator kriging, which does not assume any type or shape for the probability distribution of a random variable (non-parametric approach). The ccdf is modeled through a series of thresholds that partitions the range of variation of the physical attribute *(Goovaerts 1997)*. The joint simulation algorithm proposed by Almeida and Journel *(Almeida 1994)* is adopted to generate correlated p-field pairs. In order to avoid artificially defining a hierarchy between C and K, the first p-field (for either C or K) is generated through SGS unconditionally. This p-field serves as soft information to cosimulate the second p-field using colocated cokriging and the Markov-type approximation. The multiple, equally probable realizations of p-field pairs are used to sample the ccdfs of C and K to generate realizations of C, K. Multiple realizations of C and K are then used to simulate local mass flux. Aggregation of one local mass flux realization results in one mass discharge realization (a single value). The ensemble of simulated mass discharges provides the probability distribution of the overall mass discharge across the entire control plane.

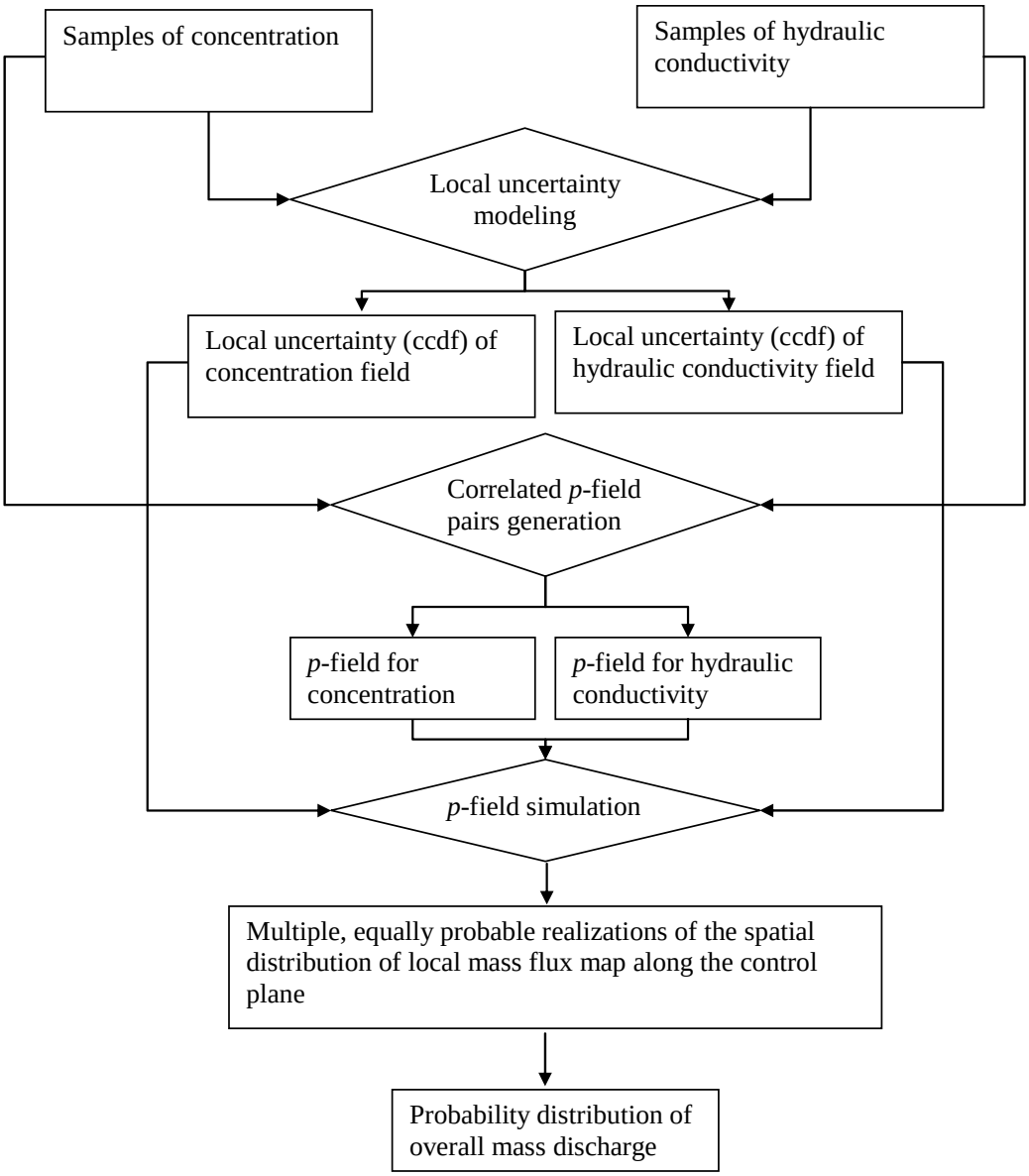

Figure 11: Flowchart of the geostatistical approach for uncertainty analysis of mass discharge using multi-level transect data. *(Li et al. 2007)*

This geostatistical approach is discussed in more details by Li et al. *(Li et al. 2007)*. The demonstration and evaluation of this approach are outlined in Section IX, using numerically simulated transect data that are part of the results of Section II 5.2.

II.5.3.2 A Multi-stage Multi-criteria Spatial Sampling Strategy for the Quantification of Contaminant Mass Discharge and the Associated Uncertainty

As demonstrated in Section IX, the accuracy of the estimated mass discharge and the magnitude of its quantifiable uncertainty depend upon the amount of information provided by the sample data. Application of the geostatistical approach presented in Section II.5.3.1 on numerical

transect data suggested that the required regional sampling density, defined as the ratio of the sampled area to the entire control plane, could be as high as 6~7% to achieve an accurate model of uncertainty for control planes that are associated with high levels of source mass removal (i.e. control planes with scattered small hot spots and large areas of near-zero concentration). This conclusion was based upon a single stage sampling design with a regular sampling pattern (rectangular). The required high sampling density was mainly attributed to the limitations of the geostatistical approach on non-representative samples and the inefficient sampling design *(Li et al. 2007)*. A more efficient sampling design to reduce the required sampling density and improve the accuracy and precision of the uncertainty model of mass discharge is highly desirable.

A multi-stage spatial sampling strategy is presented in this section to select optimal sampling locations and determine the minimum sampling density for an accurate quantification of mass discharge uncertainty. Two sampling criteria are incorporated to ensure coverage of the entire control plane and the delineation of highly concentrated areas (hot spots). The multiple criteria decision making (MCDM) theory is adapted to weight the two sampling criteria objectively based upon the information importance of each criterion. This sampling algorithm can be used in real-time to guide staged field sampling progress for mass discharge estimation.

As shown in figure 12, the multi-stage multi-criteria sampling algorithm is a dynamic and iterative process (adaptive sampling). Starting from an initial sampling dataset of contaminant concentration (9 samples in the example in figure 12), the samples are analyzed using the geostatistical approach presented in Section II.5.3.1. In addition to the quantification of mass discharge uncertainty, the sampling criteria that determine next-stage sampling locations are also computed. The optimal sampling locations for the next sampling stage are then determined by ranking all of the possible sampling locations using the two sampling criteria: conditional variance, and the “distance to the nearest sampling location”. Conditional variance can lead the sampling effort to the most uncertain location in the vicinity of hot spot areas, while the “distance to the nearest sampling locations” tends to spread sampling points evenly in the entire sampling domain. The second criterion is particularly important when none of the previous stage samples are within the vicinity of hot spot areas. In this case, the sampling effort is led to the most sparsely sampled area.

Specifically, at each possible sampling location, the two sampling criteria are computed. The weighted sums of the computed values of the two criteria are then used to rank all of the possible sampling locations. The MCDM theory was adapted in the sampling algorithm to weight the two sampling criteria objectively by using the entropy measured information importance, i.e., the more important information conveyed by a sampling criterion, the more weight the criterion will receive. For example, when none of the previous stage samples are within the vicinity of hot spot areas, i.e., there is no contrast in data values; conditional variances for all possible sampling locations are zero. In this case, the sampling criterion of conditional variance does not provide any information, thus, it receives a weight of zero.

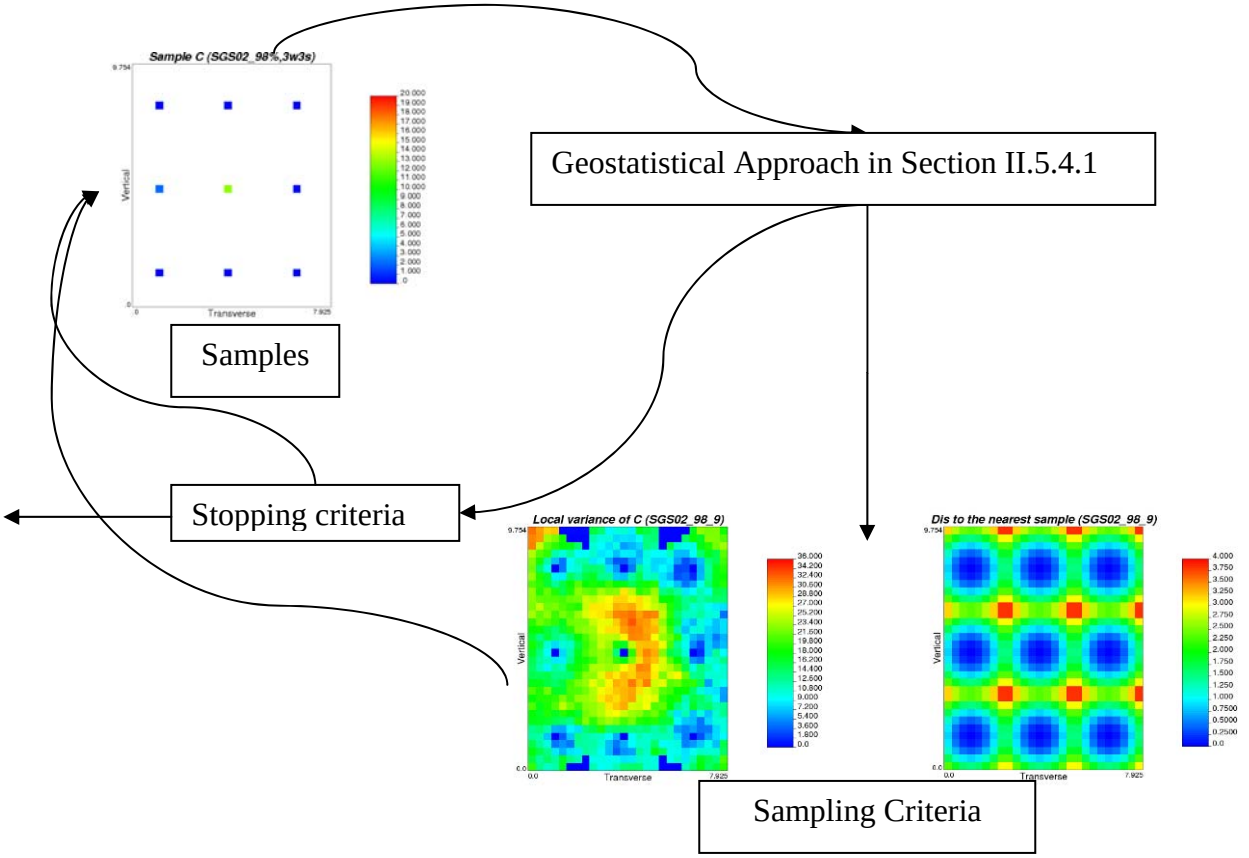

Figure 12: Flowchart of the multi-stage sampling algorithm for the optimization of sampling locations for accurate mass discharge estimation. *(Li and Abriola, in preparation)*

Once the next-stage sampling locations are selected and the sampling is performed, the new sampling data are combined with all of the data from previous sampling stages. The updated data set is then fed into the geostatistical approach to update the uncertainty quantification of mass discharge, the sampling criteria, and the weights for the criteria. With the new information, the selection for the next-stage sampling locations can be performed again.

A recommended minimum sampling density can be identified by analyzing the accuracy and precision of the probability distributions of mass discharge obtained by,applying the sampling algorithm to numerically simulated plume data that are representative of realistic permeability fields and source zone architectures. The minimum sampling density can be used as a reference value to determine when to stop sampling in the field. In addition, the stopping criteria in field implementations can also be formed by analyzing the change in the probability distribution of mass discharge, and the change in the spatial distribution of contaminant concentration.

Demonstration of the sampling algorithm is shown in Section III.2. More details of the algorithm are discussed in Li and Abriola *(in preparation)*.

II.5.3.3 Uncertainty Analysis for Near Source Zone Mass Discharge Estimated Using the Passive Flux Meter Method

This section presents an uncertainty quantification approach for mass discharge estimated in the field using mass flux [M/T•L2] measurements obtained with the Passive Flux Meter (PFM) method. Two uncertainty sources for mass discharge estimation are considered, including the uncertainty of mass flux measurements (resulting from incomplete knowledge of aquifer permeability near the flux meters) and the uncertainty introduced by the integration of local measurements. The proposed approach can provide an empirical probability distribution of mass discharge with which the uncertainty space of mass discharge is fully characterized.

PFM quantifies the local mass flux J_c using a sorptive permeable medium placed in either a borehole or monitoring well to intercept contaminated groundwater and release resident tracers. Information required in estimating mass flux using PFM at certain location includes: the mass of contaminant sorbed, the bulk volume of sorbent, the retardation of contaminant on the sorbent, volumetric water content of the sorptive matrix, and the ratio of the specific discharge in the flux meter to the undisturbed aquifer flow (α). Most of the information can be obtained from the flux meter, except for α, which requires the information of aquifer permeability near each flux measurements and obviously varies along the length of the meter for a heterogeneous aquifer. Current field applications of the PFM method, however, have typically used a uniform α based upon a single-value estimation of the aquifer permeability, which thus neglects the uncertainty associated with the heterogeneity in aquifer permeability field. In addition, mass discharge is calculated by integrating local measurements of mass flux J_c along the control plane. The integration of mass flux measurements introduces additional uncertainty into mass discharge estimate.

A geostatistical approach was developed to generate an empirical probability distribution of mass discharge using the PFM measurements, providing that several local measurements of hydraulic conductivity are available. The uncertainty contributed by the heterogeneity of the permeability field, thus the heterogeneity of α, is incorporated using the concept of soft indicators. In this approach, because of the uncertainty of α, the PFM measured mass flux is treated as a random variable, rather than a certain value. At sampled locations, the local uncertainty model, the conditional cumulative distribution function (ccdf) of mass flux J_c can be obtained from the ccdf of hydraulic conductivity. At unsampled locations, the ccdfs of J_c can be constructed from the ccdfs at sampled locations through the concept of soft indicators and a local uncertainty modeling process. Once the information about the uncertainty of α (thus the uncertainty of mass flux) is incorporated, the uncertainty of mass discharge can then be propagated from the ccdfs of J_c using an upscaling process.

Figure 13 shows the flow chart of the geostatistical approach. As shown in the figure, the geostatistical approach for the uncertainty quantification of mass discharge using the PFM mass flux measurements proceeds as follows: 1) build ccdf models of aquifer permeability using indicator kriging; 2) at sampled locations, build ccdf models of mass flux by propagating the uncertainty of aquifer permeability (ccdf) using the equations $J_c = c_F \cdot q_0 = \frac{m_c}{\pi r^2 b A_{RC} \theta R_{DC}} \cdot \frac{q_D}{\alpha}$ *(Hatfield et al. 2004)*; 3) at sampled locations, transform the

ccdfs of mass flux into soft indicators *(Saito and Goovaerts 2002)*; 4) build ccdf models of mass flux at unsampled locations using indicator kriging; 5) sample the mass flux ccdfs to generate multiple equal-probable realizations of mass flux using *p*-field simulation; and 6) integrate the mass flux realizations to build the probability distribution of mass discharge.

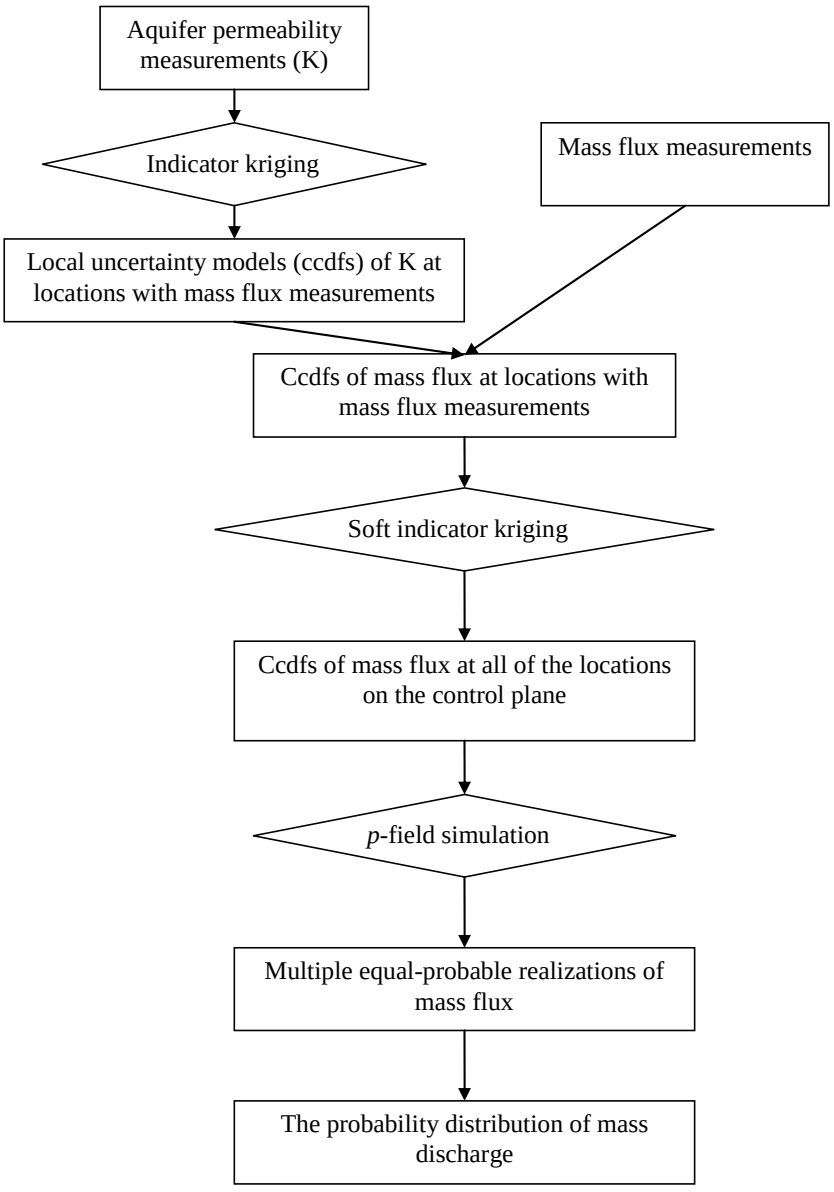

Figure 13: Flow chart of the geostatistical approach for the uncertainty analysis for the PFM method

II.5.4 Cost-Benefit Analysis Tools for Source Zone Treatment

Cost estimation tools were developed using a macro-based Microsoft Excel framework, with modular data input sheets. Output data, in both tabular and graphical forms, provided itemized cost information for each component of a particular technology (e.g., injection system, above-ground treatment system). Two levels of cost analysis tool were developed; a simplified version with generic system parameters for each technology, and a site-specific version that allows users to select and/or input options for individual components of the treatment system. Five commonly implemented DNAPL source zone treatment technologies were considered, in addition to the baseline pump-and-treat case. For the technologies considered in Tasks III and IV (i.e., surfactant flushing and air-sparging) cost estimates derived using both the simplified and advanced cost analysis tools were compared to simulated and measured post-treatment DNAPL mass flux reductions to derive cost-benefit effectiveness rankings.

III. Results and Accomplishments

Although work continues on the monitoring of dechlorination in a 2-D aquifer cell and the modeling of 1- and 2-D metabolic reductive dechlorination experiments, the objectives of the project were met. As described in detail in the following sections, this project contributed to an improved understanding of the conditions under which metabolic reductive dechlorination may be expected and quantified the influence of aggressive mass removal treatment technologies on subsequent natural attenuation. Bench-scale experiments and field-scale numerical simulations were employed to evaluate DNAPL recovery and subsequent contaminant flux from heterogeneous source zones using existing and modified multiphase compositional simulators. New tools to aid in the estimation of mass flux and mass flux uncertainty were developed to aid in site characterization and post-treatment monitoring. A cost-benefit analysis tool was developed to aid site managers in the evaluation and comparison of alternative source zone treatment technologies. Detailed discussion of these and supporting accomplishments are described below.

III.1 METABOLIC REDUCTIVE DECHLORINATION IN BATCH SYSTEMS

III.1.1 Evaluation of aqueous-phase PCE tolerance and microbially enhanced PCE dissolution

III.1.1.1 Dissolved-phase PCE tolerance of pure cultures

As described in Amos et al. *(2007a)*, experiments conducted with dissolved-phase PCE indicated that all four pure cultures tested were unable to dechlorinate when aqueous PCE concentrations exceeded 540 μM. Figure 14 shows representative results for the dechlorination performance of *Desulfuromonas michiganensis* strain BB1 in the presence of dissolved-phase PCE at tolerable and intolerable concentrations. All cultures were established with low PCE concentrations initially (Days 0-2, Figure 1), which was followed by PCE conversion to *cis*-DCE and trace levels (<2.1 μM) of *trans*-DCE, with the formation of TCE as an intermediate (Figures 1A and B). After amendment of additional PCE to a concentration of 295 ± 10 μM on Day 2, strain BB1 dechlorinated PCE to *cis*-DCE (Figure 14A). In a parallel experiment (Figure 14B), the concentration of PCE after the Day 2 addition was increased to 690 ± 10 μM. The aqueous phase concentration of PCE decreased to 560 ± 45 μM by Day 3 at which point the concentration of PCE remained relatively constant for the duration of the experiment. The initial decrease in PCE between Days 2 and 3, which also occurred when higher PCE concentrations were tested (data not shown), was attributed to partitioning of PCE from the aqueous phase to the headspace. Formation of TCE and accumulation of *cis*-DCE did not occur (Figure 14B, Days 2-6), indicating that strain BB1 did not dechlorinate PCE at the tested concentration. Additional experiments at higher PCE concentrations confirmed that strain BB1 could not dechlorinate PCE at concentrations > 560 μM (data not shown).

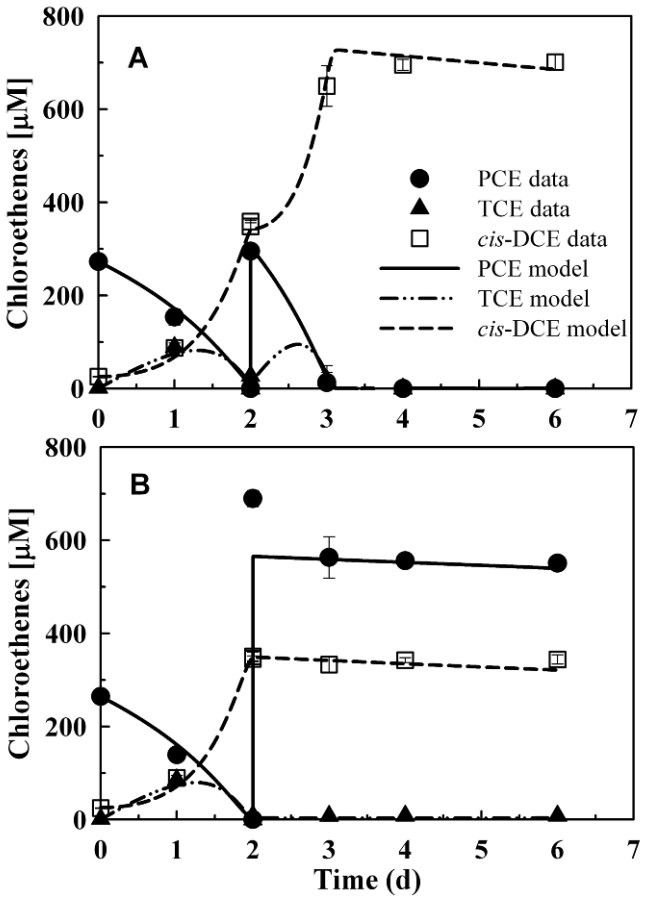

Figure 14: Dechlorination performance of *Desulfuromonas michiganensis* strain BB1 at various PCE concentrations. Low PCE concentrations were used for all initial conditions (Days 0-2), followed by amendment of additional PCE to tolerable (A) or intolerable (B) PCE concentrations. The legend is shared between the A and B. All data points represent average values from triplicate cultures, and error bars represent one standard deviation. If no error bars are shown, the standard deviations were too small to be illustrated. The lines represent simulated chlorinated ethene concentrations fitted (Figure 14A) or predicted (Figure 14B) by the developed mathematical model (see II.5.1 for details) *(Amos et al. 2007a).*

Results obtained for the other three pure cultures tested were similar in that dechlorination ceased or was severely inhibited at PCE concentrations ≥ 540 μM (data not shown). *S. multivorans* and *Geobacter lovleyi* strain SZ dechlorinated PCE to *cis*-DCE at PCE concentrations ≤ 330 μM but did not dechlorinate PCE to *cis*-DCE at PCE concentrations ≥ 540 μM. Limited dechlorination (<25% of the initial PCE mass) of PCE to TCE occurred with strain SZ at PCE concentrations of ca. 540 μM (13 day incubation, TCE production ceased on Day 8; data not shown). *Desulfitobacterium* sp. strain Viet1 dechlorinated PCE to TCE at PCE concentrations ≤ 330 μM, while only limited (<5%) accumulation of TCE occurred at PCE concentrations of ca. 540 μM; PCE dechlorination did not occur with strain Viet1 at PCE concentrations > 540 μM.

III.1.1.2 Dechlorination in the presence of PCE DNAPL

The dechlorination performance of *Desulfuromonas michiganensis* strain BB1 in the presence of PCE DNAPL is shown in Figure 15. Strain BB1 dechlorinated dissolved-phase PCE (two amendments of 300 μM each) completely to *cis*-DCE and trace levels of *trans*-DCE (<4 μM) (data not shown), before the addition of PCE DNAPL. After the addition of PCE DNAPL, PCE dissolution resulted in accumulation of PCE in the aqueous phase (Figure 15). Initially (before Day 2 following DNAPL addition), the cultures accumulated TCE, *cis*-DCE, and trace amounts of *trans*-DCE (~155, ~1,050, and < 5 μM, respectively). Dechlorination ceased after 1.4 days when the PCE concentration reached 470 ± 130 μM (Figure 15). PCE continued to accumulate in the aqueous phase until equilibrium conditions were reached around Day 6. DNAPL was visible at the conclusion of the experiment. Similar results were observed with strain SZ in the presence of PCE DNAPL, although greater amounts of TCE (310 ± 25 μM) and *cis*-DCE (1,260 ± 180 μM) accumulated in the aqueous phase after addition of PCE DNAPL (data not shown).

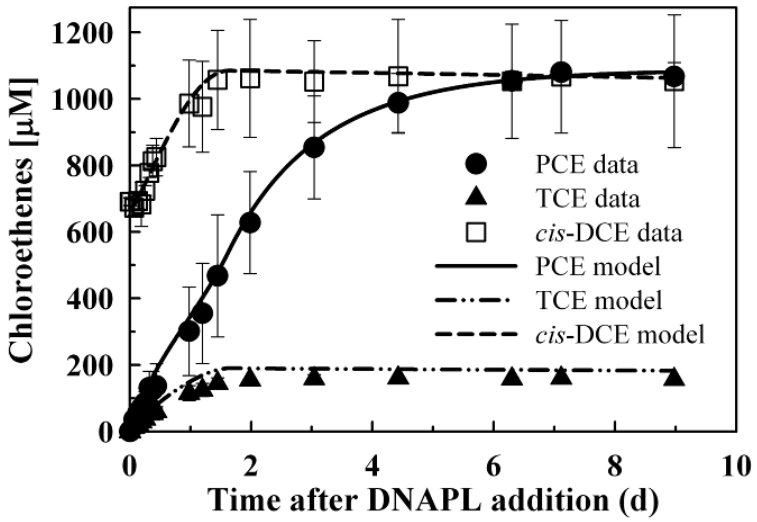

Figure 15: Dechlorination performance of triplicate cultures of *Desulfuromonas michiganensis* strain BB1 in the presence of PCE DNAPL. All data points represent average values from triplicate cultures, and error bars represent one standard deviation. If no error bars are shown, the standard deviations were too small to be illustrated. The lines represent simulated chlorinated ethene concentrations predicted by the developed mathematical model (see II.5.1 for details) *(Amos et al. 2007a)*.

The dechlorination performance of *S. multivorans* in the presence of PCE DNAPL is shown in Figure 16. *S. multivorans* dechlorinated dissolved-phase PCE (two amendments of 300 μM each) completely to *cis*-DCE and trace levels of *trans*-DCE (< 5 μM) (data not shown), before the addition of PCE DNAPL. For the inactivated controls, PCE dissolution from the DNAPL phase resulted in equilibrium conditions and saturated PCE concentrations around Day 4 (Figure 16). In the inactivated controls, dechlorination did not occur and the DNAPL droplet remained visible throughout the entire experiment. In live cultures, *S. multivorans* dechlorinated PCE and produced *cis*-DCE (Figure 16) and *trans*-DCE (data not shown). *cis*-DCE and *trans*-DCE accumulated until Day 13, at which time the production of *cis*-DCE and *trans*-DCE leveled off at

4,600 ± 200 μM and 28 ± 2 μM, respectively. Unlike similar experiments with strain BB1 (Figure 15) and strain SZ (data not shown), PCE did not accumulate in the aqueous phase when *S. multivorans* was grown in the presence of PCE DNAPL. PCE was detected in six of the twelve samples taken before or on Day 3, five of which were at levels < 6 μM, while TCE was only detected in two samples at concentrations < 40 μM. PCE and TCE were not detected in any sample after Day 3. The DNAPL droplet decreased in size (visual observation) throughout the experiment and was completely dissolved after 13 days in the live cultures, corresponding to the time at which *cis*-DCE production ceased. When the experiment with *S. multivorans* was repeated with an increased agitation speed (175 rpm), which presumably increased the rate of PCE dissolution from the DNAPL, transient accumulation of PCE and TCE to maximum aqueous phase concentrations of 124 μM and 118 μM was observed at 3 and 6 hours after DNAPL addition, respectively (see Figure 17).

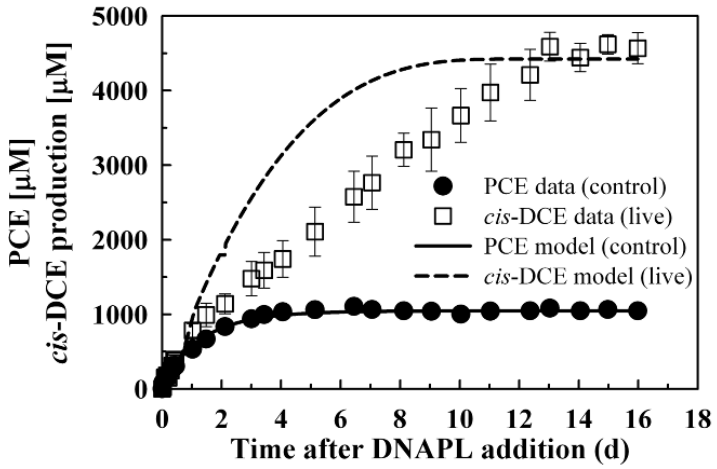

Figure 16: Dechlorination performance of *S. multivorans* cultures in the presence of PCE DNAPL. *cis*-DCE production was calculated by subtracting the *cis*-DCE aqueous phase concentration present before DNAPL addition from the *cis*-DCE aqueous phase concentration measured following DNAPL addition and is presented to aid in comparing the initial rate of *cis*-DCE accumulation to the rate of PCE dissolution in the inactivated controls. All data points represent average values from triplicate cultures shaken at 150 rpm, and error bars represent one standard deviation. If no error bars are shown, the standard deviations were too small to be illustrated. The lines represent simulated chlorinated ethene concentrations fitted (inactivated control data) or predicted (live data) by the developed mathematical model (see II.5.1 for details) *(Amos et al. 2007a)*.

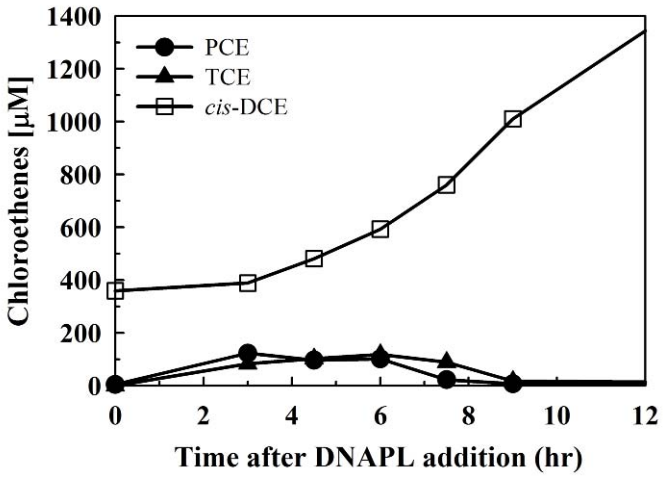

Figure 17: Dechlorination performance of *S. multivorans* in the presence of PCE DNAPL. The results for a single, representative culture shaken at 175 rpm show the transient accumulation of PCE and TCE at early times (<12 hr) *(Amos et al. 2007a).*

III.1.1.3 Implications for DNAPL source zone bioremediation

Microbially-enhanced PCE DNAPL dissolution has been suggested as a productive PCE and TCE source zone remedy *(Carr et al. 2000; Yang and McCarty 2000; Cope and Hughes 2001; Yang and McCarty 2002; Adamson et al. 2004; Sleep et al. 2006).* Several studies with pure cultures (for an extensive list, see the *Supporting Information* of Amos et al. *(2007a)*) and with mixed dechlorinating consortia (e.g., *(Isalou et al. 1998; Nielsen and Keasling 1999; Yang and McCarty 2000; Duhamel et al. 2002; Yang and McCarty 2002; Adamson et al. 2004; Yu and Semprini 2004; Sleep et al. 2006)*) have shown that bacterial PCE dechlorination occurs at or near saturated PCE concentrations. For instance, *Desulfuromonas michiganensis* strain BB1 was reported to dechlorinate at saturated PCE concentrations and to grow in the presence of PCE DNAPL *(Sung et al. 2003).* The results presented here demonstrate that strain BB1 cannot dechlorinate at PCE concentrations above 540 μM, and similar observations were made for other PCE-to-TCE and PCE-to-*cis*-DCE dechlorinating organisms (i.e., *Sulfurospirillum multivorans, Geobacter lovleyi* strain SZ, and *Desulfitobacterium* sp. strain Viet1). The discrepancies in the inhibitory PCE concentrations determined here for strain BB1 and previous results *(Sung et al. 2003)* are likely due to differences in the experimental methodology including (i) the use of Teflon-lined septa as opposed to butyl rubber stoppers to minimize contaminant loss due to sorption and (ii) the addition of PCE in a soluble carrier phase (i.e., methanol) to ensure rapid PCE dissolution and availability to the organisms. In the study by Sung et al. *(Sung et al. 2003)*, PCE was added undiluted (i.e., neat) or in a separate-phase insoluble carrier (i.e., hexadecane). The addition of PCE using these techniques is appropriate as long as adequate time is given to ensure equilibrium conditions before initiation of the experiment; otherwise, initial conditions will be at non-equilibrium, yielding PCE concentrations significantly below targeted values. DNAPL dissolution is a slow process, and time is required to establish equilibrium conditions (see inactivated control in Figure 16). The inhibitory PCE concentrations reported in this study for microbial isolates of different phylogenetic lineages accurately reflect dissolved-phase PCE concentrations and demonstrate that the cultures tested cannot dechlorinate PCE at or near the

aqueous solubility of PCE. Similar, carefully-conducted studies should be performed with other PCE-dechlorinating bacteria to elucidate culture-specific inhibitory PCE concentrations.

Although the bacterial isolates included in this study failed to dechlorinate at saturated PCE concentrations, these organisms impacted the dissolution and transformation of PCE from free-phase DNAPL. Microbial activity in the presence of PCE DNAPL occurred as long as aqueous PCE concentrations remained below inhibitory concentrations (i.e., the system was not in equilibrium). Such activity might explain one mechanism by which biologically enhanced dissolution occurs with dechlorinating microorganisms incapable of dechlorinating at high or saturated PCE concentrations. The ability to dechlorinate in the presence of DNAPL, resulting in complete DNAPL dissolution and transformation, is likely not restricted to *S. multivorans* but may be observed with the other tested dechlorinating organisms (i.e., strains BB1 and SZ) under the appropriate conditions (e.g., higher biomass concentrations, decreased PCE dissolution rates, attenuation of PCE to non-inhibitory levels due to other processes [e.g., sorption, dispersion, etc.]).

DNAPL dissolution in aquifer formations is a complex process that depends on many variables, including the DNAPL saturation distribution, DNAPL interfacial area, porous media heterogeneity, and groundwater flow. The mass transfer coefficient obtained in our experimental system falls within the range of field mass transfer coefficients predicted by commonly employed correlations (e.g., 0.13 – 4 m/d *(Powers et al. 1994)*) and is consistent with grid-scale mass transfer coefficients used in multi-dimensional numerical simulators (e.g., UTCHEM, MISER). Although many of the correlations predict equilibrium aqueous phase contaminant concentrations at the local scale under most environmental conditions (e.g., *(Powers et al. 1992)*), dispersive transport and dilution are relevant processes in source zones with heterogeneous NAPL distributions. Dispersive transport and dilution effects may reduce concentrations below levels that are inhibitory to some dechlorinating organisms. Dechlorination activity in zones with tolerable PCE concentrations would further reduce aqueous phase contaminant concentrations and sustain enhanced dissolution of downgradient NAPL ganglia or pools because of the increased mass transfer driving force. Therefore, microbial activity may enhance dissolution in PCE-DNAPL source zones even if the dechlorinating bacteria cannot tolerate high PCE concentrations or are not active in the immediate vicinity of the NAPL-water interface. Future experiments are needed to address the influence of source zone DNAPL architecture and microbial distribution within DNAPL source zones on dissolution processes.

The inability of the tested bacteria to dechlorinate PCE at concentrations >540 μM does not imply that this is a universal characteristic of PCE dechlorinators, and our results should not be used to discount bioremediation as a viable remedial option at sites where PCE concentrations exceed 540 μM. Several mixed culture studies suggest that PCE dechlorination occurs at high, saturated, concentrations of PCE (e.g., *(Isalou et al. 1998; Nielsen and Keasling 1999; Yang and McCarty 2000; Duhamel et al. 2002; Yang and McCarty 2002; Adamson et al. 2004; Yu and Semprini 2004; Sleep et al. 2006)*). The ability of these mixed cultures to dechlorinate at elevated PCE concentrations may be due to i) the presence of dechlorinating strains acclimated to high PCE concentrations or ii) dechlorinators that exhibit increased PCE tolerance as members of mixed microbial communities (e.g., biofilms). For example, an increased tolerance to high

levels of PCE may be related to the presence of large cell aggregates (i.e., granules), which characterize some dechlorinating consortia (unpublished results). The aqueous-phase concentration that dechlorinating organisms experience within such granules may be below inhibitory levels and lower than bulk (i.e., measured) concentrations due to diffusional limitations or sorption of PCE to cells on the outside of the aggregates. A similar protection mechanism from high concentrations of PCE may also occur within aquifer material biofilms, similar to what has been observed for other stressors *(Almås et al. 2005)*. In many bacteria, environmental stressors (e.g., heat) regulate the production of a large number of proteins that aid in bacterial survival, and such general stress response systems are important for microbial tolerance to other solvents (e.g., toluene) (reviewed in *(Isken and de Bont 1998)*). Recently, interspecies communication following stress exposure and the regulation of stress responses have been shown to result in stress-adapted phenotypes *(McDougald et al. 2003; Xavier and Bassler 2003)*. At present, the complex interactions among dechlorinators and other microbial populations are poorly understood. Elucidating these interactions, including their potential roles in avoiding PCE inhibition and enhancing dechlorination activity in the presence of PCE DNAPL, is likely to further promote source zone bioremediation.

III.1.2 Effects of Tween 80 on microbial reductive dechlorination

III.1.2.1 Dechlorination performance in the presence of Tween 80

As described in Amos et al. *(2007b)*, the dechlorination performance of both pure and mixed cultures in the presence of Tween 80 is summarized in Table 2 (see page 16). At the concentrations tested, Tween 80 had no effect on PCE-to-TCE and PCE-to-*cis*-DCE reductive dechlorination in all cultures tested (Table 2). Similar dechlorination performances and product patterns were observed in cultures with and without the surfactant. For example, Figure 18 shows PCE dechlorination to *cis*-DCE in cultures of "*Clostridium bifermentans*" strain DPH-1 in the presence and absence of 500 mg/L Tween 80. In contrast, Tween 80 had a profound effect on *cis*-DCE dechlorination in cultures of *Dehalococcoides* sp. strain BAV1. As shown in Figure 19, the addition of 50 mg/L Tween 80 completely inhibited *cis*-DCE dechlorination, whereas control cultures without surfactant produced stoichiometric amounts of ethene. Tween 80-amended cultures did not show any *cis*-DCE dechlorination activity even after 2 months of incubation (data not shown). Similarly, *Dehalococcoides* sp. strain FL2 did not dechlorinate TCE in the presence of Tween 80, while control cultures dechlorinated TCE to mainly VC over the 34-day incubation period (Table 2). Replicate, independent experiments yielded similar results regardless of the Tween 80 concentrations tested (50-5,000 mg/L; see Table 2). The BDI consortium dechlorinated PCE to ethene in the absence of the surfactant, but *cis*-DCE was the dechlorination end product in the presence of Tween 80 (500-5,000 mg/L; Table 2). VC or ethene formation did not occur even after extended (147 days) incubation of BDI with Tween 80 (data not shown).

III.1.2.2 Biomass effects on Tween 80 inhibition of reductive dechlorination

The biomass concentration maintained in the OW consortium was 20-fold higher compared with the BDI consortium (i.e., 820 ± 50 mg POC/L versus 40 ± 5 mg POC/L). Phase contrast light microscopy confirmed that the OW consortium contained more microbial cells than BDI and

revealed large cell aggregates ranging in size from ~10 μm to greater than 300 μm (data not shown). The aggregates consisted of bacteria with diverse morphologies dominated by small cocci and filamentous bacteria similar in morphology to *Methanosaeta* (data not shown) *(Whitman et al. 1992)*. The BDI consortium contained few cell aggregates, which were ≤ 10 μm in diameter, dominated by small cocci, and did not contain filamentous bacteria. In contrast to the observations made with BDI described above, Tween 80 (1,000 mg/L) did not inhibit dechlorination beyond *cis*-DCE with undiluted OW consortium (Table 2); both the surfactant-free control and Tween 80-amended undiluted OW cultures dechlorinated PCE to ethene following 2 days of incubation (data not shown). In experiments that used 100-fold dilutions of the OW consortium, TCE (2 mol% of the total chlorinated ethenes) and *cis*-DCE (98 mol%) accumulated in the presence of Tween 80 after 8 days of incubation, and no further dechlorination to VC and ethene occurred even after extended incubation periods (42 days). The 100-fold dilution affected the dechlorination performance of the OW consortium in the absence of Tween 80 (i.e., the surfactant-free control cultures); VC (87 mol% of total chlorinated ethenes and ethene) was the main product following a 42-day incubation period. Although dilution of the OW consortium affected complete dechlorination of PCE to ethene in the surfactant-free control cultures, comparison of dechlorination performances in the 100-fold diluted cultures (i.e., surfactant-free vs. Tween 80-amended cultures) suggested that Tween 80 inhibited *cis*-DCE dechlorination to VC and ethene.

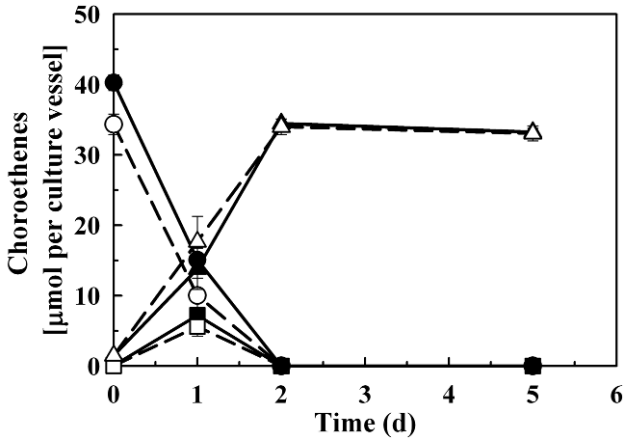

Figure 18: Reductive dechlorination of PCE to *cis*-DCE by "*Clostridium bifermentans*" strain DPH-1 in the presence (500 mg/L; open symbols, dashed lines) or absence (closed symbols, solid lines) of Tween 80. Symbols: ●, PCE; ■, TCE; ▲, *cis*-DCE. All data points represent average values from triplicate cultures, and error bars represent one standard deviation. When error bars are not visible, they are smaller than and therefore hidden behind the data symbols *(Amos et al. 2007b)*.

III.1.2.3 Effect of Tween 80 on Dehalococcoides cell numbers

The Tween 80-exposed BDI cultures initially dechlorinated VC to small amounts of ethene (8 ± 1 μmol), but additional dechlorination of VC and production of ethene was not observed after Day 4 (Figure 20A). In the absence of Tween 80, VC was dechlorinated by Day 21 with concomitant production of ethene (Figure 20A). In an independent experiment, the Tween 80-exposed BDI cultures failed to dechlorinate VC and ethene was not detected even after 58 days

of incubation (data not shown). The *Dehalococcoides* cell numbers steadily declined from 1.7 ± 1.1 × 10^8 to 2.0 ± 0.8 × 10^6 per mL during the 21 days of Tween 80 exposure (Figures 20B and 20C) and from 6.6 ± 1.5 × 10^8 to 1.3 ± 0.8 × 10^5 per mL following the 58-day Tween 80 exposure (Figure 20C). For the control cultures incubated without Tween 80, the number of *Dehalococcoides* cells increased from 1.7 ± 1.1 × 10^8 per mL on Day 0 to a maximum of 1.0 ± 0.6 × 10^9 per mL on Day 17 during dechlorination of VC to ethene (Figure 20B). The cell numbers for the electron acceptor-starved control cultures ranged from 1.4 ± 0.4 × 10^8 to 3.3 ± 1.0 × 10^8 cells per mL during the 21-day incubation period (Figure 20B). Regression analysis (R^2 = 0.85) of both the 21-day and 58-day incubations revealed that the *Dehalococcoides* cell numbers per mL decreased exponentially (pseudo first-order reaction rate of 0.13 ± 0.02 day^{-1}) with time during Tween 80 exposure (Figure 20C). At the concentrations tested, Tween 80 had no effect on DNA extraction or PCR efficacy (data not shown), indicating that the decreased cell numbers measured with qPCR analysis were not due to experimental biases introduced by the surfactant.

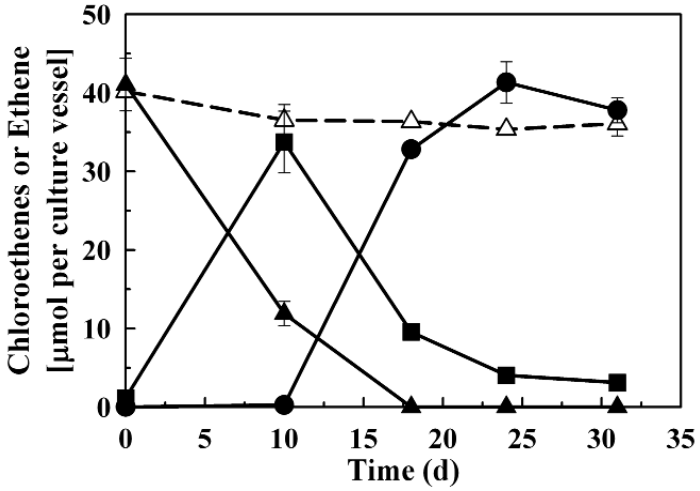

Figure 19: The dechlorination performance of *Dehalococcoides* sp. strain BAV1 in the presence (50 mg/L; open symbols, dashed line) or absence (closed symbols, solid lines) of Tween 80. Symbols: ▲, *cis*-DCE; ■, VC; ●, Ethene. All data points represent average values from triplicate cultures, and error bars represent one standard deviation. When error bars are not visible, they are smaller than and therefore hidden behind the data symbols *(Amos et al. 2007b)*.

III.1.2.4 Reversibility Experiments

The Tween 80-exposed, washed BDI cell suspensions dechlorinated VC to ethene in Tween 80-free medium. Ethene production began on Day 24 and neared completion by Day 30 (Figure 21). A much shorter lag time of 3 days was observed in the control cultures that had not experienced Tween 80 exposure (Figure 21). Ethene production also occurred in suspensions of washed, electron-acceptor starved cells (representative results are shown in Figure 21). Although the dechlorination performance of the triplicate cultures of the washed, electron-acceptor starved cells varied, complete dechlorination of VC to ethene occurred by Day 52 in all replicates (data not shown). The negative control cultures (i.e., washed, oxygen-exposed cells) did not dechlorinate VC or produce ethene (data not shown).

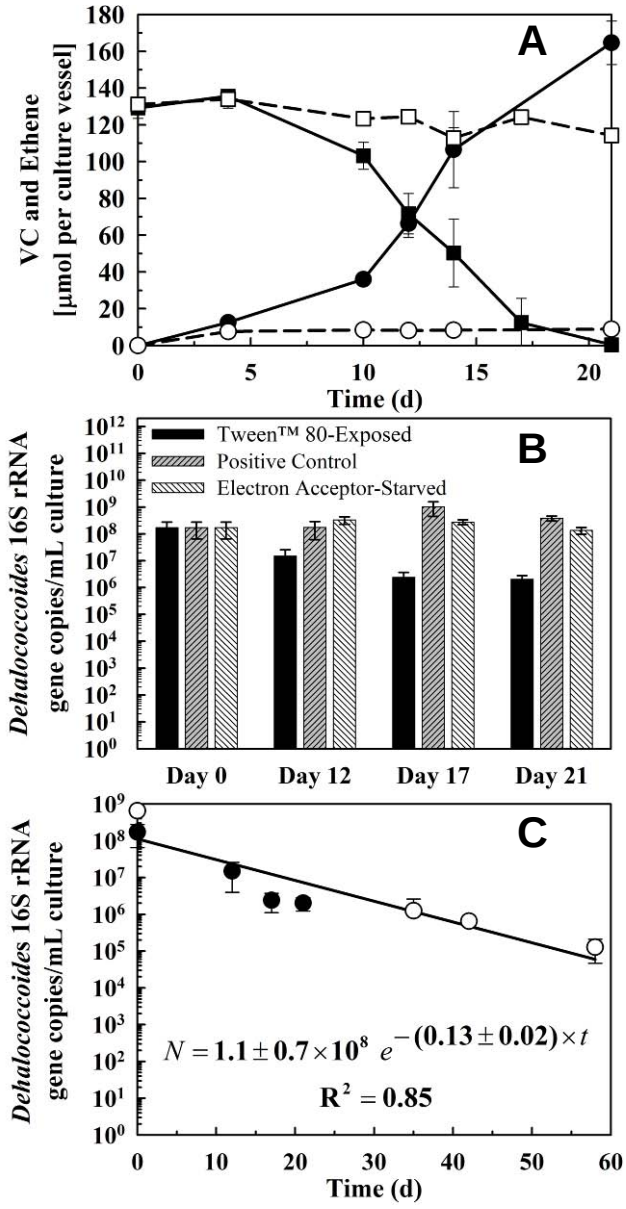

Figure 20: (A) VC dechlorination by the BDI consortium in the presence (250 mg/L; open symbols, dashed lines) or absence (closed symbols, solid lines) of Tween 80. Symbols: ■, VC; ●, Ethene. (B) qPCR analysis of *Dehalococcoides* 16S rRNA gene copy numbers during incubation under three treatments. (C) qPCR analysis showing an exponential decrease in the number of *Dehalococcoides* organisms during exposure to 250 mg/L Tween 80. The solid line in (C) represents regression of the data from both the 21-day exposure (closed symbols) and the 58-day exposure (open symbols); the line appears linear on the logarithmic axis. *N* represents the number of *Dehalococcoides* cells per mL at time *t*. Error bars represent one standard deviation. When error bars are not visible, they are smaller than and therefore hidden behind the data symbols *(Amos et al. 2007b).*

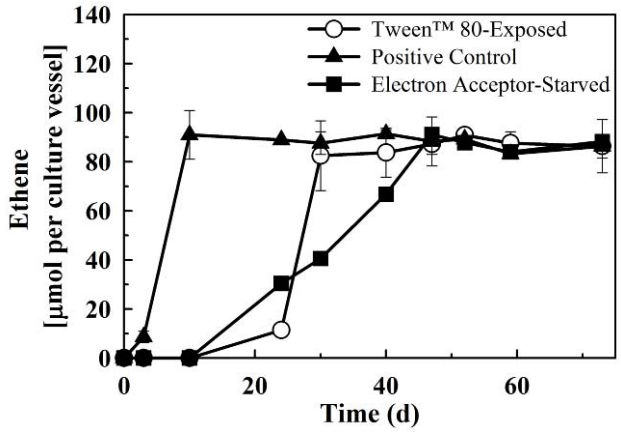

Figure 21: Reversibility experiment showing ethene production by washed cell suspensions of BDI in identical sets of fresh Tween 80-free medium. Representative data sets show values from one replicate (electron acceptor-starved cultures) or average values from duplicate (positive control) or triplicate (Tween 80-exposed) cultures. Error bars represent one standard deviation *(Amos et al. 2007b)*.

III.1.2.5 Implications for biological polishing following surfactant flushing

The presence of Tween 80 did not affect the dechlorination performance of both gram-positive and gram-negative PCE-to-TCE or PCE-to-*cis*-DCE dechlorinating isolates. The tested isolates included all major genera of PCE-to-*cis*-DCE dechlorinators except *Dehalobacter* spp. However, *Dehalobacter* spp. were detected in consortia OW *(Daprato et al. 2007)* and BDI (unpublished data), and the ability of both consortia to dechlorinate PCE to *cis*-DCE in the presence of surfactant suggests that *Dehalobacter* spp. are not affected by Tween 80. Apparently, Tween 80 does not inhibit PCE-to-TCE and PCE-to-*cis*-DCE dechlorinators, at least at surfactant concentrations similar to those observed at the Bachman Road site following SEAR (i.e., < 5,000 mg/L Tween 80) *(Ramsburg et al. 2004)*.

In contrast, Tween 80 severely inhibited dechlorination by *Dehalococcoides* organisms in both pure and mixed cultures and caused a decline in cell numbers. The sequestration of chlorinated ethenes within surfactant micelles *(Zhang et al. 2006)* may have limited the bioavailability of the terminal electron acceptor required to sustain the energy metabolism in *Dehalococcoides* cells. However, the cell numbers remained constant in electron acceptor-starved control cultures (which were not exposed to Tween 80), suggesting a direct effect of the surfactant on the *Dehalococcoides* cells. Obviously, *Dehalococcoides* organisms respond differently to Tween 80 as compared to the gram-positive and gram-negative PCE-to-TCE and PCE-to-*cis*-DCE dechlorinators, which were not affected by Tween 80 at the concentrations tested. Although the mode of Tween 80 inhibition is unclear, it is conceivable that the surfactant affects *Dehalococcoides* membrane functions and ultimately causes cell death and lysis. Phylogenetically, *Dehalococcoides* are deeply branching green non-sulfur bacteria (*Chloroflexi*) with an unusual cell wall structure and membrane composition *(Maymó-Gatell et al. 1997)*, which may be responsible for the observed Tween 80 effects. For instance, furan phospholipid fatty acids, which are not typically found in bacteria, were detected in *Dehalococcoides (White et al. 2005)*, and an archaeal-type gene (*ino1*), which has limited distribution in bacteria and may be

involved in the synthesis of cellular envelope components, was found in the genome of *Dehalococcoides ethenogenes (Nesbø et al. 2001; Empadinhas et al. 2004).*

The decrease in *Dehalococcoides* cell numbers during Tween 80 exposure were fit ($R^2 = 0.85$) to the Chick-Watson disinfection model ($N = N_o e^{-kt}$), where N and N_o are the *Dehalococcoides* 16S rRNA gene copies per mL culture at time t and initially, respectively, and k is the pseudo first-order reaction rate *(Gyürék and Finch 1998; Haas 1999).* The predictable nature of the decline in *Dehalococcoides* cells during exposure to Tween 80 allows the incorporation of decay rates in mathematical models (e.g., UTCHEM *(Delshad et al. 1996)*) used to evaluate and design remedial treatment options (e.g., SEAR followed by microbial reductive dechlorination). Since the pseudo first-order decay rate, k, is likely a function of surfactant type and concentration, type of microorganism, and environmental parameters (e.g., pH, temperature, etc.), values determined herein only apply to the experimental conditions used in this study. Future research should evaluate the effect of environmental parameters, including surfactant concentrations, degradation, sorption, and dilution on k to improve incorporation of this parameter into remedial design models.

Despite the evidence that Tween 80 inhibits dechlorination mediated by *Dehalococcoides* organisms and reduces their survival, a study by McGuire and Hughes *(McGuire and Hughes 2003)* suggested that *Dehalococcoides* can dechlorinate in the presence of Tween 80. In their study, a dechlorinating consortium dechlorinated PCE to VC and ethene when amended with 1,000 – 10,000 mg/L Tween 80 *(McGuire and Hughes 2003).* Our results with the OW consortium, which was derived from the same source as the dechlorinating consortium used by McGuire and Hughes *(McGuire and Hughes 2003; Daprato et al. 2007)*, also indicated ethene formation in the presence of 1,000 mg/L Tween 80. Microscopic analysis and POC measurements showed that the OW consortium contained at least 20-fold more biomass than the BDI consortium, which did not dechlorinate PCE beyond *cis*-DCE in the presence of Tween 80. Interestingly, the OW consortium failed to dechlorinate beyond *cis*-DCE in the 100-fold diluted cultures. These results suggest that the amount of biomass and/or type of microbes present in the OW consortium reduced the inhibitory effect of Tween 80 on *Dehalococcoides* organisms. One possible mechanism to explain this observation is sorption of Tween 80 to microbial cells. In high biomass systems (e.g., the undiluted OW consortium with 820 ± 50 mg POC/L), the mass of surfactant associated with microbial cells may be below inhibitory levels. In lower biomass systems (e.g., BDI with 40 ± 5 mg POC/L and the 100-fold diluted OW consortium with 8.2 ± 0.5 mg POC/L), the mass of surfactant associated with microbial cells may exceed a tolerable threshold and cause inhibition. For example, Yeh and Pavlostathis *(Yeh and Pavlostathis 2004)* determined that sorption of a similar surfactant (Tween 60) to biomass from a hexachlorobenzene-dechlorinating consortium reached a maximum value of 1.182 g surfactant/g biomass organic carbon. It is likely that the sorption properties of Tween 80 and Tween 60 are similar because the surfactants are structurally similar and follow Langmuir-type sorption isotherms *(Yeh and Pavlostathis 2004; Abriola et al. 2005).* Based on the Langmuir parameters reported by Yeh and Pavlostathis *(Yeh and Pavlostathis 2004)* and our experimental conditions (e.g., initial [applied] surfactant concentration), surfactant sorption to biomass was estimated at ~0.8 and ~1.0 g surfactant/g biomass POC for the undiluted and 100-fold diluted OW consortium, respectively. In both systems, the bulk aqueous-phase surfactant concentration did not decrease below the surfactant's CMC; therefore, the lack of inhibition in high biomass

systems is likely related to lower amounts of surfactant associated with the biomass as opposed to a reduction of bulk aqueous-phase surfactant concentrations. At contaminated sites, the amount of surfactant available for sorption to biomass is controlled not only by the amount of biomass present but also by the physicochemical properties of the soil (e.g., organic matter content). Sorption of Tween 80 to aquifer material will not only reduce the amount of surfactant available to associate with microbial cells (e.g., *Dehalococcoides* organisms) but also provide a long-term source of reducing equivalents (i.e., electron donors) to sustain reductive dechlorination *(Ramsburg et al. 2004)*. The surfactant sorption properties affect remedial performance in multiple ways and should be carefully considered in combined treatment applications. Another possible mechanism to explain the increased tolerance of consortium OW to the surfactant is the occurrence of large cell aggregates that may shield and protect *Dehalococcoides* organisms from exposure to and interaction with Tween 80. Association of *Dehalococcoides* organisms with other microbes may provide similar protection from exposure to Tween 80 in aquifer systems. Both proposed mechanisms, surfactant sorption and protection received within cell aggregates, may operate independently or in tandem. Future research is needed to explore the complex interactions between cell titers (i.e., biomass), aggregate and/or biofilm formation, surfactant sorption, and the ability of *Dehalococcoides* organisms to tolerate surfactant exposure under *in situ* conditions. These studies should include Tween 80 and other surfactants applicable for SEAR to develop a comprehensive understanding of the effects of these compounds on key dechlorinators (e.g., *Dehalococcoides*).

Even though Tween 80 negatively affected *Dehalococcoides* organisms in pure and enriched cultures, dechlorination activity past *cis*-DCE was recovered following the removal of the surfactant, which simulates conditions following SEAR and subsequent surfactant degradation, dilution, sorption, and transport. The effects of Tween 80 on *Dehalococcoides* organisms were reversible because at least a fraction of the cells remained viable during exposure to the surfactant, suggesting that the *Dehalococcoides* population can rebound following SEAR. These findings, combined with (i) the tolerance of PCE-to-TCE and PCE-to-*cis*-DCE dechlorinators to Tween 80, (ii) the reduced influence of Tween 80 on *Dehalococcoides* cells in systems with high biomass and/or complex microbial assemblages, and (iii) the degradation of Tween 80 to organic acids and alcohols that serve as sources of reducing equivalents supporting reductive processes *(Ramsburg et al. 2004)*, suggest that staged treatment incorporating Tween 80 flushing followed by microbial reductive dechlorination is a promising remedial strategy for chlorinated ethene-impacted source zones. The feasibility of these “treatment train” approaches for source zone remediation needs to be validated in controlled field studies that monitor the fate and transport of Tween 80 (and other surfactants applicable for SEAR), surfactant fermentation and the production of organic acids, alcohols and hydrogen, and the activity, distribution, and abundance of key microorganisms during and after source zone flushing.

III.2 METABOLIC REDUCTIVE DECHLORINATION IN 1D COLUMNS

III.2.1 Column experiments with S. multivorans

III.2.1.1 Microbial elution phase

As described in Amos et al. *(2008a)*, the inoculum for the mixed NAPL column experiment contained 8.0 ± 3.2 x 10^7 *pceA* genes (i.e., *S. multivorans* cells) per mL, and a total of 3.2 ± 1.3 x 10^{10} *S. multivorans* cells were added to the column (pore volume of 397 mL) during column packing. During the microbial elution phase, the number of cells detected in the effluent ranged from 1.2 ± 0.3 x 10^6 to 9.8 ± 1.3 x 10^6 per mL (Figure 22A), which was significantly lower than the cell titer of the inoculum. The cumulative and percent recovery of cells (i.e., *pceA* genes) in the effluent during the microbial elution phase is shown in Figure 22B. Only 26% of the biomass initially present in the column was recovered in the effluent after 4.3 PV of flushing, indicating significant retention of *S. multivorans* cells within the column. Similar results were observed in the pure PCE-DNAPL column experiment, where approximately 30% of the cells added to the column were recovered in the effluent after 3.3 PV of flushing (data not shown).

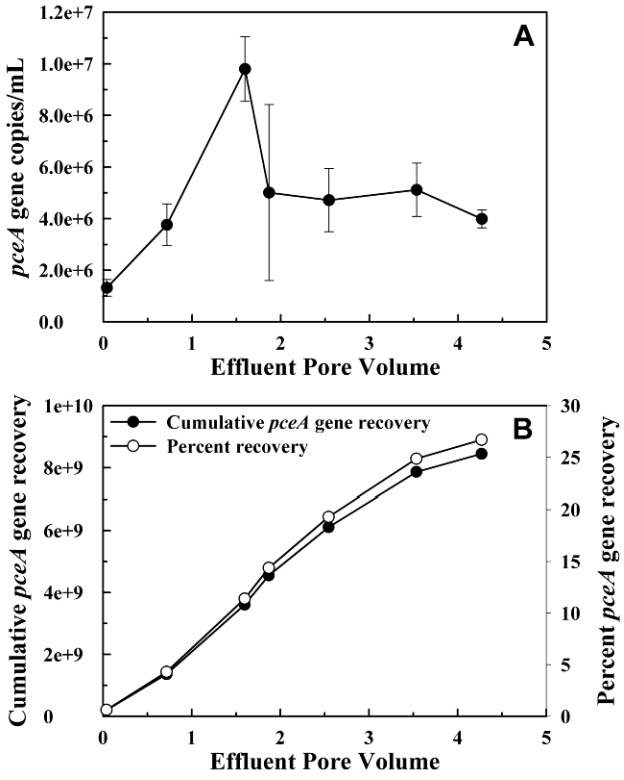

Figure 22: Effluent *pceA* gene copies per mL (A) and cumulative and percent *pceA* gene recoveries (B) during the microbial elution phase of the *S. multivorans* mixed-NAPL experiment *(Amos et al. 2008a)*.

III.2.1.2 NAPL dissolution from mixed-NAPL

III.2.1.2.1 Effluent samples

After NAPL imbibition and flushing with approximately 2 PV of pyruvate-amended medium, the number of *pceA* genes detected in the column effluent sharply increased from 10^6–10^7 per mL to approximately 2 x 10^9 per mL at 4 PV (data not shown). This 2 to 3 orders-of-magnitude increase in cell numbers was maintained over the course of the mixed-NAPL experiment, resulting in the recovery of approximately 10^{13} *S. multivorans* cells. This value is substantially greater than the total number of cells added to the column initially (ca. 3 x 10^{10}), indicating that significant growth of *S. multivorans* occurred in the column.

Effluent chlorinated ethene concentrations and pH during the mixed-NAPL column experiment are shown in Figure 23. Minimal dechlorination of PCE occurred during the initial 2 PV of flushing, which corresponds to the time when minimal growth of *S. multivorans* was observed. Following this initial lag period, dissolved-phase PCE was completely dechlorinated to *cis*-DCE and trace amounts of *trans*-DCE. After 3 PV of flushing, PCE was no longer detected in the effluent. At early time (< 5 PV), the total chlorinated ethene concentration approached the expected equilibrium value (~300 μM; dashed line in Figure 23). After 5 PV of flushing, the *cis*-DCE concentrations sharply increased to a maximum value of 3,400 μM at 8.6 PV. For most of the mixed-NAPL column experiment, *cis*-DCE concentrations were significantly higher than the expected equilibrium value, indicating bioenhanced dissolution of PCE. After 8.6 PV of flushing, the *cis*-DCE concentration declined, reaching ca. 700 μM at the conclusion of the experiment. While this value is nearly 5 fold lower than the maximum *cis*-DCE concentration observed, it was still more than 200% greater than the expected equilibrium value, indicating that bioenhanced dissolution of PCE from the mixed NAPL was ongoing even at the termination of the column experiment.

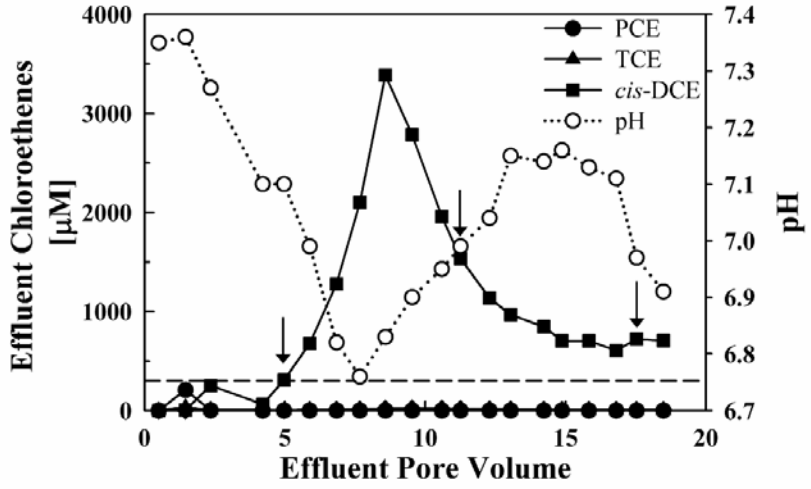

Figure 23: Effluent chlorinated ethene concentrations and pH measured during the NAPL dissolution phase of the *S. multivorans* mixed-NAPL column experiment. The expected chlorinated ethene concentration (~300 μM), based on aqueous phase solubility of PCE in equilibrium with the mixed-NAPL, is shown as the dashed line. Arrows indicate side port sampling events *(Amos et al. 2008a)*.

The decline in *cis*-DCE production and mass transfer enhancement from the NAPL could be caused by a number of factors, including (i) partial depletion of PCE from the mixed NAPL, (ii) diffusion limitations within the NAPL, or (iii) toxicity of high concentrations of *cis*-DCE to *S. multivorans*. Another possible explanation for reduced dechlorination activity after 8.6 PV is the observed decrease in pH (Figure 23). The microbial reductive dechlorination process is an acidifying process and for every mole of PCE dechlorinated to *cis*-DCE, 2 moles of protons (and chloride) are produced. In our system, changes in effluent pH generally correlated with changes in *cis*-DCE production (i.e., increasing *cis*-DCE concentrations resulted in decreasing pH) (Figure 23). The effluent pH decreased from ~7.35 to a minimum of ~6.75 when *cis*-DCE concentrations approached 3,400 μM. Reductive dechlorination by *S. multivorans* occurs optimally in a narrow pH range (7.0 – 7.5) *(Neumann et al. 1994)*, and the pH drop in the column may explain the decreased dechlorination activity. Adamson et al. *(Adamson et al. 2004)* observed that extensive PCE dechlorination lowered the pH below 5 in NAPL-containing batch systems and speculated that lower pH values decreased both the rate and extent of dechlorination. Enhancement of NAPL dissolution and subsequent microbial dechlorination could decrease the performance of such biological systems as a result of low pH. Hence, enhanced source zone bioremediation requires careful monitoring and control of the pH to achieve sustained microbial dechlorination activity.

III.2.1.2.2 Side port samples

Concentrations of chlorinated ethenes measured in aqueous side port samples are shown in Figure 24. The first side port sampling event after 5 PV of flushing (Figure 24A) coincided with the onset of bioenhanced dissolution (Figure 23). Aqueous phase PCE concentrations approached the equilibrium value (300 μM) in the source zone (Ports 1 and 2, 0-10 cm) during this sampling event. Likewise, TCE and *cis*-DCE concentrations in the same region were relatively low (< 60 μM and <105 μM, respectively). In the transition zone (Ports 3 and 4, 10-20 cm), PCE was dechlorinated to *cis*-DCE and traces of *trans*-DCE. Interestingly, *cis*-DCE concentrations in the transition zone were significantly higher than the expected equilibrium value of 300 μM, indicating bioenhanced dissolution from the NAPL ganglia in this region. *cis*-DCE concentrations were higher in the even-numbered ports (right-hand side of the column) than in the odd-numbered ports (left-hand side of the column) in the transition (Ports 3 and 4) and down-gradient (Ports 5-11, 20-60 cm) zones of the column. These concentration differences likely resulted from the nonuniformly-distributed NAPL ganglia along the right-hand side of the column (even-numbered ports), which was observed visually. The nonuniform NAPL saturation effectively increased the source zone length on one side of the column, thereby increasing the contact time between the entrapped NAPL and the aqueous phase traveling through this region. Bioenhanced dissolution from residual NAPL zones has been predicted to increase with source zone length *(Chu et al. 2004; Christ and Abriola 2007)*, and a recent study *(Glover et al. 2007)* reported greater bioenhanced dissolution from NAPL pools with transition zones compared to NAPL pools with sharp boundaries. Our results also suggest that source zone NAPL architecture (e.g., the presence of nonuniform NAPL saturation in transition zones) strongly influences the extent of bioenhanced dissolution.

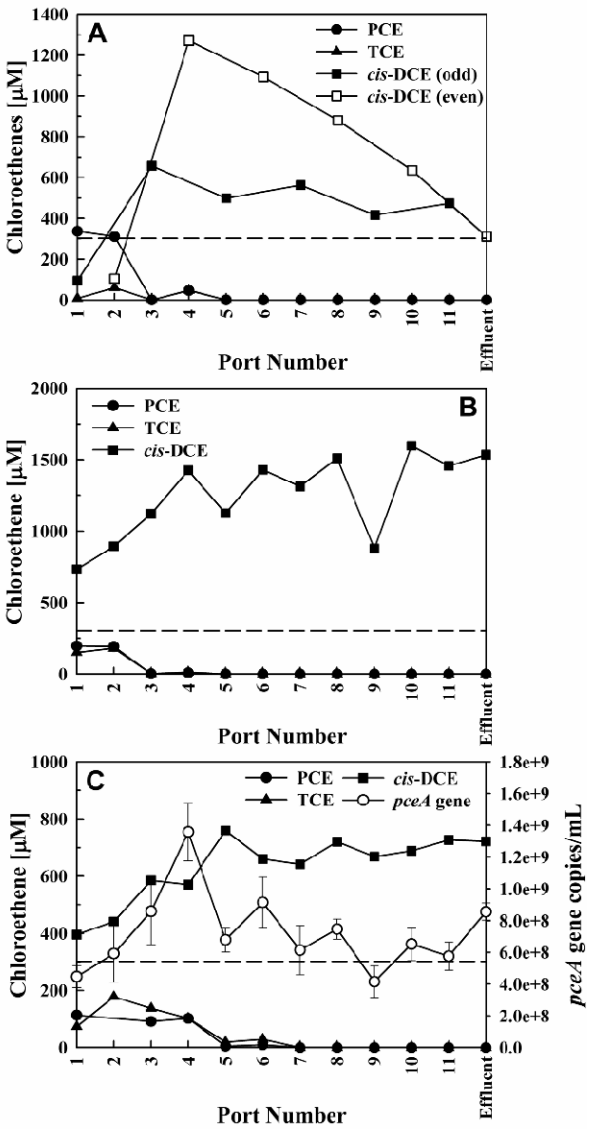

Figure 24: Profiles of chlorinated ethene concentrations and microbial cell numbers along the length of the column in the *S. multivorans* mixed-NAPL experiment after 5, 11, and 17.5 pore volumes of flushing (panels A, B, and C, respectively). Effluent concentrations taken at the same time are shown for comparison. Two profiles for *cis*-DCE are presented in panel A: one profile represents samples from the odd numbered ports and one represents samples from the even-numbered ports. The expected chlorinated ethene concentration (300 µM), based on aqueous phase solubility of PCE in equilibrium with the mixed-NAPL, is shown as the dashed lines. Port 1 is nearest the influent and in the source zone while Port 11 is nearest the effluent *(Amos et al. 2008a).*

The second side port sampling event occurred after 11 PV of flushing when effluent *cis*-DCE concentrations were declining (Figure 24B). Dissolved-phase PCE was detected in the source zone (Ports 1 and 2) but at concentrations below the expected equilibrium value. TCE (150-200 µM) was also detected in Ports 1 and 2, indicating that dechlorination activity occurred in the source zone. Both PCE and TCE were completely dechlorinated 20 cm down-gradient of the

column influent (i.e., Port 4), and *cis*-DCE concentrations increased throughout the source and transition zones (Ports 1-4), indicating bioenhanced dissolution. In the down-gradient plume region (Ports 5-11), *cis*-DCE concentrations remained relatively stable at elevated levels (1,300 - 1,500 μM) and closely matched the measured effluent concentrations. The sampling needle could not be fully inserted into the column at Ports 5 and 9 during the 11 PV side port sampling event due to blockage of the port capillaries with sand grains. As a result, samples were withdrawn from the dead-volume of Port 5 and 9, which is a likely explanation for the lower *cis*-DCE concentrations observed in these ports as compared to the rest of the plume region (Figure 4B).

The final side port sampling event (Figure 24C) occurred after 17.5 PV of flushing when effluent *cis*-DCE concentrations had declined to ca. 700 μM. Dissolved-phase PCE was detected in the source zone, but unlike the previous side port profiles, was not completely dechlorinated to *cis*-DCE until about the midpoint of the column. Both TCE and *cis*-DCE were detected in Ports 1-4, again indicating ongoing dechlorination activity in the source zone. *cis*-DCE concentrations increased throughout the source and transition zones (Ports 1-4) and reached concentrations >300 μM indicative of bioenhanced dissolution. In the down-gradient plume region (Ports 5-11), *cis*-DCE concentrations remained relatively stable at elevated levels (650 to 750 μM). Overall, chlorinated ethene concentrations were lower at 17.5 PV (Figure 24C) as compared to 11 PV (Figure 24B), which is consistent with the effluent data (Figure 23). The *pceA* genes were quantified to estimate planktonic cell numbers following 17.5 PV flushing (Figure 24C). The number of *pceA* genes increased from $4.5 \pm 0.7 \times 10^8$ to $1.4 \pm 0.2 \times 10^9$ per mL over the source and transition zones (Ports 1-4), coinciding with an increase in *cis*-DCE concentrations over the same interval (Figure 24C). In the down-gradient plume region of the column (Ports 5-11), the number of *pceA* genes was slightly lower than those observed in the transition zone. A comparable spatial distribution of *S. multivorans* within the column was observed with solid-phase (i.e., sand) samples collected after the column was sectioned (18.5 PV) (data not shown). These results demonstrate that *S. multivorans* was active and grew in the mixed-NAPL source zone, emphasize that source zone architecture affects the extent of bioenhanced dissolution, and suggest that aqueous phase sampling is a suitable approach for quantitative microbial monitoring.

III.2.1.3 NAPL dissolution from pure PCE-DNAPL

Throughout the pure PCE-DNAPL column experiment, effluent PCE concentrations approached the solubility limit of PCE (ca. 1,200 μM, Figure 25). Only minimal dechlorination occurred, resulting in trace levels of TCE (< 5 μM) and *cis*-DCE (< 8 μM) in the effluent. Thus, no enhancement in PCE dissolution occurred in the column containing the pure PCE-DNAPL source zone. In contrast to the mixed-NAPL column experiment, the number of *pceA* genes per mL detected in the effluent sharply declined following pure PCE-DNAPL addition (ca. 2 orders-of-magnitude; data not shown). Although *pceA* genes were detected at low levels throughout the experiment, the number of gene copies never exceeded those detected prior to PCE-DNAPL addition. The lack of significant dechlorination activity and absence of growth indicate that *S. multivorans* did not tolerate saturating PCE concentrations. This result is consistent with previous observations in batch culture experiments, which indicated that known PCE dechlorinators cannot tolerate elevated PCE concentrations (≥ 540 μM) *(Amos et al. 2007a)*. It

should be noted that the conditions within the pure PCE-DNAPL experiment represent a "worst case" scenario where the PCE concentration approaches the solubility limit (ca. 1,200 μM). It is unlikely that PCE would uniformly reach such high concentrations throughout a real-world DNAPL source zone due to heterogeneities in both the groundwater flow field and DNAPL saturation distribution (see further discussion in Amos et al. *(2007a)*).

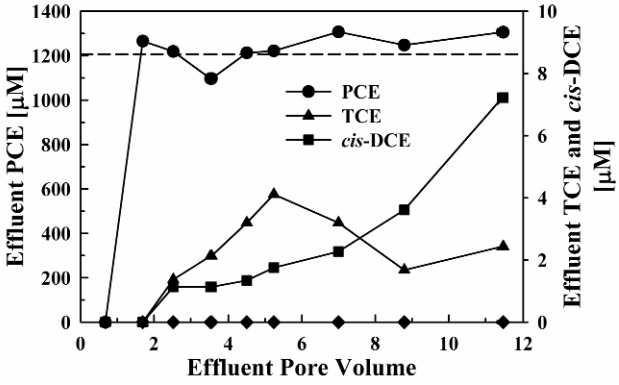

Figure 25: Effluent chlorinated ethene concentrations measured during the NAPL dissolution phase of the *S. multivorans* pure PCE-DNAPL column experiment. The expected chlorinated ethene concentration (1,200 μM), based on equilibrium aqueous phase solubility of pure PCE, is shown as the dashed line *(Amos et al. 2008a).*

III.2.1.4 Cumulative mass recoveries and mass transfer enhancement factors

For the mixed-NAPL column experiment, approximately 53% of the PCE initially present in the residual NAPL source zone was recovered in the column effluent (Figure 26A), primarily as *cis*-DCE (Table 3). This level of PCE mass recovery was significantly greater than that expected under abiotic conditions (11.6%, Table 3). As shown in Figure 26B, the cumulative mass transfer enhancement factor was approximately unity (i.e., no enhancement) for the first 5 PV of operation of the mixed-NAPL column. After 5 PV, the cumulative mass transfer enhancement increased sharply before stabilizing at ca. 4.6. An alternative method of calculating mass transfer enhancement is to compare experimental effluent concentrations to abiotic effluent concentrations (see the *Supplementary Material* of reference *(Amos et al. 2008a)*). Enhancement factors calculated in this manner (termed maximum herein) are commonly reported in the literature and are always higher than cumulative enhancement factors. For the mixed-NAPL column, the maximum mass transfer enhancement was 13.6-fold (Table 3), but this occurred at only one time point during the experiment (8.6 PV, Figure 23). The enhancement factors determined for the mixed-NAPL column experiment, either cumulative or maximum, are comparable to the enhancement factors reported in the literature, which range from 1.5 to 14 *(Carr et al. 2000; Yang and McCarty 2000; Cope and Hughes 2001; Adamson et al. 2003; Sleep et al. 2006; Glover et al. 2007).* In the pure PCE-DNAPL column experiment, approximately 6.5% of the PCE initially present in the DNAPL phase was recovered in the effluent (Table 3). This level of PCE mass recovery was virtually identical to that expected under abiotic conditions, assuming an equilibrium solubility of 1,200 μM. Due to the lack of significant microbial reductive dechlorination, enhancement of mass transfer was not observed in the pure PCE-DNAPL column experiment, resulting in no dissolution enhancement and cumulative and maximum enhancement factors close to 1 (Table 3).

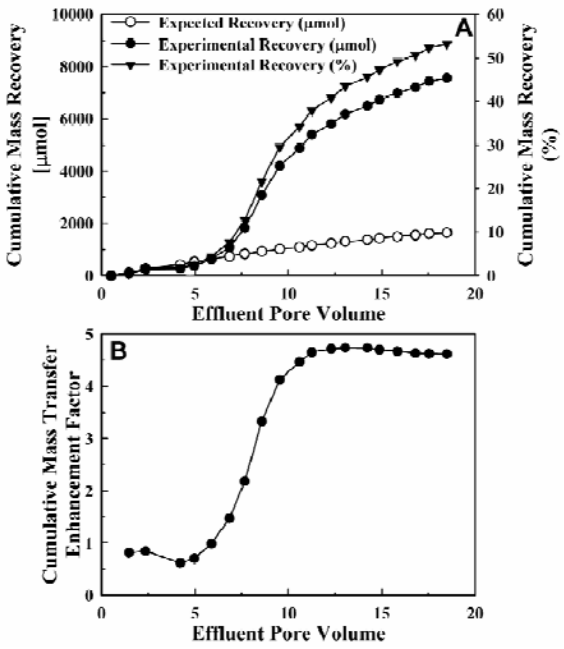

Figure 26: Cumulative chlorinated ethene mass and percent recoveries (A) and the cumulative mass transfer enhancement factor (B) for the *S. multivorans* mixed-NAPL column experiment *(Amos et al. 2008a).* Details on how the cumulative recoveries and the cumulative mass transfer enhancement factor were calculated are presented in the *Supplementary Material* of reference *(Amos et al. 2008a).*

Table 3: Cumulative chlorinated ethene recoveries and mass transfer enhancement factors for the *S. multivorans* mixed-NAPL and pure PCE-DNAPL column experiments *(Amos et al. 2008a).*

	Column Experiment	
Parameter	**Mixed-NAPL [a]**	**PCE-DNAPL**
Initial PCE Loading (μmol)	14,200	87,000
Total Chlorinated Ethenes Recovered (μmol) [%]	7,570 [53.3]	5,640 [6.48]
PCE Recovered (μmol) [%]	76 [0.5]	5,620 [6.46]
TCE Recovered (μmol) [%]	13 [<0.1]	5 [0.01]
cis-DCE Recovered (μmol) [%]	7,410 [52.2]	14 [0.02]
trans-DCE Recovered (μmol) [%]	67 [0.5]	0 [0]
Expected Abiotic PCE Recovered (μmol) [%]	1,640 [11.6]	5,430 [6.24]
Enhancement Factors		
Maximum Mass Transfer Enhancement Factor	13.6	1.09
Cumulative Mass Transfer Enhancement Factor	4.6	1.04

[a] 0.25/0.75 (mol/mol) PCE dissolved in hexadecane

III.2.1.5 Summary of the column experiments with S. multivorans

Microbial reductive dechlorination is a promising approach for the remediation of PCE-NAPL source zones, but little is known regarding microbial growth and distribution within NAPL source zones during bioenhanced PCE dissolution. Here, we presented the results of continuous-flow column experiments designed to evaluate the distribution and activity of *S. multivorans*, a PCE-to-*cis*-DCE dechlorinator, within a mixed-NAPL (0.25 mol/mol PCE in hexadecane) and a pure PCE-DNAPL source zone. The following specific conclusions can be drawn from this study:

1. For the mixed-NAPL column experiment:
   - The number of *S. multivorans* cells in the column effluent increased 2-3 orders-of-magnitude following NAPL imbibition and continuous addition of electron donor,
   - Growth of *S. multivorans* corresponded to the onset of PCE dechlorination and significant accumulation of *cis*-DCE,
   - *S. multivorans* colonized and was active within the mixed-NAPL source zone, and
   - *S. multivorans* activity resulted in enhanced PCE-NAPL dissolution, up to 13.6-fold (cumulatively 4.6-fold) relative to abiotic dissolution.
2. *S. multivorans* failed to grow, dechlorinate, or enhance contaminant dissolution in the pure PCE-DNAPL column experiment, presumably due to inhibitory concentrations of PCE.

The results of the column experiments performed under precisely controlled conditions suggest that source zone architecture (i.e., length, presence of transition zones [i.e., nonuniformly-distributed ganglia]) strongly influences bioenhanced NAPL dissolution. Hence, future research should evaluate microbial distribution and bioenhanced NAPL dissolution in heterogeneous, multi-dimensional systems (e.g., 2-D aquifer cells) to clearly delineate the effects of source zone architecture on microbially-enhanced NAPL dissolution. Further, our studies emphasize the need for efficient pH control to compensate for the acidifying effect of dechlorination, which reduces microbial dechlorination activity and dissolution bioenhancement. To date, all chlorinated ethene-dechlorinating bacteria have been enriched and isolated using cultivation conditions that maintain circumneutral pH. With the prospect of successful biological source zone remedies, the search for dechlorinators that tolerate and are active at lower pH (e.g., 5-6) should intensify.

III.2.2 Column experiment with BDI-SZ

III.2.2.1 Microbial elution phase

As described in Amos et al. *(2008b)***,** the BDI-SZ consortium used as inoculum for the column experiment contained $3.5 \pm 1.1 \times 10^5$ *Dehalobacter*, $6.3 \pm 0.9 \times 10^7$ *Geobacter*, and $1.8 \pm 0.3 \times 10^8$ *Dehalococcoides* cells per mL, resulting in a total addition of $1.4 \pm 0.4 \times 10^8$ *Dehalobacter*, $2.6 \pm 0.4 \times 10^{10}$ *Geobacter*, and $7.5 \pm 1 \times 10^{10}$ *Dehalococcoides* cells to the column (pore volume of 407 mL). The numbers of *Dehalobacter*, *Geobacter*, and *Dehalococcoides* cells recovered in the column effluent during the microbial elution phase are shown in Figure 27A. For *Dehalobacter*, a significant decrease (ca. 1.8 orders-of-magnitude) was observed between the cell titers of the inoculum and the first effluent sample (Figure 27A). For *Geobacter* and

Dehalococcoides, cell titers in the first effluent sample were only slightly lower than those measured in the inoculum (Figure 27). For all three dechlorinators, effluent cell titers remained relatively constant over the first 1.5 PV of flushing, after which the cell titers decreased (Figure 27A). At the conclusion of the 3.3 PV microbial elution phase, 2%, 65%, and 90% of the *Dehalobacter*, *Geobacter*, and *Dehalococcoides* cells initially present in the column, respectively, were recovered in the effluent (Figure 27B). In our prior column experiments with *S. multivorans*, only 26–30% of the biomass added to the columns were recovered *(Amos et al. 2008a)*. These results suggest dechlorinator specific attachment/retention characteristics and warrant further exploration of microbial attachment and transport processes relevant to bioremediation systems. Interestingly, *Dehalobacter* cell numbers were below detection throughout the rest of the experiment in aqueous-phase effluent and side port samples as well as in solid-phase (sand) samples. These results indicate that the added *Dehalobacter* organisms were not attached to the porous medium and suggest that the majority of the *Dehalobacter* cells added to the column lysed during the initial column setup. This hypothesis is consistent with the significant difference observed between the *Dehalobacter* cell titers in the inoculum and the first effluent sample. Additional studies are needed to evaluate the survival and resilience of *Dehalobacter* organisms during bioaugmentation.

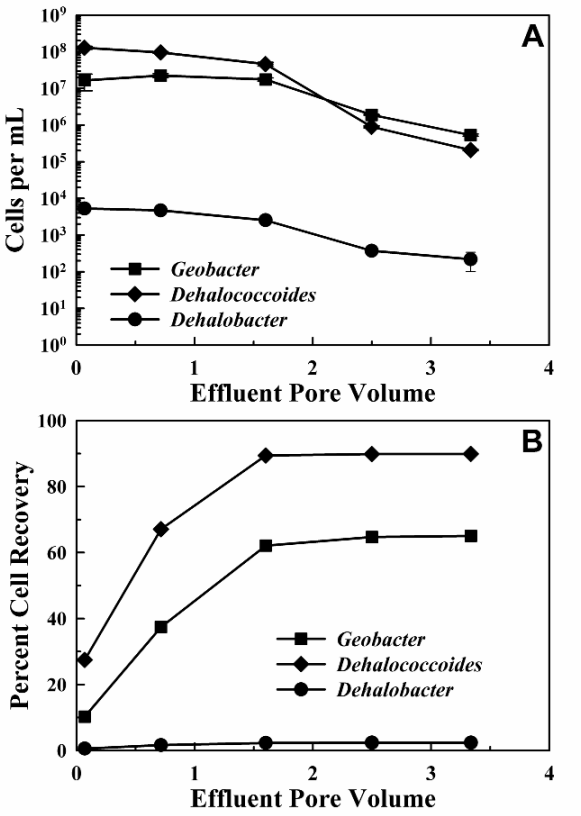

Figure 27: Effluent cell numbers per mL (A) and percent cell recoveries (B) for *Geobacter*, *Dehalococcoides*, and *Dehalobacter* during the microbial elution phase of the BDI-SZ column experiment.

III.2.2.2 NAPL dissolution phase

Effluent chlorinated ethene and ethene concentrations following NAPL imbibition are shown in Figure 28A. During the first 4 PV of flushing, minimal dechlorination of dissolved-phase PCE occurred (Figure 28A), although TCE (ca. 40 μM), *cis*-DCE (ca. 20 μM), and traces of VC (< 5 μM) were detected. Between 4 PV and 11 PV, PCE was completely dechlorinated to *cis*-DCE and small amounts of VC (4 – 25 μM). The total chlorinated ethene concentration approached the expected equilibrium value (black dashed line in Figure 28A) for approximately the first 11 PV, indicating that biologically-enhanced PCE dissolution from the NAPL did not initially occur. Side port samples collected at 8.7 PV indicated minimal dechlorination activity in the source zone but complete conversion of PCE to *cis*-DCE down gradient of the source zone (data not shown), corroborating that significant dechlorination activity is required within source zones to achieve bioenhanced NAPL dissolution. After 11 PV of operation, effluent *cis*-DCE concentrations rapidly increased before reaching a maximum of ca. 2,600 μM at 19.5 PV (Figure 28A). The *cis*-DCE concentrations following 11 PV were significantly higher than the expected equilibrium value, indicating bioenhanced dissolution of PCE from the NAPL phase. *cis*-DCE concentrations gradually declined after 19.5 PV of flushing, falling below 5 μM by 30 PV. *cis*-DCE concentrations initially rebounded following the flow rate reduction at 21.6 PV, likely a result of the increased column residence time.

VC was detected in the effluent throughout the NAPL dissolution phase, although at concentrations significantly lower than *cis*-DCE (Figure 28A). VC concentrations slowly increased after NAPL imbibition before leveling off at ca. 50 μM by 14 PV (Figure 28A). A spike in VC concentrations to ca. 200 μM was observed following the flow interruption at 16.8 PV, but when column operation resumed, VC concentrations returned to levels similar to those observed before the flow interruption. After the flow rate was reduced at 21.6 PV, VC concentrations steadily increased to a maximum of ca. 300 μM (28.5 PV, Figure 28A). These results suggest that the column residence time was insufficient for significant dechlorination beyond *cis*-DCE.

The sharp decrease in the total chlorinated ethene concentration (primarily *cis*-DCE and VC) by 30 PV indicated complete depletion of PCE from the mixed-NAPL (Figure 28A). This decline corresponded to the onset of ethene production. In fact, ethene (21 μM) was first detected at 29.3 PV when *cis*-DCE and VC concentrations reached 6 μM and 105 μM, respectively. These results suggest that VC dechlorination to ethene was inhibited by the presence of elevated concentrations of *cis*-DCE, as has been previously documented for other dechlorinating consortia *(Yu and Semprini 2004; Yu et al. 2005).* Accumulation of *cis*-DCE, therefore, might limit complete detoxification of PCE to ethene unless system residence times are sufficiently long for sequential conversion of *cis*-DCE to VC before VC conversion to ethene. Future work is needed to address the influence of residence times *(Da Silva et al. 2006)* and *cis*-DCE toxicity *(Chu et al. 2004; Chu et al. 2006)* on complete detoxification of PCE during bioenhanced dissolution.

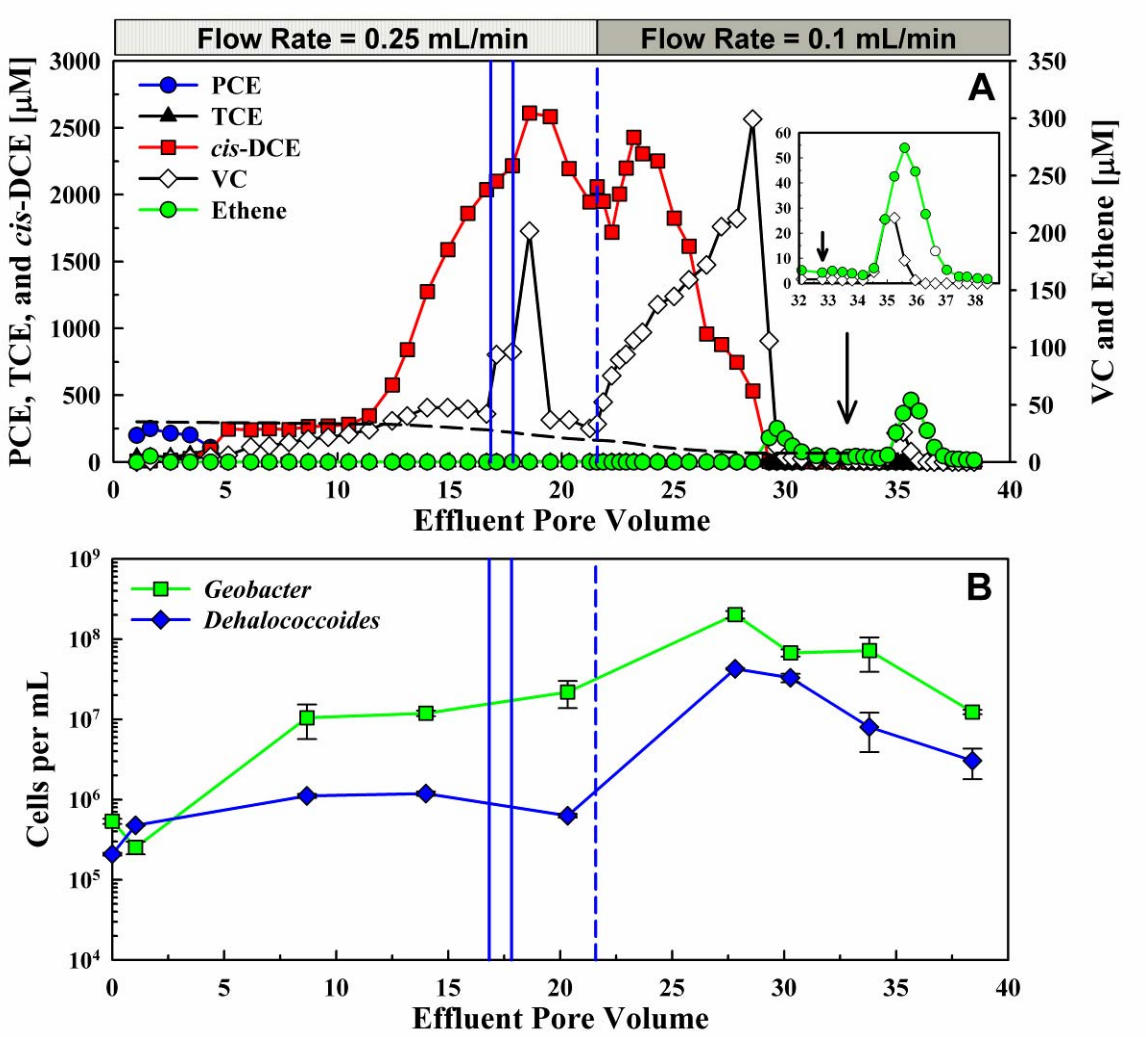

Figure 28: Effluent chlorinated ethene concentrations (A) and effluent cell titers (B) measured during the NAPL dissolution phase of the BDI-SZ column experiment. In (A), the expected chlorinated ethene concentration based on equilibrium solubility of PCE is shown with the black dashed line (left-hand-side y-axis); the expected value was initially ca. 300 μM but decreased with changing NAPL composition due to PCE mass depletion (see text for details). The inset in (A) shows effluent VC and ethene concentrations after a ca. 1.1 PV pulse of VC-amended medium was flushed through the column (the pulse began at 32.8 PV; see arrows). In both (A) and (B), the pore volume residing in the column during the flow interruption (ca. 22 hours at 16.8 PV) is bracketed by the solid blue lines, and the change in flow rate from 0.25 mL/min to 0.1 mL/min is demarcated by the dashed blue line (21.6 PV) (*Amos et al. 2008b)*.

III.2.2.3 Vinyl chloride (VC) pulse

To determine if conditions within the column were conducive to significant dechlorination of VC to ethene and to assess the performance of VC-to-ethene dechlorinating organisms (i.e., *Dehalococcoides* strains), the influent medium was amended with VC for ca. 1.1 PV at 32.8 PV. As shown in the inset of Figure 28A, effluent VC and ethene concentrations began to increase over background levels at 34.5 PV of column operation (1.7 pore volumes after initiation of the

pulse of VC-amended medium). VC concentrations increased to a maximum value of 26.1 μM at 35.2 PV before returning to background levels by 35.9 PV. Ethene concentrations (53.9 μM at 35.6 PV) were observed at approximately twice the level of VC, and ethene remained above background levels for much longer than VC. For both VC and ethene, the delay in VC and ethene breakthrough and the spreading (widening) of the breakthrough curves indicate that some VC and ethene retardation occurred in the column. The retardation was attributed to partitioning of VC and ethene into residual hexadecane (data not shown) and discrete gas bubbles formed within the column during operation. Approximately 97.4% of the chlorinated ethene mass associated with the VC pulse was recovered in the effluent, with 75.6% of the total VC added to the column recovered as ethene in the effluent and the remaining 21.8% recovered as VC. Calculation of these recoveries corrected for the background levels of VC and ethene, which were assumed to be constant at 1.3 μM and 4.2 μM, respectively, based on effluent concentrations prior to the VC pulse. The results of the VC pulse indicate that ethene formation within the column was possible and provide further evidence that the lack of significant ethene production throughout most of the column experiment was likely due to inhibition by polychlorinated ethenes (i.e., the presence of significant amounts of *cis*-DCE).

III.2.2.4 Effluent pH

Periodic pH measurements were taken during the NAPL dissolution phase (data not shown). While the pH trends were not as clear as those demonstrated in the *S. multivorans* column experiment *(Amos et al. 2008a)*, increasing concentrations of PCE dechlorination products generally correlated to decreases in effluent pH. The pH decrease was attributed to the production of hydrochloric acid during each reductive dechlorination step. Even though the influent medium was well buffered (60 mM $NaHCO_3$), effluent pH decreased from 7.25 to a minimum of 6.77, which is comparable to the pH reduction observed in the *S. multivorans* column experiment *(Amos et al. 2008a)*. pH levels below the optimum levels of dechlorinators (e.g., 7.2-7.4 for *Dehalococcoides (He et al. 2003; He et al. 2003)*) may have contributed to the minimal VC and ethene production (for further discussion, see above and reference *(Adamson et al. 2004)*).

III.2.2.5 Effluent cell titers

Although *Dehalobacter* organisms were not detected after the microbial elution phase and NAPL imbibition (see above), growth of both *Geobacter* and *Dehalococcoides* populations was observed during the NAPL dissolution phase (Figure 28B). The number of *Geobacter* and *Dehalococcoides* cells increased from $5.4 \pm 0.4 \times 10^5$ cells per mL and $2.1 \pm 0.1 \times 10^5$ cells per mL, respectively, directly after NAPL imbibition and lactate amendment to $1.1 \pm 0.5 \times 10^7$ per mL and $1.1 \pm 0.1 \times 10^6$ per mL, respectively, at 8.7 PV (Figure 28B). The number of *Geobacter* (ca. 10^7) and *Dehalococcoides* (ca. 10^5-10^6) cells detected in the effluent remained relatively constant over the first 21 PV of column operation. In general, *Geobacter* cell numbers were more than one order-of-magnitude higher than *Dehalococcoides* cell numbers during this period, which is consist with the production of substantial quantities of *cis*-DCE, limited production of VC, and no ethene formation (Figure 28A). Although cell numbers of both organisms increased after the flow rate was reduced, *Dehalococcoides* cell numbers increased by approximately 2 orders-of-magnitude while *Geobacter* cell numbers only increased by approximately one order-

of-magnitude (Figure 28B). The relative changes in *Dehalococcoides* and *Geobacter* cell numbers are consistent with decreased *cis*-DCE production and increased VC production between 21 PV and 30 PV (Figure 28A). After reaching maxima at 27.8 PV, the number of *Geobacter* and *Dehalococcoides* cells declined throughout the remainder of the experiment, coinciding with the sharp decrease in the total chlorinated ethene concentration after PCE depletion from the mixed-NAPL.

III.2.2.6 Side port samples

During the NAPL dissolution phase, the side ports along the length of the column were sampled at 8.7, 14, 20.3, 27.8, and 30.3 PV of continuous flushing. The results from the side ports support the conclusions drawn from the effluent data (Figure 28) and confirm that both *Geobacter* and *Dehalococcoides* cells were present and active in the mixed-NAPL source zone. The results from all of the side port sampling events are generally consistent with one another; therefore, only representative results are presented here.

The results from the side port samples taken at 14 PV are shown in Figure 29, where Port 1 is nearest the influent and Port 11 is nearest the effluent. Ports 1 and 2 were within the source zone, and Ports 4-11 were in the plume region down gradient of the source zone. Due to some fingering of the imbibed NAPL, Port 3 was in a transition zone between the source zone and the plume region. The data presented in Figure 29A indicate significant dechlorination activity in the source zone. Although PCE was detected at levels close to the expected concentration (269 μM; dashed line in Figure 29A) in the source zone, TCE (100 μM) and *cis*-DCE (1,500 μM) were also observed. The high levels of *cis*-DCE within the source zone and adjacent ports show that bioenhanced dissolution was occurring, a result that is consistent with the effluent data at 14 PV (see Figure 28A). VC was not detected in the source zone (Ports 1-3). Down gradient of the source zone, PCE and TCE were completely dechlorinated, *cis*-DCE concentrations remained relatively stable, and VC concentrations increased (Ports 4-11). VC was produced at significantly lower levels than *cis*-DCE (Figure 29A). Ethene was not observed in any sample from the 14 PV side port sampling event (Figure 29A). As shown in Figure 29B, the distribution of *Geobacter* and *Dehalococcoides* generally correlated with the chlorinated ethene concentration profile. For example, the number of *Geobacter* cells detected in the source zone (4.7×10^7 to 9.7×10^7 per mL) was slightly higher than the number detected in the plume region (1.2×10^7 to 2.8×10^7 per mL), consistent with complete conversion of PCE to *cis*-DCE by Port 4. In contrast, *Dehalococcoides* cell numbers were significantly lower in the source zone (4.6×10^4 to 1.1×10^5 per mL) than in the plume region (8.3×10^5 to 5.8×10^6 per mL), consistent with VC production only occurring down gradient of the source zone.

Although VC was not produced in the source zone at the 14 PV side port sampling event, VC was detected at trace levels (<10 μM) within the source zone at later times. For example, Figure 30 shows that VC was produced in the source zone (Ports 1 and 2) at the 27.8 PV sampling event. *Dehalococcoides* cell numbers within the source zone at 27.8 PV (Figure 30) were approximately an order-of-magnitude greater than those observed at 14 PV (Figure 29B). These results indicate that *Dehalococcoides* organisms successfully colonized and were active within a PCE-NAPL source zone. Interestingly, *Dehalococcoides* cell numbers generally increased 1 to 2 orders-of-magnitude over the length of the column (e.g., from the source zone area to the column

exit) (Figures 29B and 30). In fact, the increase in *Dehalococcoides* cell numbers throughout the column often paralleled increases in VC concentrations, as illustrated in the side port samples from 27.8 PV (Figure 30).

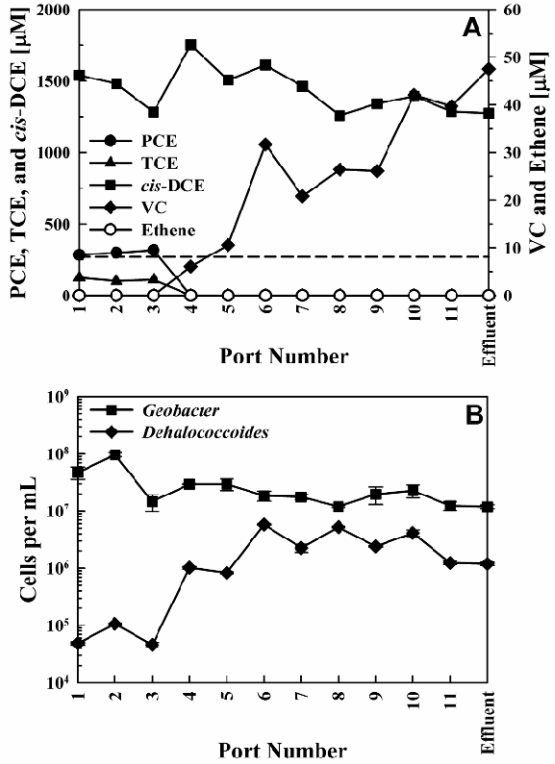

Figure 29: Profiles of chlorinated ethene concentrations (A) and microbial cell titers (B) along the length of the column following 14 pore volumes of flushing during the BDI-SZ column experiment. Effluent concentrations taken at the same time are shown for comparison. The expected chlorinated ethene concentration (269 μM) at 14 PV, based on equilibrium solubility of PCE and accounting for changing NAPL composition due to PCE mass depletion (see text for details), is shown with the dashed line in (A). Port 1 is nearest the influent and in the source zone while Port 11 is nearest the effluent (*Amos et al. 2008b)*.

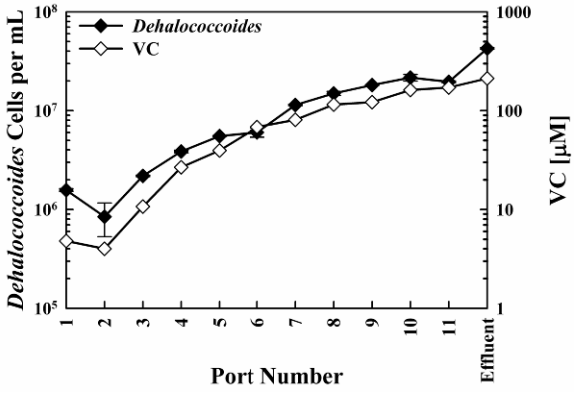

Figure 30: Profiles for VC and *Dehalococcoides* cell titers along the length of the column following 27.8 pore volumes of flushing during the BDI-SZ column experiment. Effluent concentrations taken at the same time are shown for comparison. Port 1 is nearest the influent and in the source zone while Port 11 is nearest the effluent (*Amos et al. 2008b)*.

III.2.2.7 Final microbial distribution

At the conclusion of the experiment, the final microbial distribution was determined with both solid-phase (sand) samples (Figure 31A) and side port (liquid) samples (Figure 31B). The solid-phase samples were taken after termination of column operation (at 38.5 PV), while the side port samples were taken at 38.4 PV. Although high numbers of *Geobacter* and *Dehalococcoides* cells were detected in the source zone and over the entire length of the column in the solid-phase and aqueous phase samples (Figures 31A and 31B), differences between the profiles were observed. For example, *Geobacter* organisms were detected at 1.8×10^7 to 2.6×10^7 cells per gram of sand in the source zone (Ports 1-3; Figure 31A). In the down gradient plume region (Ports 4-11), the number of *Geobacter* cells was approximately 1-2 orders-of-magnitude lower (4.8×10^5 to 3.5×10^6 cells per gram sand) than in the source zone (Figure 31A). Therefore, the solid-phase (sand) samples indicate that *Geobacter* organisms not only grew within the source zone but also attached to the porous medium within the source zone. This trend was not observed in the side port (liquid) samples (Figure 31B), where *Geobacter* cell numbers ranged from 3.9×10^6 to 3.5×10^7 per mL. In contrast to the profiles for *Geobacter*, the profiles for *Dehalococcoides* from the solid-phase (sand) and side port (liquid) samples were relatively similar to one another (Figures 31A and 31B). Additional studies are needed to evaluate the role of microbial attachment and possibly biofilm formation in bioenhanced dissolution and in promoting complete contaminant detoxification (i.e., ethene formation). The differences between the liquid and solid-phase profiles observed here also suggest that the form of environmental sample (aquifer solids or groundwater) might influence bioremediation monitoring and assessment with molecular biological tools (e.g., qPCR); additional work is needed to evaluate the differences between liquid and solid-phase samples for accurate microbial analysis.

III.2.2.8 Cumulative mass recoveries and mass transfer enhancement factors

Cumulative chlorinated ethene recoveries, on a molar as well as a percent basis, are summarized in Table 4 and Figure 32A. A detailed description of how cumulative mass recoveries and mass transfer enhancement factors were calculated is provided in the *Supplementary Material* of reference *(Amos et al. 2008a)*. Cumulative mass recoveries include data from the NAPL dissolution phase (0 - 32.8 PV), but not from the pulse of VC-amended influent medium. Approximately 83% of the PCE initially present in the NAPL source zone was recovered in the column effluent (Figure 32A), primarily as *cis*-DCE (Table 4). This recovery is lower than expected since several lines of evidence indicate that the mixed-NAPL became completely depleted of PCE. A number of factors may have contributed to the mass balance discrepancy: (i) observations of side port septa swelling suggests PCE mass was lost via sorption to septa, especially in Port 1, (ii) visually observed mobilization of the mixed-NAPL around the bottom end-cap of the column removed some NAPL from the column, (iii) some NAPL was unintentionally, but unavoidably, removed from the column during side port sampling events, and (iv) partitioning into residual hexadecane and/or discrete gas bubbles formed within the column during operation may have acted as a sink for *cis*-DCE, VC, and ethene. Mass losses by these mechanisms could not be accurately quantified. These factors highlight the complexity of the column system and imply that the observed mass recovery is not unreasonable.

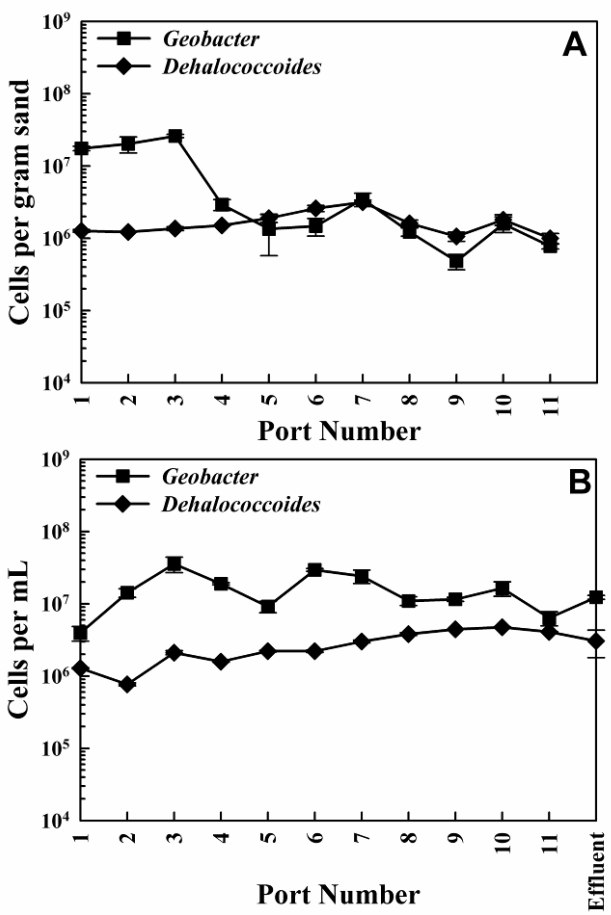

Figure 31: Microbial distribution of *Geobacter* and *Dehalococcoides* determined with (A) solid-phase (sand) samples and (B) side port (liquid) samples for the BDI-SZ column experiment. The solid-phase samples were taken after column dissection at 38.5 PV, and the side port samples were taken after 38.4 PV of column operation. Port 1 is nearest the influent and in the source zone while Port 11 is nearest the effluent. Effluent concentrations taken at the same time are shown in (B) for comparison (*Amos et al. 2008b)*.

Although some contaminant mass was unaccounted for, the observed, experimental recovery of 83% is still significantly greater than the expected mass recovery under abiotic conditions (16%; see Table 4) (see the *Supplementary Material* of Amos et al. *(2008a)* for more information on these calculations). The expected abiotic mass recovery was estimated by assuming an initial aqueous PCE solubility of ca. 300 μM, accounting for changing NAPL composition with PCE mass depletion (i.e., PCE mass depletion lowered the PCE mole fraction in the mixed-NAPL), and assuming equilibrium mass transfer at both operational flow rates. Initially (<12 PV), the cumulative experimental and expected abiotic mass recoveries were almost identical (Figure 20A). This is consistent with the data shown in Figure 28A, which also indicates little bioenhanced dissolution at < 12 PV. At ca. 12 PV, the experimental mass recovery increased significantly faster than the expected abiotic recovery, indicating bioenhanced dissolution and suggesting microbial colonization of the source zone. To quantify the extent of the enhancement, a cumulative mass transfer enhancement factor was calculated by dividing the experimental mass recovery by the expected mass recovery (see the *Supplementary Material* of Amos et al. *(2008a)*). As shown in Figure 32B, the cumulative mass transfer enhancement factor

was approximately unity (i.e., no enhancement) for the first 12 PV of column operation. After this time, the cumulative mass transfer enhancement rapidly increased before leveling off and reaching a final value of 5.2 at 32.8 PV. An alternative way of calculating mass transfer enhancement is by comparing the experimental effluent concentration to the abiotic (expected) effluent concentration for a given effluent sample (see the *Supplementary Material* of Amos et al. *(2008a)*). Enhancement factors calculated in this manner (termed maximum herein) are the ones most commonly reported in the literature and are always higher than cumulative enhancement factors. For the current experiment, 21-fold maximum enhancement of mass transfer was observed utilizing this alternative definition. This maximum enhancement occurred at a single time point (24.2 PV; Figure 28A). The enhancement factors are consistent with those observed during the *S. multivorans* mixed-NAPL column experiment and are comparable to the enhancement factors reported in the literature *(Carr et al. 2000; Yang and McCarty 2000; Cope and Hughes 2001; Yang and McCarty 2002; Adamson et al. 2003; Sleep et al. 2006; Glover et al. 2007).*

Table 4. Cumulative chlorinated ethene recoveries and mass transfer enhancement factors for the column experiment [a] (*Amos et al. 2008b).*

Parameter	**μmol**	**%**
Initial PCE Loading	16,300	–
Total Chlorinated Ethenes Recovered	13,500	83
PCE Recovered	300	1.8
TCE Recovered	90	0.6
cis-DCE Recovered	12,300	75.5
trans-DCE Recovered	30	0.2
VC Recovered	790	4.9
Ethene Recovered	20	0.1
Expected Abiotic PCE Recovered	2,610	16.0
Enhancement Factors		
Maximum Mass Transfer Enhancement Factor	21	
Cumulative Mass Transfer Enhancement Factor	5.2	

[a] Calculated with data only from the NAPL dissolution phase (0-32.8 PV) and not including the pulse of VC-amended influent medium

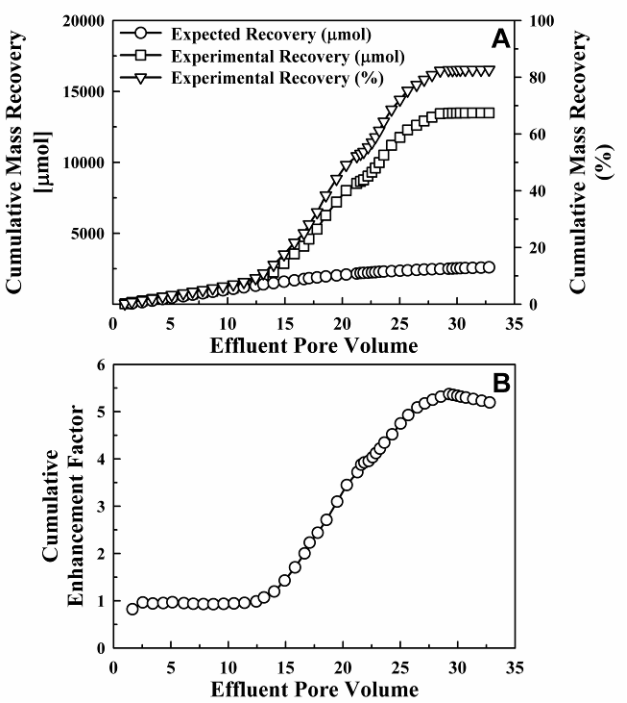

Figure 32: Cumulative chlorinated ethene mass and percent recoveries (A) and the cumulative mass transfer enhancement factor (B) for the BDI-SZ column experiment (*Amos et al. 2008b).*

III.2.2.9 Summary of the column experiment with BDI-SZ

Although previous studies have demonstrated biological activity within NAPL source zones, the contributions of individual dechlorinating populations to bioenhanced dissolution are currently unknown. The involvement of key dechlorinating populations in enhanced contaminant dissolution, therefore, was explored with a 1-D continuous-flow column inoculated with BDI-SZ, a PCE-to-ethene dechlorinating microbial consortium containing multiple *Dehalococcoides* strains and two PCE-to-*cis*-DCE dechlorinating populations (*Geobacter lovleyi* strain SZ and a *Dehalobacter* species). Interestingly, the results suggest that the *Dehalobacter* population did not survive the initial stages of column operation (i.e., column packing) and, therefore, played a limited role, if any, in PCE dechlorination and bioenhanced dissolution. In contrast, growth of *Geobacter* and *Dehalococcoides* organisms was directly linked to the observed 5.2-fold cumulative bioenhanced dissolution, which is comparable to the dissolution enhancements observed with *S. multivorans* (see above) and in previous experiments *(Carr et al. 2000; Yang and McCarty 2000; Cope and Hughes 2001; Yang and McCarty 2002; Adamson et al. 2003; Sleep et al. 2006; Glover et al. 2007).*

Results from both chemical (e.g., chlorinated ethene) and qPCR analyses indicate that *Geobacter* and *Dehalococcoides* organisms were present and active in the mixed-NAPL (0.25/0.75 mol/mol PCE dissolved in hexadecane) source zone. These results corroborate the findings presented above for *S. multivorans* and suggest that successful source zone colonization by dechlorinating organisms is possible. *Geobacter* cell numbers were typically 1-3 orders-of-magnitude higher than *Dehalococcoides* cell numbers in samples from either the side ports or the column effluent. Spatial and temporal changes in both populations tracked closely with changes in the production

of PCE dechlorination products (i.e., *cis*-DCE and VC). Interestingly, *Dehalococcoides* cell numbers generally increased 1-2 orders-of-magnitude over the length of the column, often correlating to increases in VC concentrations.

Despite the observed growth of both dechlorinating populations, PCE dechlorination generally stalled at *cis*-DCE, which reached concentrations as high as 2,600 μM. Similar dechlorination stalls have been reported in the literature *(Carr et al. 2000; Yang and McCarty 2000; Cope and Hughes 2001; Yang and McCarty 2002; Adamson et al. 2003; Da Silva et al. 2006; Sleep et al. 2006; Glover et al. 2007)*. In this study, increasing the column residence time from 1.1 days to 2.8 days increased VC formation (up from < 50 μM to 300 μM), suggesting that the column residence time was insufficient to achieve significant dechlorination beyond *cis*-DCE. Ethene production was not observed until PCE was depleted from the mixed-NAPL and *cis*-DCE concentrations were reduced to low levels (< 10 μM), suggesting that *cis*-DCE may be inhibitory to complete dechlorination. Results from the pulse of VC-amended influent medium indicated that ethene formation within the column was possible and provide further evidence that the lack of ethene production throughout most of the column experiment was likely due to inhibition (i.e., the presence of significant amounts of *cis*-DCE). Accumulation of *cis*-DCE, therefore, might limit complete detoxification of PCE to ethene unless system residence times are sufficiently long for sequential conversion of *cis*-DCE to VC before VC conversion to ethene. Future studies should identify the mechanisms limiting complete PCE detoxification during source zone bioremediation and consider alternative remediation strategies, such as using biological activity as a tertiary (polishing) step following physical-chemical treatment (see above).

III.3 2D AQUIFER CELL EXPERIMENTS

III.3.1. TCE-DNAPL mass recovery and saturation distributions during surfactant flushing

To realize the potential benefits of aggressive source zone treatment, including mass removal and reduced source longevity, more comprehensive remediation strategies must be developed to address residual contaminant mass and corresponding dissolved-phase plumes. One promising approach is to combine aggressive DNAPL mass removal by surfactant flushing with longer-term bioremediation strategies to address dissolved-phase contaminants emanating from treated source zones *(Christ et al. 2005)*. Biodegradable surfactants that provide reducing equivalents for reductive dechlorination of chlorinated ethenes, and can be tolerated by relevant microbial populations (e.g., *Dehalococcoides* sp.) would particularly well-suited for sequential treatment of chlorinated solvents.

Two promising surfactant candidates for coupled source zone treatment were evaluated; Tween 80, a non-ionic, food-grade surfactant, and Aerosol MA, an anionic surfactant widely used in pharmaceutical coatings. In a recent field test, a 6% (wt.) aqueous solution of Tween 80 was used to recover PCE-DNAPL from a shallow aquifer formation *(Ramsburg et al. 2005)*. Post-treatment monitoring of the treated source zone revealed elevated concentrations of volatile fatty acids (e.g., acetate, generated from the fermentation of T80), *cis*-1,2-dichloroethene (*cis*-DCE), and vinyl chloride (VC) *(Ramsburg et al. 2004)*. A subsequent laboratory study revealed that Tween 80, at concentrations ranging from 50 to 5,000 mg/L, did not inhibit reductive dechlorination of PCE and TCE to *cis*-DCE by pure and mixed cultures *(Amos et al. 2007b)*.

Although the presence of Tween 80 prevented ethene formation and reduced *Dehalococcoides* cell numbers, activity was recovered when Tween 80 was removed from the aqueous phase. In addition, *(McGuire and Hughes 2003)* reported that 40% of Tween 80 in a 1% (wt.) solution was degraded by mixed anaerobic culture after 70 days, and that Tween 80 exhibited no adverse effect on PCE conversion to VC, although subsequent transformation of VC to ethene occurred more slowly than in surfactant-free controls. Evidence of post-treatment stimulation of TCE reductive dechlorination has also been reported for Aerosol MA, which was used to flush a TCE-DNAPL source zone at Hill Air Force Base, Operational Unit 2 *(Londergan et al. 2001)*. Several years after surfactant flushing was completed, methyl isobutyl ketone, a known breakdown product of Aerosol MA, and cis-DCE were detected in ground water monitoring wells located down-gradient from the treated source zone.

Surfactant-based remediation technologies typically involve two primary recovery mechanisms; micellar solubilization and/or NAPL displacement (mobilization). In this context, Tween 80 is generally considered to be a solubilization agent for chlorinated solvents *(Taylor et al. 2001; Schaerlaekens and Feyen 2004)*, while Aerosol MA has the potential to both solubilize and mobilize DNAPL contaminants due to the lower interfacial tension (IFT) achieved upon salt addition *(Pennell et al. 1996; Dwarakanath et al. 1999; Zhong and Pope 2003)*. In general, the solubilization capacity of a surfactant increases as the interfacial tension is reduced *(Bourrel and Schechter 1988)*, yet this benefit is often offset by the risk of uncontrolled mobilization of DNAPL, which could enter lower permeability layers and migrate to greater depths in the subsurface, e.g., *(Ramsburg and Pennell 2001)*. Employment of either a solubilization or mobilization recovery mechanism requires careful design of the hydraulic and treatment systems *(Abriola et al. 2005; Jin et al. 2007)*. An important aspect of the design of surfactant flushing treatments is the onset and extent of DNAPL mobilization, which can be described by the total trapping number *(Pennell 1996)*:

$$N_T = \sqrt{N_{Ca}^2 + 2N_{Ca}N_B \sin\alpha + N_B^2} \tag{6}$$

where α is the angle of aqueous-phase flow relative to the horizontal axis. The capillary number (N_{Ca}) and Bond number (N_B) are defined as:

$$N_{Ca} = \frac{q_w \mu_w}{\sigma_{ow} \cos\theta}, \quad N_B = \frac{\Delta\rho g k k_{rw}}{\sigma_{ow} \cos\theta} \tag{7}$$

where q_w is the Darcy velocity of the aqueous phase (upward direction is taken as positive), μ_w is the dynamic viscosity of the aqueous phase, σ_{ow} is the interfacial tension between the organic and aqueous phases, θ is the contact angle between the aqueous and solid phases, $\Delta\rho$ is the difference between the aqueous and organic phase densities ($\rho_w - \rho_o$), g is the gravitational constant, k is the intrinsic permeability of the porous medium, and k_{rw} is the relative permeability of the aqueous phase. For the case of horizontal flow ($\alpha = 0^o$), Eq. 6 reduces to:

$$N_T = \sqrt{N_{Ca}^2 + N_B^2} \tag{8}$$

Results of column studies conducted with PCE-DNAPL suggest that the threshold trapping number corresponding to the onset of ganglia mobilization is approximately 2 x 10^{-5}, with nearly complete displacement observed at N_T values exceeding 1 x 10^{-3}. However, the ability of the trapping number approach to describe DNAPL displacement and subsequent free product migration has received only limited consideration in multi-dimensional, heterogeneous systems *(Ramsburg and Pennell 2001; Conrad et al. 2002; Jin et al. 2007).*

The specific objectives of these studies were to assess the ability of Tween 80 and Aerosol MA to recover TCE-DNAPL from heterogeneous 2-D aquifer cells and to evaluate the utility of the total trapping number to predict TCE-DNAPL mobilization behavior in a heterogeneous source zone. We hypothesized that Tween 80 would exhibit a lower TCE solubilization capacity than Aerosol MA, but would result in only limited mobilization of TCE-DNAPL during aquifer cell flushing. Furthermore, we hypothesized that the relationship between solubilization capacity and IFT for both surfactant formulations could be accurately represented by the Huh correlation *(Huh 1979)*, and that the total trapping number concept could be used to predict and modify TCE-DNAPL mobilization behavior. In addition to the aquifer cell studies, batch experiments were performed to determine relevant surfactant solution properties, including density, viscosity, solubilization capacity, and interfacial tension.

III.3.1.1 TCE Solubility and Interfacial Tension

The equilibrium solubilities of TCE in micellar solutions of Tween 80 and Aerosol MA are shown in Figure 2a. For the 4% (~40 g/L) Tween 80 and 3.3% (~33 g/L) Aerosol MA formulations used in the aquifer cell experiments, the solubility of TCE was approximately 63,500 and 39,100 mg/l, respectively, which represent 57- and 35-fold enhancements over the aqueous solubility of TCE (1,100 mg/l). The observed solubility of TCE in the 3.3% Aerosol MA solution was consistent with data reported by Dwarakanath and coworkers *(Dwarakanath et al. 1999)*. However, the sizable capacity of 4% Tween 80 to solubilize TCE was not anticipated. To further explore and confirm this behavior, the solubility of TCE in solutions of Tween 80 was measured over a Tween 80 concentration range of 6 to 60 g/L. The solubility of TCE increased linearly with Tween 80 concentration, consistent with Winsor Type I behavior of an oil-in-water microemulsion *(Winsor 1954)*. The capacity of a surfactant to solubilize an organic compound can be expressed as a weight solubilization ratio (WSR);

$$WSR = \frac{C_O - C_{O,CMC}}{C_S - C_{S,CMC}} \tag{9}$$

where C_O is the concentration of the organic compound in the aqueous phase, $C_{O,CMC}$ is the concentration of the organic at the CMC, generally assumed to be equal to the aqueous solubility of the organic species, C_S is the aqueous phase concentration of surfactant, and $C_{S,CMC}$ is the CMC of the surfactant. The solubility data for TCE in Tween 80 were fit to Eq. 10 using a least-squares, linear regression procedure to obtain a WSR of 1.74 (r^2 = 0.997, Figure 33). For Aerosol MA, a WSR of 1.21 was calculated from the measured equilibrium solubility of TCE in the 3.3% Aerosol MA formulation. Based on the molecular weight of the surfactant and TCE,

the WSR values were converted to molar solubilization ratios (MSRs), which were then used the compute the Log micelle-water partition coefficients (K_{mw}) *(Edwards et al. 1991)*;

$$K_{mw} = \frac{X_m}{X_w};\ X_m = \frac{MSR}{1 + MSR},\ X_w = \frac{C_{O,CMC}}{V_w} \tag{10}$$

where X_m is the mole fraction of organic in the micellar phase, X_w is the mole fraction of organic in the free aqueous phase, and V_w is the molar volume of water (55.4 M at 25^{o}C).

Despite the capacity of Tween 80 to solubilize TCE, the interfacial tension (IFT) between the aqueous surfactant solution and TCE only decreased from 35.2 (water) to 10.4 dyn/cm. In contrast, the Aerosol MA formulation, which contained 6 g/l NaCl and 8% (wt) IPA, yielded a substantially lower IFT (0.19 dyn/cm) even though the solubilization capacity for TCE was approximately 40% less. In general, the solubilization capacity of a surfactant formulation increases as the IFT is reduced, which is often achieved by addition of salt to anionic surfactant formulations *(Bourrel and Schechter 1988)*. If a middle-phase microemulsion (Winsor Type III system) forms, extremely low IFTs (< 0.01 dyn/cm) and high solubilization capacities can be achieved. For example, when the NaCl concentration in a 4% Aerosol MA formulation is increased to 9.35 g/l, the resulting middle-phase microemulsion yields a TCE solubility of 516,000 mg/l (WSR = 12.9) and an IFT of 0.02 dyn/cm *(Dwarakanath et al. 1999)*. In the enhanced oil recovery literature, this inverse relationship between IFT and the solubilization capacity is typically described by the Huh correlation *(Huh 1979)*:

$$\sigma_{ow} = c / SP^2 \tag{11}$$

where σ_{ow} is the interfacial tension (dyn/cm), *SP* is the solubilization parameter (mL organic/mL surfactant), and *c* is a constant, which is equal to 0.3 dyn/cm for hydrocarbons and chlorinated organics *(Pope 1995)*.

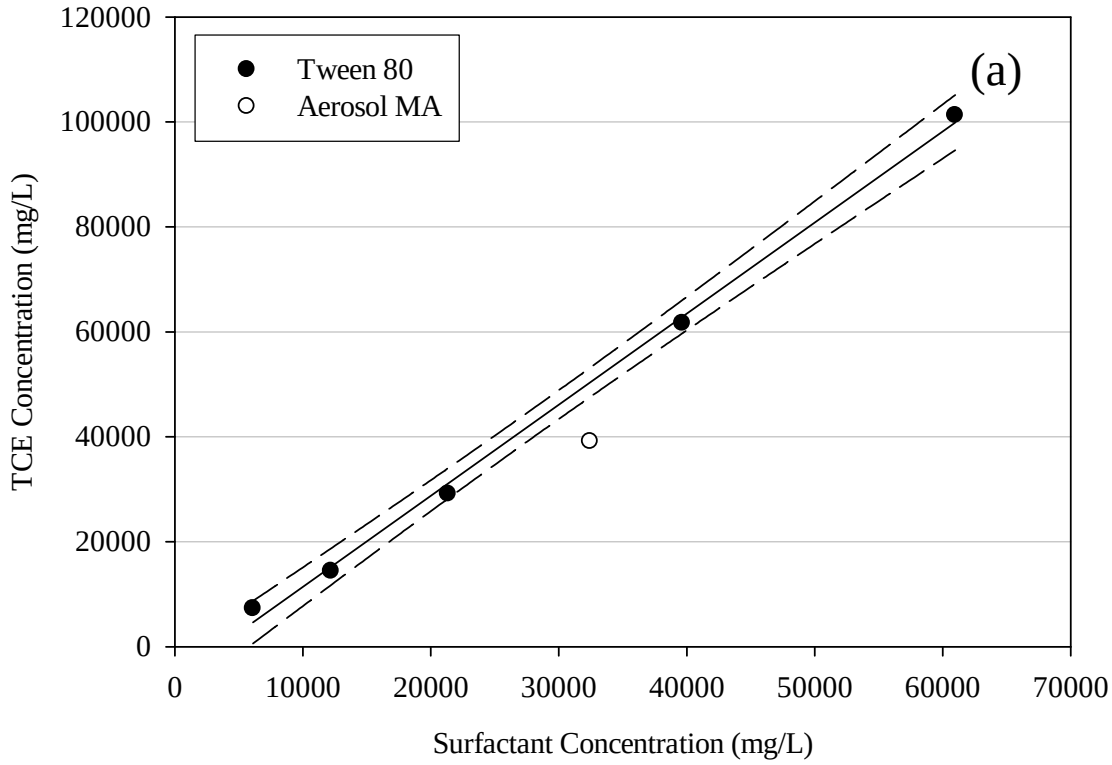

Figure 33: Aqueous solubility of TCE as a function of surfactant concentration at 22±1ºC *(Suchomel et al. 2007).*

Based on the measured WSR values, solubilization parameters of 1.26 and 0.91 mL TCE/mL surfactant were calculated for Tween 80 and Aerosol MA, respectively. The measured solubility parameter and IFT data are plotted against the Huh correlation (c = 0.3 dyn/cm) in Figure 34, along with published data for several relevant chlorinated ethene-surfactant systems. In general, the Huh correlation captures the experimental data, consistent with the findings of *(Pope and Wade 1995)*. For example, the IFT predicted for the TCE/Aerosol MA system (0.36 dyn/cm) compares favorably with the measured value of 0.19 dyn/cm. One notable exception to this trend is the TCE/Tween 80 system, for which the measured IFT (10.4 dyn/cm) was 55 times greater than the value predicted by the Huh correlation (0.18 dyne/cm). This finding further confirms the unique behavior of Tween 80, for which a large TCE solubilization capacity is accompanied by a relatively small IFT reduction. The behavior could be due to the ability of Tween 80 to solubilize TCE in both the hydrophobic and hydrophilic mantle as noted above, with minimal changes in the tendency for the surfactant to accumulate at the DNAPL-water interface. The combination of a large solubilization capacity coupled with a relatively small IFT reduction makes Tween 80 an attractive option for surfactant-based remediation because it offers the potential to achieve efficient TCE mass recovery via solubilization with reduced risk of mobilization. For example, if one considers a solution of Tween 80 flowing through a porous medium containing residual TCE-DNAPL droplets at a horizontal pore-water velocity of 1.0 m/day, a porosity of 0.35, and an effective permeability 1.0 x 10^{-11} m^2, the total trapping number

(N_T) would be 4.4 x 10^{-6}. This value is 5 times less than the value corresponding to the onset of PCE-DNAPL mobilization (2.0 x 10^{-5}) reported by Pennell et al. *(Pennell 1996)* for similar size fractions of Ottawa sand.

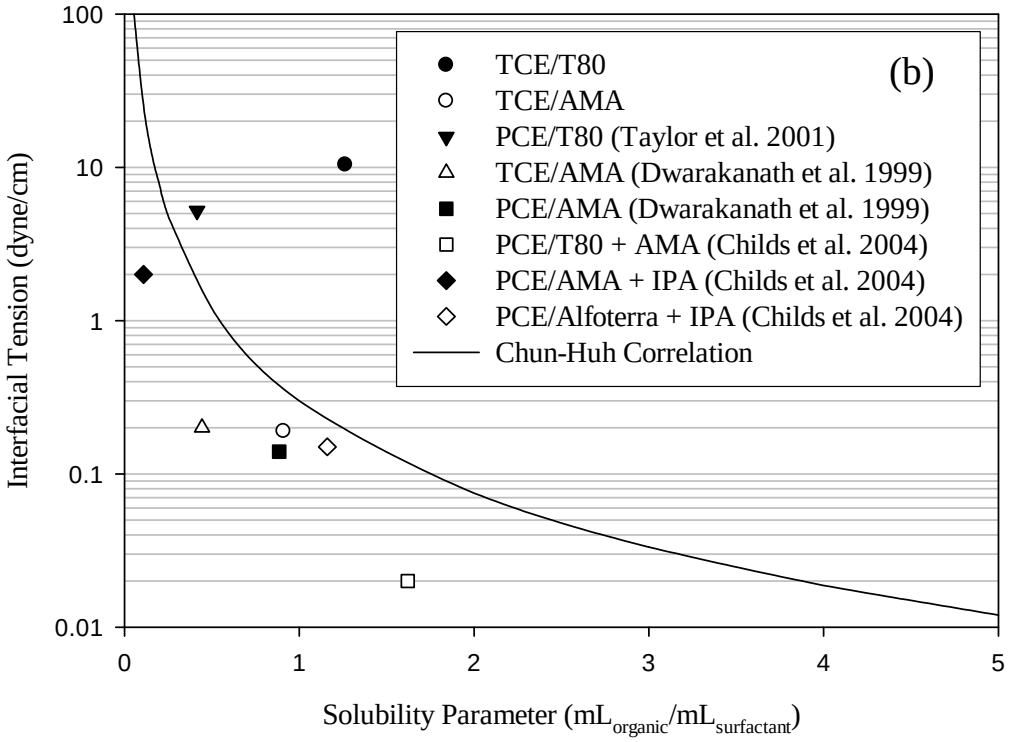

Figure 34: Measured and estimated *(Huh 1979)* PCE and TCE solubility versus interfacial tension (T80 = Tween 80, AMA = Aerosol MA-80, IPA = 2-propanol) *(Suchomel et al. 2007)*.

A total of five aquifer cell studies were conducted to quantify TCE recovery from heterogeneous source zones with TCE-DNAPL saturation distributions that ranged from ganglia-dominated to pool-dominated. The initial conditions of each aquifer cell are summarized in Table 5. Three aquifer cell experiments (T80-1, T80-2, T80-3) were conducted to evaluate the ability of Tween 80 to recover TCE-DNAPL from a heterogeneous porous medium, and to investigate the effects of the TCE-DNAPL saturation distribution on recovery efficiency. The total pore volume of these cells, which were packed with either Federal Fine Ottawa sand (T80-1), a 1:1 mixture of 20-30 and 40-50 mesh Accusands (T80-2), or 20-30 mesh Accusand (T80-3) as the background medium, ranged from 1,180 to 1,370 ml, while the overall hydraulic conductivity ranged from 3.2 to 39.6 cm/min (Table 5).

Following TCE-DNAPL release and redistribution, 26.1 to 32.7 ml of TCE-DNAPL were retained in the aquifer cells, yielding overall TCE-NAPL saturations of 2.0 to 2.7 %. Although the Federal Fine Ottawa sand did not permit LT analysis, a GTP ratio of 1.8 was estimated for T80-1 cell based on a digital image of the front panel. The GTP ratio of 1.8 indicates that 64% (21 ml) of the TCE-DNAPL existed as entrapped ganglia or droplets, while the remaining 36% (11.7 ml) was present in high saturation (S_{TCE} > 13%) zones or pools. In the two aquifer cells packed with Accusands, LT analysis yielded GTP ratios of 1.5 (T80-2) and 0.2 (T80-3),

indicating that 40% (11.8 ml) and 83% (21.7 ml), respectively, of the TCE-DNAPL initially existed in high saturation (S_{TCE} > 11%) zones. Digital images of the T80-2 and T80-3 aquifer cells and their corresponding TCE-DNAPL saturation distribution profiles prior to surfactant flushing are shown in Figure 35. Two additional aquifer cells (AMA-1 and AMA-2) were packed with Federal Fine Ottawa sand as the background medium to evaluate the recovery of TCE by Aerosol MA at two flow rates. The total pore volume of these cells was 1,330 and 1,340 ml, which is consistent with the T80-1 cell packed with Federal Fine Ottawa sand. Approximately 28 and 39 ml of TCE-DNAPL were retained in the AMA-1 and AMA-2 aquifer cells, yielding overall TCE-DNAPL saturations of 2.2 and 2.9%, respectively. The corresponding GTP ratios were 1.1 and 1.2, indicating that slightly more than half of the TCE-DNAPL existed as ganglia prior to surfactant flushing.

Table 5: Experimental conditions of the TCE-DNAPL aquifer cells. (Suchomel et al., 2007)

Experimental Parameter	Aquifer Cell Experiment				
	T80-1	T80-2	T80-3	AMA-1	AMA-2
Background porous medium	Federal Fine Ottawa sand	Accusand mixture[a]	20-30 mesh Accusand	Federal Fine Ottawa sand	Federal Fine Ottawa sand
Mean grain dia., d_{50} (mm)	0.305	0.544	0.725	0.305	0.305
Pore volume (ml)	1,370	1,180	1,280	1,340	1,330
Hydraulic conductivity (cm/min)	3.19±0.32[b]	9.55±1.35	39.59±1.31	5.21±0.13	2.98±0.55
Volume of TCE (ml)	32.7	29.5	26.1	28.7	39.3
Overall TCE sat. (%)	2.4	2.7	2.0	2.2	2.9
Initial GTP[c] ratio	1.8[d]	1.5[e]	0.2[e]	1.2[d]	1.1[d]

[a] 1:1 mixture of 20-30 and 40-50 mesh Accusand; [b] ± one standard deviation; [c] GTP = ganglia to pool ratio (TCE vol. ≤ residual saturation /TCE vol. > residual saturation);

III.3.1.2 Tween 80 Aquifer Cell Results

For all three Tween 80 experiments flow through the aquifer cell was maintained at a rate of approximately 4.0 mL/min, which corresponds to a pore-water velocity of 2.7 m/day, equal to a residence time of 5.6 hr. Flow conditions, dimensionless parameter analysis, and TCE recoveries for each aquifer cell experiment are summarized in Table 5. Approximately 7 pore volumes (9,600 ml) of 4% Tween 80 solution were flushed through the T80-1 aquifer cell, while only 2 pore volumes of solution were injected in experiments T80-2 and T-80-3. Following each surfactant pulse, several pore volumes of surfactant-free water were flushed through the cells to recover any dissolved phase TCE or surfactant. The resulting flux-averaged effluent Tween 80 and TCE concentrations versus the number of pore volumes of solution injected are plotted in Figure 36. In all cases, effluent Tween 80 and TCE concentrations increased sharply after approximately 0.6 pore volumes of Tween 80 were introduced, indicating that sorption had minimal effects on Tween 80 delivery and TCE solubilization. This finding is consistent with the relatively small Langmuir sorption capacity of Ottawa sand for Tween 80 (S_{max} = 0.16 mg/g),

which yields a retardation factor of 1.00005 *(Taylor et al. 2001)*. Based on this analysis, less than 2% (0.8 g) of the Tween 80 mass injected during the first pore volume of surfactant flushing would be associated with the solid phase, after which time no additional net loss of surfactant would occur.

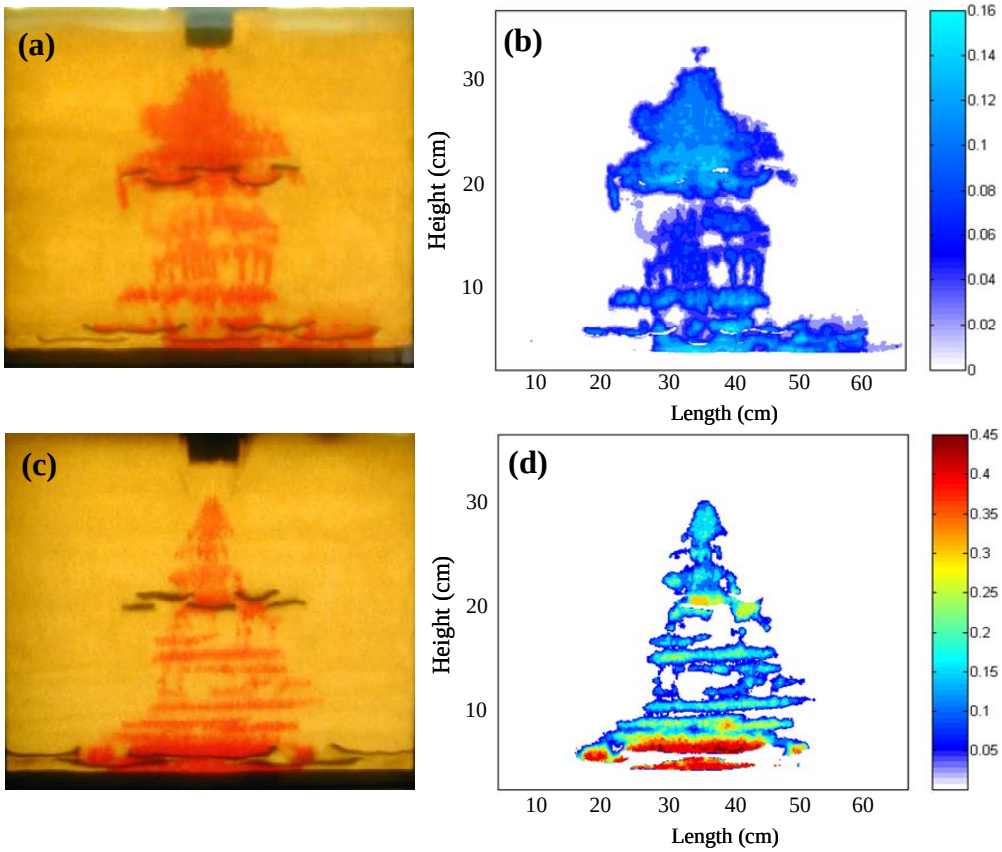

Figure 35: Initial TCE-DNAPL saturation distributions for experiments: T80-2 (GTP = 1.5) (a) digital image with back lighting and (b) light transmission saturation distribution profile; and T80-3 (GTP = 0.2) (c) digital image with back lighting and (d) light transmission saturation distribution profile. *(Suchomel et al. 2007)*

In experiments T80-1 and T80-2, effluent TCE concentrations approached a maximum value of 25,000 mg/L after 1.2 pore volumes (1,800 mL) of Tween 80 had been injected, and then declining steadily to relatively low levels (<1,000 mg/L) after approximately 3 pore volumes of surfactant solution had been injected (Figure 36). The observed maximum value is approximately 40% of the equilibrium TCE solubility (63,500 mg/l) measured in completely-mixed batch reactors. Similar behavior was reported by *(Taylor et al. 2001)* for the solubilization of entrapped PCE-DNAPL by Tween 80, which was described using a modified Sherwood number (Sh')-Reynolds number (Re) correlation ($Sh' = 0.741Re^{0.71}$) where;

$$Sh' = \frac{K_e d_{50}^2}{D_l}, \; Re = \frac{d_{50} q \rho_w}{\mu_w} \tag{12}$$

and K_e is the effective mass transfer coefficient, d_{50} is the median grain size, and D_l is the free liquid diffusion coefficient of the dissolved solute.

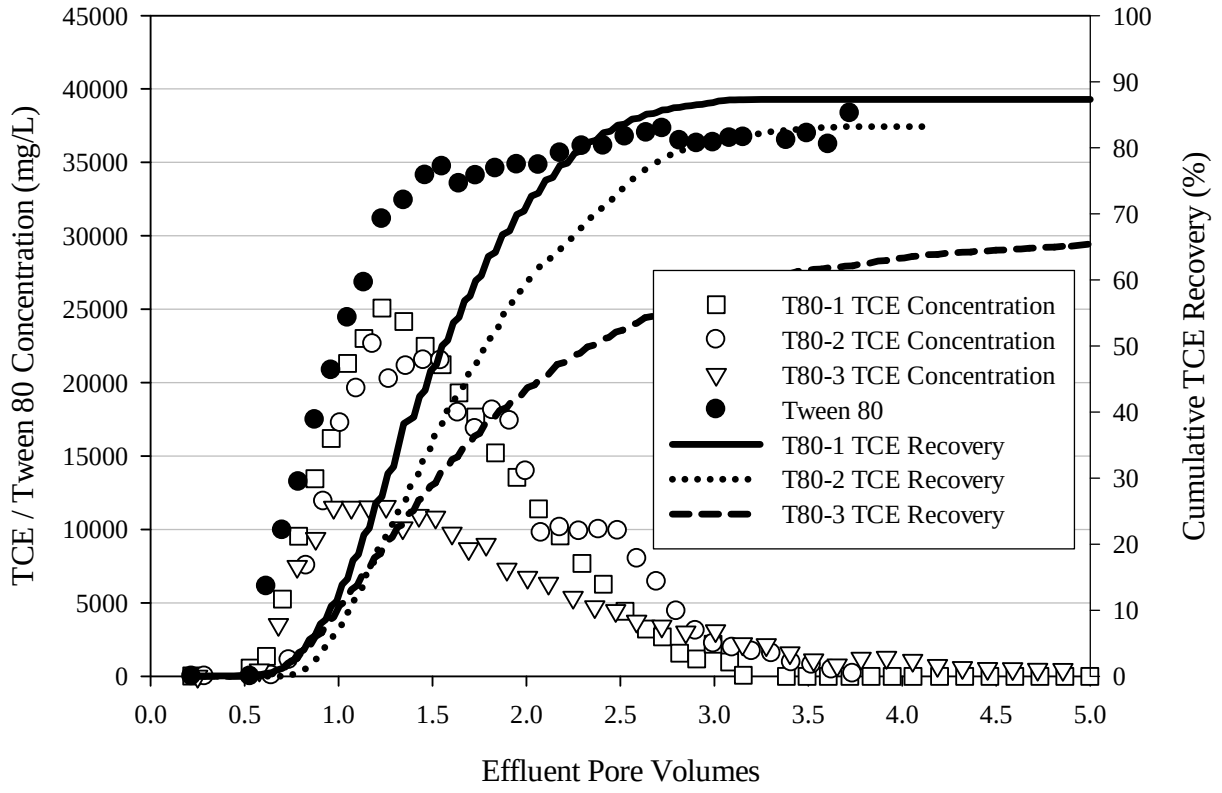

Figure 36: Effluent TCE and surfactant concentrations and cumulative mass recoveries for experiments T80-1, T80-2, and T80-3. *(Suchomel et al. 2007)*

If one assumes that the initial surfactant flood can be approximated by horizontal, one-dimensional flow through a 15 cm zone of entrapped TCE-DNAPL droplets, the effluent concentration can be estimated from *(Powers et al. 1991)*:

$$\frac{C_O}{C_{O,sat}} = 1 - \exp\left(\frac{1-\sqrt{1+4Da/Pe}}{2/Pe} X^*\right) \tag{13}$$

where *Da* is the Damköhler number ($Da = K_e L/q_w$), *Pe* is the Peclet number ($Pe = v_w L/D_H$) where v_w is the pore-water or interstitial velocity and D_H is the hydrodynamic dispersion coefficient, and X^* is x/L where x is the distance and L is the length of the DNAPL zone. Inserting the value of K_e obtained from Eq. 12 (0.16 1/hr), $X = 1$, and $D_H = 1.18$ cm^2/hr *(Rathfelder et al. 2001)* into Eq. 13, yields an effluent TCE concentration (C_O) of 26,000 mg/l. The similarity in the measured and estimated maximum concentrations suggests that the rate of TCE solubilization was similar to that reported for PCE, and will control early time effluent concentrations in ganglia-dominated source zones.

Based on visual observation and LT analysis, TCE-DNAPL ganglia were rapidly solubilized during the initial 3 pore volumes of Tween 80 flushing, which corresponded to the relatively

sharp rise and fall of the effluent TCE concentration curves. The remaining TCE-DNAPL consisted primarily of higher saturation zones located above the lower permeability lenses near the bottom of the aquifer cell as evidenced by LT saturation distribution profiles of the T80-2 and T80-3 cells (Figure 37). These high saturation zones dissolved slowly to yield the persistent low effluent TCE concentrations and mass discharge observed at late flushing times.

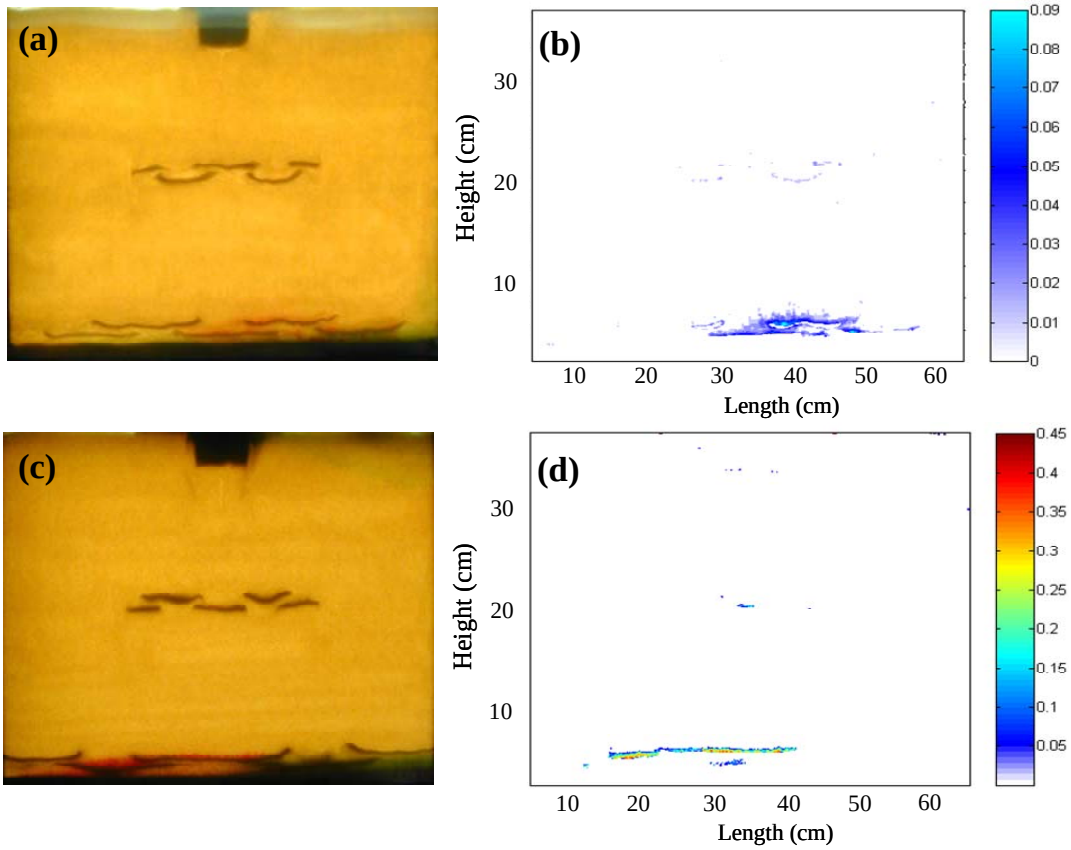

Figure 37: Final TCE-DNAPL saturation distributions for experiment T80-2 (GTP = 0.5) (a) digital image with back lighting and (b) light transmission saturation distribution profile; and experiment T80-3 (GTP = 0.16) (c) digital image with back lighting and (d) light transmission saturation distribution profile. *(Suchomel et al. 2007)*

The similarity in effluent TCE concentration profiles obtained for experiments T80-1 and T80-2 was attributed to relatively large and similar volume of TCE-DNAPL existing as high interfacial area ganglia (21.0 and 17.7 ml, respectively) as indicated by the GTP values (1.8 and 1.5, respectively). In experiment T80-3, effluent TCE concentrations reached a lower maximum value of 11,000 mg/L after injecting approximately 1.0 pore volume of Tween 80 solution, remained relatively constant until 1.5 pore volumes, and then declined slowly over time. The lower maximum effluent TCE concentration obtained in experiment T80-3 was attributed to the substantially smaller volume of TCE-DNAPL existing as ganglia (4.3 ml), which was reflected in the initial GTP value of 0.2. These results are consistent with the numerical simulations of PCE-NAPL solubilization in 2-D aquifer cells *(Rathfelder et al. 2001)*, where unobstructed NAPL ganglia were readily solubilized early in the surfactant flood, leading to a rapid rise in effluent contaminant concentrations as high interfacial area ganglia dissolved. Following

removal of DNAPL ganglia, contaminant recovery is controlled by the volume and distribution of the remaining zones of higher saturation or pooled DNAPL. These DNAPL pools are characterized by relatively low interfacial areas, and can serve as long-term, mass transfer limited sources of dissolved-phase contaminant mass during later stages of surfactant or water flushing, or post-treatment natural gradient conditions as illustrated in Figure 37.

Visual observation of the aquifer cells indicated that entrapped ganglia underwent minimal or slight mobilization and subsequent re-entrapment during Tween 80 flushing. These observations are consistent with anticipated behavior based on a total trapping number analysis of experiments T80-1 and T-80-2, which yielded N_T values of 2.14×10^{-5} and 6.14×10^{-5} (Table 6). These N_T values are similar to the threshold or critical value of 2.0×10^{-5} that was required for the onset of PCE-DNAPL mobilization in columns packed with Ottawa sand *(Pennell 1996)*. In experiment T80-3, which contained the highest permeability Ottawa sand (20-30 mesh), an N_T value of 2.65×10^{-4} was obtained. Although this value corresponds to the displacement of approximately 80% of the PCE-DNAPL in one-dimensional column studies *(Pennell et al. 1996)*, only minor TCE mobilization and re-entrapment were observed in the T80-3 aquifer cell. This discrepancy is likely due to inherent differences between the flow in 1-D column and 2-D aquifer cell experimental systems, which (i) permit flow bypassing that limits contact between the surfactant and DNAPL and (ii) allow re-entrapment of the mobilized DNAPL.

III.3.1.3 Aerosol MA Aquifer Cell Results

Two aquifer cell studies were conducted with Aerosol MA 80 in order to compare mass recoveries obtained with Tween 80 to those of an anionic surfactant formulation that possessed a similar TCE solubilization capacity, but also had the potential to displace TCE-DNAPL as free product due to a substantially lower IFT (10.4 dyn/cm vs. 0.19 dyn/cm). The Aerosol MA 80 experiments were conducted at two flow rates, 4 ml/min (AMA-1) and 10 ml/min (AMA-2), to evaluate the effects of flushing velocity on TCE mass recovery and DNAPL bank formation. In both experiments, effluent Aerosol MA and TCE concentrations increased sharply after introducing approximately 0.75 pore volumes of the Aerosol surfactant solution, reaching maximum values of 23,100 and 31,600 mg/L, respectively, at 1.1 pore volumes (Figure 38). The maximum effluent TCE concentrations were 60 and 82% of equilibrium solubility of TCE in the Aerosol MA solution (39,100 mg/L). The solubilization rate parameter reported for TCE in a similar Aerosol MA formulation is approximately 50 times greater than that of 4% Tween 80 *(Zhong and Pope 2003)*, and thus, local TCE concentrations were expected to approach the equilibrium solubility. The greater divergence from equilibrium observed in experiment AMA-1 was attributed to the smaller amount of entrapped TCE-DNAPL present in the source zone (29 ml vs. 39 ml). In addition, a shallow bank of TCE-DNAPL formed along the lower layer of F-70 Ottawa sand after flushing with approximately 0.5 pore volumes of Aerosol MA solution (Figure 39).

Table 6: Recovery parameters for TCE-DNAPL aquifer cell experiments. *(Suchomel et al. 2007)*

Recovery Parameter	Aquifer Cell Experiment				
	T80-1	T80-2	T80-3	AMA-1	AMA-2
Surfactant formulation	36.2 g/l Tween 80[a]	37.6 g/l Tween 80	40.2 g/l Tween 80	32.0 g/l Aersol MA[b]	34.0 g/l Aersol MA
Volume injected (ml)	9,600	2,520	2,800	1,520	1,590
Flow rate (ml/min)	4.29±0.18	3.84±0.34	4.47±0.88	4.24±0.22	9.89±0.85
Darcy velocity (cm/hr)	4.81±0.18	4.33±0.38	4.82±0.99	4.79±0.25	11.16±0.96
Capillary number, N_{Ca}	1.66×10^{-6}	1.49×10^{-6}	1.66×10^{-6}	1.15×10^{-4}	2.68×10^{-4}
Bond number, N_B	2.14×10^{-5}	6.40×10^{-5}	2.65×10^{-4}	1.94×10^{-3}	1.11×10^{-3}
Total trapping number, N_T	2.14×10^{-5}	6.40×10^{-5}	2.65×10^{-4}	2.06×10^{-3}	1.38×10^{-3}
Bank number, N_{Ba}	NA	NA	NA	0.06	0.24
Angle of mobilization, τ	NA	NA	NA	86.6	76.4
TCE recovered (ml)	28.6	26.1	17.3	17.3	32.0
TCE recovery (% vol)	87.4	83.1	66.2	56.3	81.3
Final GTP ratio	0.5	0.6	0.15	ND	ND

[a] Tween 80 + 0.5 g/L $CaCl_2$; [b] Aersol MA-80 + 8% (wt.) IPA + 6.0 g/L NaCl.

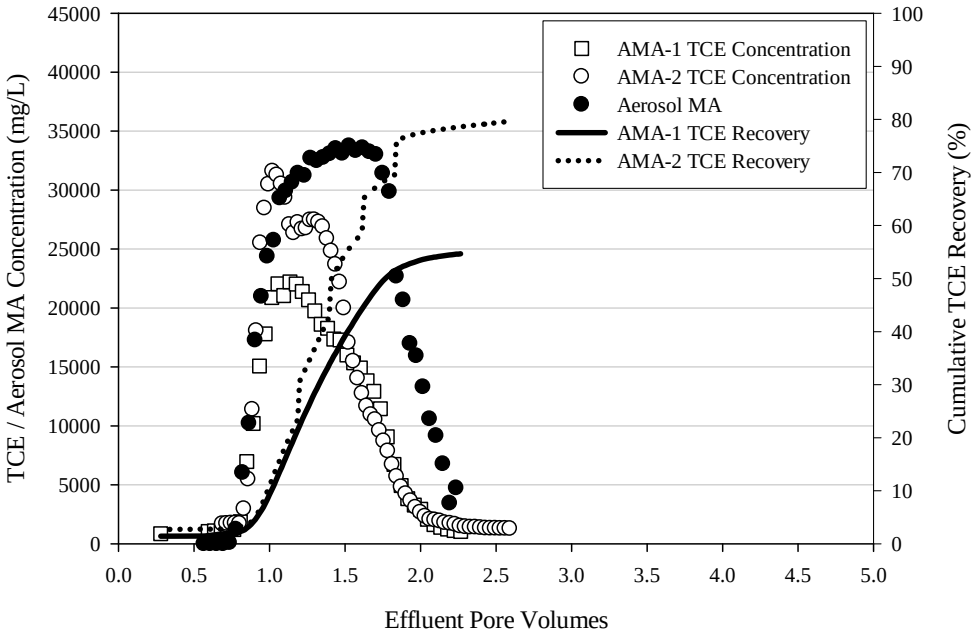

Figure 38: Effluent TCE and surfactant concentrations and cumulative mass recoveries for experiments AMA-1 and AMA-2. *(Suchomel et al. 2007)*

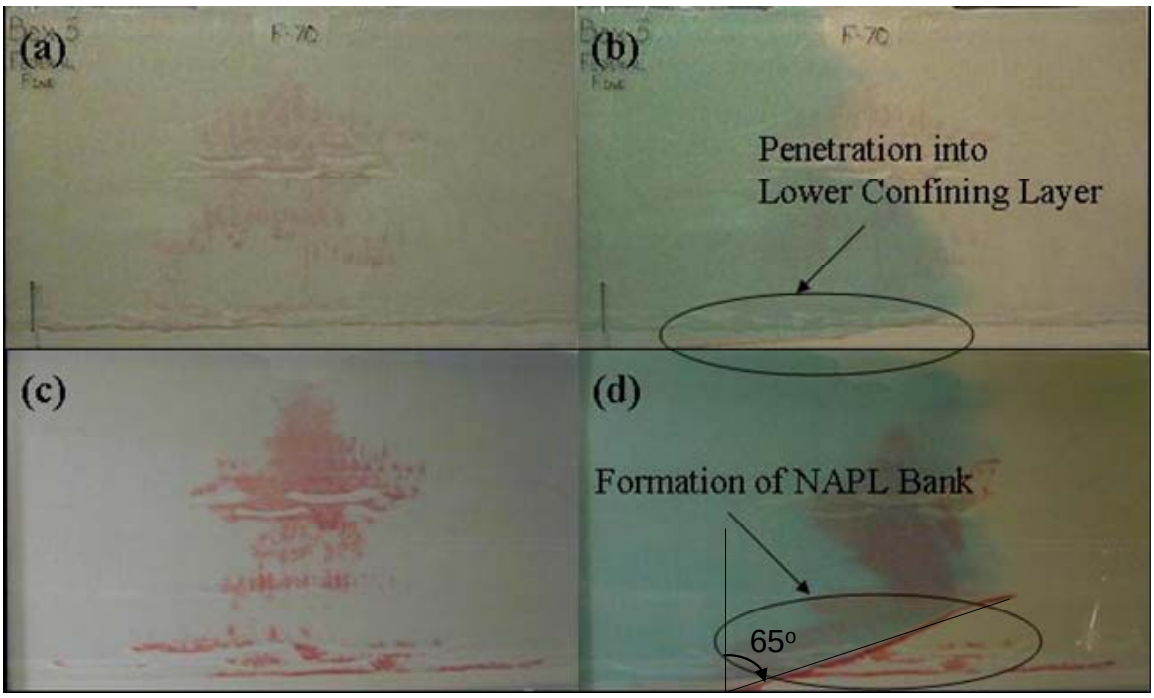

Figure 39: Initial TCE-DNAPL distributions and representative images of TCE-DNAPL mobilization and bank formation for experiments AMA-1 (a, b) and AMA-2 (c, d). *(Suchomel et al. 2007)*

Mobilization of TCE-DNAPL in experiment AMA-1 was anticipated based on total trapping number analysis, which yielded an N_T value of 2.06 x 10^{-3} (Table 6). This value is more than one order-of-magnitude greater than the values obtained for the Tween 80 aquifer cell experiments, which is due primarily to the lower IFT of the Aerosol MA solution (i.e., 0.19 vs. 10.4 dyn/cm). For horizontal aqueous-phase flow, the angle of displacement for mobilized NAPL relative to the x-axis (τ) can be predicted from the ratio of the Bond and capillary numbers by:

$$\tau = \arctan\left(\frac{N_B}{N_{Ca}}\right) \tag{14}$$

where a value of 0° corresponds to purely horizontal DNAPL migration (formation of a vertical DNAPL bank) and a value of 90° indicates vertical purely (downward) DNAPL migration (formation of a horizontal DNAPL bank) *(Jin et al. 2007)*. For experiment AMA-1, the displacement angle was calculated to be 87°, consistent with the nearly vertical (downward) migration of TCE-DNAPL visible in Figure 39b. An alternative representation of this concept was presented by *(Willson et al. 1999)*, where a dimensionless bank number (N_{Ba}) was developed that relates the forces acting on DNAPL ganglia in the direction of flow to the forces acting perpendicular to flow. Based on the previously developed capillary and Bond numbers (Eqs. 6-8), the bank number (N_{Ba}) can written as:

$$N_{Ba} = \frac{N_{Ca} + N_B \sin\alpha}{N_B \cos\alpha} \tag{15}$$

which reduces to $N_{Ba} = N_{Ca}/N_B$ in the case of horizontal flow ($\alpha = 0^o$). The value of N_{Ba} calculated for experiment AMA-1 was 0.03, consistent with the results of small-scale cell (1.5 cm height x 20 cm length) experiments conducted by *(Willson et al. 1999)* in which mobilized PCE-DNAPL flowed downward, and accumulated along the bottom of the tube at bank numbers less than 0.8.

In the second Aerosol MA experiment (AMA-2) the flow rate was increased by a factor 2.3 to examine the effects of flow rate on bank formation and free product recovery. The volume of TCE-DNAPL released into the cell was also increased to better visualize bank formation and free product migration. As anticipated from the N_T value of 1.38×10^{-3}, TCE-DNAPL mobilization was observed during experiment AMA-2, resulting in the formation of TCE-DNAPL bank that flowed toward the effluent well (Figure 39). A total of 18.1 ml of TCE were recovered as free product from the effluent chamber, accounting for 57% if the TCE volume recovered in experiment AMA-2. The observed angle of the TCE-DNAPL bank decreased to approximately 65º at the higher flow rate (Figure 39), which is less than the calculated value of 76º (Eq. 10). A further increase in the applied flow rate may provide for additional TCE mass recovery, and limit downward migration of mobilized DNAPL *(Jin et al. 2007)*. Consideration of higher flow rates as a means of attaining greater mass recovery under a mobilization scenario should be accompanied by careful assessment of site-specific hydraulics *(Abriola et al. 2005)*. The bank number obtained for experiment AMA-2 was 0.28 (Eq. 10), well below the reported value of 3 required for bank flow through porous media *(Willson et al. 1999)*. This discrepancy may be due to the very small aspect ratio (0.075) and relatively coarse sand fraction employed by *(Willson et al. 1999)*.

III.3.1.4 Comparison of TCE recoveries with different surfactant formulations

The cumulative amount of TCE recovered versus the number of pore volumes of surfactant solution injected are shown in Figure 40 for all five aquifer cell studies. For experiments T80-1 and T80-2, TCE recoveries of 87% and 83%, respectively, were reached after injecting only 2.5 pore volumes of 4% Tween 80 solution. The efficient recovery of TCE was attributed to the large TCE solubilization capacity of Tween 80 (WSR = 1.74) and the relatively large fraction of TCE-DNAPL existing as entrapped ganglia (initial GTP ratio of 1.8 and 1.5, respectively) in the source zones. In contrast, only 66% of the initial TCE-DNAPL volume was recovered in experiment T80-3 after flushing with 2.5 pore volumes of 4% Tween 80 solution, which was attributed to greater percentage of TCE-DNAPL existing in high-saturation pools (initial GTP ratio of 0.2). Once most of the high-interfacial area ganglia had dissolved, DNAPL recoveries plateau at a level corresponding to the difference between the initial mass and the amount remaining in persistent low-interfacial area pools despite continued injection of surfactant, as observed in experiment T80-1.

The limitations of a solubilizing surfactant to efficiently treat high-saturation DNAPL zones, motivated consideration of Aerosol MA formulations, which can be tailored with alcohol and salt addition to yield relatively high solubilization capacity with moderate IFT reduction. In experiment AMA-1, a total of 18.1 mL of TCE was recovered in the dissolved-phase effluent, yielding a cumulative recovery of 56.3%. Although a substantial fraction of TCE-DNAPL was

mobilized (~40%), the DNAPL bank was nearly horizontal and accumulated within the lower layer of F-70 Ottawa sand, severely limiting further TCE recovery. To address this issue, the aqueous flow rate was increased by a factor of 2.3, which resulted in a free product bank angle of approximately 65º in experiment AMA-2. Approximately 10 ml of free product were recovered from the effluent chamber, with an additional 22 ml recovered as dissolved-phase effluent, yielding an overall recovery of 81% after 3 pore volumes, which is comparable to the T80-1 experiment even though the GTP ratio was lower in the AMA-2 aquifer cell (1.1 versus 1.8).

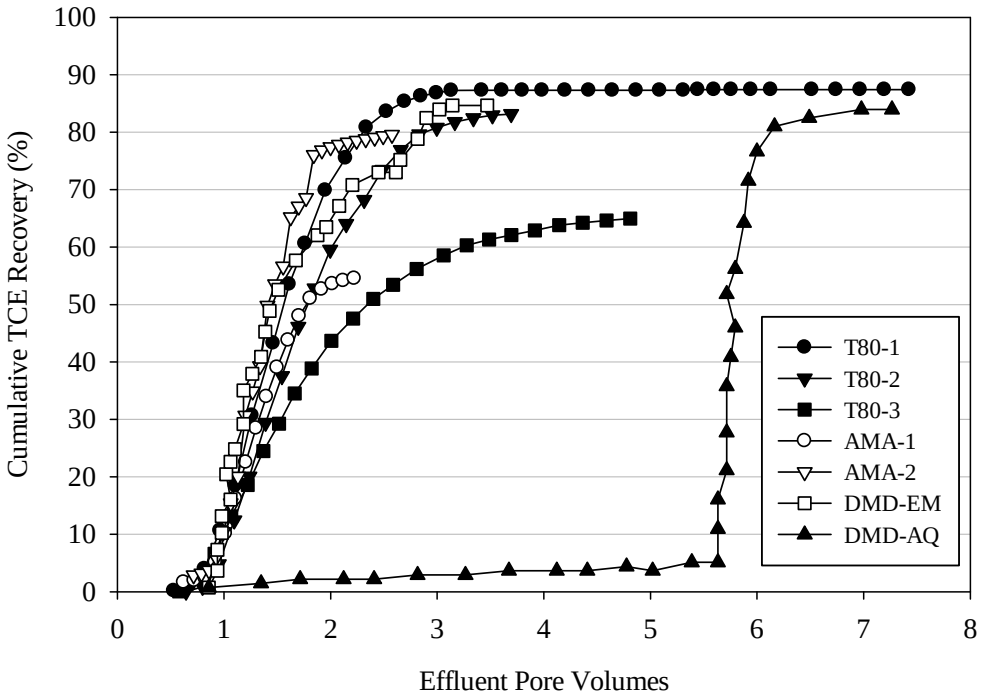

Figure 40: Comparison of cumulative TCE mass recoveries as a function of total pore volumes of Tween 80 and Aerosol MA injected, along with TCE recoveries obtained in similar aquifer cells using the density modified displacement (DMD) method with aqueous phase *(Ramsburg CA 2002)* and emulsion *(Ramsburg 2003)* delivery of butanol. *(Suchomel et al. 2007)*

For comparison purposes, cumulative TCE recoveries achieved using the density modified displacement (DMD) method *(Ramsburg CA 2002; Ramsburg 2003)* are also presented in Figure 40. In these experiments, TCE was converted *in situ* to a light NAPL via partitioning of n-butanol, which was delivered either in aqueous solution containing 6% butanol (DMD-AQ) or in a surfactant-stabilized macroemulsion containing 15% butanol (DMD-EM). Following density conversion the TCE-DNAPL was displaced using a low-IFT surfactant solution consisting 10% Aerosol MA + 5% n-butanol + 15 g/l NaCl + 1 g/l $CaCl_2$. The recovery of TCE in both DMD experiments approached 85%, however, this was achieved after only 3 pore volumes with the emulsion preflood while a total of 7.5 pore volumes was required for the aqueous preflood. Hence, both Tween 80 and Aerosol MA yielded recovery efficiencies that were comparable to the DMD-EM flood for GTP ratios greater than 1.0. As discussed above and noted by

(Ramsburg 2003), the advantage of a DMD-EM displacement flood will be more pronounced for source zones that are dominated by high saturation pools (GTP ratios < 0.5).

The key findings of the TCE-DNAPL aquifer cell studies are:

- Aqueous solutions of Tween 80 exhibited an unexpectedly large capacity to solubilize TCE, yielding a weight solubilization ratio (WSR) of 1.74, which was approximately 40% greater than the WSR value (1.21) obtained for a 3.3% Aerosol MA formulation.
- The relationship between TCE solubilization by Tween 80 and IFT was not accurately captured using a widely-accepted empirical correlation *(Huh 1979)*, which predicted a substantially lower IFT (0.18 vs. 10.4 dyn/cm).
- Flushing aquifer cells containing a heterogeneous TCE-DNAPL source zone with less than 2.5 pore volumes of 4% Tween 80 resulted in TCE mass recoveries ranging from 66 to 85% with minimal mobilization of TCE.
- Comparable TCE mass recoveries were obtained with the 3.3% Aerosol MA formulation provided that the flow rate was sufficient to transport mobilized TCE-DNAPL to the effluent chamber.
- The total trapping number provided reasonable estimates of the onset and extent of TCE-DNAPL mobilization, and supports the use of this approach to predict and design for displacement behaviors in multi-dimensional domains.
- Based on their high solubilization capacities and potential to stimulate post-treatment microbial reductive dechlorination, these surfactants are promising candidates for DNAPL source zone remedial actions that incorporate aggressive mass removal followed by enhanced bioremediation.

III.3.2. Changes in source zone architecture and down-gradient plumes following surfactant flushing of PCE-DNAPL source zones.

A total of four aquifer cell experiments were conducted to quantify the effects of partial mass removal on dissolved-phase PCE concentrations and mass discharge as a function of the initial source zone architecture. The initial source zone PCE saturation distribution profiles obtained by LT analysis were expressed in terms of the ganglia-to-pool (GTP) volume ratio, yielding values of 1.60 (HI-GTP), 0.40 (MID-GTP), 0.26 (MID/LO-GTP) 0.16 (LO-GTP) for the four aquifer cells. In the HI-GTP cell, the GTP value of 1.60 indicates that 62% of the PCE volume existed as discrete ganglia or droplets, while the remaining 38% was present in high-saturation (S_{PCE} > 13%) pools (Figure 41, top row). For the two intermediate GTP cells, 20-30 mesh Accusand was used as the background porous media to reduce the amount of PCE entrapped as residual ganglia. Approximately 15 mL of PCE was introduced into the MID-GTP aquifer cell, resulting in an overall PCE saturation of 0.4%, and a GTP value of 0.4 (28.6% as ganglia). In the MID/LO-GTP aquifer cell, the volume of PCE released was increased to 25.5 mL, which further reduced the relative amount of residual PCE (GTP = 0.26, 21% as ganglia). The LO-GTP cell was packed with 20-30 mesh Accusand and the PCE injection rate was lowered from 1.0 to 0.1 mL/min to achieve a source zone that was characterized by extensive pooling. Of the 25.1 mL of PCE introduced into the LO-GTP aquifer cell, 86% existed in high-saturation pools (GTP = 0.16), which were primarily located immediately above the lower confining layer of the cell. The initial properties of the four aquifer cell experiments are summarized in Table 7.

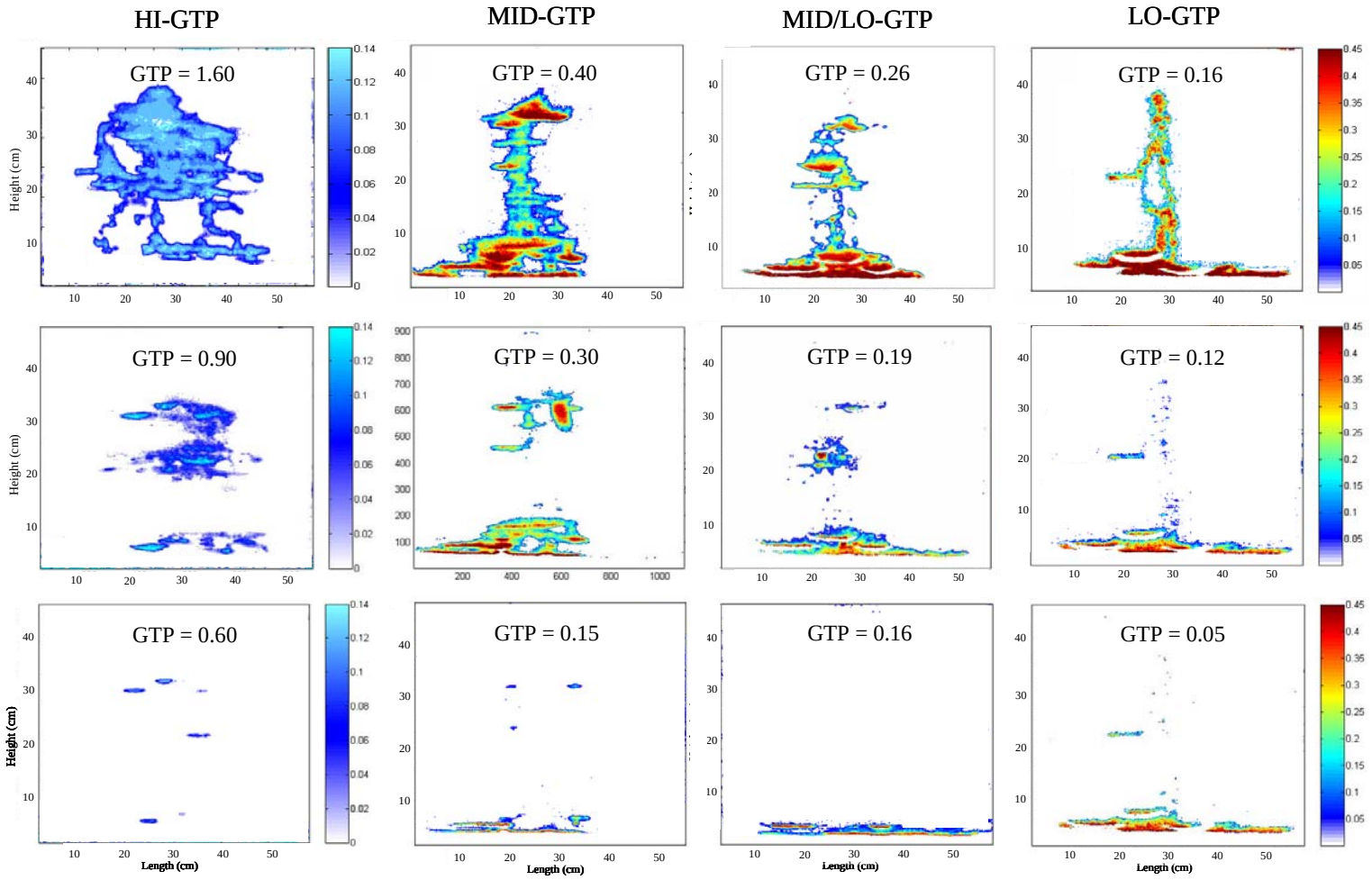

Figure 41: PCE saturation distribution profiles for the HI-GTP, MID-GTP, MID/LO GTP and LO-GTP aquifer cells prior to surfactant flushing (top row), after the first surfactant flood (middle row), and after the final surfactant flood (bottom row). *(Suchomel and Pennell 2006)*

Table 7: Summary of PCE-DNAPL aquifer cell (1.5 m) experimental conditions. *(Suchomel and Pennell 2006)*

2-D Cell Parameter	HI-GTP	MID-GTP	MID/LO-GTP	LO-GTP
Background porous medium	Mixed Accusand	20/30 mesh Accusand	20/30 mesh Accusand	20/30 mesh Accusand
Total pore volume (mL)	3630	3950	3950	3820
Hydraulic conductivity (cm/min)	2.75	5.83	12.05	33.33
PCE injection rate (mL/min)	1.0	1.0	1.0	0.1
PCE injection volume (mL)	40.9	15.3	25.5	25.1
Overall PCE saturation (%)	1.1	0.4	0.6	0.6
Initial PCE GTP	1.60	0.40	0.26	0.16
Surfactant Flood 1				
Volume injected (mL)	4500	3210	5360	3370
Flow rate (mL/min)	5.72±0.50	5.71±1.84	6.05±0.35	8.59±2.27
Pore-water velocity (cm/hr)	14.18	13.07	13.85	20.18
Surfactant Flood 2				
Volume injected (mL)	4500	3210	5360	3370
Flow rate (mL/min)	5.47±0.21	8.12±1.81	5.52±0.46	7.12±2.50
Pore-water velocity (cm/hr)	13.57	18.59	12.64	16.72
Surfactant Flood 3				
Volume injected(mL)		4480		3630
Flow rate (mL/min)		8.00±2.47		7.38±2.26
Pore-water velocity (cm/hr)		18.32		17.34

III.3.2.1 PCE-DNAPL Mass Recovery

Two sequential 4% Tween™ 80 surfactant floods, separated by a water flood, were conducted in the HI-GTP (GTP = 1.60) aquifer cell, resulting in a total PCE recovery of approximately 75% (31 mL). Cumulative PCE mass recovery of over the course of the entire experiment is shown in Figure 42. Here, the shaded areas correspond to the injection of 4% Tween 80 solution, while the non-shaded areas correspond to water flushing. In the first surfactant flood of the HIGH-GTP cell, 21 mL of PCE were recovered after flushing with 4,500 mL (1.23 PVs) of 4% Tween 80 solution, while the second surfactant flood (2.25 PVs) yielded the additional recovery of 10 mL of PCE. Both the rate and extent of PCE recovery were greater during the first surfactant flood

compared to the second flood, as indicated by the PCE to surfactant recovery efficiency (g PCE recovered/g Tween 80 injected), which declined from 0.12 g/g in the first flood down to 0.06 g/g in the second flood. This behavior was attributed to the dissolution of high-interfacial area ganglia, which accounted for 62% of the initial PCE volume, followed by less favorable dissolution of PCE from lower-interfacial area pools. Recovery parameters for each of the PCE-DNAPL aquifer cell experiments are summarized in Table 7.

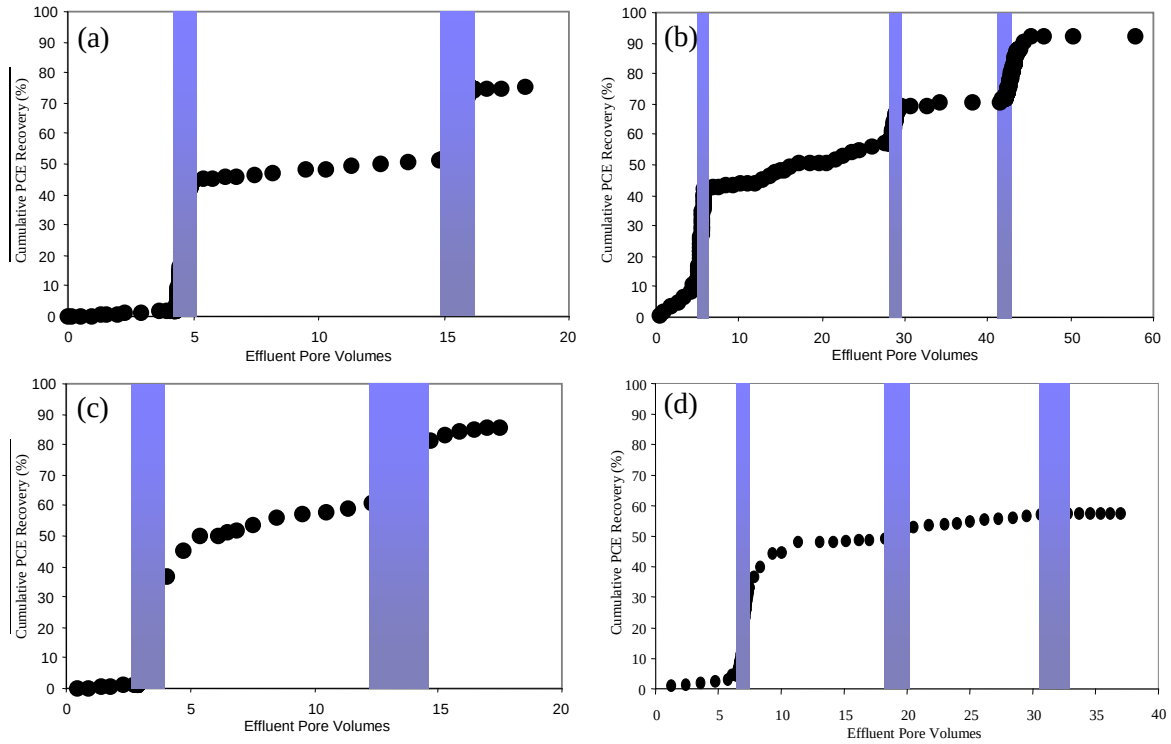

Figure 42: Cumulative PCE mass recovery from the (a) HI-GTP, (b), MID-GTP, (c), MID/LO-GTP, and (d) LO-GTP aquifer cells. *(Suchomel and Pennell 2006)*

In the second PCE-DNAPL aquifer cell experiment (MID-GTP; GTP = 0.4), three surfactant (4% Tween 80) floods, separated by two water floods, yielded an overall PCE mass recovery of 92% (Table 8, Figure 42). The relatively steep rise in PCE mass recovery observed in the MID-GTP cell at early time is the result of PCE dissolution during the initial water flood, which is more pronounced than in the other experiments due to the smaller initial volume of PCE-DNAPL (15 mL). Of the total volume of PCE recovered (14.1 mL) from the MID-GTP cell, 55.0% was removed during the first 0.81 PVs 4% Tween 80 flood, while an additional 3.0 and 3.3 mL of PCE were recovered during the second (0.8 PVs) and third (1.13 PVs) 4% Tween 80 floods, respectively. Thus, the three sequential Tween 80 floods yielded PCE to surfactant recovery efficiencies of 0.10, 0.04 and 0.03 g/g, respectively.

In the third PCE-DNAPL aquifer cell experiment (MID/LO-GTP, GTP = 0.26) experiment, a total of 21.7 mL (85%) of PCE were recovered after flushing with 1.36 and 2.10 PVs of 4% Tween 80 solution (Table 8, Figure 42). The corresponding PCE to surfactant recovery efficiencies for each Tween 80 flood were 0.10 and 0.4 g/g, respectively. These recovery efficiencies obtained for the MID- and MID/LO-GTP experiments are similar despite differences

in the initial PCE volume (15.3 versus 25.5 mL) and number of surfactant floods. This finding indicates that the fraction of PCE mass existing as ganglia (28 and 20%, respectively), as represented by the GTP ratio, strongly governs partial mass recovery resulting from a dissolution process such as micellar solubilization.

Table 8: Effect of surfactant flushing on PCE mass removal, GTP ratio, effluent concentrations, and mass discharge from the aquifer cells. *(Suchomel and Pennell 2006)*

2-D Cell Parameter	HI-GTP	MID-GTP	MID/LO-GTP	LO-GTP
initial GTP [% ganglia]	1.6 [61.5]	0.40 [28.6]	0.26 [20.6]	0.16 [13.8]
initial flux-averaged conc. (mg/L)	95.0±20.0[b]	101.0±6.0	157.0±10.7	57.0±3.8
initial mass discharge (mg/min)	1.26±0.017	1.54±0.006	3.04±0.014	1.31±0.006
total PCE recovered (mL) [%]	30.7 [75.2]	14.1 [92.2]	21.7 [85.1]	14.4 [57.4]
Post Surfactant Flood 1				
PCE recovered (mL) [cum. %]	20.9 [51.3]	7.8 [51.0]	13.2 [51.8]	12.0 [47.9]
GTP [% ganglia]	0.90 [47.4]	0.30 [23.1]	0.19 [16.0]	0.12 [10.7]
flux-ave. effluent conc. (mg/L)	113.0±12.0	63.6±7.6	76.1±16.3	20.0±2.0
relative effluent conc. (C/C_o)	1.00±0.12[b]	0.68±0.06	0.48±0.10	0.35±0.10
effluent mass discharge (mg/min)	0.105±0.011	0.090±0.011	0.112±0.024	0.026±0.003
relative mass discharge (MD/MD_o)	1.07±0.17	0.77±0.07	0.50±0.12	0.35±0.10
Post Surfactant Flood 2				
PCE recovered (mL) [cum. %]	9.8 [75.2]	3.0 [70.6]	8.5 [85.1]	1.2 [52.5]
GTP [% ganglia]	0.60 [37.5]	0.25 [20.0]	0.16 [13.8]	0.06 [5.7]
flux-ave. effluent conc. (mg/L)	36.7±3.6	59.7±13.8	6.3±1.8	14.8±2.4
relative effluent conc. (C/C_o)	0.36±0.04	0.59±0.27	0.04±0.04	0.26±0.13
effluent mass discharge (mg/min)	0.033±0.003	0.077±0.022	0.090±0.003	0.018±0.003
relative mass discharge (MD/MD_o)	0.31±0.02	0.74±0.27	0.04±0.04	0.26±0.13
Post Surfactant Flood 3				
PCE recovered (mL) [cum. %]		3.3 [92.2]		0.3 [53.8]
GTP [% ganglia]		0.15 [13.0]		0.05 [4.7]
flux-ave. effluent conc. (mg/L)		28.9±5.6		12.6±2.2
relative effluent conc. (C/C_o)		0.27±0.11		0.23±0.15
effluent mass discharge (mg/min)		0.039±0.007		0.016±0.003
relative mass discharge (MD/MD_o)		0.35±0.11		0.23±0.15

In the LO-GTP (GTP = 0.16) aquifer cell experiment, which was designed to simulate a source zone dominated by a single PCE-DNAPL pool above the lower confining layer, a total of 14.4 mL (57.4%) of PCE were recovered after three sequential surfactant floods (Table 8, Figure 42). The first 0.9 PV surfactant flood yielded a PCE to surfactant recovery efficiency of 0.14 g/g, which is similar to the values obtained for the initial 4% Tween 80 floods in the other aquifer cell experiments. The observed consistency in initial mass recovery efficiencies regardless of the GTP ratio is attributed to the dissolution of PCE-DNAPL ganglia, which accounted for at least 14% of the initial PCE mass in all of the aquifer cell experiments. However, as the PCE-DNAPL ganglia were depleted in the LO-GTP experiment, mass recovery efficiencies declined substantially; to 0.014 g/g in the second flood and 0.004 g/g in the third flood. These data indicate that in strongly pool-dominated source zones (low GTP), where ganglia represent a relatively small fraction (e.g., < 25%) of the initial DNAPL mass, remediation strategies based, or dependent upon, dissolution will exhibit reduced mass recovery efficiency over time as the total NAPL interfacial area available for mass transfer decreases. This finding is consistent with cumulative mass recovery data obtained for surfactant and cosolvent flushing of heterogeneous source zones at both laboratory and field scales *(Rao 1997; Taylor et al. 2001; Soga et al. 2004)*.

III.3.2.2 Change in PCE-DNAPL saturation distributions

The change in GTP ratios as a function of PCE mass removal are shown in Table 8 for each aquifer cell experiment, along with the corresponding percentage of PCE-DNAPL remaining as ganglia (i.e., $S_{PCE} \leq 11\%$ or 13%). In addition, LT images of the PCE saturation distribution profile obtained after the first and final surfactant flood are shown in Figure 42 (middle and bottom rows, respectively) for each aquifer cell experiment. The GTP ratios decreased with increasing PCE recovery in all experiments, providing further evidence that high interfacial area ganglia are readily removed during micellar solubilization surfactant floods. Reductions in the volume of ganglia (Figure 43) and GTP ratio (Table 8) were most pronounced in the HI-GTP experiment, for which the GTP ratio decreased from an initial value of 1.60 (25.1 mL as ganglia) to a final value of 0.60 (3.8 mL as ganglia). In contrast, for the LO-GTP experiment the GTP ratio decreased from an initial value of 0.16 (3.46 mL as ganglia) to a final value of 0.05 (0.55 mL as ganglia). The sizable decrease in the GTP ratio observed after surfactant flushing of the HI-GTP cell was attributed to dissolution of the relatively large volume of ganglia initially present in the source zone (62%). In contrast, the low GTP ratio (0.05) obtained at the conclusion of the LO-GTP experiment was consistent with the persistent high-saturation pools existing above the lower layer of F70 Ottawa sand (Figure 41).

III.3.2.3 Plume concentrations and mass discharge

The effects of source zone mass removal on down-gradient plume concentrations and flux-averaged effluent concentrations were monitored after each surfactant flood. Representative dissolved-phase PCE concentrations are shown in Figure 44 for the HI-GTP aquifer cell, along with the corresponding source zone saturation distribution. Following the first surfactant flood of the HI-GTP cell, which achieved 51% mass removal, dissolved-phase concentrations remained near the equilibrium solubility of PCE (200 mg/L) immediately down-gradient from the most highly contaminated region of the source zone, in which high interfacial area ganglia persisted (Figure 43, middle row). Following the second surfactant flood which resulted in 75%

PCE mass removal, however, concentrations of PCE in the plume did not exceed 40 mg/L (Figure 44, bottom row). Corresponding values of mass flux (mass/area·time) within the dissolved-phase plume are shown in Figure 45 as function of vertical position and PCE mass removal. The highest mass flux values occurred immediately down-gradient from the source zone regions with the greatest contamination since the flow profile was relatively uniform throughout the cell despite the presence of lower-permeability lenses and entrapped PCE.

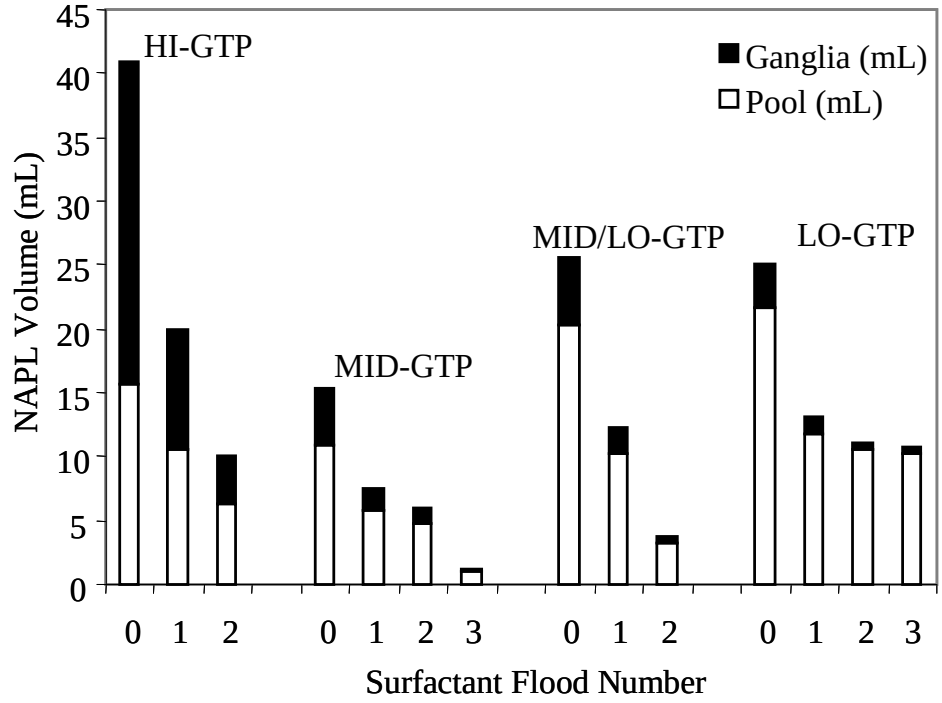

Figure 43: Comparisons of the PCE-DNAPL volume existing as ganglia and pools in the source zone of the aquifer cells following each sequential surfactant flood. (Suchomel and Pennell, 2006)

Relative effluent (flux-averaged) concentrations and mass discharge (mass/time), normalized to the initial condition (i.e., prior to the first surfactant flood) are summarized in Table 8 and plotted as a function of cumulative PCE recovery in Figure 45. For the HI-GTP experiment, relative PCE effluent concentrations and mass discharge remained essentially constant after 50% PCE mass removal, which was attributed to the persistence of PCE ganglia over much of the source zone. However, a 60% reduction in relative mass discharge occurred following the second surfactant flood, at which time 85% of PCE mass initially present as ganglia had been removed (Table 8, Figure 43).

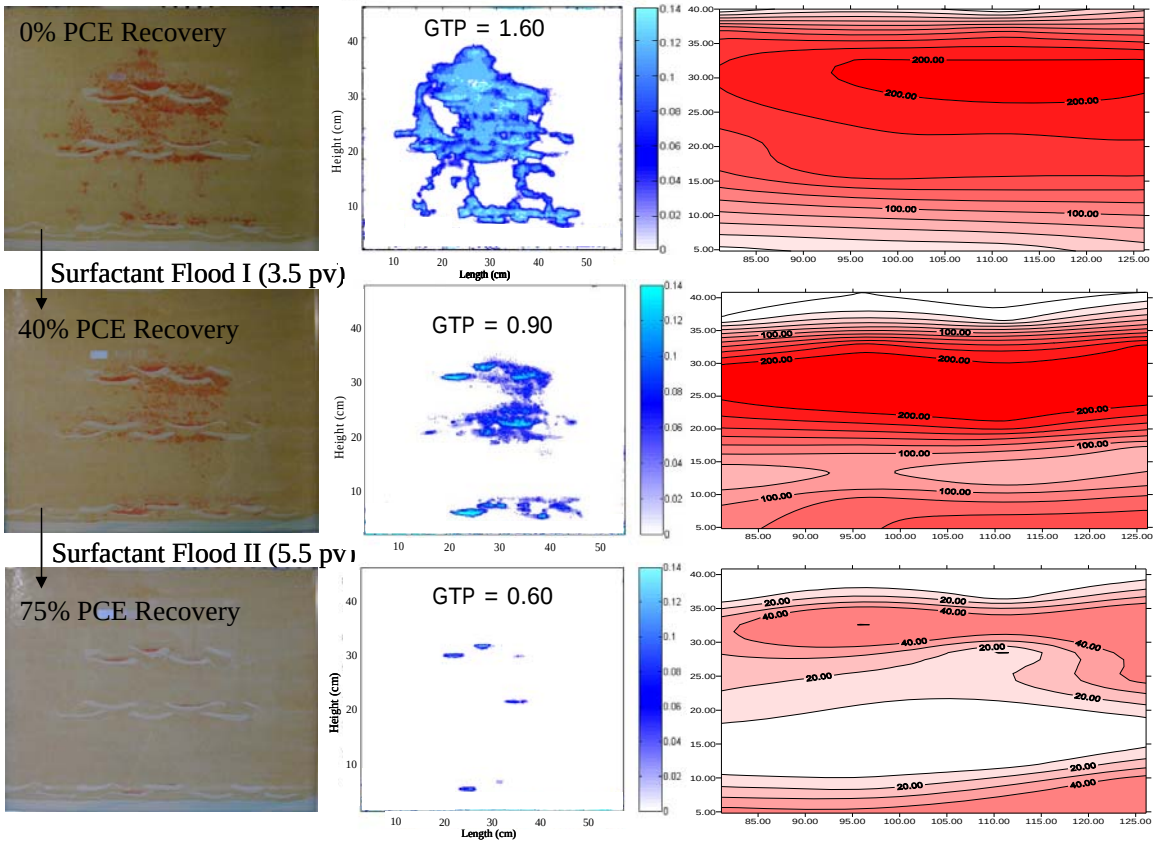

Figure 44: Change in source zone saturation distribution and corresponding down-gradient plume concentrations for the HI-GTP aquifer cell prior to surfactant flushing (top row), after the first surfactant flood (middle row), and after the second surfactant flood (bottom row). *(Suchomel and Pennell 2006)*

In the remaining aquifer cell experiments, incremental reductions in relative PCE effluent concentrations and mass discharge occurred after each sequential surfactant flood, with the greatest reductions observed in the LO-GTP aquifer cell. This trend is consistent with the fraction of initial PCE mass existing as ganglia, which was reflected in GTP ratio. For example, the observed reduction in relative mass discharge was the greatest in the LO-GTP cell (65% reduction after 55% PCE mass removal). However, it should be noted that during the second and third surfactant floods of the LO-GTP cell, when the remaining PCE mass existed in high saturation pools (GTP < 0.06), very little additional PCE mass was recovered. Hence, the effectiveness of dissolutiuon-based surfactant recovery technologies is diminished as the source zone became more pool-dominated (GTP decreased), although mass discharge stabilized at a relatively low level (0.016 mg/min) in the LO-GTP case.

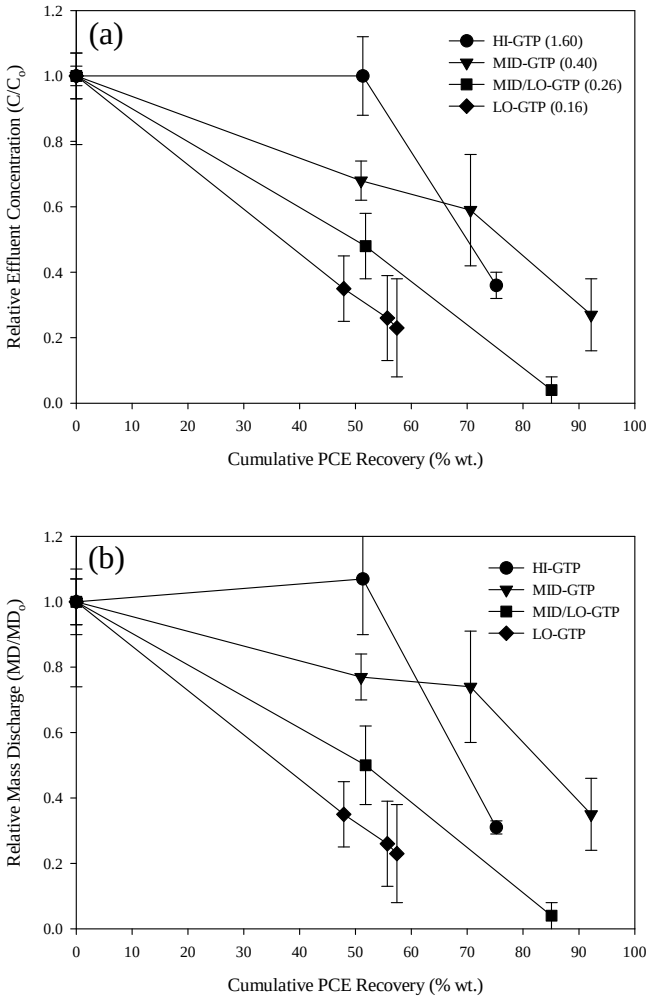

Figure 45: Relative flux-averaged effluent concentration (a) and mass discharge (b) as a function of increasing cumulative PCE recovery for the four aquifer cell experiments. *(Suchomel and Pennell 2006)*

The key findings of the PCE-DNAPL aquifer cell studies are:

- Flux-averaged effluent concentrations and mass discharge are expected to decrease substantially (> 40%) following partial (50-85%) source zone mass removal.
- The relationship between mass removal achieved by enhanced dissolution (i.e., micellar solubilization) and reductions in mass discharge is strongly dependent upon the source zone saturation distribution; specifically, the relative fraction of PCE mass existing as ganglia and pools which can be expressed as the GTP ratio.
- In ganglia-dominated source zones (GTP > 1.0; > 50% ganglia), substantial mass removal (>70%) may be required before meaningful reductions in mass discharge are realized.
- In pool-dominated source zones (GTP < 0.5, 33% ganglia) may exhibit substantial reductions in mass discharge following relatively modest mass removals (e.g., 50-70%).

- Local plume concentrations and overall mass discharge following partial treatment of low-GTP source zones may be compatible with lower-capitol cost, longer-term treatment strategies, or may fall below the attenuation capacity of the down-gradient aquifer formation.

III.3.3 Biotic aquifer cell experiments

As discussed in Section II.4, a 2-D aquifer cell was designed and operated under anaerobic conditions to evaluate potential enhancements in chlorinated ethene dissolution in heterogeneous DNAPL source zones undergoing metabolic reductive dechlorination. After the introduction of the PCE-DNAPL and the initial 7-10 pore volume plume development period, the resulting ganglia-to-pool (GTP) ratio measured by light transmission analysis in the source zone was 1.6, indicating that 60% of the DNAPL volume consisted of entrapped ganglia while the remaining 40% corresponded to high-saturation pools (So>0.13). Following the initial light transmission analysis, two separate surfactant floods, corresponding to a total of 2.3 pore volumes of 4% (wt.) Tween 80 solution, were injected into the aquifer cell at a flow rate of 4.0 mL/min to reduce the NAPL mass in the source zone and the aqueous phase PCE concentrations. Prior to the first surfactant flood, the down-gradient plume and flux-averaged effluent concentrations were high, approaching the aqueous solubility of PCE (>150 mg/L). Following the first surfactant flood, approximately 28% of the initial PCE-DNAPL mass was removed, and flux-averaged effluent concentrations dropped to 130 mg/L. However, side port sample measurements indicated that the majority of down-gradient plume concentrations still approached or exceeded aqueous solubility of PCE (>150 mg/L). These dissolved phase PCE concentrations were above inhibitory levels determined for several dechlorinating cultures (~90 mg/L; *(Amos et al. 2008a)*). Therefore, an additional surfactant flood was undertaken to further reduce PCE-DNAPL mass and the corresponding PCE concentrations.

After the second surfactant (4% Tween 80) flood, an additional 20% of the PCE-DNAPL mass was removed from the aquifer cell, which resulted in a further reduction in the flux-averaged effluent PCE concentration to 80 mg/L. Concentrations of PCE were below 60 mg/L in half of the side ports and below the aqueous solubility of PCE in most down-gradient locations. The highest dissolved-phase PCE concentrations (>150 mg/L) were located near the box outlet. After each surfactant flood the PCE-DNAPL saturation was quantified using the light transmission system, which indicated that GTP ratio decreased incrementally from 1.60 to 1.38 (1^{st} surfactant flood), and from 1.37 to 1.07 (2^{nd} surfactant flood). The aquifer cell was also flushed with approximately 22-30 pore volumes of de-aired water at a nominal flow rate of 1.0 mL/min to monitor post-treatment dissolved-phase plume development and mass flux, which resulted in an additional 3-4% mass removal, following each surfactant flush. Approximately 58% of the initial PCE-DNAPL mass was recovered over the course of the two surfactant floods and subsequent water flushes.

Immediately prior to the introduction of the mineral salts medium to support biological reductive dechlorination, the PCE concentrations measured in the effluent had decreased to 50 mg/L, and all down-gradient plume side port sample concentrations were below less than <150 mg/ L. High concentrations (>100 mg/L) were now only measured in two locations; a) near the bottom of the aquifer cell where approximately 8 mL of pooled PCE-DNAPL remained, and b)

in two side-port samples located next to the effluent outlet of the aquifer cell and directly down-gradient from the remaining ~8 mL of entrapped PCE-DNAPL ganglia (NAPL saturation < 0.13). These volumes of remaining PCE-DNAPL correspond to a final GTP ratio of 1.06 prior to bioaugmentation. Over 80% of the side sampling locations measured PCE concentrations < 25 mg/L, indicating that PCE concentrations were below the inhibitory levels determined in batch studies (~90 mg/L), and therefore, metabolic reductive dechlorination would be expected in most of the aquifer cell.

After flushing with less than 1 pore volume after bioaugmentation with BDI inoculum, evidence of reductive dechlorination activity was observed in the aquifer cell. Flux-averaged effluent PCE concentrations decreased from 45 mg/L (300 μM) before bioaugmentation to below 1 mg/L (6 μM) only 12 pore volumes after bioaugmentation. Flux-averaged effluent *cis*-DCE concentrations increased from below the detection limit to approximately 28 mg/L (292 μM) at 6 pore volumes and decreased down to less than 2 mg/L (30 μM) after 26 pore volumes of flushing following bioaugmentation . Vinyl chloride (VC) and ethene concentrations increased to ≤ 0.8 mg/L (13 μM) and ≤ 0.4 mg/L (14 μM), respectively, during the same 26 pore volume time frame. The flux-averaged molar chlorinated ethene concentration in the effluent 26 pore volumes after bioaugmentation was 2.95:1.4:1 *cis*-DCE to VC to ethene. After 26 PVs of flushing a 14-day flow interruption was initiated. Upon restarting flow in the aquifer cell, concentrations of cis-DCE (33 mg/L), VC (11.3 mg/L) and ethene (3.6 mg/L) all spiked to concentrations exceeding those measured previously. After an additional 5 PVs of flushing (31 PVs since bioaugmentation), concentrations of cis-DCE returned close to levels (3.7 mg/L, 38μM) measured prior to flow-interruption, as did VC (1.5 mg/L, 25.5μM) and ethene (0.7 mg/L, 25.5μM)

Aqueous phase measurements obtained from side ports located immediately down-gradient from the original PCE-DNAPL source zone and near the bottom of the aquifer cell indicated concentrations of PCE that were less than or equal to 70 mg/L (430 μM), with *cis*-DCE concentrations up to 60 mg/L (620 μM) in the same location. Interestingly, VC (≤ 3.6 mg/L, 57 μM) and ethene (≤ 0.8 mg/L, 27.5 μM) were detected down-gradient from the elevated PCE concentrations. Organic acid measurements obtained from side port and effluent samples, along with effluent hydrogen analysis, verified that sufficient electron donor was available throughout the aquifer cell. Therefore, lack of available electron donor did not limit reductive dechlorination activity in the aquifer cell. Alternatively, the dechlorinating populations (i.e., *Dehalococcoides*) in BDI are likely to be inhibited in presence of high concentrations of polychlorinated ethenes (i.e., PCE and *cis*-DCE). Similar inhibition was observed in the bioenhanced dissolution column experiments (Section *III.2.3*). Therefore, production of VC and/or ethene is likely to be limited until additional PCE-DNAPL mass is removed from the aquifer cell and aqueous phase *cis*-DCE concentrations have declined below 10 μM (Section *III.2.3*).

The results of this combined remedy experiment indicate that surfactant flushing followed by bioaugmentation is feasible for enhanced PCE-DNAPL source zone remediation. However, biologically enhanced dissolution is likely to be limited near persistent DNAPL pool sources and greatest mass transfer enhancement is most probable to occur in high GTP source zones (ganglia dominated).

III.4 MATHEMATICAL MODELING

III.4.1 Modeling metabolic reductive dechlorination

III.4.1.1 Batch Systems

The model described in II.5.1 was used to model batch experiments described in III.1 and obtain best-fit dechlorination kinetic coefficients. Model simulations of dissolved phase chlorinated ethene concentrations undergoing dechlorination by strain BB1 are shown in Figure 46. These results demonstrate that the fitted model provided a good representation of the concentration data from the dissolved-phase experiments. Incorporation of a substrate inhibition expression correctly predicted the cessation of dechlorinating activity when PCE concentrations approached the experimentally-derived inhibitory PCE concentration (i.e., ~540 μM for strain BB1, Figure 46b). Differences between the simulated and experimental PCE concentrations following amendment of additional PCE on Day 2 (Figure 46b) stem from the model assumption that equilibrium between the gas and aqueous phases occurred instantaneously, while the experimental results suggest a short period (< 1 day) of equilibration.

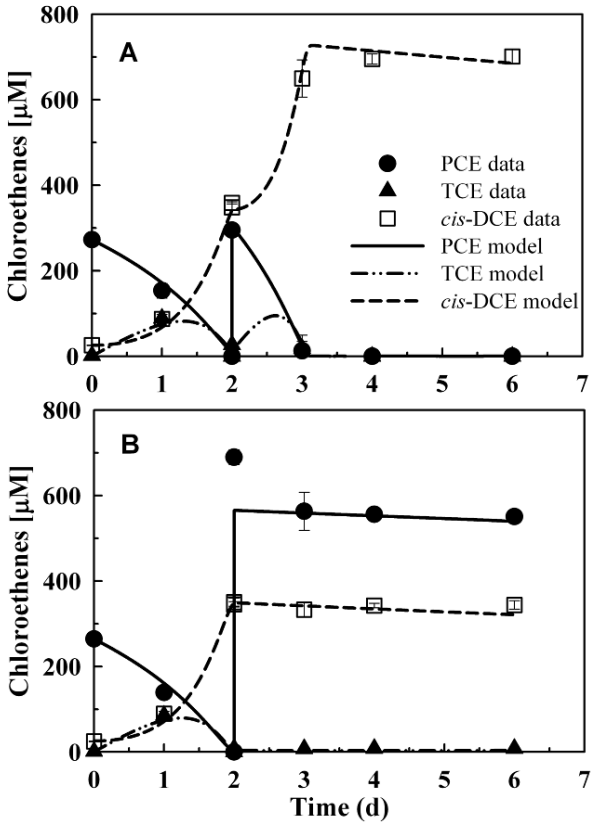

Figure 46: Dechlorination performance of *Desulfuromonas michiganensis* strain BB1 at various PCE concentrations. Low PCE concentrations were used for all initial conditions (Days 0-2), followed by amendment of additional PCE to tolerable (a) or intolerable (b) PCE concentrations. The lines represent simulated chlorinated ethene concentrations fitted (a) or predicted (b) by the developed mathematical model *(Amos et al. 2007a)*.

The best-fit kinetic coefficients were then used along with a fitted dissolution mass-transfer coefficient obtained from an abiotic dissolution experiment (Figure 48) to predict dechlorination in a batch reactor contaminated with PCE-DNAPL. As shown in Figure 47, the model accurately predicted dechlorination in the presence of PCE DNAPL using the best-fit kinetic coefficients obtained from the dissolved-phase simulations and a best-fit mass transfer coefficient (κ^{PCE} = 1.84 ± 0.03 m/d, $C_{ao}^{PCE\text{-}e}$ = 1043 ± 2 μM) obtained by fitting the model with X_0 = 0 mg/L to PCE dissolution from the PCE DNAPL in the inactivated control (Figure 48). Initial biomass concentrations were assumed to be equal to the initial biomass concentration from the dissolved-phase experiments and biomass growth attributed to the supply of dissolved-phase PCE concentrations below inhibitory values was simulated to estimate the biomass concentration at the time of PCE DNAPL addition. For strain BB1, the model predicted PCE dechlorination to TCE and *cis*-DCE before accumulation of PCE in the aqueous phase to inhibitory concentrations (~540 μM), as was observed experimentally (Figure 47). Furthermore, the model correctly predicted that the dechlorination activity of *S. multivorans* would prevent significant PCE accumulation, resulting in accumulation of *cis*-DCE and ultimately the complete dissolution of the PCE DNAPL, as was observed experimentally (Figure 48). Although the simulated rate of *cis*-DCE accumulation slightly exceeded the observed value, the simulated and experimental time to complete dissolution of the PCE DNAPL is approximately the same (13 days after DNAPL addition). The difference between the measured and predicted rates of *cis*-DCE accumulation could be attributed to (i) assumptions used to model dissolution (e.g., diminishing sphere model), (ii) changes in the dissolution rate due to microbial growth on or near the surface of the DNAPL, (iii) inhibition of microbial activity at increasing *cis*-DCE concentrations, and/or (iv) changes in PCE dissolution rates from the NAPL due to partitioning of *cis*-DCE into the NAPL.

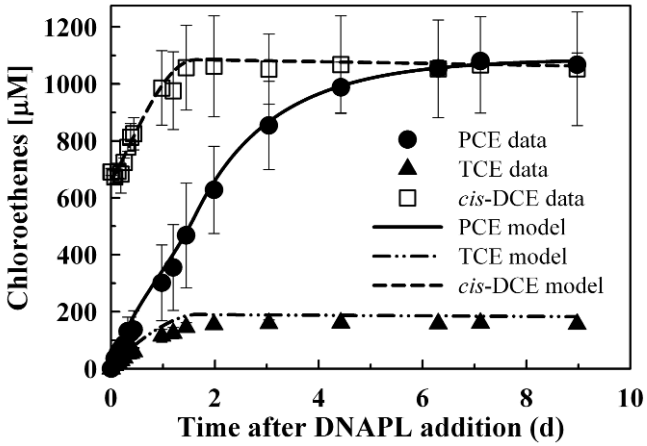

Figure 47: Dechlorination performance of triplicate cultures of *Desulfuromonas michiganensis* strain BB1 in the presence of PCE DNAPL. All data points represent average values from triplicate cultures, and error bars represent one standard deviation. If no error bars are shown, the standard deviations were too small to be illustrated. The lines represent simulated chlorinated ethene concentrations predicted by the developed mathematical model *(Amos et al. 2007a)*.

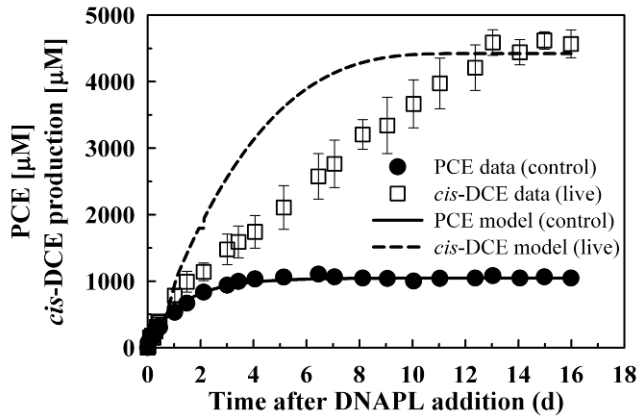

Figure 48: Dechlorination performance of *S. multivorans* cultures in the presence of PCE DNAPL. The lines represent simulated chlorinated ethene concentrations fitted (inactivated control data) or predicted (live data) by the developed mathematical model *(Amos et al. 2007a)*.

III.4.1.2 One and two dimensional bench-scale systems

The validated model described in II.5.1.2 was used to examine bioenhanced dissolution in hypothetical one and two dimensional experimental systems to explore the expected range of behavior and potential sensitivity to system parameters. Dechlorination kinetics, source zone characteristics (e.g., NAPL contaminated length, saturation), flushing conditions (e.g., ground water velocity, electron donor amendment), and biomass distribution were varied in the sensitivity analysis. Following the methods used in existing experimental studies (e.g., *(Yang and McCarty 2002)*), dissolution enhancement due to biological activity was computed in the numerical model as the ratio of the total simulated chloroethene flux (i.e., DNAPL component plus dechlorination products including ethene) through the down-gradient boundary of a biotic (J_{biotic}) and abiotic ($J_{abiotic}$) system:

$$E = \frac{J_{biotic}}{J_{abiotic}} \qquad (16)$$

Computing dissolution enhancement in this manner facilitates the determination of reductions or increases in mass flux due to bioenhanced dissolution.

Past experimental work has considered the role of the dechlorination rate on dissolution enhancement only indirectly through the use of different dechlorinating cultures. Depending upon the culture, these experiments have revealed that the rate of dechlorination may vary by up to an order-of magnitude. Thus, the modeled PCE maximum utilization rate, based on the value used to simulate the Yang and McCarty *(Yang and McCarty 2002)* experiment (see II.5.1.2), was increased and decreased by an order-of-magnitude. Results are plotted in Figure 49. The lower dechlorination rate simulation demonstrates essentially no enhancement. In this scenario, the rate of dechlorination is too slow to affect the rate of dissolution. Simulation results for the higher dechlorination rate, however, indicate that mild increases in enhancement may be realized for dechlorinating cultures with rapid rates of PCE degradation. More appreciable enhancements may be realized by eliminating dechlorination rate limitations, such as electron donor limitations.

Length and configuration of the NAPL zone are also likely to be important factors in the success of a bioenhanced dissolution remediation strategy. To examine the affect of NAPL zone length on dissolution enhancement, the NAPL zone length was changed from 30cm to 60cm and reduced from 30cm (i.e., the entire column) to 20cm and 10cm (see Figure 50 a-c). All other parameters were kept constant. Simulation results are plotted in Figure 51. As expected, reductions in the NAPL zone length lead to reductions in dissolution enhancement. Or, put another way, increases in the NAPL zone length (e.g., 20 cm versus 10 cm) lead to increases in dissolution enhancement. However, increases in dissolution enhancement with NAPL length appear to decline in the numerical simulations, suggesting the existence of a maximum dissolution enhancement corresponding to the length at which electron donor becomes depleted.

To investigate the influence of NAPL saturation and configuration on dissolution enhancement predictions, two alternative initial organic phase saturations, two additional 10 cm DNAPL source-zone configurations in the one-dimensional column (Figure 50 d and e), and a hypothetical two-dimensional 15 cm DNAPL source zone (Figure 50 f) were modeled. These scenarios were selected to examine the effect of DNAPL saturation, total NAPL length, and system dimensionality on dissolution enhancement.

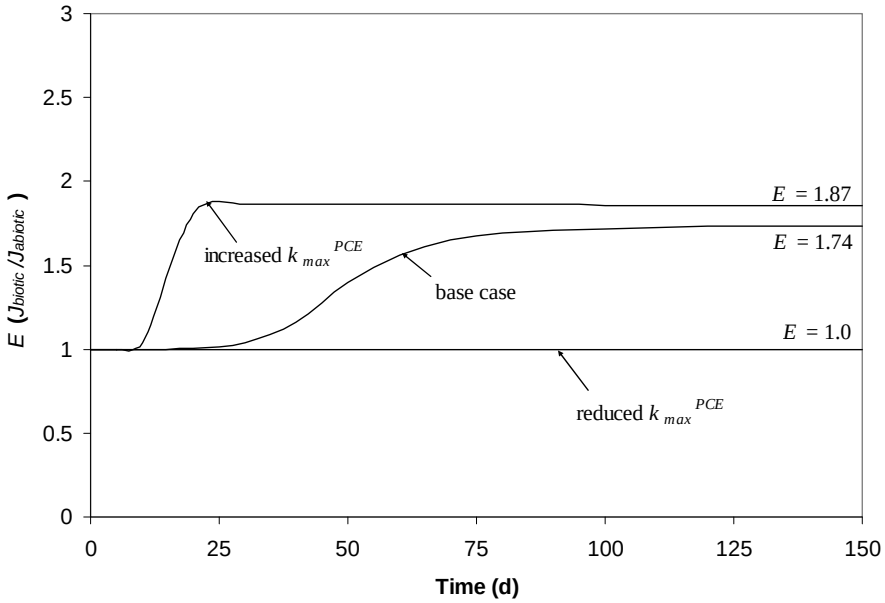

Figure 49: Dissolution enhancement as a function of time for three alternative k_{max}^{PCE} values. All other simulation parameters remain unchanged *(Christ and Abriola 2007)*.

An increase in the uniform DNAPL saturation distributed along the length of the column led to sustained rates of high mass transfer, which result in an increase in the simulated dissolution enhancement. For example, increasing the organic phase saturation from 0.02 to 0.2 (column retention time was kept at ~14 days), resulted in a dissolution enhancement prediction of 1.9. This value represents a ~10% increase in the predicted bioenhanced dissolution factor. Increasing the organic saturation to 0.5 resulted in a further increase in dissolution enhancement to 2.14. Changing the location of the 10 cm NAPL zone from the influent end of the column to

the center of the column (Figures 50 c and d) delayed the initial on-set of dissolution enhancement, however, the impact on the predicted steady-state dissolution enhancement was minimal (Figure 52). Although the microbial competitors thrived in the initial 10 cm of the column in the absence of high PCE concentrations, sufficient electron donor was present to drive the dechlorination reactions in the DNAPL zone. Dissecting the 10 cm NAPL zone into two 5 cm NAPL zones separated by a 5 cm zone that was initially uncontaminated (Figure 50e) increased the dissolution enhancement (E = 1.33 versus E = 1.2) (Figure 52). Although NAPL was not present in the 5cm zone separating the NAPL zones, dechlorination continued, resulting in reduced PCE concentrations that increased the dissolution driving force in the down gradient NAPL zone. This same observation appears to hold for two-dimensional systems. As shown in Figure 52 for a hypothetical laboratory scale two-dimensional domain (Figure 50f), with a 20 cm long non-uniform source-zone (10 cm NAPL length), the predicted dissolution enhancement is greater than that expected for a 10 cm NAPL zone length. This observation is important given the likelihood that DNAPL will be distributed non-uniformly due to tortuous migration paths and DNAPL fingering.

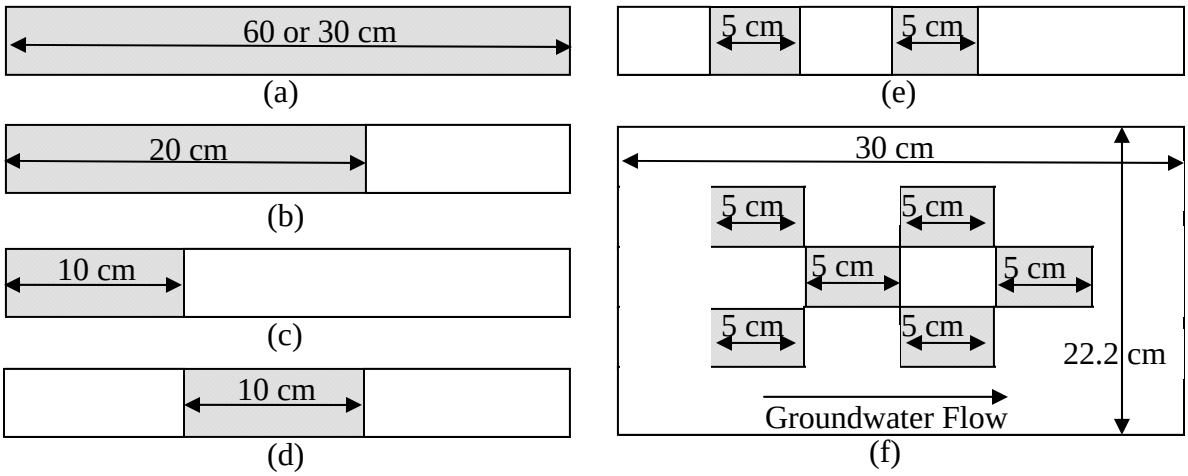

Figure 50: NAPL configuration (shaded area) used in simulations *(Christ and Abriola 2007)*.

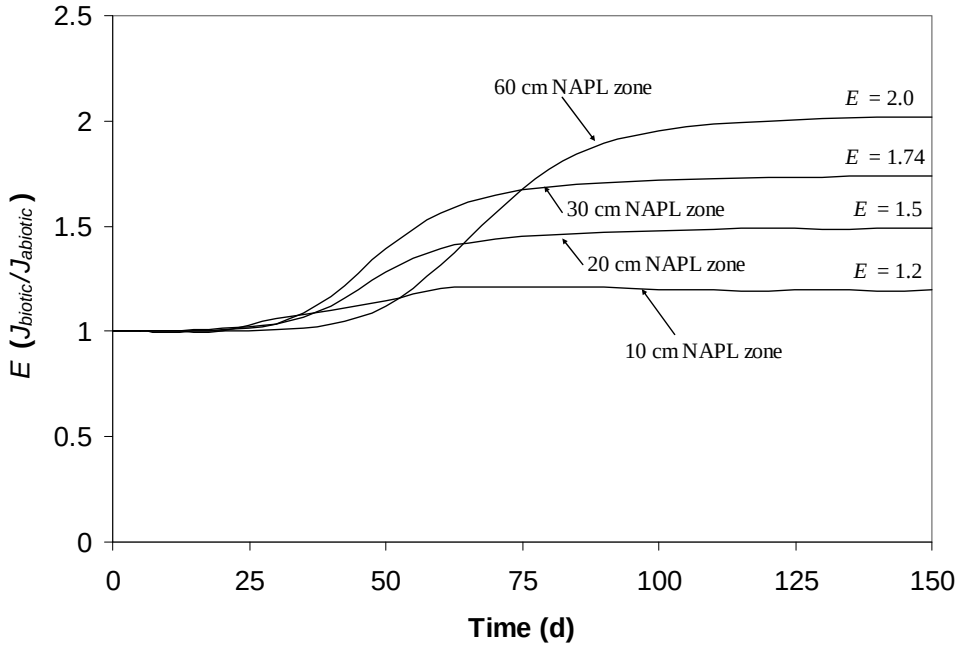

Figure 51: Dissolution enhancement factor as a function of time for the 60 cm, 30 cm, 20 cm, and 10 cm NAPL zone length *(Christ and Abriola 2007).*

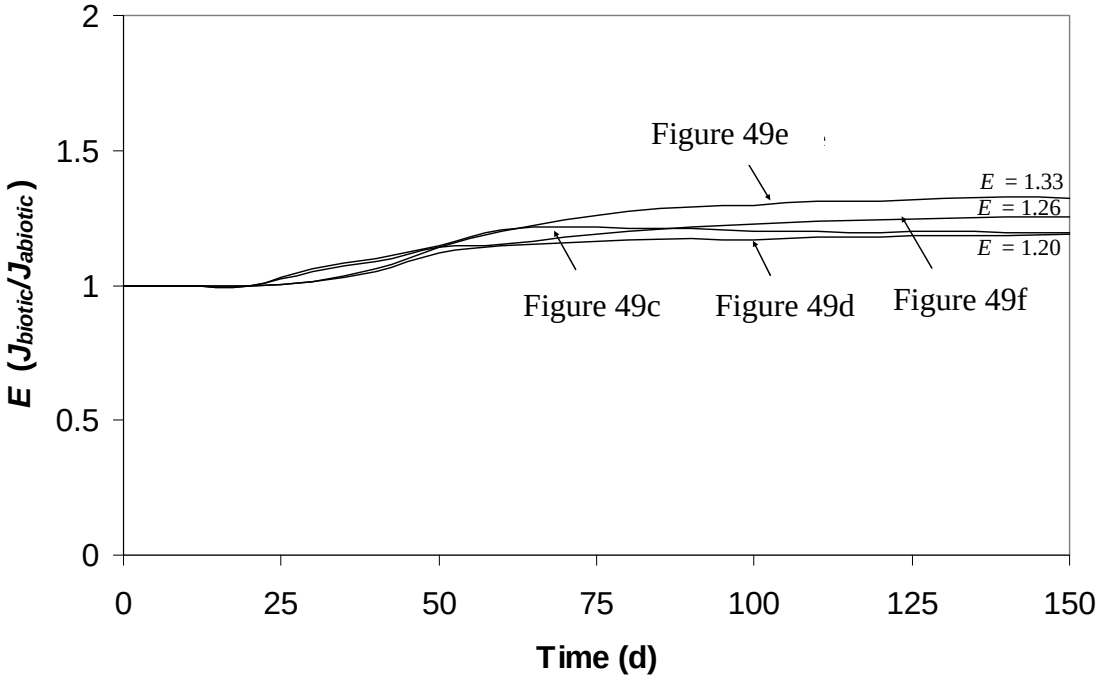

Figure 52: Dissolution enhancement factor as a function of time for alternative NAPL source configurations. See Figure 50 c – f *(Christ and Abriola 2007).*

The time required to completely dissolve residual NAPL in 1-D column experiments has typically exceeded the time-frame of an experiment. Thus, bioenhanced dissolution factors published in the literature generally represent the quasi-steady-state value. Although the time required to reach this steady-state value may be on the order of 50 to 100 days, relatively short compared to the longevity of the NAPL source, past research has failed to consider the length of time the system remains at the quasi-steady-state value. As NAPL dissolves, the rate of dissolution will likely change, leading to a reduction in the dissolution enhancement factor. Figure 53 demonstrates the eventual decline in the dissolution enhancement factor as the source-zone length (L_x) decreases due to dissolution. Eventually the system becomes dissolution limited and the bioenhanced dissolution factor is reduced to 1.0 (see 10 cm NAPL length curve in Figure 53). A failure to consider this behavior could lead to the erroneous estimation of source longevity at a site with active microbial reductive dechlorination. For example, in the 10 cm NAPL zone simulation, bioenhanced dissolution is sustained at the quasi-steady-state value for less than 50% of the time required to effect DNAPL removal. Failing to account for this transient effect could lead to overly-optimistic predictions of reductions in DNAPL source longevity due to bioenhanced dissolution.

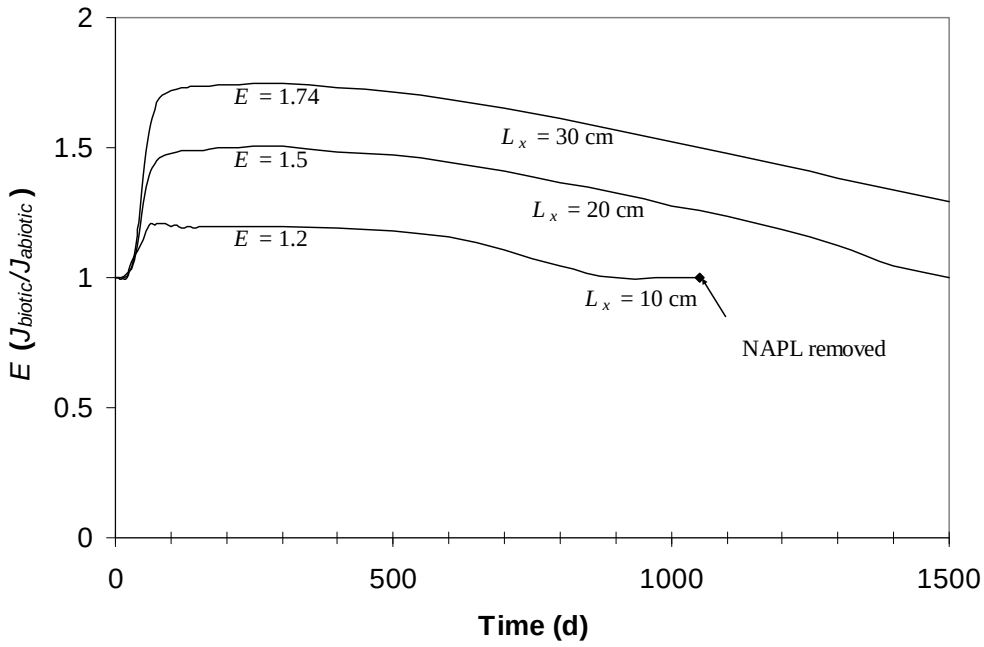

Figure 53: Bioenhanced dissolution as a function of time for 30 cm, 20 cm, and 10 cm NAPL zone lengths. Point on 10cm NAPL length curve indicates the time when NAPL was completely dissolved *(Christ and Abriola 2007).*

III.4.2 Modeling mass recovery from field-scale heterogeneous source zones

III. 4.2.1 Two-dimensional simulations

The suite of numerical simulators described in II.5.2 was employed to examine the relationship between source zone architecture and plume response. Two types of aquifer ensembles, described in II 5.2, tend to produce different DNAPL source zone architecture characteristics. Typical distributions of pool (high saturation area) and ganglia (low saturation area) cells are illustrated in Figure 54 for example realizations of correlated (a1) and independent (a2) ensembles. Here pools are defined as areas with organic liquid saturation higher than the maximum residual saturation, while ganglia as areas with saturation lower than the maximum residual saturation. *Lemke and Abriola (2004b)* found a GTP ratio ranging from 0.9 to 65.6 for the independent ensemble, while a range from 2.1 to 14.3 was found for the correlated ensemble. In addition, simulations suggested that increased depth of penetration, decreased spreading, and higher organic saturations for the independent ensemble.

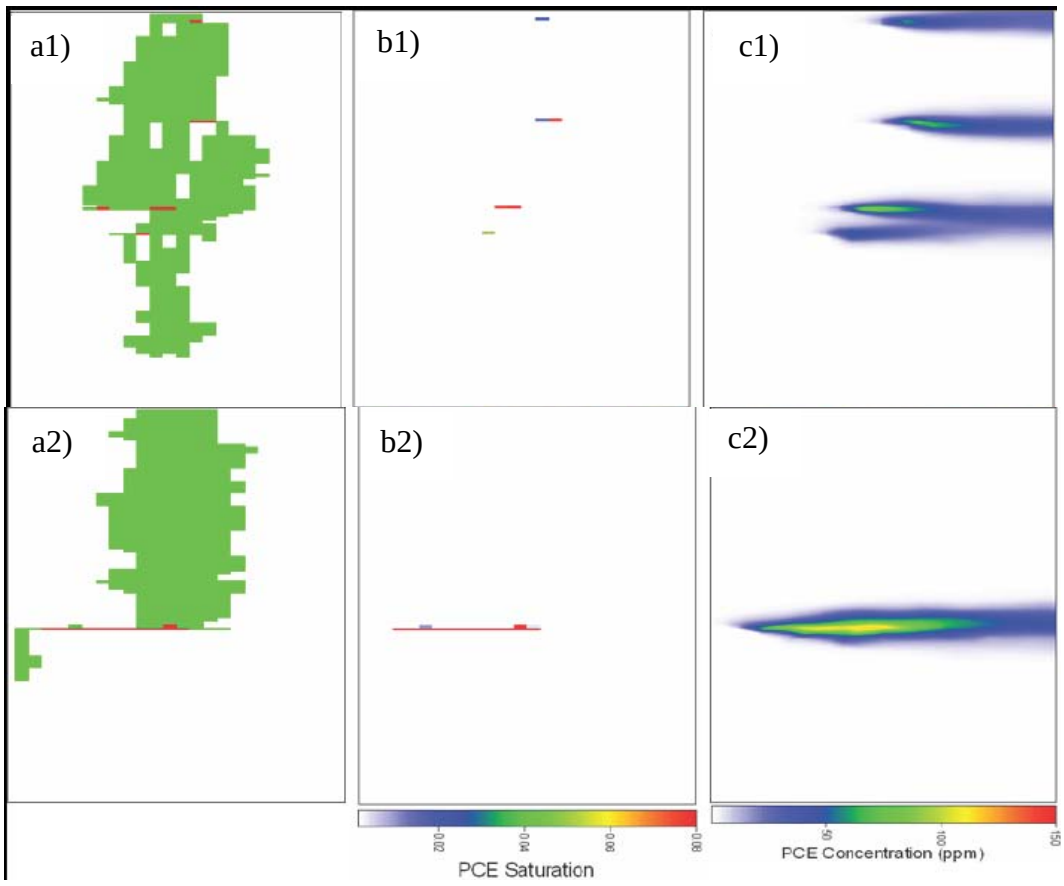

Figure 54. Example PCE DNAPL source zone architecture and dissolved PCE concentration from numerical simulation in correlated (row1) and independent (row2) ensembles: (a) presurfactant flush pool (red) and ganglia (green) cell; (b) postsurfactant flush saturation, and (c) postsurfactant flush aqueous PCE concentration under natural gradient flow from left to right across the profile. *(Lemke and Abriola 2006)*

MISER simulation results demonstrate that aqueous phase contaminant mass flux, predicted in response to % DNAPL removal, differs for source zone realizations with different DNAPL saturation architectures. Figure 55 shows the predicted mass flux reduction at a given level of DNAPL mass reduction for 8 different saturation distribution 'realizations'. Each of these realizations is based upon geostatistical models of the same formation. Six of these simulations (closed symbols) have DNAPL saturation distributions dominated by ganglia. The two saturation distributions that are dominated by pools (open symbols) show remarkably different behavior in mass flux reduction, suggesting the potential for significant flux reductions at moderate DNAPL mass reductions in such formations and supporting the use of the ganglia to pool (GTP) ratio as a quantitative metric to estimate mass flux behavior for a given level of mass removal.

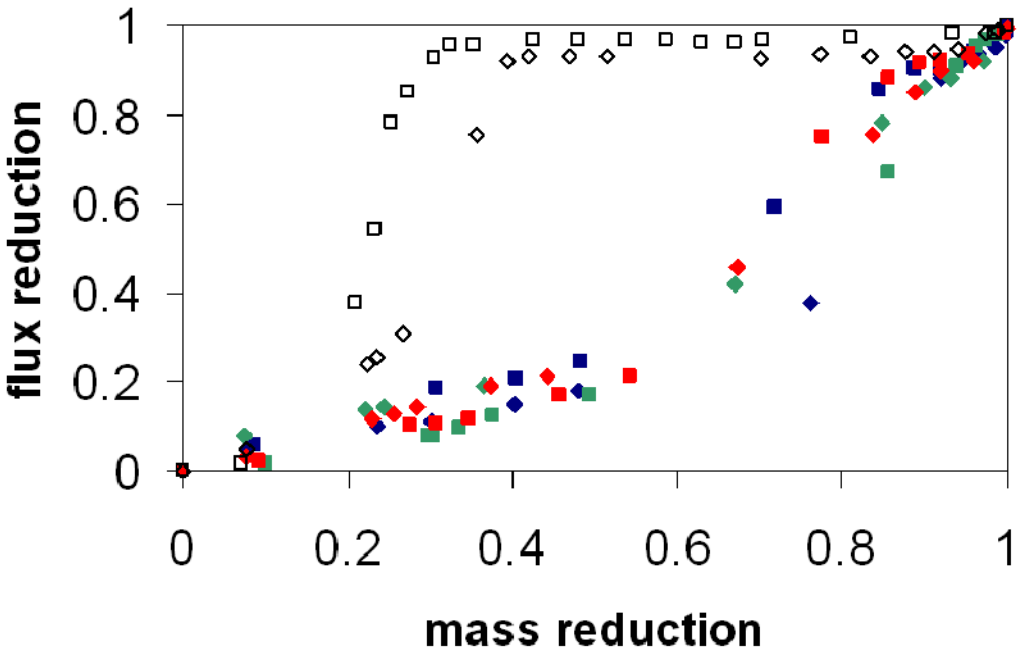

Figure 55: Flux reduction at the downstream model boundary following surfactant flush plotted as a function of DNAPL mass removal. See text for description of symbols.

Flux-weighted effluent PCE concentration was plotted as a function of PCE removal in Figure 56 for several independent realizations with ganglia-to-pool (GTP) ratios ranging from 0.9 to 65.6. Based on Figure 56, one order of magnitude or more decrease in aqueous phase effluent concentrations was predicted after only 60–70% PCE removal for low GTP ratio realizations. On the other hand, source zone with high GTP will require removal of 98 to 99% of entrapped PCE to achieve a second order of magnitude reduction in mass flux. This striking feature indicates that a low GTP ratio may be a favorable characteristic for partial mass removal of the DNAPL source zone, since considerable mass flux reduction can result from removal of less than 70% of the DNAPL mass.

These results suggested that source zone characterization at field sites would benefit from inclusion of an estimate of the overall GTP. In addition, GTP could serve as a useful metric to distinguish between DNAPL source zones, based on their different response in terms of mass removal per remediation effort applied.

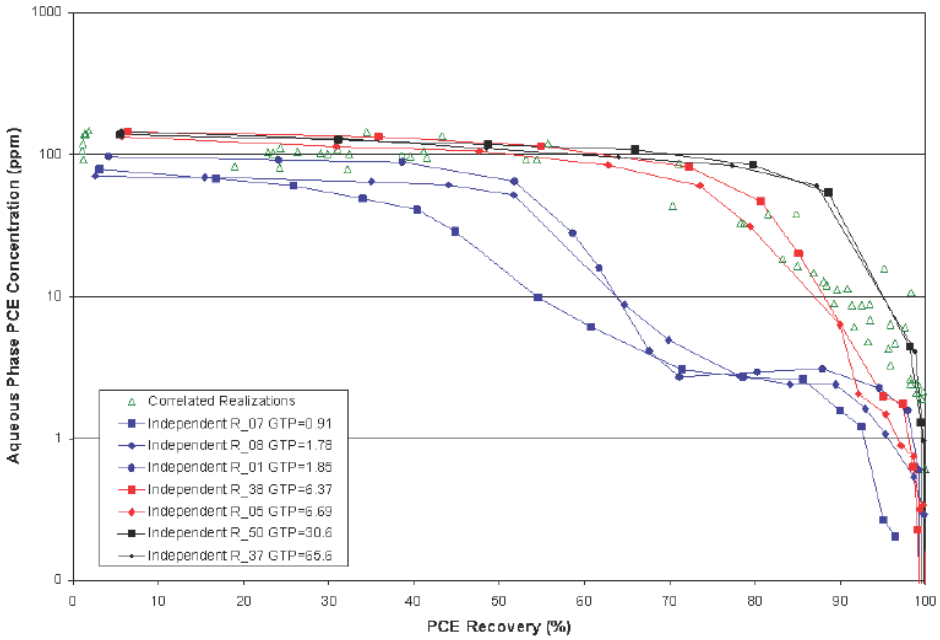

Figure 56. Flux-weighted effluent tetrachloroethene (PCE) concentrations versus PCE removal for seven independent realizations with ganglia-to-pool (GTP) ratios ranging from 0.9 to 65.6. Open triangles represent correlated realizations. Blue, red, and black lines and symbols represent low, moderate, and high ganglia-to-pool ratios in independent ensemble realizations. *(Lemke and Abriola, 2006)*

III. 4.2.2 Three-dimensional simulations

Simulations described in Section II.5.2.2 were conducted to investigate the influence of dimensionality on the DNAPL infiltration and mass recovery from a DNAPL source zone. Results demonstrated that a reduction in dimensionality from 3D to 2D had only a limited impact on the predicted characteristics of the DNAPL source zone. Figure 57 compares 3 saturation distribution metrics (maximum organic saturation, spreading in the x-direction, and spreading in the z-direction) calculated using an ensemble of 2D simulations and the same 2D cross-section extracted from an ensemble of 3D simulations. The dimensionality of the numerical experiment was the only difference between the two simulations.

Statistical analyses showed that all 3 metrics calculated from the 2D slices extracted from the fully 3D domain are statistically lower at the 95% confidence level than the metrics calculated for the same slice simulated in 2D. Based on these results, it was assumed that 2D simulations will likely result in slightly conservative estimates of contaminant flux and source longevity, supporting the use of two dimensional simulations for mass recovery analyses. Figure 58 shows that the GTP mass ratio simulated in 3D (closed boxes) and 2D cross-sections extracted from 3D (open boxes) are generally higher than the GTP mass ratio in the corresponding 2D realization.

These results confirm that 2D simulations will likely result in slightly conservative estimates of contaminant flux and source longevity.

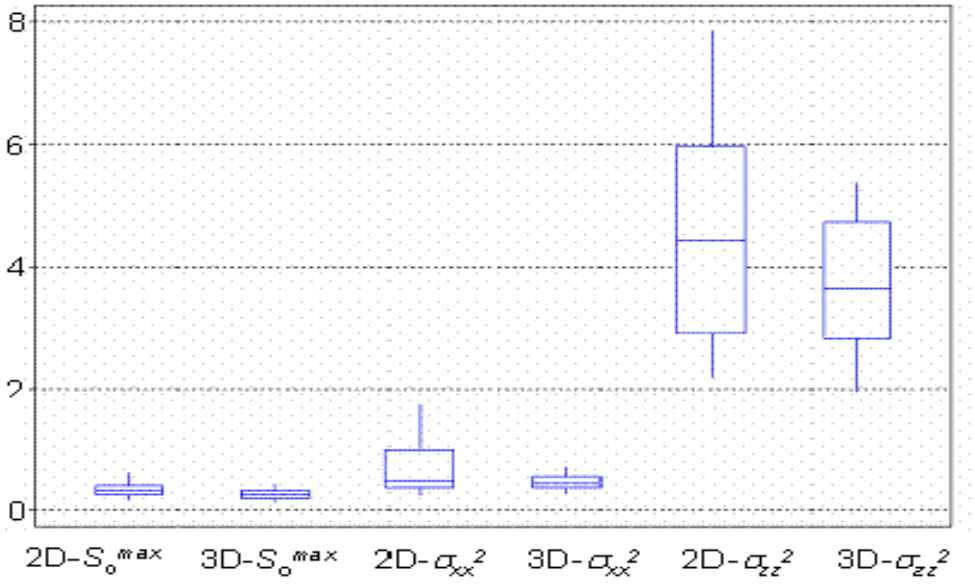

Figure 57: Box-and-whisker plot comparing metric values calculated from 2D numerical simulations (2D) with metric values calculated from the same x-z cross section in 3D simulations (3D) *(Christ et al. 2005).*

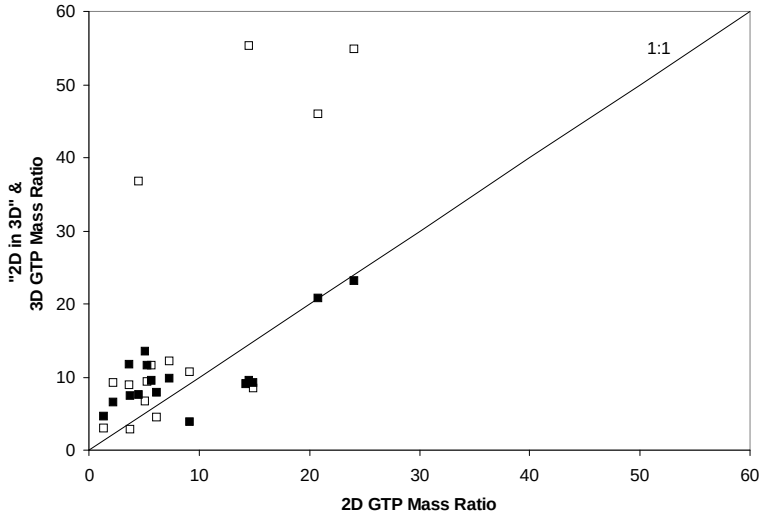

Figure 58: GTP mass ratios for saturation distributions generated in 3D along with the GTP mass ratio for the center x-z cross section in the 3D domain (2D in 3D) versus GTP mass ratios simulated in the corresponding 2D realization *(Christ et al. 2005).*

Figure 59 demonstrates that mass recovery curves simulated in 2D and 3D exhibit the same behavior, however, 2D simulations predict a flux-weighted contaminant concentration up to 3.5 times larger than the corresponding 3D simulation. Subsequent analysis has demonstrated that this difference is primarily due to dilution of the flux-weighted concentration at the down gradient boundary and not to flow by-passing.

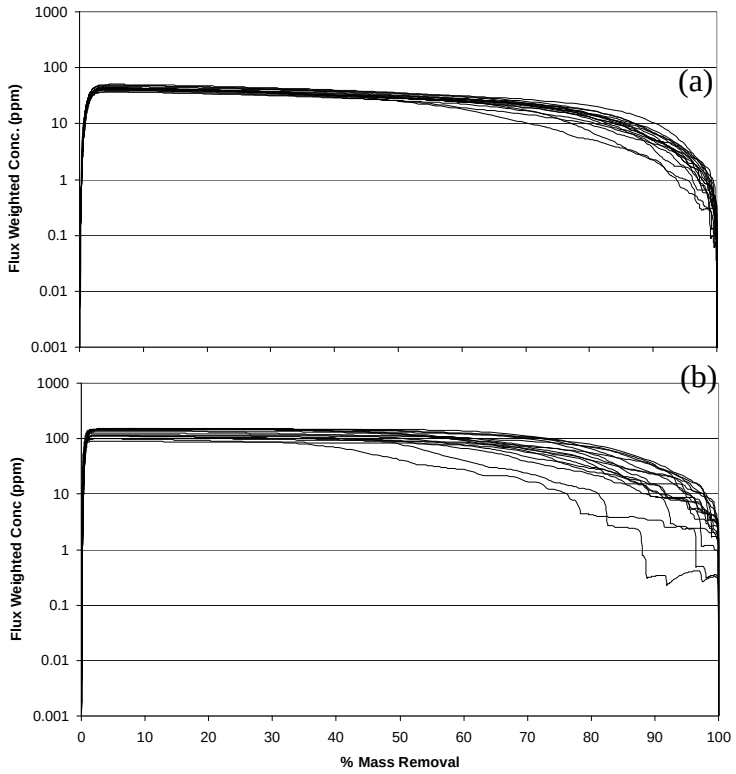

Figure59: Flux weighted concentration versus %-mass removal for (a) 3D simulations and (b) 2D simulations.

Source longevity predictions for 2D and 3D simulations are presented in Figure 60. In this figure the closed diamonds represent the primary set of realizations examined and the open boxes are for 3 simulations conducted at an increased $\sigma^2 ln(K)$. This plot demonstrates that 2D and 3D source longevity predictions will usually be different for a single realization. However, as depicted by the solid line, there is a statistically significant (p-value = 0.0077) positive correlation (0.6387) between the 2D and 3D source longevity predictions, indicating that a higher source longevity value predicted in 2D will generally correspond to a higher value in 3D. Additionally, a statistical analysis demonstrated that the mean difference between 2D and 3D source longevity values is not significantly different from zero at the 95% confidence level. This suggests that, on average, the source longevity simulated in 2D will be approximately equal to the source longevity simulated in 3D. However, as shown in Figure 10, equivalent mean values of source longevity do not necessarily translate into equivalent source longevity values for an individual realization.

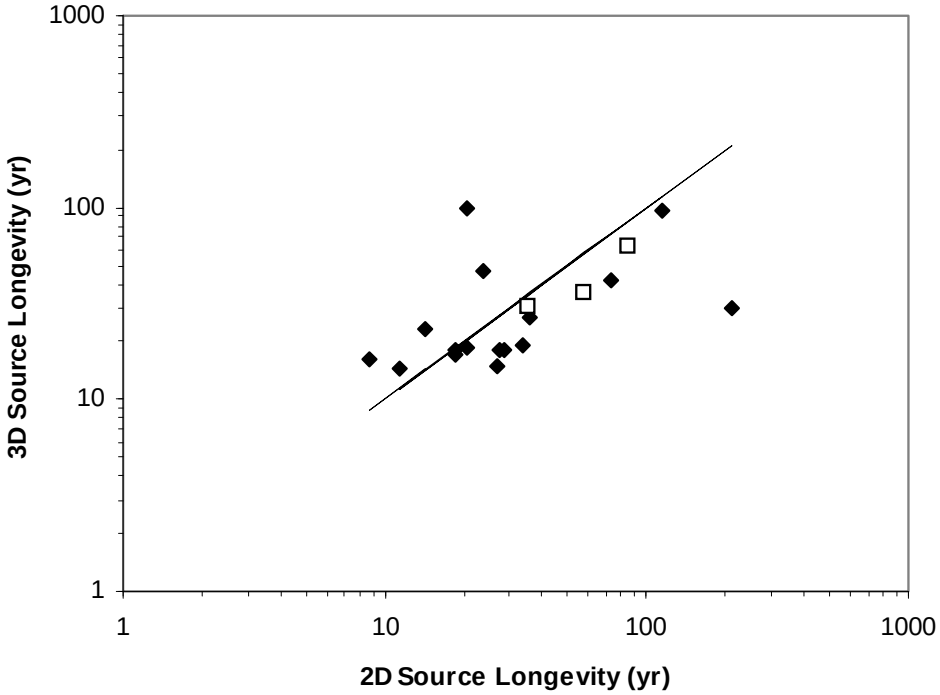

Figure 60: 3D versus 2D source longevity values predicted using a modified version of MT3D. Closed diamonds are for a set of 16 simulations conducted in a relatively homogeneous permeability field ($\sigma^2 ln(K)$ = 0.29). Open boxes are for 3 simulations in a permeability field with a $\sigma^2 ln(K)$ scaled to 1.0. *(Christ, et al. 2005a)*

III. 4.2.3 Upscaling

Based on an analysis of the 16 numerical simulations as described in Section II 5.2.3, a correlation between mass depletion exponent (β) and the initial GTP saturation distribution was developed. Figure 61 presents a plot of β versus the GTP for each of the numerical simulations. A statistically significant (p-value = 0.0039) negative correlation was obtained between β and GTP, which can be expressed through a power-law model (r^2 = 0.6373) in the following form:

$$\beta = 1.5 \cdot GTP^{-0.26} \quad \text{for } 1.5 < \text{GTP} < 24.0 \tag{17}$$

Incorporation of this correlation results in an upscaled mass transfer model capable of simulating both the pseudo-steady-state flux-weighted concentration and the transition from ganglia- to pool-dominated dissolution:

$$\frac{\overline{C}(L)}{C^{eq}} = 1 - \left(1 - \frac{\overline{C_o}}{C^{eq}}\right)^{\left(M/M_o\right)^{1.5 \cdot GTP^{-0.26}}} \tag{18}$$

In this equation, average contaminant concentration is expressed as a function of two site-specific parameters, the initial flux-weighted concentration ($\overline{C_o}$) and the source-zone GTP. Their inclusion results in a model that does not require fitting to obtain upscaled parameters. A RMSE of approximately 2 mg/L was obtained when comparing the flux-weighted concentration predicted from the proposed upscaled model prediction with the mean of the numerical simulation, which is almost identical to the RMSE for the original best fit upscaled model.

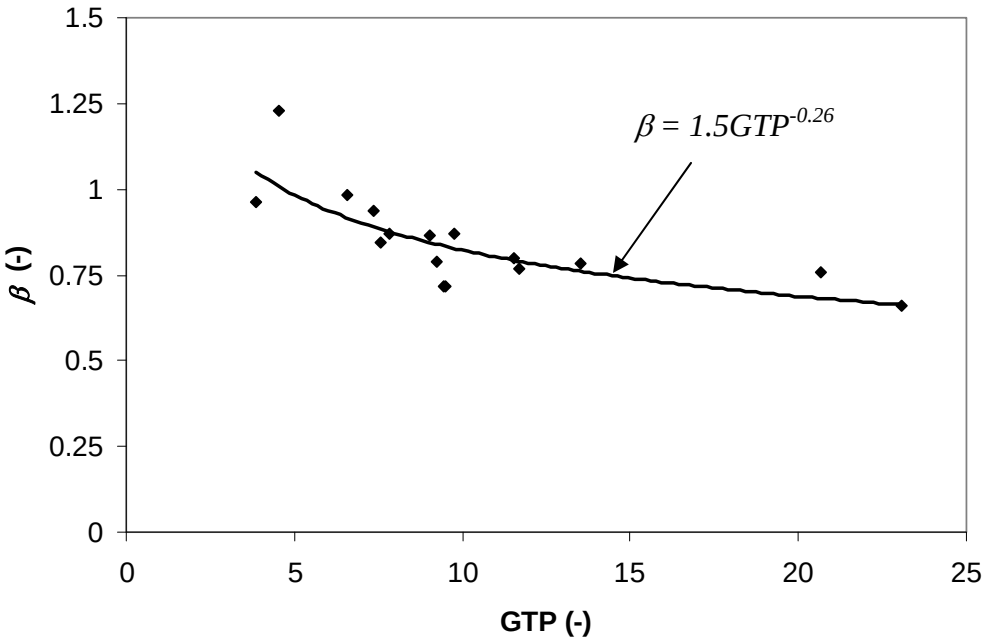

Figure 61: Mass depletion parameter (β) as a function of ganglia-to-pool (GTP) mass ratio for 16 numerical simulations. *(Christ et al. 2005b)*

The proposed upscaled model was further validated on the source-zone scenarios other than those used to develop the correlation. Eight realizations of source-zone scenarios were selected from *Lemke and Abriola (2006)*, where GTP ratios ranged from 0.9 to 65. Two additional scenarios were based on the work by *(Zhu and Sykes 2004)* and *(Parker and Park 2004)*, which have GTP mass ratios of infinity and ~0.41, respectively. Figure 62 present a comparison of the flux-weighted concentration predicted using the proposed upscaled model (solid line) and the numerical simulation results (open symbol). The RMSE values for the predicted flux-weighted concentrations ranged from 3 mg/L to 20 mg/L, which is generally three to five times less than the RMSE values obtained when the previously published models were used for prediction. The analysis presented herein clearly demonstrates the importance of incorporation of site-specific parameters into upscaled mass transfer models and highlights the need for innovations in *in situ* characterization techniques as an important area for future research.

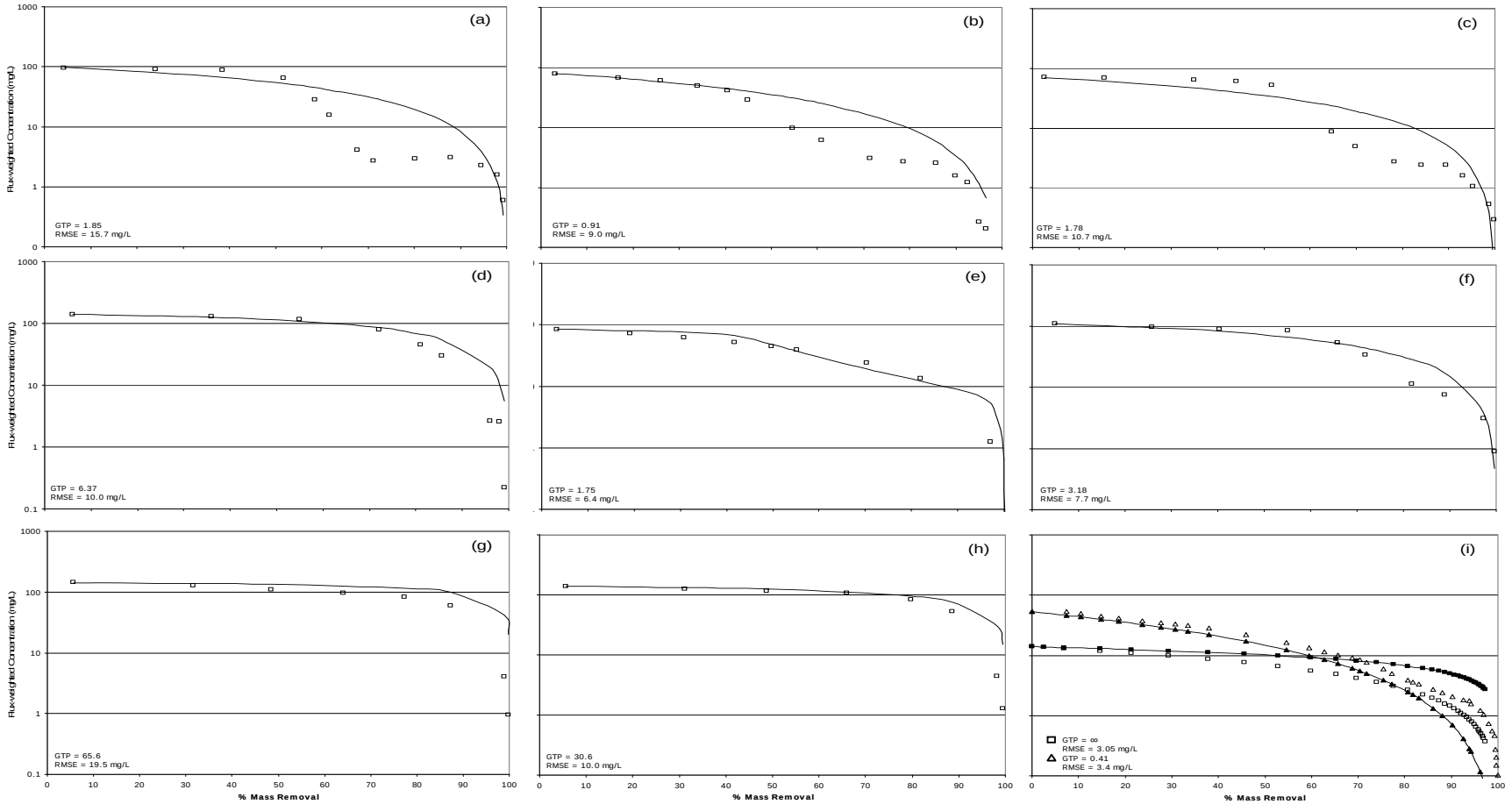

Figure 62: Comparisons of numerical simulation (open symbols) and proposed upscaled mass transfer model predictions (solid lines) of flux-weighted PCE concentrations as a function of mass removal for: (a) – (h) realizations selected from *Lemke and Abriola* (2006) and (i) *Zhu and Sykes* (2004) source-zone scenario (GTP = ∞), and *Parker and Park* (2004) source-zone scenario (GTP = 0.414). GTP mass ratios and RMSE are (a) 1.85 & 15.7 mg/L, (b) 0.91 & 9.0 mg/L, (c) 1.78 & 10.7 mg/L, (d) 6.37 & 10.0 mg/L, (e) 1.75 & 6.4 mg/L, (f) 3.18 & 7.7 mg/L, (g) 65.6 & 19.5 mg/L, (h) 30.6 & 10.0 mg/L, and (i) ∞ & 3.05 mg/L for *Zhu and Sykes* (2004) and 0.41 & 3.4 mg/L for *Parker and Park* (2004), respectively. *(Christ et al., 2005b)*

III.4.3 Uncertainty Modeling

The uncertainty quantification approaches and the multi-stage spatial sampling algorithm described in II.5.3 were tested and demonstrated using the numerically simulated plume data obtained as part of the results of Section II.5.2. The plume data were generated based upon a real field site *(Abriola et al. 2005)*. The generation process was designed to produce physically realistic plume transect data associated with heterogeneous source zones.

III.4.3.1 A Geostatistical Approach for Quantification of Contaminant Mass Discharge Uncertainty Using Multi-level Sampler Measurements

The geostatistical approach was evaluated using numerically simulated plume data. A series of sampling events with different sampling densities (regular sampling design) was "applied" on 48 numerical transects (reference fields). The probability distributions of mass discharge were calculated using the geostatistical approach. The accuracy and precision of the probability distributions were analyzed, and statistics were obtained to evaluate the quantified uncertainty of mass discharge.

III.4.3.1.1 The Accuracy Plot - Combination Measure of Accuracy and Precision

The accuracy plot (e.g. Figure 63) was used to assess the accuracy and precision of models of uncertainty. The accuracy plot was originally proposed by Deutsch *(Deutsch 1997)* to evaluate local uncertainty models (ccdfs) and plots the frequencies (computed from ccdfs) for which local true values fall within a series of symmetric p-probability intervals (PI) bounded by the (1-p)/2 and (1+p)/2 quantiles. An uncertainty model is accurate if the frequency of true values falling in the p-PI exceeds p for all p-PIs. The precision of an accurate uncertainty model is measured by the closeness of the computed frequency to p. In this demonstration, the accuracy plot was adapted to evaluate the uncertainty space of the mass discharge modeled by the proposed approach. Given a certain sampling strategy (number of samples, measurement support, sampling locations) the probability distributions derived from different reference fields were analyzed to compute the frequency of occurrence of the true values within a series of symmetric p-PIs. The accuracy plot then depicts the calculated frequencies as a function of the expected probabilities (p). For example, to create one curve (representing one sampling density) on the accuracy plot in Figure 63, 16 reference fields were used and 16 true values of mass discharge were calculated for each reference field. A series of symmetric p-PIs with p varying from 2% to 100% (50 p-PIs in total) was calculated from the 16 output probability distributions. Theoretically the frequency with which the p-PI includes the true value should be close to the expected probability p, i.e. all of the points should fall along the 45° line. If all the points fall above the 45° line the observed frequency is higher than the expected probability, indicating that the model of uncertainty is accurate, but is not as precise as expected.

Because the spatial distribution of concentration varies remarkably among the reference fields with 1%, 50% and 98% source mass removal, the approach was assessed separately on three sets of reference fields (each set has 16 reference fields). Regular sampling with sampling densities varying from 1% to 25% (number of samples from 9 to 208) was applied on each reference field. For each set of reference fields, accuracy plots for all of the sampling densities used were grouped into one figure. Different symbols represent different sampling densities. Figure 56 shows the grouped accuracy plots for the 1%, 50% and 98% mass removal cases, which leads to the following findings:

1) For concentration distributions that display large continuous regions of high concentration (corresponding to low levels of mass removal), the approach provides an accurate model of uncertainty for all of the sampling densities used in this study. All of the points fall above the 45° line, indicating that the frequency of capturing the true value is higher than the theoretical (i.e. expected) probability value, which means that the uncertainty model is accurate but conservative
2) For concentration distributions that consist of scattered hot spots and large areas of near-zero concentration (the case for high levels of mass removal), a sampling density of 6~7% (corresponding to 50~60 samples in an area of 77.3m^2) is required to obtain an accurate model of uncertainty, according to the accuracy plots. This sampling density appears unrealistic for field applications. For example, King et al. (1999) used 21 points (6 wells) in an area of 50m^2. Assuming the same measurement support of 0.0929m^2, the sampling density is 3.9%. Kao and Wang (2001) had 20 points (5 wells) in an area of 283.8m^2. The screen length is 0.6m. If it is assumed that the horizontal scale of each sample is 0.3048m as in this work, their sampling density is 1.3%. Einarson and Mackay used 49 points (7 wells) in an area of 154.29m^2 with unknown measurement support. Again assuming 0.0929m^2 measurement support, the sampling density is 3.0%.

III.4.3.1.2 Individual Measure of Accuracy and Precision

According to the definition of the accuracy plot, whether or not the uncertainty model is accurate is not only influenced by the closeness of the median of the probability distribution to the true value, but also by the width of the p-PIs. Therefore, to further elucidate the performance of the proposed approach, the accuracy and precision of the uncertainty models were assessed respectively by the following two statistics: 1) magnitude of the normalized mean absolute error of prediction (MAEP), which is defined as the absolute value of the difference between the mean of the probability distribution and the true value, normalized by the true value (Figure 64), and 2) the width of the 95% confidence interval that is calculated as the difference between the 97.5% quantile and the 2.5% quantile (Figure 65). Figure 64 reveals that, if using the mean of the probability distribution as the mass discharge estimate, the absolute error of prediction does not exceed 20% of the true value at most sampling densities for the concentration distributions corresponding to 1% and 50% mass removal. Beyond a sampling density of about 4~5%, this error is below 10% of the true value. For these cases, Figure 63 also suggests that the MAEP is much less sensitive to the increase of the sampling density, compared to the 98% mass removal case. This is likely because the concentration distribution is more continuous and its spatial structure is easier to recognize. For the 98% mass removal case the MAEP improves quickly with more samples initially and the improvement slows down at about a sampling density of 6~7%, which corresponds to a prediction error of about 50% of the true value. This behavior is attributed to a slow improvement in the recognition of spatial structure. Figure 64 shows that the 95% confidence intervals are quite large at low sampling densities, and their width decrease (precision increases) slowly as the sampling density increases, indicating the need for reporting the uncertainty of mass discharge, in addition to the "best estimate". Note that the probability distribution of mass discharge is typically highly skewed; therefore the uncertainty cannot be quantified simply by confidence intervals which are typically used for symmetric distributions. In addition to insufficient sampling density, the large confidence interval may also be caused by

the regular sampling design. where a large portion of samples are placed in the near-zero concentration areas, which does not tend to contribute significantly to the mass discharge and therefore does not help to refine the mass discharge estimate. The impacts of the sampling design are discussed in Section II.5.3.2 and III.4.3.1.

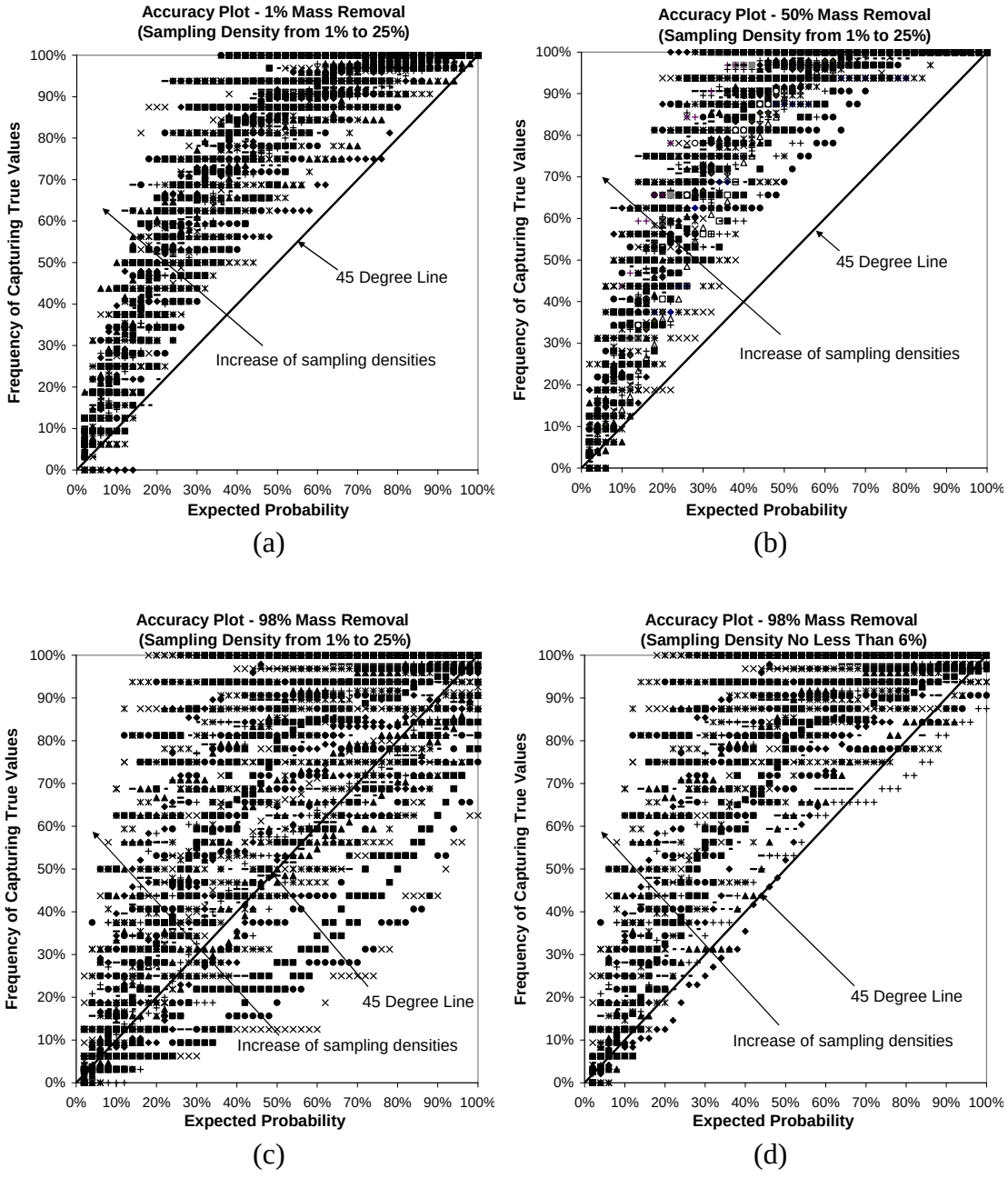

Figure 63: Grouped accuracy plots for the samples with a screen length of 0.3048m (Different symbols represent different sampling densities). (a) 1% mass removal cases (sampling density from 1% to 25%); (b) 50% mass removal cases (sampling density from 1% to 25%); (c) 98% mass removal cases (sampling density from 1% to 25%); (d) 98% mass removal cases with sampling density higher than 6%.

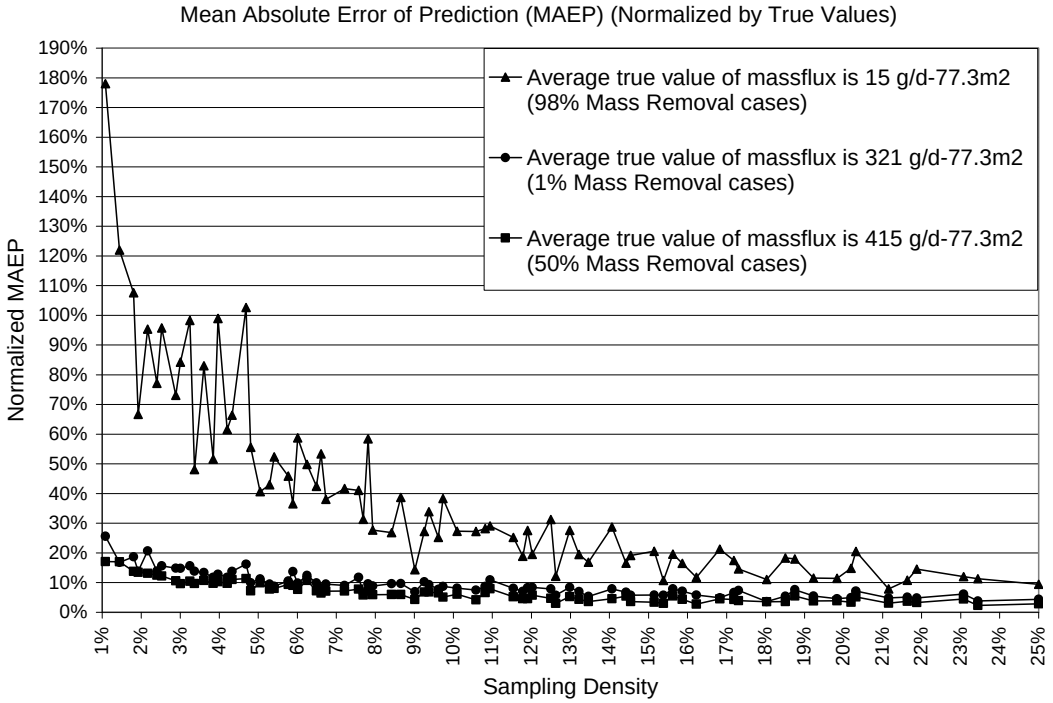

Figure 64: Normalized mean absolute error of prediction, averaged over 16 reference fields

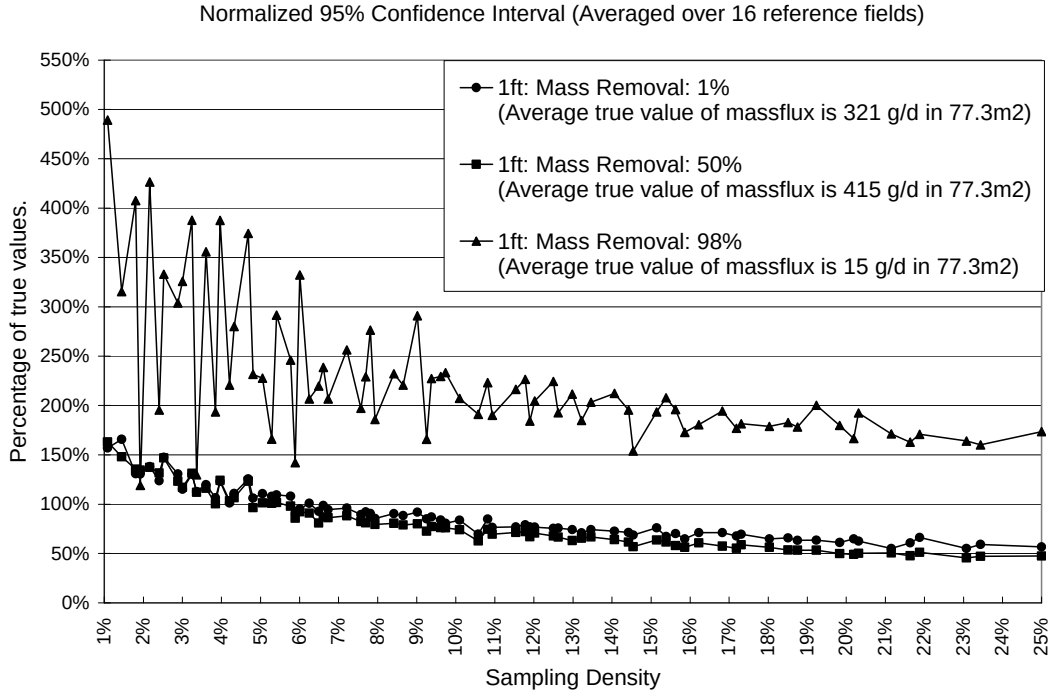

Figure 65: The 95% confidence interval of the probability distributions averaged over 16 reference fields

III.4.3.1.3 Impact of Measurement Support

All of the results above are for a screen length of 0.3048m (1ft). To explore the impact of screen length on the mass discharge uncertainty, a 0.6096m (2ft) vertical sampling scale was applied for the same 48 reference fields. Thus, for the same sampling densities the number of samples was reduced to half of the amount collected in the corresponding 1ft sample case. The normalized MAEP and the 95% confidence interval were used to compare the accuracy and precision of the probability distributions modeled from the two different measurement supports. The comparison of the normalized MAEP is shown for equal sampling density in Figure 66.

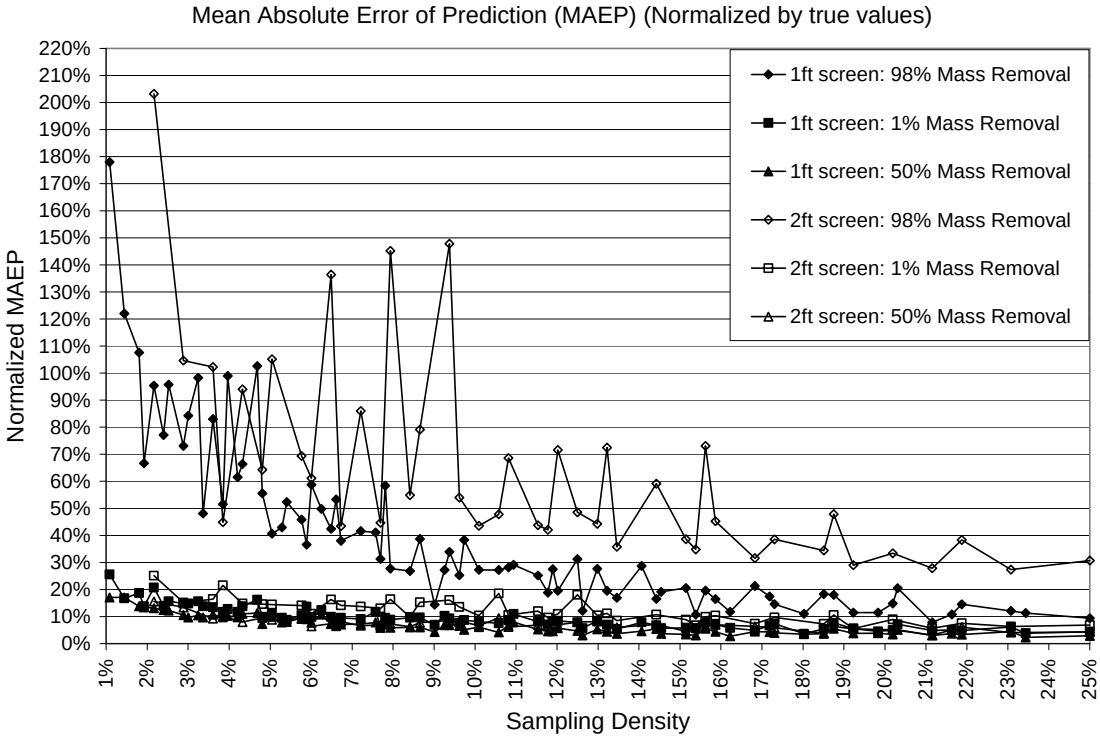

Figure 66: The comparison of the mean absolute error of prediction expressed in sampling densities for the 0.3048m (1ft) screen and the 0.6096m (2ft) screen samples

The comparison reveals that using a 2ft sampling interval does not lead to more accurate results. For the same number of samples, there is no discernible difference in accuracy for the 1ft and 2ft screen samples (Figure 67). For the same sampling density (same sampling volume), Figure 66 reveals that the 2ft screen samples generate less accurate probability distributions for the mass discharge than the 1ft screen samples. The reduction in the accuracy is especially remarkable for the concentration distribution associated with 98% source mass removal.

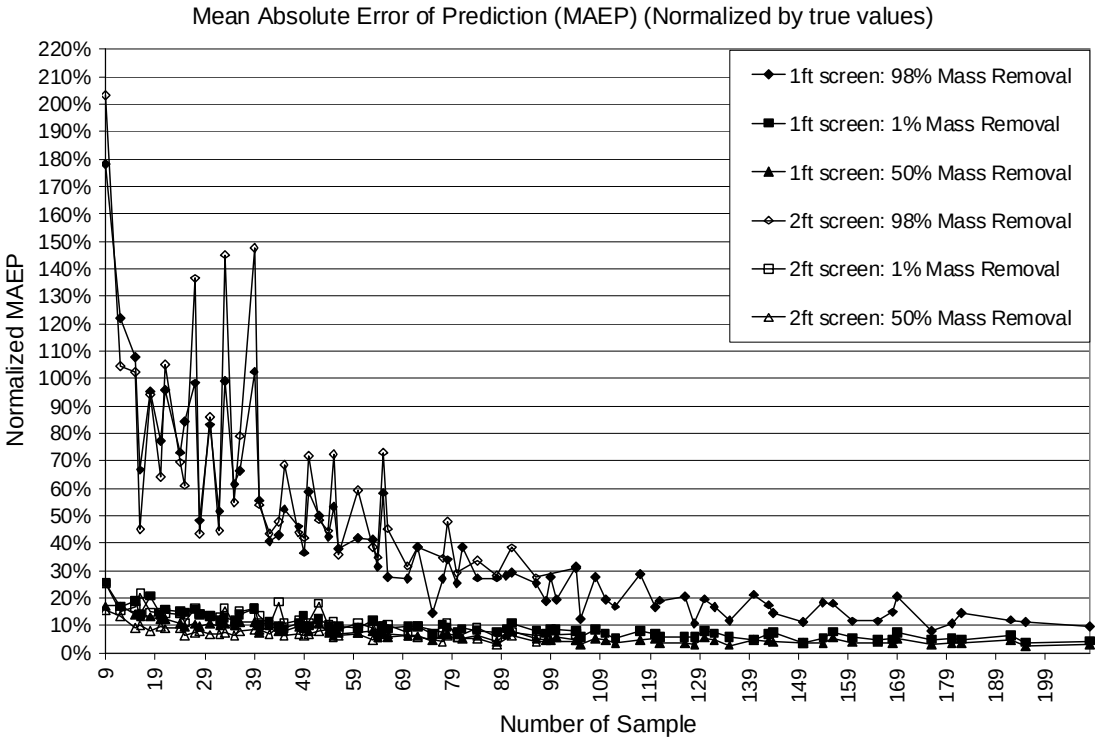

Figure 67: The comparison of the mean absolute error of prediction expressed in the number of samples for the 0.3048m (1ft) screen and the 0.6096m (2ft) screen samples

When comparing the 95% confidence intervals for the samples with 1ft and 2ft screens at the same sampling density, the probability distributions of 2ft screen samples were slightly less precise. In terms of sample numbers, there was little difference in precision between the two measurement supports (not shown).

This comparison suggests that increasing the measurement support (sampling volume) does not improve the quality of the probability distribution of mass discharge. This may be explained through the change in the sample statistics. Indeed, increasing the measurement support results in changes in the statistics of sample data such as the histogram (spread, asymmetry and standard deviation) *(Isaaks 1989)* and semivariogram (nugget, range, sill) *(Journel 1978)*. Typically, larger measurement support reduces the spread of samples values (smoothing effect) while the histogram becomes more symmetric. The elimination of the spatial variance within the sampling volume causes a reduction of variance, which changes the structure of the experimental semivariogram. Most simulation algorithms, including *p*-field simulation, aim to reproduce sample histogram and semivariogram; thus, the changes in sample statistics directly affect the generated realizations.

The magnitude of the impact of increasing measurement support depends upon the spatial structure of the data set. Spatially uncorrelated data are affected the most. As the spatial continuity increases, the statistics become more robust *(Isaaks 1989)*. Note that two data sets

with the same semivariogram may exhibit different degrees of robustness to measurement support as it is increased. The data set with larger spatial disorder (i.e. extreme values are poorly connected) is affected more readily. Thus, the optimal screen length will be site specific, related to the spatial pattern of the target attribute. It may be determined by analyzing the degree of heterogeneity (e.g. the variance), the correlation length, and the degree of spatial disorder (i.e. entropy, see *(Journel 1993)*). However, this topic is beyond the scope of this project. The proposed approach cannot automatically choose an appropriate measurement support.

III.4.3.2 A Multi-stage Multi-criteria Spatial Sampling Strategy for the Quantification of Contaminant Mass Discharge and the Associated Uncertainty

The sampling strategy is illustrated in this section, using numerically simulated plume data. The applications of the algorithm focus on the reference fields that are correlated with the 98% source mass removal case because this is the most difficult situation as identified in Section III.5.1.

III.4.3.2.1 Conceptual Sampling Locations Based Upon Conditional Variance

Conditional variance was selected as one of the sampling criteria because it can guide sampling effort to the most uncertaint locations in the vicinity of hot spot areas. Figure 68 shows the conceptual sampling locations if sampling based upon conditional variance.

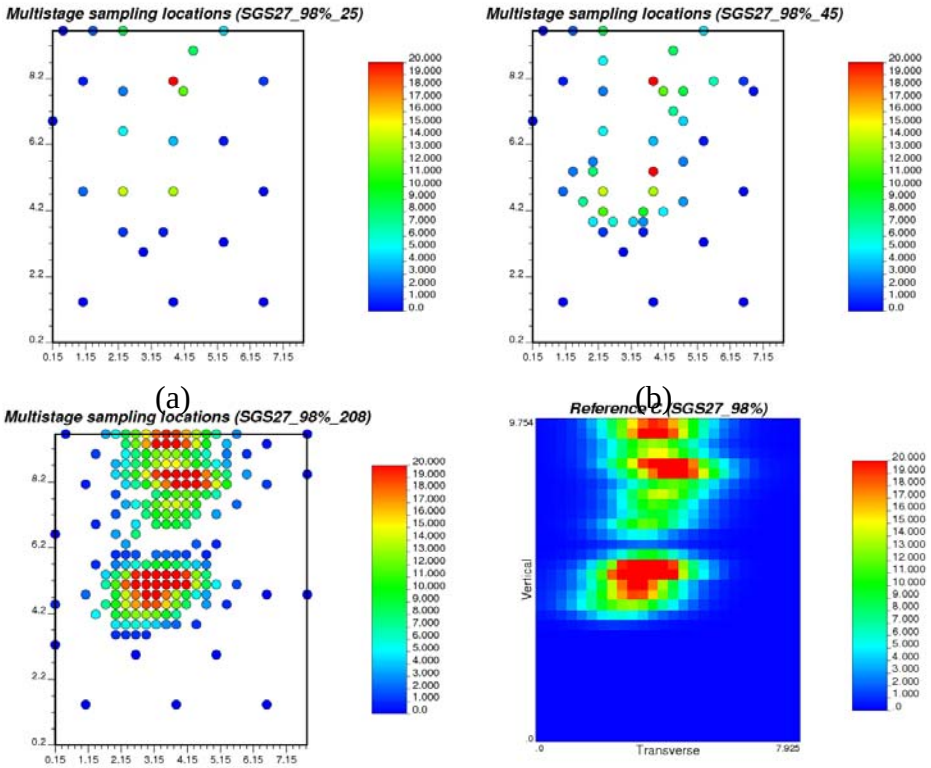

Figure 68: An example of the multi-stage sampling locations detected based upon conditional variance (a): 25 observations (b) 45 observations (c) 208 observations (d) reference field

Figure 68 shows that the hot spots can be successfully identified and delineated as sampling progresses if based upon conditional variance. The delineation of hot spots occurred from the boundary towards the center, because boundaries are the most uncertain locations in the hot spot areas. At locations that are adjacent to "hot" observations, conditional variance is low because there is less local uncertainty due to existing observations. However, locations that are close to near-zero observations also have low conditional variances because data values are low. As a result, the boundaries of hot spots are the most uncertain locations, and thus they are the sampling priorities.

Figure 68 shows the conceptual sampling locations. In the field, sampling can only occur along vertical lines (wells). The benefit of the sampling design on hot spot identification and delineation is further illustrated in Figure 69 through an example of the comparison of the regular sampling design and the staged sampling design (sampling along vertical lines). It can be found that using the same number of observations, the staged sampling design identified all of the three hot spots and the shape of each hot spot area was delineated, while the regular sampling design located only one hot spot. The comparison of the probability distributions derived from the two sets of sample data also shows that the staged sampling design provided mass discharge estimates with less uncertainty.

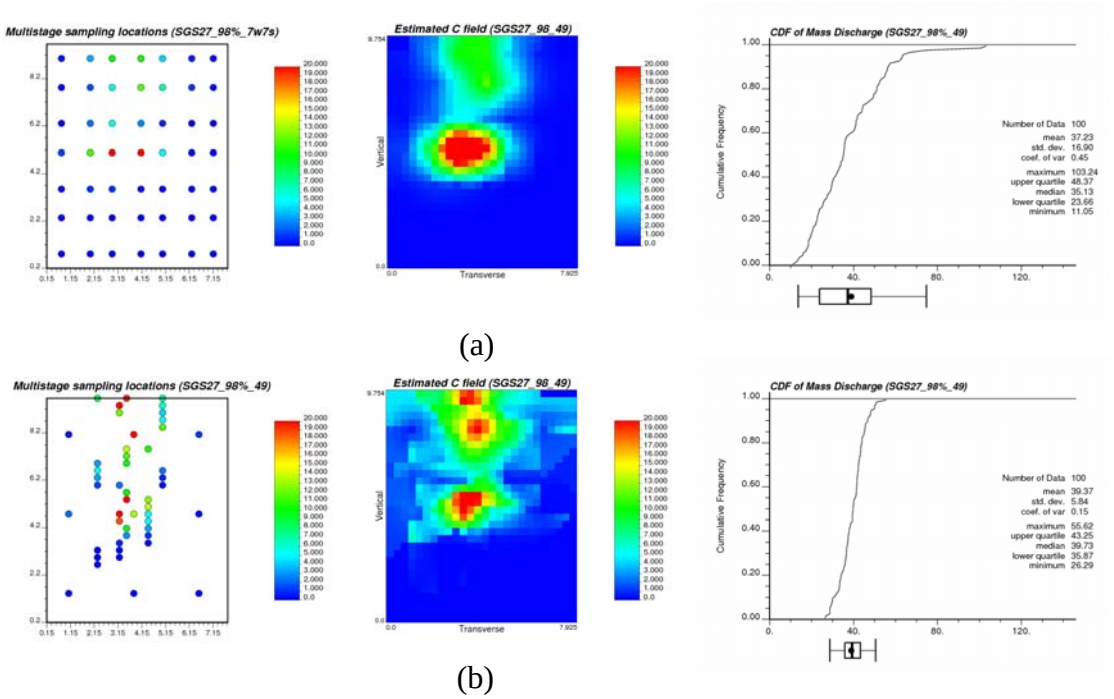

Figure 69: An example of the difference between the regular sampling design (a) and staged sampling design (b) with 49 observations. Left: map of sampling locations; Middle: estimated concentration map (using ordinary kriging); Right: the probability distribution of mass discharge. Dot: true value; center line in the "box": the mean of the probability distribution; "box": the 50% confidence interval, bounded line: the 95% confidence interval (See the reference concentration map in Figure 68(d))

III.4.3.2.2 Reduction in Sampling Density Due to Accuracy and Precision Improvement

According to the accuracy plot for one stage sampling design with a regular (rectangular) sampling pattern, a sampling density no less than 6~7% is needed for an accurate model of mass discharge uncertainty for the type of concentration distributions correlated with 98% source mass removal, where a few hot spots are scattered in large areas of near-zero concentration *(Li et al. 2007)*. Using the same reference fields, the accuracy plots for the multi-stage sampling design are shown in Figure 70. Figures 63a and 63b indicate that for the ideal situation (no vertical sampling constraints, as shown in Figure 68), when sampling density is higher than about 2.5%, the uncertainty model is accurate. For the restricted situation (sampling along vertical lines, as shown in Figure 69), a sampling density of about 2~3% is needed (Figure 70c, 63d). Thus, compared to one stage sampling design, the minimum sampling density is reduced by at least 50% when using the multi-stage sampling design. This improvement is achieved through the improved accuracy and precision of the probability distribution of mass discharge.

III.4.3.3 Uncertainty Analysis for Near Source Zone Mass Discharge Estimated Using the Passive Flux Meter Method

The uncertainty analysis approach for the PFM method was applied to numerically simulated plume data. The results suggest that the portion of the mass discharge uncertainty contributed by the uncertainty of mass flux measurements is negligible in comparison to the portion of the uncertainty contributed by the integration of mass flux measurements. The recommended maximum sampling spacing is 3 m.

III.4.3.3.1 Uncertainty of the Mass Flux Measurement

The uncertainty contributed by mass flux measurements is contributed by incomplete knowledge of aquifer permeability near the flux meters and the assumption of the aquifer permeability used in the calculation of mass flux in the PFM method. This uncertainty source is incorporated in the analysis by using the concept of soft indicators.

However, results suggest that comparing to the uncertainty introduced by regionalization of local mass flux values, uncertainty contributed by mass flux measurement is negligible. The accuracy and precision of the probability distribution of mass discharge show no discernible difference no matter whether the uncertainty of mass flux measurements is considered or not. This is because the PFM method is not very sensitive to the variability of the aquifer permeability field due to its design, i.e., if the permeability of the flux meter is designed to be much larger than the aquifer permeability, the influence of the variability of the aquifer permeability is very limited.

III.4.3.3.2 The Recommended Maximum Sampling Spacing

One way to determine the maximum recommended horizontal sampling spacing is to use the accuracy plot, i.e. it is the maximum sampling spacing for an accurate model of uncertainty for mass discharge. Figure 71 shows the accuracy plot for the reference fields generated in Section

II.5.2. Data series in the accuracy plot represent different sampling densities, and critical sampling spacings were also reported in brackets. Figure 71 suggests that, except for the sampling spacing of 3.81m, all of the other data series are above the 45° line, indicating that the frequency of capturing the true value is higher than the theoretical (i.e. expected) probability value, and the uncertainty model is accurate but conservative. Thus, to assure accurate estimation of the associated uncertainty, a maximum sampling spacing of about 3 m is recommended.

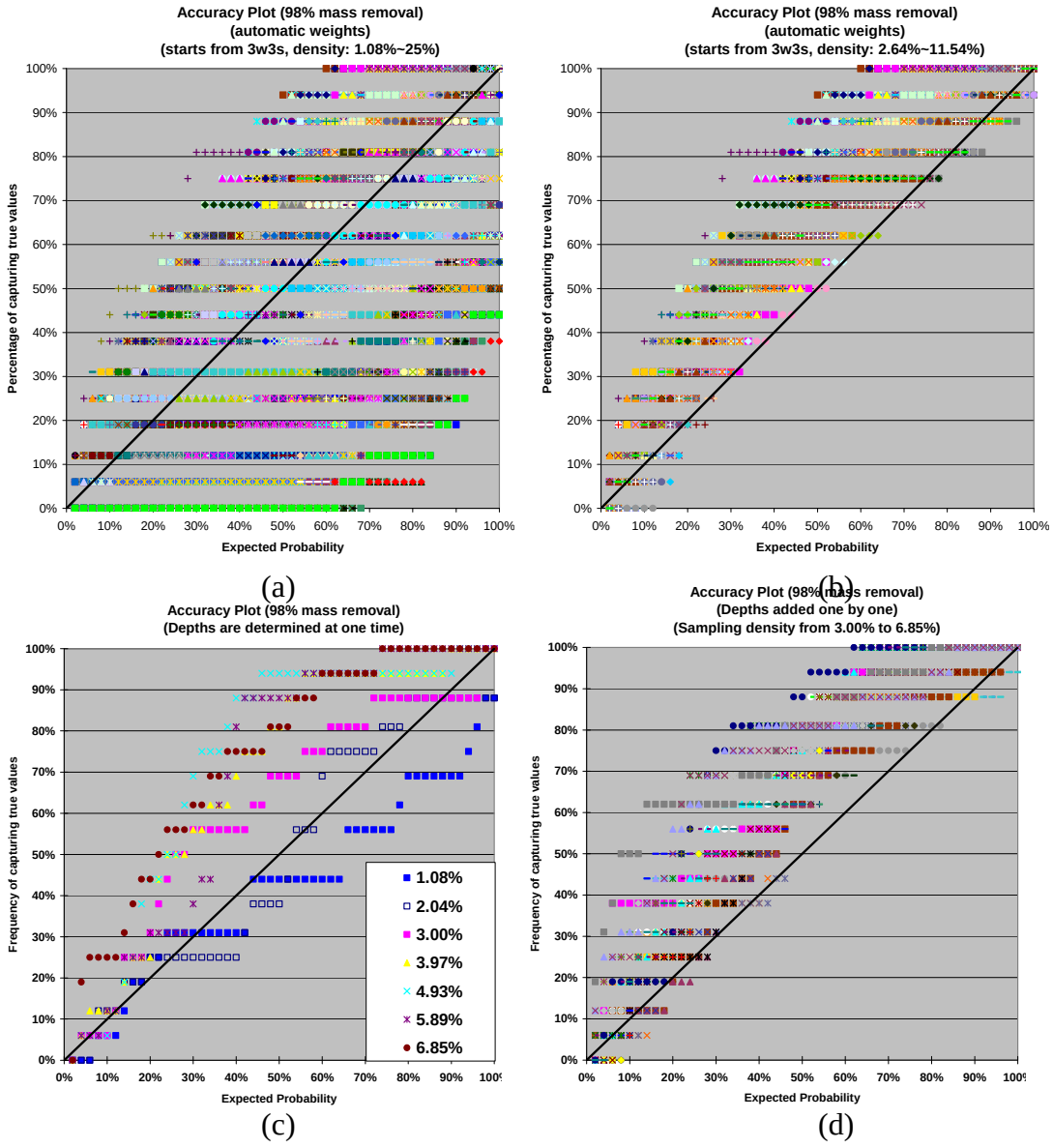

Figure 70: Grouped Accuracy plot of multi-stage sampling. Different symbols represent different sampling densities. (a) Grouped accuracy plot for the ideal situation (sampling density: 1% –25%); (b) Grouped accuracy plot for the ideal situation (sampling density: 2.64% – 10.54%); (c) Grouped accuracy plot for the restricted situation (depths added in one time); (d) Grouped accuracy plot for the restricted situation (depths added one by one)

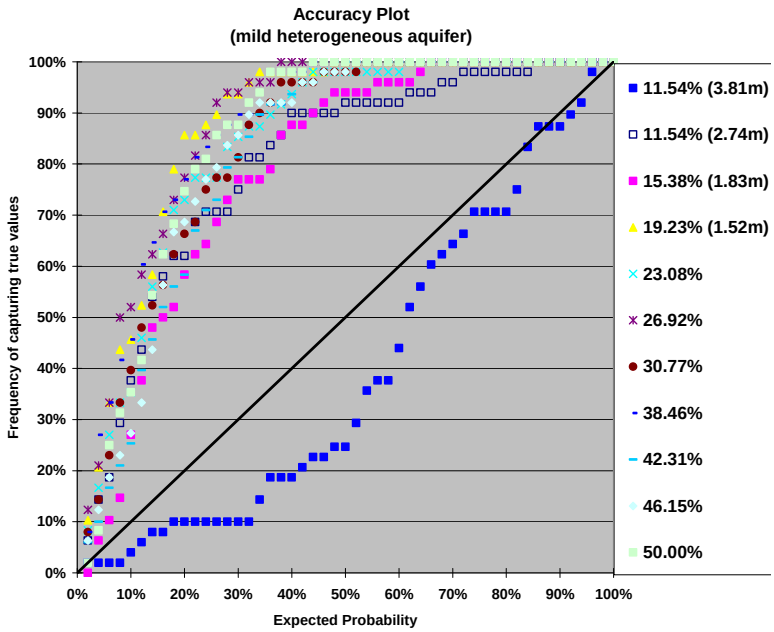

Figure 71: Grouped accuracy plots for the uncertainty models of mass discharge (Different data series represent different sampling densities, bracket values are corresponding horizontal sampling spacing)

III.4.4 Cost-Benefit Analysis Tools for Source Zone Treatment

Modular cost components were developed for surfactant flushing. The components considered include the injection well system, the extraction well system, the surfactant solution mixing and storage system, and the post-treatment extraction system. Each modular component was further broken down into individual components within the system (e.g. storage tanks, mixing tanks, transfer pumps, etc. for the surfactant solution mixing and storage system). All costs were computed based on user-defined treatment parameters (e.g., well number and well depth for the injection and extraction well systems), and itemized for labor, equipment and materials.

The cost model was further evaluated and refined to include a new front-end input utility, which will allow users to specify a treatment strategy (e.g. pump-and-treat or surfactant flushing), key parameters relating to the treatment (e.g. pumping rate and above ground treatment), and relevant site-specific parameters. In addition, a preliminary tool for SEAR cost analysis based on the modular cost components has been developed. Based on user defined treatment parameters, two spreadsheets are generated to analyze system cost. The first (see Figure 72) includes a general cost breakdown (i.e. fixed capital costs, operation and maintenance costs, etc.) of the SEAR system employed and calculates the estimated cost of treatment on a per volume treated basis. The second includes a detailed breakdown of the itemized costs generated by the cost analysis spreadsheet.

Total Fixed Capital Costs	$200,900
Total Chemical Cost	$155,800
Total O&M (Present Value)	$49,200
Fees	
Administrative (15% of Total Fixed Capital and O&M)	$37,500
Engineering (10% of Total Fixed Capital and O&M)	$25,000
Piping (13% of Total Fixed Capital)	$26,100
Contingencies (15% of Total Fixed Capital)	$30,100
Total Fees	$118,800
Recoverable Equipment Cost (MACRS)	$126,300
Total Cost (Including Location Factor)	**$378,400**
$/ft3 Source Zone Treated	**$9.51**
$/gal NAPL Treated	**$50.88**
Treatment Time (Days)	**36**

Figure 72: General SEAR costs generated by cost analysis tool.

Estimates of total remediation cost and detailed component cost breakdowns for pilot-scale surfactant flushing have been generated for the Bachman Road site using the SEAR Cost Analysis Tool (SEAR-CAT). Cost estimates generated with the SEAR Cost Analysis Tool compared favorably to published values for the Bachman site, with the SEAR-CAT tool estimating a total treatment cost of $378,000 compared to the reported cost of $382,000. Further evaluation of the Cost Analysis Tool was conducted using published data from three additional pilot-scale field tests (cosolvent flushing at Sage's Dry Cleaner, and surfactant flushing at Hill AFB-OU2 and Camp Lejune). SEAR-CAT results were comparable to published data in all cases, although some underestimation of equipment costs was observed. In addition, personnel from HSI-Geotrans evaluated SEAR-CAT.

Based on results of the HSI-Geotrans and co-investigator evaluations, additional refinements to the SEAR Cost Analysis Tool (SEAR-CAT) were completed. The completed refinements include development of application "wizards" to assist users in the design of above-ground treatment components (e.g. air-strippers, GAC units) and incorporation of more complex, multi-component NAPL compositions (Figure x1). In addition, the SEAR-CAT tool was modified to include the DNAPL mass recovery/effluent contaminant mass flux type curves for different initial source zone architectures based on results obtained in 2-D box studies. Incorporation of these type curves allows the user to specify the source zone DNAPL distribution and estimate either a) the volume of surfactant flushing required to attain a specific flux reduction or b) the flux reduction accompanying a given volume of surfactant flushing. Based on these type curve estimations, overall treatment cost as a function of either mass flux reduction and/or source zone mass removal is now included in SEAR-CAT. A manual for SEAR-CAT has also been developed based on feedback from the evaluations and includes instructions for using SEAR-

CAT, as well as example inputs/results from a PCE-DNAPL contaminated site (i.e. Bachman Road).

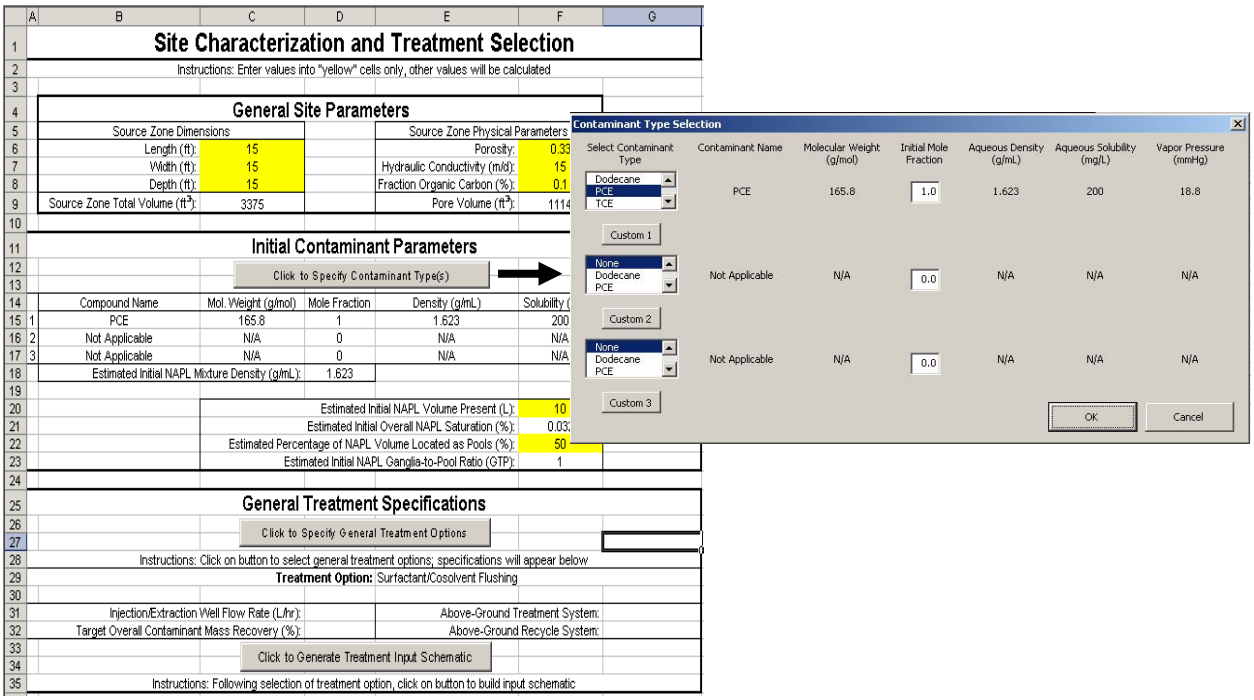

Figure 73: Representative image of site characterization portion of SEAR-CAT tool and contaminant specification menu.

Excel-based modular cost components for in-situ remediation technologies in addition to SEAR were developed. Technologies considered include pump-and-treat, air sparging, and thermal remediation. The modular components are similar to those previously developed for SEAR. For example, pump-and-treat remediation includes components for the monitoring well system, extraction well systems, and effluent treatment, while air sparging includes an additional module for the inclusion of air blowers. For all components, calculated costs were itemized for labor, equipment and materials.

The cost comparison tool (CCT) is designed to allow the user to input cost estimate results for each technology considered by the SEAR-CAT tool (e.g., pump-and-treat, surfactant flushing, cosolvent flushing) into a single worksheet. The CCT worksheet contains the total estimated cost for each project, along with a more detailed breakdown of specific costs for each product, among them total capital costs, operation and maintenance, and salvage.

Following cost input into the CCT, the tool is then able to calculate several simple performance metrics, such as cost per volume of NAPL removed, cost per volume of soil treated, and cost as a function of treatment time for each of the considered technologies. The cost metrics for innovative treatments (i.e., surfactant and cosolvent flushing) are compared to baseline pump-and-treat values. Once the performance metrics are calculated, a series of graphical displays (as well as tables) allow for rapid comparisons of the different treatment technologies.

IV. Conclusions

The research described in this work provides a suite of assessment information and tools to guide remediation site managers during the characterization of DNAPL source zones and the selection and design of alternative remediation technologies. Research results are encouraging. Significant reductions in contaminant flux may be realized at moderate levels of DNAPL mass removal at sites characterized by a low GTP. The level of mass recovery may be tied to the source zone architecture through novel metrics such as the ganglia to pool ratio. Stimulation of indigenous or augmented microorganisms in a DNAPL source zone will lead to significant metabolic reductive dechlorination and may lead to significant enhancement in DNAPL dissolution. Residual flushing solution following aggressive mass removal can provide a sustained stimulant for metabolic reductive dechlorination in the field. The developed geostatistical approaches are able to quantify not only the contaminant mass discharge emanating from a DNAPL source zone, but also the uncertainty associated with that estimate. The developed multi-stage adaptive sampling algorithm can be used to drastically reduce the down-gradient area sampled to quantify contaminant mass discharge and achieve uncertainty reduction. All of these results may be combined to guide remediation site managers as done in the SEAR-CAT for surfactant enhanced aquifer remediation. These results, combined with the developed tools provide a profound improvement in the understanding of significant mechanisms controlling DNAPL source zone behavior. In fact, these results (e.g., the GTP metric) have already found their way into language describing new research needs (e.g., FY08 SON) and are fully expected to provide improved DNAPL site management strategies. The following sections provide a summary of lessons learned from this work, the limitations of some of the findings, and suggestions for future research directions.

IV.1. Lessons Learned:

1. Mass flux v. mass removal

- Significant reductions in contaminant mass flux (2 orders of magnitude) can be realized with only moderate mass removal (e.g., 50%) for *in situ* surfactant flushing technologies in sandy, unconsolidated, porous media.
- The relationship between reductions in dissolved-phase mass flux and mass recovery will depend on DNAPL architecture, which can be described quantitatively by the source zone DNAPL ganglia-to-pool (GTP) ratio.
- The ganglia-to-pool ratio of the DNAPL source zone may be estimated *a priori* at sites with extensive knowledge of the DNAPL volume, rate of release, and spatial variability in subsurface hydraulic and capillary (pressure-saturation) parameters.
- Cumulative DNAPL mass recovery that can be realized via *in situ* flushing technologies strongly depends on DNAPL architecture, which can be described by the ganglia-to-pool ratio, and DNAPL composition.
- Following aggressive DNAPL source zone treatment, significant contaminant mass may persist, which can result in locally-high aqueous phase concentrations.

2. Source zone dechlorination

- Under appropriate conditions, reductive dechlorination can be achieved within a DNAPL source zone; chlororespiring bacteria exist, dechlorinate, and grow in the presence of pure and mixed DNAPLs.
- Without aggressive mass removal, bioenhanced DNAPL dissolution can reduce source longevity, but such enhancements are unlikely to result in source zone treatment times that are acceptable within a regulatory framework.
- Use of aggressive mass removal technologies that can be readily coupled with in situ bioremediation approaches offer considerable promise for DNAPL source zone restoration and long-term plume management.
- Polyoxyethylene (20) sorbitan monooleate (Tween 80), a nonionic surfactant, which functions as a solubilizing agent in surfactant enhanced aquifer remediation (SEAR) applications, has negligible effects on PCE-to-*cis*-DCE dechlorinating bacteria. In contrast, Tween 80 inhibits chloroethene-dechlorination by *Dehalococcoides* spp. The inhibition, however, is reversible, and dechlorination resumes following the removal (e.g., sorption, dilution, microbial degradation) of the surfactant.

3. Estimating mass discharge uncertainty

- Geostatistical approaches can be used successfully to estimate down gradient contaminant mass discharge and quantify the associated uncertainty using multi-level transect measurements or flux meter measurements.
- For transects associated with low levels of mass removal (in this study, 1% to 50%), i.e. transects that have large contaminated regions, mass discharge and the associated uncertainty can be accurately quantified for all of the sampling densities (ratio of the sampled area over the entire area of the transect) employed in this study (from 1% to 25%).
- For transects associated with high levels of mass removal (98% in this study) that feature only a few hot spots and a large near-zero concentration region, a minimum sampling density of 6-7% is required to obtain accurate quantification of uncertainty. Such densities are not economically feasible for most field-scale applications, suggesting that many existing sites may have not even collected sufficient data to accurately quantify the uncertainty associate with their mass flux estimates.
- Multi-stage sampling algorithm can reduce the required sampling density for an accurate quantification of uncertainty with the additional benefit of hot spot identification and delineation.

IV.2. Limitations:

Through the course of this project continuing challenges have been identified. Although this work identified the link between mass recovery and down-gradient contaminant mass flux, there is currently no method deployed in the field capable of quantifying the GTP or similar metrics. Future work must improve site characterization techniques to better resolve the source zone architecture. Failure to improve this resolution will limit future predictive capability. Stimulation of metabolic reductive dechlorination is still a complex, poorly understood process.

While this work made major contributions to this remediation strategy there are still a number of unresearched factors that may significantly influence metabolic reductive dechlorination, namely solvent toxicity, electron donor limitations, biogenic gas production, and pH. Future efforts may focus on novel methods for the delivery of electron donor to the DNAPL aqueous phase interface to ensure maximized dissolution enhancement. Additionally, much of the modeling accomplished in this project employed multi-dimensional, multi-phase compositional simulators. While well-suited for research, these models are difficult to use and are rarely applied by practitioners. Thus, a major effort to transition this knowledge to the field has focused on the development and application of simplified screening models that may be used to guide future site characterization and remediation technology selection. These models are designed to incorporate relevant mechanisms without requiring extensive site characterization or skilled user know-how. Finally, although the geostatistical approaches developed in this work can provide a much needed tool for improved site characterization and decision-making processes, the beneficial use of the tool has not been established systematically at actual sites. In addition, refinement of the tool for actual field settings is also required. Further, a user's guide and an easy-to-use interface are also needed to provide a vehicle for straightforward application of this tool.

IV.3. Suggestions for Future Research

Based on the findings of this research, the following suggestions are provided for future research that is relevant to the practice of source remediation.

- Quantification of DNAPL source zone mass and distribution (i.e., architecture) - this plays a critical role in remedial design, assessment, and performance.
- Bioenhanced dissolution can potentially increase the risk of downgradient exposure if reductive dechlorination is not complete and chlorinated daughter products persist. Factors influencing microbial transformation processes in source zones should be explored, including pH effects, chloroethene toxicity to the dechlorinating organisms, and electron donor limitations.
- DNAPL dissolution may become the controlling and rate-limiting step for microbial reductive dechlorination over time. The relative importance of this process on overall DNAPL mass removal and dechlorination should be explored.
- Alternative methods for sustained electron donor delivery in heterogeneous DNAPL source zones should be developed and evaluated under a range of probable *in situ* conditions.
- The effects of aggressive DNAPL mass removal technologies on key dechlorinators (e.g., *Dehalococcoides* spp.) should be explored to ensure the feasibility of biopolishing approaches.
- The development of simplified (and predictive) tools for the design, monitoring, and assessment of *in situ* remediation technologies, and in particular coupled technologies, for effective restoration and long-term management of DNAPL source zones should be pushed forward. These efforts should include the design of protocols to assess the uncertainty of mass flux measurements and estimation procedures for all current mass flux estimation technologies.

V. References

(ITRC), I. T. R. C. (2004). Strategies for Monitoring the Performance of DNAPL Source Zone Remedies.

AATDF (1997). Technology Practices Manual for Surfactants and Cosolvents. A. A. T. D. F. Program. Houston, TX.

Abriola, L. A., K. Rathfelder, et al. (1992). VALOR Code Version 0.0: A PC Code for Simulating Immiscible Contaminant Transport, Final Report RP2879-08. Palo Alto, CA, Electric Power Research Institute.

Abriola, L. M., T. J. Dekker, et al. (1993). "Surfactant-Enhanced Solubilization Of Residual Dodecane In Soil Columns .2. Mathematical-Modeling." Environmental Science & Technology **27**(12): 2341-2351.

Abriola, L. M., C. D. Drummond, et al. (2005). "Pilot-scale demonstration of surfactant-enhanced PCE solubilization at the Bachman road site. 1. Site characterization and test design." Environmental Science & Technology **39**(6): 1778-1790.

Abriola, L. M., J. Lang, et al. (1997). Michigan Soil Vapor Extraction Remediation (MISER) Model: A Computer Program to Model Soil Vapor Extraction and Bioventing of Organic Chemicals in Unsaturated Geologic Materials, U.S. Environmental Protection Agency, EPA/600/R-97/099, National Risk Management Research Laboratory, Ada, OK.

Abriola, L. M., J. R. Lang, et al. (1997). Michigan Soil-Vapor Extraction Remediation (MISER) Model - A Computer Program to Model Bioventing of Organic Chemicals in Unsaturated Geological Material, U. S. Environmental Protection Agency.

Adamson, D. T., D. Y. Lyon, et al. (2004). "Flux and product distribution during biological treatment of tetrachloroethene dense non-aqueous-phase liquid." Environmental Science & Technology **38**(7): 2021-2028.

Adamson, D. T., J. M. McDade, et al. (2003). "Inoculation of a DNAPL source zone to initiate reductive dechlorination of PCE." Environmental Science & Technology **37**(11): 2525-2533.

Adeel, Z. and R. G. Luthy (1995). "Sorption and transport kinetics of a nonionic surfactant through an aquifer sediment." Environmental Science & Technology **29**(4): 1032-1042.

Almås, Å. R., J. Mulder, et al. (2005). "Trace metal exposure of soil bacteria depends on their position in the soil matrix." Environmental Science & Technology **39**(16): 5927-5932.

Almeida, A. S., and A. G. Journel (1994). "Joint Simulation of Multiple-Variables with a Markov-Type Coregionalization Model." Math. Geol. **26**: 565-588.

Amos, B. K., J. A. Christ, et al. (2007a). "Experimental evaluation and mathematical modeling of microbially enhanced tetrachloroethene (PCE) dissolution." Environmental Science & Technology **41**: 963-970.

Amos, B. K., R. C. Daprato, et al. (2007b). "Effects of the nonionic surfactant Tween 80 on microbial reductive dechlorination of chlorinated ethenes." Environmental Science & Technology **41**: 1710-1716.

Amos, B. K., E. J. Suchomel, et al. (2008a). "Microbial activity and distribution during enhanced contaminant dissolution from a NAPL source zone." Water Research **In Press**.

Amos, B. K., E. J. Suchomel, et al. (2008b). Distribution of Geobacter lovleyi and Dehalococcoides spp. during bioenhanced NAPL dissolution. Environmental Science & Technology **In Preparation**.

Amos, B. K., Y. Sung, et al. (2007c). "Detection and quantification of *Geobacter lovleyi* strain SZ: implications for bioremediation at tetrachloroethene- and uranium-impacted sites." Applied and Environmental Microbiology **73**(21): 6898-6904.

Annable, M. D., K. Hatfield, J. Cho, H. Klammler, B. L. Parker, J. A. Cherry, and P. S. C. Rao (2005). "Field-scale evaluation of the passive flux meter for simultaneous measurement of groundwater and contaminant fluxes." Environmental science & technology **39**(18): 7194-7201.

Aziz, C. E., C. J. Newell, et al. (1999). BIOCHLOR Naturatl Attenuation Decision Support System User's Manual. San Antonio, TX, Prepared for the Air Force Center for Environmental Excellence, Brooks AFB.

Bockelmann, A., T. Ptak, and G. Teutsch (2001). "An analytical quantification of mass fluxes and natural attenuation rate constants at a former gasworks site; Natural attenuation of organic pollutants in groundwater. ." J. Contam. Hydrol. **53**: 429-453.

Borden, R. C., R. A. Daniel, et al. (1997). "Intrinsic biodegradation of MTBE and BTEX in a gasoline-contaminated aquifer." Water Resources Research **33**(5): 1105-1115.

Bourrel, M., Schechter, RS. (1988). Microemulsions and Related Systems. . Surfactant Science Series. New York, NY, Marcel Dekker, Inc. **30**.

Bradford, S. A., L. M. Abriola, et al. (1998). "Flow and entrapment of dense nonaqueous phase liquids in physically and chemically heterogeneous aquifer formations." Advances In Water Resources **22**(2): 117-132.

Brown, C. L., G. A. Pope, et al. (1994). "Simulation Of Surfactant-Enhanced Aquifer Remediation." Water Resources Research **30**(11): 2959-2977.

Carr, C. S., S. Garg, et al. (2000). "Effect of dechlorinating bacteria on the longevity and composition of PCE-containing nonaqueous phase liquids under equilibrium dissolution conditions." Environmental Science & Technology **34**(6): 1088-1094.

Chang, Y. C., M. Hatsu, et al. (2000). "Isolation and characterization of a tetrachloroethylene dechlorinating bacterium, *Clostridium bifermentans* DPH-1." Journal of Bioscience and Bioengineering **89**: 489-491.

Chouke, R. L., P. van Meurs, et al. (1959). "The instability of slow, immisible, viscous liquid - liquid displacements in porous media." Transactions AIME **216**: 188-194.

Christ, J. A. and L. M. Abriola (2007). "Modeling metabolic reductive dechlorination in dense non-aqueous phase liquid source-zones." Advances in Water Resources **30**(6-7): 1547-1561.

Christ, J. A., L. D. Lemke, et al. (2005). "Comparison of two- and three-dimensional simulations of dense nonaqueous phase liquid (DNAPL) migration and entrapment in a nonuniform permeability field." Water Resources Research **41**(1): w01007, doi: 1029/2004WR003239.

Christ, J. A., C. A. Ramsburg, et al. (2005). "Coupling aggressive mass removal with microbial reductive dechlorination for remediation of DNAPL source zones - A review and assessment." Environmental Health Perspectives **113**(4): 465-477, doi: 10.1289/ehp.6932.

Christ, J. A., C. A. Ramsburg, et al. (2006). "Estimating mass discharge from dense nonaqueous phase liquid source zones using upscaled mass transfer coefficients: An evaluation using multiphase numerical simulations." Water Resources Research **42**: W11420.

Chu, M., P. K. Kitandidis, et al. (2003). "Effects of biomass accumulation on microbially enhanced dissolution of a PCE pool: a numerical simulation." Journal of Contaminant Hydrology **1906**: 1-22.

Chu, M., P. K. Kitanidis, et al. (2004). "Possible factors controlling the effectiveness of bioenhanced dissolution of non-aqueous phase tetrachloroethene." Advances in Water Resources **27**(6): 601-615.

Chu, M., P. K. Kitanidis, et al. (2006). Inhibition-related limitation to biologically enhanced dissolution of chlorinated solvents, abstr. B-24. Remediation of chlorinated and recalcitrant compounds. Proceedings of the Fifth International Conference on Remediation of Chlorinated and Recalcitrant Compounds. B. M. Sass. May 21-25, 2006, Monterey, CA.

Clement, T. P. (2001). "Generalized solution to multispecies transport equations coupled with a first-order reaction network." Water Resources Research **37**: 157-163.

Conrad, S., Glass, RJ, Peplinski, WJ. (2002). "Bench-scale visualization of DNAPL remediation processes in analog heterogeneous aquifers: surfactant floods and in situ oxidation using permanganate." J. Contam. Hydrol. **58**: 13-49.

Cope, N. and J. B. Hughes (2001). "Biologically-enhanced removal of PCE from NAPL source zones." Environmental Science & Technology **35**(10): 2014-2021.

Da Silva, M. L., R. C. Daprato, et al. (2006). "Comparison of bioaugmentation and biostimulation for the enhancement of dense nonaqueous phase liquid source zone bioremediation." Water Environment Research **78**(13): 2456-2465.

Daprato, R. C., F. E. Löffler, et al. (2007). "Comparative analysis of three tetrachloroethene to ethene halorespiring consortia suggests functional redundancy." Environmental Science & Technology **41**: 2261-2269.

Darnault, C., Throop, JA, DiCarlo, DA, Rimmer, A, Steenhuis, TS, Parlange, J.–Y. (1998). "Visualization by light transmission of oil and water contents in transient two-phase flow fields. ." J. Contam. Hydrol. **31**: 337-348.

Dekker, T. J. and L. M. Abriola (2000). "The influence of field-scale heterogeneity on the infiltration and entrapment of dense nonaqueous phase liquids in saturated formations." Journal Of Contaminant Hydrology **42**(2-4): 187-218.

Dekker, T. J. and L. M. Abriola (2000). "The influence of field-scale heterogeneity on the surfactant-enhanced remediation of entrapped nonaqueous phase liquids." Journal Of Contaminant Hydrology **42**(2-4): 219-251.

Delshad, M., G. A. Pope, et al. (1996). "A compositional simulator for modeling surfactant enhanced aquifer remediation .1. Formulation." Journal Of Contaminant Hydrology **23**(4): 303-327.

Delshad, M., G. A. Pope, et al. (1996). "A compositional simulator for modeling surfactant enhanced aquifer remediation, 1 formulation." Journal of Contaminant Hydrology **23**(4): 303-327.

Deutsch, C. V. (1997). "Direct assessment of local accuracy and precision. ." Geostatistics Wollongong '96, Vols 1 and 2 **8**: 115-125.

Duhamel, M. and E. A. Edwards (2006). "Microbial composition of chlorinated ethene-degrading cultures dominated by *Dehalococcoides*." FEMS Microbiology Ecology **58**: 538-549.

Duhamel, M. and E. A. Edwards (2007). "Growth and yields of dechlorinators, acetogens, and methanogens during reductive dechlorination of chlorinated ethenes and

dihaloelimination of 1,2-dichloroethane." Environmental Science & Technology **41**: 2303-2310.

Duhamel, M., K. Mo, et al. (2004). "Characterization of a highly enriched *Dehalococcoides*-containing culture that grows on vinyl chloride and trichloroethene." Applied and Environmental Microbiology **70**: 5538-5545.

Duhamel, M., S. D. Wehr, et al. (2002). "Comparison of anaerobic dechlorinating enrichment cultures maintained on tetrachloroethene, trichloroethene, *cis*-dichloroethene and vinyl chloride." Water Research **36**(17): 4193-4202.

Dwarakanath V, K. K., Pope GA, Shotts D, Wade WH. (1999). "Anionic surfactant remediation of soil columns contaminated by nonaqueous phase liquids." J. Contam. Hydrol. **38**: 465-488.

Edwards, D., Luthy, RG, Liu, Z. (1991). "Solubilization of polycyclic aromatic hydrocarbons in micellar nonionic surfactant solutions. ." Environ. Sci. Technol. **25**: 127-133.

Einarson, M. D., and D. M. Mackay (2001). "Predicting impacts of groundwater contamination." Environmental Science & Technology **35**: 66A-73A.

Empadinhas, N., L. Albuquerque, et al. (2004). "A gene from the mesophilic bacterium *Dehalococcoides ethenogenes* encodes a novel mannosylglycerate synthase." Journal of Bacteriology **186**(13): 4075-4084.

Essaid, H. I. and K. M. Hess (1993). "MONTE-CARLO SIMULATIONS OF MULTIPHASE FLOW INCORPORATING SPATIAL VARIABILITY OF HYDRAULIC-PROPERTIES." Ground Water **31**(1): 123-134.

Fennell, D. E. and J. M. Gossett (1998). "Modeling the production of and competition for hydrogen in a dechlorinating culture." Environmental Science & Technology **32**: 2450-2460.

Field, J., Sawyer, TE. (2000). "High-performance liquid chromatography diode array detection of trichloroethene and aromatic and aliphatic anionic surfactants used for surfactant-enhanced aquifer remediation." J. Chromat. A **893**: 253-260.

Fountain, J. C., R. C. Starr, et al. (1996). "A controlled field test of surfactant-enhanced aquifer remediation." Ground Water **34**(5): 910-916.

Geosyntec. (2005) *Bioaugmentation for remediation of chlorinated solvents: technology development, status and research needs*; Environmental Security Technology Certification Program (ESTCP), U.S. Department of Defense: Washington, DC; http://www.estcp.org/viewfile.cfm?Doc=BioaugmentationWhitePaper%2Epdf.

Glover, K. C., J. Munakata-Marr, et al. (2007). "Biologically enhanced mass transfer of tetrachloroethene from DNAPL source zones: experimental evaluation and influence of pool morphology." Environmental Science & Technology **41**(4): 1384-1389.

Goovaerts, P. (1997). Geostatistics for Natural Resources Evaluation. New York, Oxford University Press.

Gossett, J. M. (1987). "Measurement of Henry's law constants for C_1 and C_2 chlorinated hydrocarbons." Environmental Science & Technology **21**: 202-208.

Gyürék, L. L. and G. R. Finch (1998). "Modeling water treatment chemical disinfection kinetics." Journal of Environmental Engineering **124**(9): 783-793.

Haas, C. N. (1999). Disinfection. Water quality & treatment. R. D. Letterman. New York, McGraw-Hill, Inc**:** 14.22-14.23.

Hatfield, K., M. Annable, J. Cho, P. S. Rao, and H. Klammler (2004). "A direct passive method for measuring water and contaminant fluxes in porous media." J. Contam. Hydrol. **75**: 155-181.

He, J., K. M. Ritalahti, et al. (2003). "Complete detoxification of vinyl chloride (VC) by an anaerobic enrichment culture and identification of the reductively dechlorinating population as a *Dehalococcoides* species." Applied and Environmental Microbiology **69**(2): 996-1003.

He, J., K. M. Ritalahti, et al. (2003). "Detoxification of vinyl chloride to ethene coupled to growth of an anaerobic bacterium." Nature **424**: 62-65.

He, J., Y. Sung, et al. (2005). "Isolation and characterization of *Dehalococcoides* sp. strain FL2, a trichloroethene (TCE)- and 1,2-dichloroethene-respiring anaerobe." Environmental Microbiology **7**: 1442-1450.

Helton, R. R., F. E. Löffler, et al. (2000). Microbial dynamics in a SERB treated Tetrachloroethene (PCE)-contaminated aquifer. Hanzardous Substance Research Centers Research Symposium. Asilomar, CA.

Holder, T. G., T. G. Teutsch, et al. (1998). New approach for source zone characterization: The Neckar Valley study. IAHS (International Assoication of Hydrological Sciences).

Homsy, G. M. (1987). "Viscous fingering in porous media." Annual Review of Fluid Mechanics **19**: 271-311.

Huh, C. (1979). "Interfacial-tensions and solubilizing ability of a microemulsion phase that coexists with oil and brine. ." J. Colloid Interface Sci. **71**: 408-426.

Huling, S. and J. W. Weaver (1991). Ground water issue: dense nonaqueous phase liquids (EPA/540/4-91-002). Washington, D.C., U. S. Environmental Protection Agency. **Washington, DC**.

Isaaks, E. H., and R. M. Srivastava (1989). An Introduction to Applied Geostatistics. . New York, Oxford University Press.

Isalou, M., B. E. Sleep, et al. (1998). "Biodegradation of high concentrations of tetrachloroethene in a continuous flow column system." Environmental Science & Technology **32**(22): 3579-3585.

Isken, S. and J. A. M. de Bont (1998). "Bacteria tolerant to organic solvents." Extremophiles **2**(3): 229-238.

Jawitz, J. W., M. D. Annable, et al. (1998). "Field implementation of a Winsor type I surfactant/alcohol mixture for in situ solubilization of a complex LNAPL as a single phase microemulsion." Environmental Science & Technology **32**(4): 523-530.

Jin M, H. G., Jackson RE, Kostarelos K, Pope GA. (2007). "Control of downward migration of dense nonaqueous phase liquid during surfactant flooding by design simulations. ." Water Resour. Res. **43**: W01412.

Journel, A. G., Deutsch, C.V. (1993). "Entropy and Spatial Disorder. ." Math. Geol. **25**: 329-355.

Journel, A. G., Huijbregts, C.J. (1978). Mining Geostatistics. New York, Academic Press.

Kao, C. M., and Y. S. Wang (2001). "Field investigation of the natural attenuation and intrinsic biodegradation rates at an underground storage tank site. ." Environ. Geol. **40**: 622-631.

King, M. W. G., J. F. Barker, J. F. Devlin, and B. J. Butler (1999). "Migration and natural fate of a coal tar creosote plume; 2, Mass balance and biodegradation indicators; Transport and fate of coal-tar compounds in the subsurface. ." J. Contam. Hydrol. **39**: 281-307.

Kube, M., A. Beck, et al. (2005). "Genome sequence of the chlorinated compound respiring bacterium *Dehalococcoides* species strain CBDB1." Nature Biotechnology **23**(10): 1269-1273.

Kueper, B. H. and E. O. Frind (1991). "2-PHASE FLOW IN HETEROGENEOUS POROUS-MEDIA .2. MODEL APPLICATION." Water Resources Research **27**(6): 1059-1070.

Kueper, B. H., D. Redman, et al. (1993). "A Field experiment to study the behavior of tetrachloroethylene below the water-table-spatial-distribution of residual and pooled DNAPL." Ground Water **31**(5): 756-766.

Lee, I.-S., J.-H. Bae, et al. (2004). "Simulated and experimental evaluation of factors affecting the rate and extent of reductive dehalogenation of chloroethenes with glucose." Journal of Contaminant Hydrology **74**: 313-331.

Lemke, L. D. and L. M. Abriola (2006). "Modeling DNAPL mass removal in nonuniform formations: Linking source zone architecture and system response." Geosphere **2**: 74-82.

Lemke, L. D., L. M. Abriola, et al. (2004). "DNAPL source zone characterization: Influence of hydraulic property correlation on predictions of DNAPL infiltration and entrapment." Water Resources Research **40**(1): W01511 doi: 10.1029/2003WR001980.

Lemke, L. D., L. M. Abriola, et al. (2004). "Influence of hydraulic property correlation on predicted DNAPL source zone architecture, mass recovery and contaminant flux." Water Resources Research **40**(12): W12417 doi: 10.1029/2004WR003061.

Li, K. B., and L. M. Abriola (in preparation). "A Multi-stage Multi-criteria Spatial Sampling Strategy for the Quantification of Contaminant Mass Discharge and the Associated Uncertainty ".

Li, K. B., P. Goovaerts, and L. M. Abriola (2007). "A geostatistical approach for quantification of contaminant mass discharge uncertainty using multilevel sampler measurements." Water Resources Research **43**(6): W06436.

Löffler, F. E., J. E. Champine, et al. (1997). "Complete reductive dechlorination of 1,2-dichloropropane by anaerobic bacteria." Applied and Environmental Microbiology **63**: 2870-2875.

Löffler, F. E., K. M. Ritalahti, et al. (1997). "Dechlorination of chloroethenes is inhibited by 2-bromoethanesulfonate in the absence of methanogens." Applied and Environmental Microbiology **63**: 4982-4985.

Löffler, F. E., R. A. Sanford, et al. (1996). "Initial characterization of a reductive dehalogenase from *Desulfitobacterium chlororespirans* Co23." Applied and Environmental Microbiology **62**: 3809-3813.

Löffler, F. E., J. M. Tiedje, et al. (1999). "Fraction of electrons consumed in electron acceptor reduction and hydrogen thresholds as indicators of halorespiratory physiology." Applied and Environmental Microbiology **65**: 4049-4056.

Londergan JT, M. H., Mariner PE, Jackson RE, Brown CL, Dwarakanath V, Pope GA, Ginn JS, Taffinder S. (2001). "DNAPL removal from a heterogeneous alluvial aquifer by surfactant-enhanced aquifer remediation. ." Ground Water Monitor. Remed. **21**: 57-67.

Luijten, M. L. G. C., J. de Weert, et al. (2003). "Description of *Sulfurospirillum halorespirans* sp. nov., an anaerobic, tetrachloroethene-respiring bacterium, and transfer of *Dehalospirillum multivorans* to the genus *Sulfurospirillum* as *Sulfurospirillum multivorans* comb. nov." International Journal of Systematic and Evolutionary Microbiology **53**(3): 787-793.

Luong, J. H. T. (1987). "Generalization of Monod kinetics for analysis of growth data with substrate inhibition." Biotechnol. Bioeng. **29**: 242-248.

Major, D. W., M. L. McMaster, et al. (2002). "Field demonstration of successful bioaugmentation to achieve dechlorination of tetrachloroethene to ethene." Environmental Science & Technology **36**(23): 5106-5116.

Maymó-Gatell, X., Y.-T. Chien, et al. (1997). "Isolation of a bacterium that reductively dechlorinates tetrachloroethene to ethene." Science **276**: 1568-1571.

McDougald, D., S. Srinivasan, et al. (2003). "Signal-mediated cross-talk regulates stress adaptation in *Vibrio* species." Microbiology **149**: 1923-1933.

McGuire, T. and J. B. Hughes (2003). "Effects of surfactants on the dechlorination of chlorinated ethenes." Environmental Toxicology and Chemistry **22**(11): 2630-2638.

Mravik, S. C., R. K. Sillan, et al. (2003). "Field evaluation of the solvent extraction residual biotreatment technology." Environmental Science & Technology **37**(21): 5040-5049.

Nesbø, C. L., S. L'Haridon, et al. (2001). "Phylogenetic analyses of two "archaeal" genes in *Thermototga maritima* reveal multiple transfers between archaea and bacteria." Mol. Biol. Evol. **18**(3): 362-375.

Neumann, A., H. Scholz-Muramatsu, et al. (1994). "Tetrachloroethene metabolism of *Dehalospirillum multivorans*." Archives of Microbiology **162**(4): 295-301.

Nielsen, R. B. and J. D. Keasling (1999). "Reductive dechlorination of chlorinated ethene DNAPLs by a culture enriched from contaminated groundwater." Biotechnology and Bioengineering **62**(2): 160-165.

Niemet, M., Selker, JS. (2001). "A new method for quantification of liquid saturation in 2-D translucent porous media systems using light transmission. ." Adv. Water Res. **24**: 651-666.

NRC (1997). Innovation in Ground Water and Soil Cleanup. N. A. Press. Washington, D.C.

Okutman Tas, D., I. N. Thomson, et al. (2006). "Kinetics of the microbial reductive dechlorination of pentachloroaniline." Environmental Science & Technology **40**: 4467-4472.

Parker, J. C. and E. Park (2004). "Modeling field-scale dense nonaqueous phase liquid dissolution kinetics in heterogeneous aquifers." Water Resources Research **40**(5).

Parkhill, J., B. W. Wren, et al. (2000). "The genome sequence of the food-borne pathogen *Campylobacter jejuni* reveals hypervariable sequences." Nature **403**(6770): 665-668.

Pennell, K., Abriola, LM, Pope, GA. (1996). "Influence of viscous and buoyancy forces on the mobilization of residual tetrachloroethylene during surfactant flushing. ." Environ. Sci. Technol. **30**: 1328-1335.

Pennell, K. D. and L. M. Abriola (1997). Surfactant enhanced aquifer remediation: Fundamental processes and practical application. Bioremediation: Principles and Practice. S. K. Sikdar and R.L.Irvine. Lancaster, PA, Technomic Publ.**:** 693-750.

Pennell, K. D., A. M. Adinolfi, et al. (1997). "Solubilization of dodecane, tetrachloroethylene, and 1,2-dichlorobenzene in micellar solutions of ethoxylated nonionic surfactants." Environmental Science & Technology **31**: 1382-1389.

Perry, R. H., D. W. Green, et al., Eds. (1997). Perry's chemical engineers' handbook. New York, McGraw-Hill.

Pfaffl, M. W. (2001). "A new mathematical model for relative quantification in real-time RT-PCR." Nucleic Acids Research **29**(9): e45.

Phelan, T. J., L. D. Lemke, et al. (2004). "Influence of textural and wettability variations on predictions of DNAPL persistence and plume development in saturated porous media." Advances in Water Resources **27**(4): 411-427.

Pope, G., Wade, WH. (1995). Lessons from enhanced oil recovery research for surfactant-enhanced aquifer remediation. . Surfactant-Enhanced Subsurface Remediation. D. A. Sabatini, Knox, R.C., Harwell, J.H. . Washington, D.C., American Chemical Soceity**:** 142-160.

Powers, S. E., L. M. Abriola, et al. (1994). "Phenomenological models for transient NAPL-water mass-transfer processes." Journal of Contaminant Hydrology **16**: 1-33.

Powers, S. E., L. M. Abriola, et al. (1992). "An experimental investigation of nonaqueous phase liquid dissolution in saturated subsurface systems: steady state mass transfer rates." Water Resources Research **28**(10): 2691-2705.

Powers, S. E., C. O. Loureiro, et al. (1991). "Theoretical study of the significance of nonequilibrium dissolution of nonaqueous phase liquids in subsurface systems." Water Resources Research **27**(4): 463-477.

Ramakrishnan, V., A. V. Ogram, et al. (2005). "Impacts of co-solvent flushing on microbial populations capable of degrading trichloroethylene." Environmental Health Perspectives **113**(1): 55-61.

Ramsburg, C., Pennell, KD, Kibbey, TCG, Hayes, KF. (2003). "Use of a surfactant-stabilized macroemulsion to deliver n-butanol for density-modified displacement trichloroethene-NAPL. ." Environ. Sci. Technol. **37**: 4246-4253.

Ramsburg, C., Pennell, KD. (2001). "Experimental and economic assessment of two surfactant formulations for source zone remediation at a former dry cleaning facility. ." Ground Water Monitor. Remed. **21**: 68-82.

Ramsburg, C. A., L. M. Abriola, et al. (2004). "Stimulated microbial reductive dechlorination following surfactant treatment at the Bachman Road site." Environmental Science & Technology **38**: 5902-5914.

Ramsburg, C. A., K. D. Pennel, et al. (2005). "Pilot-scale demonstration of surfactant-enhanced PCE solubilization at the Bachman Road site. 2. System operation and evaluation." Environmental Science & Technology: DOI: 10.1021/es049563r.

Ramsburg CA, P. K. (2002). "Density-modified displacement for DNAPL source zone remediation: Density conversion and recovery in heterogeneous aquifer cells. ." Environ. Sci. Technol. **36**: 3176-3187.

Ramsburg CA, P. K., Kibbey TCG, Hayes KF. (2003). "Use of a surfactant-stabilized macroemulsion to deliver n-butanol for density-modified displacement trichloroethene-NAPL. ." Environ. Sci. Technol. **37**: 4246-4253.

Rao, P., Annable, MD, Sillan, RK, Dai, D, Hatfield, K, Graham, WD, Wood, AL, Enfield, CG (1997). "Field-scale evaluation of in situ cosolvent flushing for enhanced aquifer remediation." Water Resour. Res. **33**: 2673-2686.

Rao, P. S. C., J. W. Jawitz, C. G. Enfield, R. W. Falta Jr, M. D. Annable, and A. L. Wood (2002). "Technology integration for contaminated site remediation; clean-up goals and performance criteria; Groundwater quality; natural and enhanced restoration of groundwater pollution." IAHS-AISH Publication **275**: 571-578.

Rathfelder, K. and L. M. Abriola (1998). "The influence of capillarity in numerical modeling of organic liquid redistribution in two-phase systems." Advances In Water Resources **21**(2): 159-170.

Rathfelder, K. M., L. M. Abriola, et al. (2001). "Surfactant enhanced recovery of tetrachloroethylene from a porous medium containing low permeability lenses 2. Numerical simulations." Journal of Contaminant Hydrology **48**: 351-374.

Rathfelder, K. M., L. M. Abriola, et al. (2003). "Surfactant enhanced recovery of tetrachloroethylene from a porous medium containing low permeability lenses 2. Numerical simulation." Journal of Contaminant Hydrology **64**(3-4): 227-252.

Rathfelder, K. M., J. R. Lang, et al. (2000). "A numerical model (MISER) for the simulation of coupled physical, chemical and biological processes in soil vapor extraction and bioventing systems." Journal Of Contaminant Hydrology **43**(3-4): 239-270.

Regeard, C., J. Maillard, et al. (2004). "Development of degenerate and specific PCR primers for the detection and isolation of known and putative chloroethene reductive dehalogenase genes." Journal of Microbiology Methods **56**(1): 107-118.

Ritalahti, K. M., B. K. Amos, et al. (2006). "Quantitative PCR targeting 16S rRNA and reductive dehalogenase genes simultaneously monitors multiple *Dehalococcoides* strains." Applied and Environmental Microbiology **72**(4): 2765-2774.

Ritalahti, K. M., F. E. Löffler, et al. (2005). "Bioaugmentation for chlorinated ethene detoxification: bioaugmentation and molecular diagnostics in the bioremediation of chlorinated ethene-contaminated sites." Industrial Biotechnology **1**(2): 114-118.

Saito, H., and P. Goovaerts (2002). "Accounting for measurement error in uncertainty modeling and decision-making using indicator kriging and p-field simulation: application to a dioxin contaminated site. ." Environmetrics **13**: 555-567.

Sale, T. C. and D. B. McWhorter (2001). "Steady state mass transfer from single-component dense nonaqueous phase liquids in uniform flow fields." Water Resources Research **37**(2): 393-404.

Schaerlaekens, J., Feyen, J. (2004). "Effect of scale and dimensionality on the surfactant-enhanced solubilization of a residual DNAPL contamination." J. Contam. Hydrol. **71**: 283-306.

Scholz-Muramatsu, H., A. Neumann, et al. (1995). "Isolation and characterization of *Dehalospirillum multivorans* gen. nov., sp. nov., a tetrachloroethene-utilizing, strictly anaerobic bacterium." Archives of Microbiology **163**: 48-56.

Schroth, M., Ahearn, SJ, Selker, JS, Istok, JD. (1996). "Characterization of Miller-similar silica sands for laboratory hydrologic studies." Soil Sci. Soc. Am. J. **60**: 1331-1339.

Schwarz, R., T. Ptak, et al. (1998). Groundwater risk assessment at contaminantd sites: A new investigation approach. IAHS (International Assoication of Hydrological Sciences).

Schwarzenbach, R. P., P. M. Gschwend, et al. (2003). Environmental organic chemistry. New Jersey, John Wiley & Sons, Inc.

Semprini, L., P. Kitandidis, et al. (1995). "Anaerobic transformation of chlorinated aliphatic hydrocarbons in a sand aquifer based on spatial chemical distributions." Water Resources Research **31**(4): 1051-1062.

Seshadri, R., L. Adrian, et al. (2005). "Genome sequence of the PCE-dechlorinating bacterium *Dehalococcoides ethenogenes*." Science **307**(5706): 105-108.

Sleep, B. E., D. J. Seepersad, et al. (2006). "Biological enhancement of tetrachloroethene dissolution and associated microbial community changes." Environmental Science & Technology **40**(11): 3623-3633.

Smith, J. A., D. Sahoo, et al. (1997). "Surfactant-enhanced remediation of a trichloroethene-contaminated aquifer .1. Transport of triton X-100." Environmental Science & Technology **31**(12): 3565-3572.

Smits, T. H. M., C. Devenoges, et al. (2004). "Development of a real-time PCR method for quantification of the three genera *Dehalobacter*, *Dehalococcoides*, and *Desulfitobacterium* in microbial communities." Journal of Microbiology Methods **57**: 369-378.

Soga, K., J. W. E. Page, and T. H. Illangasekare (2004). "A review of NAPL source zone remediation efficiency and the mass flux approach. ." J. Hazard. Mater. **110**: 13-27.

Stroo, H. F., M. Unger, C. H. Ward, M. C. Kavanaugh, C. Vogel, A. Leeson, J. A. Marqusee, and B. P. Smith (2003). "Remediating chlorinated solvent source zones. ." Environ. Sci. Technol. **37**: 224A-230A.

Stroo, H. F., M. Unger, et al. (2003). "Remediation chlorinated solvent source zones." Environmental Science & Technology **37**: 224A-230A.

Suchomel, E., Pennell, KD. (2006). "Reductions in contaminant mass discharge following partial mass removal from DNAPL source zones. ." Environ. Sci. Technol. **40**: 6110-6116.

Suchomel, E. J., C. A. Ramsburg, et al. (2007). "Evaluation of trichloroethene recovery processes in heterogeneous aquifer cells flushed with biodegradable surfactants." Journal of Contaminant Hydrology **93**(3-4): 195-214.

Sung, Y., K. E. Fletcher, et al. (2006). "*Geobacter lovleyi* sp. nov. strain SZ, a novel metal-reducing and tetrachloroethene-dechlorinating bacterium." Applied and Environmental Microbiology **72**(4): 2775-2782.

Sung, Y., K. M. Ritalahti, et al. (2003). "Characterization of two tetrachloroethene-reducing, acetate-oxidizing anaerobic bacteria, and their description as *Desulfuromonas michiganensis* sp. nov." Applied and Environmental Microbiology **69**(5): 2964-2974.

Taylor, T. P., K. D. Pennell, et al. (2001). "Surfactant enhanced recovery of tetrachloroethylene from a porous medium containing low permeability lenses - 1. Experimental studies." Journal Of Contaminant Hydrology **48**(3-4): 325-350.

Taylor, T. P., K. D. Pennell, et al. (2001). "Surfactant enhanced recovery of tetrachloroethylene from a porous medium containing low permeability lenses. 1. Experimental Studies." Journal of Contaminant Hydrology **48**(3-4): 325-350.

Tidwell, V., Glass, RJ. (1994.). "X-ray and visible light transmission for laboratory measurement of two-dimensional saturation fields in thin-slab systems. ." Water Resour. Res. **30**: 2873-2882.

Toride, N., F. J. Leij, et al. (1995). The CXTFIT code for estimating transport parameters from laboratory or field tracer experiments, version 2.0. Riverside, CA, USDA Salinity Lab.

USEPA (1997). Cleaning up the Nation's Waste Sites: Markets and Technology Trends. U. S. E. P. Agency.

White, D. C., R. Geyer, et al. (2005). "Phospholipid furan fatty acids and ubiquinone-8: Lipid biomarkers that may protect *Dehalococcoides* strains from free radicals." Applied and Environmental Microbiology **71**(12): 8426-8433.

Whitman, W. B., T. L. Bowen, et al. (1992). The methanogenic bacteria. The Prokaryotes. A. Balows, H. G. Trüper, M. Dworkin, W. Harder and K.-H. Schleifer. New York, Springer-Verlag. **1:** 719-767.

Willson, C., Hall, JL, Miller, CT, Imhoff, PT. (1999). "Factors affecting bank formation during surfactant enhanced mobilization of residual NAPL. ." Environ. Sci. Technol. **33**: 2440-2446.

Wilson, J. T., J. S. Cho, et al. (2000). Natural attenuation of MTBE in the subsurface under methanogenic conditions, US Environmental Protection Agency.

Winsor, P. (1954). Solvent Properties of Amphiphilic Compounds. London, UK, Butterworth.

Xavier, K. B. and B. L. Bassler (2003). "LuxS quorum sensing: more than just a numbers game." Current Opinion in Microbiology **6**: 191-197.

Yang, Y. and P. L. McCarty (2000). "Biologically enhanced dissolution of tetrachloroethene DNAPL." Environmental Science & Technology **34**(14): 2979-2984.

Yang, Y. and P. L. McCarty (2002). "Comparison between donor substrates for biologically enhanced tetrachloroethene DNAPL dissolution." Environmental Science & Technology **36**(15): 3400-3404.

Yang, Y. and P. L. McCarty (2002). "Comparison between donor substrates for biologically enhanced tetrachloroethene DNAPL dissolution." Environmental Science and Technology **36**: 3400-3404.

Yeh, D. H. and S. G. Pavlostathis (2004). "Phase distribution and hexachlorobenzene in a suspended-growth culture amended with a polysorbate surfactant." Water Environment Research **76**(2): 137-148.

Yu, S., M. E. Dolan, et al. (2005). "Kinetics and inhibition of reductive dechlorination of chlorinated ethylenes by two different mixed cultures." Environmental Science & Technology **39**(1): 195-205.

Yu, S. and L. Semprini (2004). "Kinetics and modeling of reductive dechlorination at high PCE and TCE concentrations." Biotechnol. Bioeng. **88**: 451-464.

Yu, S. and L. Semprini (2004). "Kinetics and modeling of reductive dechlorination at high PCE and TCE concentrations." Biotechnol. Bioeng. **88**(4): 451-464.

Zhang, C., G. Zheng, et al. (2006). "Micellar partitioning and its effects on Henry's law constants of chlorinated solvents in anionic and nonionic surfactant solutions." Environmental Science & Technology **40**(1): 208-214.

Zhong LR, M., AS, Pope, GA. (2003). "The effects of surfactant formulation on nonequilibrium NAPL solubilization. ." J. Contam. Hydrol. **60**: 55-75.

Zhu, J. and J. F. Sykes (2000). "The influence of NAPL dissolution characteristics on field-scale contaminant transport in subsurface." Journal of Contaminant Hydrology **41**(1-2): 133-154.

Zhu, J. T. and J. F. Sykes (2004). "Simple screening models of NAPL dissolution in the subsurface." Journal of Contaminant Hydrology **72**(1-4): 245-258.

VI. Appendices

Appendix A

Peer-reviewed Publications

Abriola, L.M., J.A. Christ, K.D. Pennell, and C.A. Ramsburg. Chapter 10: Source Zone Remediation Challenges. *In* Delivery and Mixing in the Subsurface: Processes and Design Principles for In Situ Remediation, P.K. Kitanidis and P.L. McCarty (Eds.). in review.

Amos, B.K., J.A. Christ, L.M. Abriola, K.D. Pennell, F.E. Löffler. 2007. Experimental evaluation and mathematical modeling of microbial enhanced tetrachloroethene (PCE) dissolution, *Environmental Science & Technology*, 41(3): 963-970, doi: 10.1021/es061438n.

Amos, B.K., R.C. Daprato, J.B. Hughes, K.D. Pennell, and F.E. Löffler. 2007. Effects of the nonionic surfactant Tween 80 on microbial reductive dechlorination of chlorinated ethenes, *Environmental Science & Technology*, 41(5): 1710-1716, doi: 10.1021/es061926v.

Amos, B.K., E.J. Suchomel, K.D. Pennell, F.E. Löffler. 2008. Microbial activity and distribution during enhanced contaminant dissolution from a NAPL source zone. *Water Research*, in press, doi: 10.1016/j.waters.2008.03.015.

Christ, J.A., C.A. Ramsburg, L.M. Abriola, K.D. Pennell, and F.E. Löffler. 2005. Coupling aggressive mass removal with microbial reductive dechlorination for remediation of DNAPL source zones: A review and assessment, *Environmental Health Perspectives*, 113(4): 465-477, doi: 10.1289/ehp.6932.

Christ, J.A., L.D. Lemke, and L.M. Abriola. 2005. Comparison of two- and three-dimensional simulations of dense nonaqueous phase liquids (DNAPLs): Migration and entrapment in a nonuniform permeability field, *Water Resources Research*, 41(1): W01007, doi: 10.1029/2004WR003239.

Christ, J.A., C.A. Ramsburg, K.D. Pennell, and L.M. Abriola. 2006 Estimating mass discharge from dense nonaqueous phase liquid source zones using upscaled mass transfer coefficients: An evaluation using multiphase numerical simulations, *Water Resources Research*, 42(11): W11420, doi:10.1029/2006WR004886.

Christ, J.A. and L.M. Abriola. 2007. Modeling metabolic reductive dechlorination in dense non-aqueous phase liquid source-zones, *Advances in Water Resources*, 30(6-7): 1547-1561, doi: 10.1016/j.advwatres.2006.05.024.

Lemke, L.D., and L.M. Abriola. 2003, Predicting DNAPL entrapment and recovery: the influence of hydraulic property correlation, *Stochastic Environmental Research and Risk Assessment*, 17(6): 408-418, doi: 10.1007/s00477-003-0162-4.

Lemke, L.D., L.M. Abriola, and P. Goovaerts. 2004. Dense nonaqueous phase liquid (DNAPL) source zone characterization: Influence of hydraulic property correlation on predictions of DNAPL infiltration and entrapment, *Water Resources Research,* 40(1): W01511, doi: 10.1029/2003WR001980.

Lemke, L.D., L.M. Abriola, and J.R. Lang. 2004. Influence of hydraulic property correlation on predicted dense nonaqueous phase liquid source zone architecture, mass recovery and contaminant flux, *Water Resources Research,* 40(12): W12417, doi: 10.1029/2004WR003061.

Lemke, L.D., W.A. Barrack, L.M. Abriola, and P. Goovaerts. 2004. Matching solute breakthrough with deterministic and stochastic aquifer models, *Ground Water,* 42(6): 920-934, doi: 10.1111/j.1745-6584.2004.t01-10-.x

Lemke, L.D., L.M. Abriola, and P. Goovaertz. 2005. Correction to "Dense nonaqueous phase liquid (DNAPL) source zone characterization: Influence of hydraulic property correlation on predictions of DNAPL infiltration and entrapment." *Water Resources Research*, 41(6): W06015, doi: 10.1029/2005WR004213.

Lemke, L.D. and L.M. Abriola. 2006. Modeling dense nonaqueous phase liquid mass removal in nonuniform formations: Linking source-zone architecture and system response, *Geosphere*, 2(2): 74-82, doi: 10.1130/GES00025.1.

Li, Y.S., L.M. Abriola, T.J. Phelan, C.A. Ramsburg, and K.D. Pennell. 2007. Experimental and numerical validation of the total trapping number for prediction of DNAPL mobilization, *Environmental Science & Technology,* 41(23): 8135-8141, doi: 10.1021/es070834i

Li K.B., P. Goovaerts, L.M. Abriola. 2007. A geostatistical approach for quantification of contaminant mass discharge uncertainty using multilevel sampler measurements, *Water Resources Research,* 43(6): W06436, doi:10.1029/2006WR005427.

Phelan, T.J., S.A. Bradford, D.M. O'Carroll, L.D. Lemke, and L.M. Abriola. 2004. Influence of textural and wettability variations on predictions of DNAPL persistence and plume development in saturated porous media, *Advances in Water Resources*, 27(4): 411-427, doi: 10.1016/j.advwatres.2004.02.011.

Ramsburg, C.A., L.M. Abriola, K.D. Pennell, F.E. Löffler, M. Gamache, B.K. Amos, and E.A. Petrovskis. 2004. Stimulated microbial reductive dechlorination following surfactant treatment at the Bachman Road site, *Environmental Science & Technology,* 38(22): 5902-5914, doi: 10.1021/es049675i.

Suchomel, E.J. and K.D. Pennell. 2006. Reductions in contaminant mass flux following partial mass removal from DNAPL source zones. *Environmental Science & Technology*. 40(19): 6110-6116, doi: 10.1021/es060298e.

Suchomel, E.J., C.A. Ramsburg, and K.D. Pennell. 2007. Evaluation of tricholoethene recovery processes in heterogeneous aquifers flushed with biodegradable surfactants. *Journal of Contaminant Hydrology*, 94(3-4): 195-214, doi: 10.1016/j.jconhyd.2007.05.011.

Conference Proceedings, Technical Abstracts and Scientific Presentations

Abriola, L.M. and L.D. Lemke, The influence of hydraulic property correlation on predictions of DNAPL entrapment and recovery, ModelCare 2002: 4th International Conference on Calibration and Reliability in Groundwater Modelling; June 17-20, 2002, Prague, Czech Republic.

Abriola, L.M., Goovaerts, P., and Lemke, L.D., Source Zone Remediation: The influence of hydraulic property correlation on predictions of DNAPL infiltration, entrapment, and recovery. SERDP/ESTCP Partners in Environmental Technology Technical Symposium & Workshop, December 3-5, 2002, Washington, District of Columbia.

Abriola, L.M., C.A. Ramsburg, K.D. Pennell, F.E. Löffler, M. Gamache, and E.A. Petrovskis. Post treatment monitoring and biological activity at the Bachman Road surfactant-enhanced aquifer remediation site. 225th American Chemical Society National Meeting, March 23-27, 2003, New Orleans, Louisiana.

Abriola, L.M., T.J. Phelan, and D.M. O'Carroll. Exploring the influence of medium wettability on DNAPL migration and retention behavior: Bench scale experiments and field scale implications. Society for Industrial and Applied Mathematics Conference on Mathematical & Computational Issues in the Geosciences, March 17-20, 2003, Austin, Texas.

Abriola L.M. Effectiveness of DNAPL source zone treatment in heterogeneous media: The role of interphase mass transfer. 226th ACS National Meeting, September 7-11, 2003, New York, New York.

Abriola, L.M., J.A. Christ, L.D. Lemke, C.A. Ramsburg, F.E. Löffler, and K.D. Pennell, Quantifying benefits of partial mass removal from chlorinated DNAPL source zones, to be presented at the 4th International conference on remediation of chlorinated and recalcitrant compounds, May 24-27, 2004, Monterey, California.

Abriola, L.M. DNAPL Source Zone Treatment Trains: Coupling Aggressive Mass Removal and Microbial Reductive Dechlorination. Invited presentation at the Regenesis sponsored luncheon program on "The Future of Bioremediation", held in conjunction with the Eighth International Conference on In Situ and On-Site Bioremediation, June 6, 2005, Baltimore, Maryland.

Abriola, L.M. DNAPL Source Zones: Progress and Challenges for Site Management, Keynote Luncheon Speaker, 21st Annual International Conference on Soils, Sediments, and Water, October 20, 2005, University of Massachusetts, Amherst.

Abriola, L.M., J.A. Christ, K. Li, and C.A. Ramsburg. Modeling Tools for Assessing the Benefits of DNAPL Source-Zone Remediation. *SERDP/ESTCP Partners in Environmental Technology Technical Symposium & Workshop*, November 29-December 1, 2005, Washington, District of Columbia.

Abriola, L.M., Subsurface contamination: Application of innovative technology or perpetual stewardship. *Lichtenstein Distinguished Lecture*, April 28, 2006, Ohio State University.

Abriola, L.M., Invited Presenter/Instructor and Panel Member in the DNAPL Remediation Session at the *EPA National Association of Remedial Project Managers Annual Training Conferenc*e, June 19, 2006, New Orleans, Louisiana.

Abriola, L.M., K.D. Pennell, F.E. Löffler, C.A. Ramsburg, J.A. Christ, B.K. Amos, and E.J. Suchomel. 2006. Experimental and modeling assessment of dissolution enhancement due to source zone bioremediation. *SERDP/ESTCP Partners in Environmental Technology Technical Symposium & Workshop*, November 28-30, 2006, Washington, District of Columbia.

Abriola, L.M., K.D. Pennell, F.E. Löffler, C.A. Ramsburg, J.A. Christ, B.K. Amos, and E.J. Suchomel. Exploring the influence of bioremediation on dissolution in DNAPL source zones. *Eos Transactions AGU, 87*(52), Fall Meeting Supplement, Abstract H331-01., December 11-15, 2006, San Francisco, California.

Abriola, L.M., B.K. Amos, N. Capiro, J.A. Christ, K. Li, Y. Li, F.E. Löffler, K.D. Pennell, and C.A. Ramsburg. Investigating the Benefits of DNAPL Source Zone Treatment: Source Zone Architecture, Partial Mass Removal, and Contaminant Flux Reduction. Partners in Environmental Technology Technical Symposium & Workshop, Sponsored by SERDP and ESTCP, 04-06 December 2007, Washington, District of Columbia.

Amos, B.K., Y. Sung, F.E. Löffler. Evaluation of the Reductive Dechlorination Process in the Presence of Free Phase Tetrachloroethene (PCE). 103rd General Meeting of the American Society for Microbiology, May 18-22, 2003, Washington, District of Columbia.

Amos, B.K., F.E. Löffler, K.D. Pennell, and E.J. Suchomel. Evaluation of Microbial Reductive Dechlorination of Chloroethenes in the Presence of the Surfactant Tween 80. Poster presentation at *SERDP/ESTCP Partners in Environmental Technology Technical Symposium & Workshop*, December 2-4, 2003, Washington, District of Columbia.

Amos, B.K., R. Krajmalnik-Brown, J. He, Y. Sung, J. Waddell, K. Ritalahti, F.E. Löffler, and S. Koenigsberg. New Approaches for Initiating and Monitoring Reductive Dechlorination at Chloroethene-Contaminated Sites. Fourth International Conference on Remediation of Chlorinated and Recalcitrant Compounds. May 24-27, 2004, Monterey, California.

Amos, B.K. and F.E. Löffler. Microbial Reductive Dechlorination at High Tetrachloroethene (PCE) Concentrations and In the Presence of PCE-DNAPL. *Tenth International Symposium on Microbial Ecology.* August 22-27, 2004, Cancun, Mexico.

Amos, B.K. Is Bioremediation Feasible Following Physical-Chemical Treatment at Chloroethene-Contaminated Sites? *EPA STAR Graduate Fellowship Conference*. October 11-13, 2004, Washington, District of Columbia.

Amos, B.K., F.E. Löffler, K.D. Pennell, and E.J. Suchomel. Microbial Reductive Dechlorination at High Tetrachloroethene (PCE) Concentrations and In the Presence of PCE-DNAPL.

SERDP/ESTCP Partners in Environmental Technology Technical Symposium & Workshop, November 30-December 2, 2004, Washington, District of Columbia.

Amos, B.K., S. Koenigsberg, and F.E. Löffler. Improved Understanding of Microbial Reductive Dechlorination at High Tetrachloroethene (PCE) Concentrations and in the Vicinity of PCE-DNAPL. *National Ground Water Association: 2005 Ground Water Summit.* April 17-20, 2005, San Antonio, Texas.

Amos, B.K., R.C. Daprato, J.B. Hughes, and F.E. Löffler. Real Time (RTm) PCR Monitoring of *Dehalococcoides*, *Sulfurospirillum*, and *Dehalobacter* Species During Exposure to Surfactants. *105th General Meeting of the American Society of Microbiology*, June 5-9, 2005, Atlanta, Georgia.

Amos, B.K., E.J. Suchomel, K.D. Pennell, and F.E. Löffler. Assessment of Microbial Reductive Dechlorination Performance and Microbial Distribution in the Immediate Vicinity of a NAPL Source Zone. *SERDP/ESTCP Partners in Environmental Technology Technical Symposium & Workshop*, November 29-December 1, 2005, Washington, District of Columbia.

Amos, B.K., E.J. Suchomel, K.D. Pennell, and F.E. Löffler. Microbial distribution and microbial reductive dechlorination performance in the immediate vicinity of a NAPL source zone. The *Fifth International Conference on Remediation of Chlorinated and Recalcitrant Compounds*. May 22 – 25, 2006, Monterey, California.

Amos, B.K., E.J. Suchomel, K.D. Pennell, and F.E. Löffler. Experimental assessment of bioenhanced dissolution and microbial distribution during PCE-NAPL source zone bioremediation. *Eos Transactions AGU, 87*(52), Fall Meeting Supplement, Abstract H331-06, December 11-15, 2006, San Francisco, California.

Amos, B.K., C. Cruz-Carcia, E. Padilla-Crespo, K.E. Fletcher, K.M. Ritalahti, and F.E. Löffler. Oxygen sensitivity of *Dehalococcoides*: effects on viability and quantification. Presented at the *Incredible Anaerobes: From Physiology to Genomics to Fuels Symposium*, March 2-3, 2007, Athens, Georgia.

Daprato, R.C., B.K. Amos, F.E. Löffler, and J.B. Hughes. Evaluation of Microbial Reductive Dechlorination to Remove Residual Contamination After Surfactant Treatment. *Tenth International Symposium on Microbial Ecology.* August 22-27, 2004, Cancun, Mexico.

Christ, J.A., L.M. Abriola, J.L Lang, L.D. Lemke, F.E. Löffler, K.D. Pennell, and C.A. Ramsburg. Coupling Chlororespiration with Aggressive Mass Removal to Reduce DNAPL Source Longevity. Partners in Environmental Technology Technical Symposium & Workshop, Sponsored by SERDP and ESTCP, 2-4 December 2003, Washington, District of Columbia.

Christ, J.A., C.A. Ramsburg, K.D. Pennell, and L.M. Abriola. Upscaled Mass Transfer Correlations for Estimating Mass Discharge from DNAPL Source Zones: Comparisons to Field-Scale Numerical Simulations. American Geophysical Union Fall Meeting, 13-17 December 2004, San Francisco, California.

Christ, J.A., C.A. Ramsburg, L.M. Abriola, and K.D. Pennell. Estimation of Mass Discharge Emanating from DNAPL Source-Zones using Upscaled Mass Transfer Coefficients. *The Fifth International Conference on Remediation of Chlorinated and Recalcitrant Compounds* May 22-25, 2006, Monterey, California.

Lemke, L.D., L.M. Abriola, and P. Goovaerts, Exploration of the influence of hydraulic property correlation on predictions of DNAPL infiltration and entrapment, Groundwater 2002 IAHR Groundwater Symposium Proceedings; March 25-29, 2002, Berkeley, California.

Lemke, L.D., W.A. Barrack, L.M. Abriola, and P. Goovaerts, Influence of Conceptual Model Selection on Three-Dimensional Tracer Transport: Comparison of Predictions and Observations in a Nonuniform Sand Aquifer. American Geophysical Union Fall Meeting, December 6-10, 2002, San Francisco, California.

Lemke, L.D., W.A. Barrack, and L.M. Abriola. Use of Advective Particle Tracking Metrics to Identify Stochastic Realizations with Extreme Advective-dispersive Transport Behavior in a Nonuniform Sand Aquifer. MODFLOW and More 2003: Understanding Through Modeling, September 17-19, 2003, Golden, Colorado.

Li, Y., K.D. Pennell, C.A. Ramsburg, and L.M. Abriola. Simulation of Low Interfacial Tension DNAPL Mobilization in Porous Media Using the Total Trapping Number Approach. American Geophysical Union Fall Meeting, paper no. H23G-07,11-15 December 2006, San Francisco, California.

Li, K. B. and L. M. Abriola, 2006, A multi-stage multi-criteria spatial sampling strategy for the quantification of contaminant mass discharge and the associated uncertainty, American Geophysical Union Fall Meeting, December, 2006, San Francisco, California.

Pennell, K.D., F.E. Löffler, C.A. Ramsburg, E.J. Suchomel, and B.K. Amos. Comparisons of Surfactant-Based DNAPL Source Zone Remediation Strategies: Solubilization, Mobilization and Density Modified Displacement. SERDP/ESTCP Partners in Environmental Technology Technical Symposium & Workshop, December 3-5, 2002, Washington, District of Columbia.

Pennell, K.D., L.M. Abriola, F.E. Löffler, B.K. Amos, E.J. Suchomel, and J. Costanza. Combined Remediation Technologies: Surfactants + Bioremediation, Thermal + Bioremediation. Presented to the Remediation Technologies Development Forum (RTDF) Combined Remedies Group at the *Eighth International Symposium on In Situ and On-Site Bioremediation*. June 8, 2005, Baltimore, Maryland.

Phelan, T.J., C.A. Ramsburg, and L.M. Abriola. Compositional Simulation of Subsurface Remediation via Density Modified Displacement. American Geophysical Union Fall Meeting, 13-17 December 2004, San Francisco, California.

Preston, K.E., F.E. Löffler, H. Moura, A. Woolfitt, B.K. Amos, Y. Sung, S. Henry, and J.R. Barr. Detection of *Anaeromyxobacter dehalogenans* Biomarkers by MALDI-TOF-MS Analysis of Whole Cells. Association of Biomolecular Resource Facilities Annual Meeting, February 5-8, 2005. Savannah, Georgia.

Preston, K.E., F.E. Löffler, H. Moura, A. Woolfitt, B.K. Amos, Y. Sung, S. Henry, and J.R. Barr. MALDI-TOF MS Profiling of Environmentally Relevant Bacteria Including *Anaeromyxobacter*, *Geobacter*, and *Desulfuromonas* Species. *105th General Meeting of the American Society of Microbiology*, June 5-9, 2005, Atlanta, Georgia.

Preston, K.E., J.R. Barr, H. Moura, A. Woolfitt, B.K. Amos, Y. Sung, S. Henry, and F.E. Löffler. MALDI-TOF MS Profiling of Metal-Reducing Bacteria Including *Anaeromyxobacter*, *Geobacter*, and *Desulfuromonas* Species. The Joint International Symposia for Subsurface Microbiology and Environmental Biogeochemistry, August 17, 2005, Jackson Hole, Wyoming.

Ramsburg, C.A., E.J. Suchomel, and K.D. Pennell. Comparison of surfactant-based DNAPL source zone remediation technologies. 225th American Chemical Society National Meeting, March 23-27, 2003, New Orleans, Louisiana.

Ramsburg, C.A., L.M. Abriola, K.D. Pennell, F.E. Löffler, M. Gamache, and E.A. Petrovskis. Impacts of Residual Surfactant on Tetrachloroethene (PCE) Degradation Following Pilot-Scale SEAR Treatment at a Chloroethene-Impacted Site. European Geophysical Society-American Geophysical Union-European Union of Geosciences Joint Assembly, Nice, France, Apr 6-11, 2003.

Ramsburg, C.A., J.A. Christ, and L.M. Abriola. Implications of Degradation Product Partitioning on Dissolution Bioenhancements in Heterogeneous DNAPL Source Zones. *The Fifth International Conference on Remediation of Chlorinated and Recalcitrant Compounds* May 22-25, 2006, Monterey, California.

Ramsburg, C.A., J.A. Christ, and L.M. Abriola. Lab-scale Investigation of Degradation Product Partitioning in Source Zones Containing Chlorinated Solvents. *Eos Transactions AGU, 86*(52), Fall Meeting Supplement, Abstract H23A-1412, December 11-15, 2006, San Francisco, California.

Suchomel, E.J. and K.D. Pennell. Assessment of Contaminant Plume Development Following Surfactant-Based DNAPL Source Zone Treatment. Frontiers in Assessment Methods in the Environment, Sponsored by AEESP, 10-13 August 2003, Minneapolis, Minnesota.

Suchomel, E.J. and K.D. Pennell. Assessment of Contaminant Plume Development Following Surfactant-Based DNAPL Source Zone Treatment. Fourth International Conference on Remediation of Chlorinated and Recalcitrant Compounds, May 24-27, 2004, Monterey, California.

Suchomel, E.J. and K.D. Pennell. Plume Development and Mass Flux Following Surfactant-Based Treatment of Heterogeneous PCE-DNAPL Source Zones. American Geophysical Union Fall Meeting, December 13-17, 2004, San Francisco, California.

Suchomel, E.J., B.K. Amos, F.E. Löffler, and K.D. Pennell. Quantitative PCR correlates microbial activity and distribution with enhanced contaminant dissolution from a PCE-NAPL source zone. *231P stP American Chemical Society National Meeting and Exposition.* March 26-30, 2006, Atlanta, Georgia.

Appendix B

Intellectual Property Patents

Li, K. B., P. Goovaerts, L. M. Abriola, *Method for Multi-Stage Spatial Sampling with Multiple Criteria,* US Provisional Patent Application 60/874,214, disclosure filed on December 11, 2006.

Li, K. B., P. Goovaerts, L. M. Abriola, *Method for Multi-Stage Spatial Sampling with Multiple Criteria*, PCT Patent Application PCT/US2007/25440, disclosure filed on December 11, 2007.

Awards

Strategic Environmental Research and Development Program *Environmental Restoration Project of the Year* 2006.

2006 AGU Fall Meeting Outstanding Student Paper Award, Hydrology Section – awarded to Dr. K. Betty Li for the presentation: A Multi-stage Multi-criteria Spatial Sampling Strategy for the Quantification of Contaminant Mass Discharge and the Associated Uncertainty by K.B. Li and L.M. Abriola.

Frank J. Seiler Research Award for Research Excellence in Engineering, US Air Force Academy, CO – awarded to Dr. John A. Christ.

Dr. Robert Farvolden National Ground Water Research and Education Foundation Best Student Paper Award at the *National Ground Water Association's 2005 Ground Water Summit* – awarded to Dr. Benjamin K. Amos for the presentation: Improved Understanding of Microbial Reductive Dechlorination at High Tetrachloroethene (PCE) Concentrations and in the Vicinity of PCE-DNAPL by B.K. Amos, S.S. Koenigsberg, and F.E. Löffler.

2007 Geosyntec Consultants Student Research Contest – awarded to Dr. Benjamin K. Amos for the whitepaper: Quantitative PCR Correlates Microbial Activity and Distribution with Enhanced Contaminant Dissolution by B.K. Amos, E.J. Suchomel, K.D. Pennell, and F. E. Löffler.